

# **Studies on Development of Micro-Solid Lubricant Coating on Cutting Tools**

**THESIS**

Submitted in partial fulfilment of  
the requirements for the degree of

**DOCTOR OF PHILOSOPHY**

by

**UMAMAHESHWERA REDDY P**

**ID. No. 2011PHXF017H**

Under the Supervision of

**Prof. SURESH KUMAR REDDY NARALA**



**BIRLA INSTITUTE OF TECHNOLOGY AND SCIENCE, PILANI,  
INDIA**

**2014**

**BIRLA INSTITUTE OF TECHNOLOGY AND SCIENCE, PILANI,  
HYDERABAD CAMPUS, HYDERABAD, TELANGANA**

**CERTIFICATE**

This is to certify that the thesis entitled “**Studies on Development of Micro-Solid Lubricant Coating on Cutting Tools**” and submitted by **UMAMAHESHWERA REDDY P**, ID No. **2011PHXF017H** for award of Ph.D. of the Institute embodies original work done by him under my supervision.

Signature of the Supervisor:

Name in capital letters:

**SURESH KUMAR REDDY NARALA**

Designation:

**Associate Professor**

Department of Mechanical Engineering

BITS-Pilani Hyderabad Campus, Jawahar Nagar

Shameerpet (Mandal), Hyderabad – 500 078

Telangana, India.

Date:

## ACKNOWLEDGEMENTS

I feel very fortunate to have an opportunity to acknowledge various persons involved in my research work and for their help in one way or the other.

First of all, I would like to thank the *Almighty* for giving me the opportunity to do the research work with good health and prosperity.

My deep sense of gratitude to *Prof. Bijendra Nath Jain*, Vice Chancellor, BITS-Pilani for permitting me to carry out my doctoral work in the institute.

My heart-felt gratitude to *Prof. V. Sambasiva Rao*, Director, BITS-Pilani, Hyderabad Campus, for permitting me to carry out my research work in the campus.

I wish to express my earnest gratitude and heartfelt thanks to my **research supervisor**, *Prof. Suresh Kumar Reddy Narala*, Department of Mechanical Engineering, BITS-Pilani, Hyderabad Campus, for his excellent guidance, constant encouragement, enormous patience and good advice with a smiling face throughout my research work. I would like to acknowledge him for his moral support every instance, careful reviews, technical comments, constructive criticism through all my research work and dissertation, and his highly appreciated instruction, without which, this work would not have been completed. I owe it to you sir.

I am thankful to *Prof. Amit Kumar Gupta* and *Dr. S. Sandeep Deshmukh*, Doctoral Advisory Committee members, Department of Mechanical Engineering, BITS-Pilani, Hyderabad Campus, for their valuable time in reviewing this thesis and suggestions.

I am thankful to *Prof. Suman Kapur*, Dean, IPCD, *Prof. Vidya Rajesh*, Associate Dean, ARD and *Prof. P. Yogeeswari*, Associate Dean, SRCD, BITS-Pilani, Hyderabad Campus, for their support to my research work.

I wish to express my thanks and take immense pleasure in acknowledging all the *faculty* of Department of Mechanical Engineering, BITS-Pilani, Hyderabad Campus for their support and encouragement to carry out my research work.

My special thanks to *Prof. Y.V. Daseswara Rao*, current HOD and *Prof. Srinivasa Prakash Regalla*, former HOD, Department of Mechanical Engineering, BITS-Pilani, Hyderabad Campus, for permitting me to carry out my research work in the Department of Mechanical Engineering.

I express my thanks to all laboratory staff and technicians of Mechanical Engineering Department, especially, *Mr. B. Chandra Shekar* for the warm-hearted assist and patient in my experimental work.

Thanks to all the members in the institute for the unforgettable happy time in the past three years, especially my colleague, *Mr. J. Sravan Kumar*, for his uncountable and unselfish help in artwork for thesis writing. I also thank to my colleague, *Mr. G. Rakesh Kumar*, for proof reading.

I deeply acknowledge the research support of BITS-Pilani ([www.bits-pilani.ac.in](http://www.bits-pilani.ac.in)) through *BITS Seed Grant Scheme* (Mission 2012 TF8).

I would like to thank my research group, my friends in and out of the department who have made the last few years an exciting and memorable experience.

Last, but not least, I place my deep sense of gratitude and thanks to my *family* and *parents* for their unconditional support and loving encouragement throughout my life.

Date:

UmaMaheshwera Reddy P

## ABSTRACT

Conventional metal cutting processes involve massive consumption of energy where the specific cutting energy is usually high. A major division of this energy is converted into heat which creates detrimental effects on cutting tool wear, tool life and surface quality of machined workmaterial. Although cutting fluids are effective to coerce this energy transfer, but the growing challenge to deal with the environmental and health aspects stood by coolant machining is imposing manufacturers to limit the usage of cutting fluids. Alternative to cutting fluid application, the aim of the current research work is to develop the concept of an approach to product manufacturing in producing novel coatings. In view of this, present work introduces an electrostatic micro-solid lubricant (EMSL) coating on carbide tool with molybdenum disulfide ( $\text{MoS}_2$ ) as a solid lubricant. To explore the level of success of this novel coating, efficacies of coatings were investigated in tribological as well as machining applications.

The tribological behavior of EMSL coatings in dry sliding conditions is evaluated as per the ASTM G99 standard. A pin-on-disc tribological testing is conducted to examine the friction and wear behavior of EMSL coatings under dry sliding conditions at various sliding speeds and applied loads. The surfaces of the wear samples were examined under scanning electron microscopy and optical microscopy. Further, in order to assess the performance of developed EMSL coated cutting tool in machining process, an attempt has been made in comprehending the results on cutting forces, cutting temperatures, tool wear, chip formation and surface finish of machined workmaterial.

Tribological studies reveal that the EMSL coating has the lowest friction coefficient on average of about 50% less at all the sliding conditions when compared to that of uncoated one. Wear volume of the specimens is linear satisfying the Archard's wear law and directly

dependent on the mechanical energy dissipated in the sliding contact. Further, the specific wear rate of EMSL coated specimen is very low when compared to that of uncoated one.

Machining with EMSL coated cutting tools results in lower frictional values at tool-work interface leading to reasonable lower cutting forces than those in machining with uncoated cutting tools. Further, tool flank wear in EMSL coated cutting tools is very less as compared to that of the uncoated cutting tool. Shear deformation to form chips was judged and observed favorable tool-chip interaction in machining with EMSL coated tools. Surface quality of machined workmaterial when machining with EMSL coated cutting tool showed a much better improvement when compared to that of machining with uncoated cutting tool.

In addition to the above, the current research work also analyzes finite element (FE) modelling of metal cutting process to comprehend the physical cutting process variables such as cutting temperature, cutting force, chip thickness and shear angle by relating the same with practical conditions when machining with and without coated cutting tools. FE modelling of machining process by taking into account the both shear and Coulomb friction and workmaterial flow based on the formulated constitutive model was demonstrated with the help of numerical code, DEFORM<sup>TM</sup>.

**Keywords:** EMSL coating, MoS<sub>2</sub>, tribological tests, machining tests, cutting parameters, FE simulations, DEFORM<sup>TM</sup>

# TABLE OF CONTENTS

---

<b>Contents</b>	<b>Page No.</b>
Certificate -----	i
Acknowledgements -----	ii
Abstract -----	iv
Table of contents -----	vi
List of tables -----	x
List of figures -----	xii
List of abbreviations -----	xvii
List of symbols -----	xix
<b>Chapter 1 INTRODUCTION</b>	<b>1-12</b>
1.1. Background-----	1
1.2. Motivation and research methodology -----	5
1.3. Aim and scope of the current research -----	7
1.4. Organization of the dissertation -----	10
<b>Chapter 2 LITERATURE REVIEW</b>	<b>13-43</b>
2.1. Introduction -----	13
2.2. Surface coating -----	21
2.2.1. Classification of coating deposition methods -----	22
2.2.2. Classification of coating materials -----	26
2.3. Significance of MoS <sub>2</sub> based coatings -----	27
2.4. Finite element (FE) modelling approach of machining process -----	32
2.4.1. Modelling of chip formation process -----	34
2.4.2. Material constitutive modelling -----	35
2.4.3. Tool-chip interfacial friction modelling -----	36
2.5. Gaps in the existing research -----	39
2.6. Summary -----	42
<b>Chapter 3 DESIGN &amp; FABRICATION OF NOVEL MICRO-SOLID LUBRICANT COATING SYSTEM</b>	<b>44-66</b>
3.1. Introduction -----	44
3.2. Basics of electrostatic coating deposition process -----	45
3.3. Design & fabrication of EMSL coating deposition process setup -----	48

3.3.1. EMSL coating system -----	49
3.3.2. Nozzle assembly -----	51
3.3.3. EMSL coating process operating parameters -----	53
3.3.3.1. Air pressure -----	53
3.3.3.2. Electric potential -----	53
3.3.3.3. Nozzle tip to substrate distance -----	54
3.4. Optimal deposition process parameters -----	55
3.4.1. Material and tool substrate -----	55
3.4.2. Plan of EMSL coating experiments -----	56
3.4.3. Experimental results -----	58
3.4.4. Correlations and confirmations -----	64
3.5. Summary -----	66
<b>Chapter 4 EXPERIMENTAL INVESTIGATION TO ASSESS THE</b>	<b>67-89</b>
<b>TRIBOLOGICAL PERFORMANCE OF EMSL COATINGS</b>	
4.1. Introduction -----	67
4.2. Experimental approach -----	68
4.2.1. Materials -----	68
4.2.2. Preparation of EMSL coatings -----	68
4.2.3. Sliding wear tests -----	69
4.2.4. Analysis of the EMSL coatings -----	73
4.2.4.1. Mechanical properties of coatings -----	73
4.2.4.2. Coating strength -----	74
4.2.5. Dry sliding behavior -----	74
4.3. Results and discussion -----	75
4.3.1. Particle surface charge to mass ratio, coating thickness, hardness, elastic modulus and coating strength -----	75
4.3.2. Friction and wear behavior -----	79
4.4. Summary -----	88
<b>Chapter 5 EXPERIMENTAL INVESTIGATION TO STUDY THE</b>	<b>90-122</b>
<b>EFFECT OF EMSL COATED TOOLS ON MACHINABILITY</b>	
<b>PARAMETERS</b>	
5.1. Introduction -----	90
5.2. Material and machining tests -----	92



5.3. Results and discussion -----	94
5.3.1. Cutting forces -----	95
5.3.2. Tool flank wear -----	100
5.3.3. Chip formation -----	105
5.3.4. Surface roughness -----	108
5.3.4.1. Surface roughness under varying cutting conditions -----	110
5.3.4.1.1. Plan of experiments -----	110
5.3.4.1.2. Results and discussion -----	112
5.3.4.1.2.1. ANOVA results -----	112
5.3.4.1.2.2. Correlations and confirmations-----	118
5.4. Summary -----	121
<b>Chapter 6 FINITE ELEMENT (FE) MODELLING AND SIMULATION OF MACHINING PROCESS</b>	<b>123-147</b>
6.1. Introduction -----	123
6.2. FE modelling of the machining process -----	124
6.2.1. Selection of material constitutive model-----	125
6.2.1.1. Johnson-Cook (JC) model -----	127
6.2.1.2. Zerilli-Armstrong (ZA) model -----	129
6.2.1.3. Arrhenius (Arr) model -----	130
6.2.1.4. Norton-Hoff (NH) model -----	131
6.2.2. Tool-chip interfacial friction modelling -----	132
6.3. FE machining simulations -----	134
6.4. Machining experiments -----	136
6.5. Results and discussion -----	138
6.6. Summary -----	146
<b>Chapter 7 CONCLUSIONS AND FUTURE WORK</b>	<b>148-153</b>
7.1. Summary -----	148
7.2. Specific contribution -----	148
7.3. Conclusions -----	149
7.4. Future work -----	153
<b>APPENDICES</b>	<b>154-158</b>
Appendix A -----	154
Appendix B -----	157

<b>REFERENCES</b>	159
List of publications -----	180
Biography of the candidate -----	182
Biography of the supervisor -----	183

## LIST OF TABLES

Table No.	Details	Page No.
2.1	Methods of fabricating coatings	23
2.2	Classification of tribological coatings, depending on the nature of the constituting material	27
3.1	The EMSL coating deposition conditions	55
3.2	Assignment of levels to the factors used in experiments	56
3.3	Selected electrostatic coating deposition process parameters and measured coating thickness	59
3.4	ANOVA results for coating thickness	61
3.5	The optimum values of EMSL coating deposition process parameters	62
3.6	Input process parameters employed in confirmation tests and comparison of measured and predicted results	65
4.1	The MoS <sub>2</sub> coating deposition conditions	69
4.2	Critical load of EMSL coatings	78
5.1	Material and experimental conditions adopted in machining tests	93
5.2	Assignment of levels to the control factors (machining parameters)	110
5.3	Measured surface roughness ( $R_a$ ) on the machined workmaterial at varying cutting conditions	111
5.4	ANOVA results for average surface roughness ( $R_a$ )	113
5.5	The optimum values of cutting parameters	113
5.6	Percentage of error (%) between measured and predicted surface roughness	119
6.1	Material constants for JC model	129
6.2	Material constants for ZA model	130
6.3	Material constants for Arr model	131
6.4	Material constants for NH model	132
6.5	Mechanical and thermo-physical properties of materials used in FE simulations	135
6.6	Percentage of error (%) between experimental and FE simulated results of cutting forces with different constitutive models for different strain rates	136
6.7	Conditions adopted in FE simulations and machining experiments	137

6.8	Percentage of error (%) between experimental and FE simulated results of cutting forces and cutting temperatures when machining AA7075-T6 material with and without coated cutting tool	141
6.9	Percentage of error (%) between experimental and FE simulated results of chip thickness ratio and shear angle when machining AA7075-T6 material with and without coated cutting tool	146
B.1	Wear volume, wear rate and dissipated energy obtained from sliding tests	158

## LIST OF FIGURES

Figure No.	Details	Page No.
1.1	The overall objectives of the research work	8
1.2	Organization of the dissertation	10
2.1	Schematic illustration of layered crystal structures of solid lubricants: (a) $H_3BO_3$ , (b) graphite, (c) HBN, and (d) $MoS_2$	16
2.2	The life curves of tools with and without $MoS_2$	28
2.3	Coefficient of friction of $MoS_2$ and $MoS_2/Ti$ coatings: (a) in fretting test, and (b) in pin-on-disk test	29
2.4	(a) Coefficient of friction in different atmospheric conditions at sliding speed of 66 mm/s, and (b) specific wear rate of coatings after 4000 cycles	30
2.5	Results from pin-on-disc testing at 10, 40 and 80 N loads showing friction coefficient and wear rates for low and high-Ti MoST coatings	31
2.6	(a) Friction coefficient with sliding distance of the specimens when sliding against a hard steel ring at 200 r/min, load of 20 N, and (b) Flank wear of the inserts in dry cutting of the hard steel	32
2.7	Stress distribution on tool-chip interface	37
3.1	The most common components of electrostatic coating equipment	45
3.2	Schematic of experimental process used in corona charging EMSL coating deposition system	46
3.3	Electrostatic micro-solid lubricant (EMSL) coating deposition system: (a) schematic view of the experimental setup, and (b) photograph of the developed EMSL coating experimental setup	49
3.4	Details of control block: (a) working schematic view, and (b) photograph of the control block	50
3.5	EMSL coating nozzle assembly: (a) schematic view of the nozzle assembly, and (b) photograph of the fabricated nozzle assembly	52
3.6	Coating thickness measurement using tool measuring microscope	57
3.7	Photograph of EMSL coated carbide substrates: (a) pin specimen used in tribological pin-on-disc tests, and (b) cutting tool inserts used in machining experiments	57

3.8	(a) SEM images, and (b) microscopic images, showing the uniformity and cross-sectional views of coatings at different process conditions	60
3.9	MEP of experimental plan for coating thickness	61
3.10	Surface plot for electric potential and pressure effects on coating thickness	62
3.11	Surface plots for electric potential and distance effects on coating thickness	63
3.12	Surface plots for pressure and distance effects on coating thickness	63
4.1	Pin-on-disc tribological testing setup used in tribological tests	70
4.2	Schematic of tribological pair designs: (a) WC-Co alloy specimen, and (b) Ti-6Al-4V alloy counter material	70
4.3	(a) Magnified view of pin and disc used in tribological tests, and (b) a sample thermal infrared image at sliding contact	71
4.4	Surface roughness profiles: (a) disc with $R_a = 0.256 \mu\text{m}$ , and (b) pin specimen with $R_a = 0.24 \mu\text{m}$	72
4.5	Coating strength test using standard scratch tester (Ducom Instruments)	74
4.6	Optical micrographs: (a) EMSL coated surface, and (b) typical microindentations on the coated surface at various loads	77
4.7	Scratch images on coated surface: (a) no failure in the coating, (b) corresponding to a load of 52 N, (c) corresponding to a load of 61 N, and (d) corresponding to a load of 69 N	78
4.8	Mean coefficient of friction against sliding speed at different loads: (a) 40 N, (b) 60 N, (c) 80 N, and (d) all loads corresponding to (a), (b) and (c)	79
4.9	Pin contact temperatures as the function of normal load at different sliding speeds for two tested tribological pairs	80
4.10	Dissipated energy ( $\Delta E$ ) in the sliding contact as the function of normal load at different sliding speeds for two tested tribological pairs	80
4.11	Specimen wear volume ( $WV$ ) as the function of normal load at different sliding speeds for two tested tribological pairs	82
4.12	Specimen wear rates ( $WR$ ) as the function of normal load at different sliding speeds for two tested tribological pairs	82
4.13	Specimen wear volume ( $WV$ ) against mechanical energy ( $F_n * L$ ) in the sliding contact for the two tested tribological pairs at normal load of 60 N (Archard's approach)	83

4.14	SEM images and EDS observations on the specimen surfaces in tribopair-1 at applied load of 60 N: (a) worn surface at sliding speed of 100 m/min, (b) EDS chemical composition on the worn surface corresponding to (a), (c) worn surface at sliding speed of 200 m/min, and (d) EDS chemical composition on the worn surface corresponding to (c)	85
4.15	SEM images and EDS observations on the specimen surfaces in tribopair-2 at applied load of 60 N: (a) worn surface at sliding speed of 100 m/min, (b) EDS chemical composition on the worn surface corresponding to (a), (c) worn surface at sliding speed of 200 m/min, and (d) EDS chemical composition on the worn surface corresponding to (c)	86
4.16	Wear tracks and surface finish on counterpart against uncoated and EMSL coated specimens at sliding speed of 150 m/min at different loads: (a)-(b) 40 N, and (c)-(d) 80 N	88
5.1	(a) Turning experiments using a high precision lathe, and (b) a sample of thermal infrared image captured at tool-chip contact, and (c) a schematic view of the experimental setup	94
5.2	(a) Cutting forces with induced specific cutting energy ( $u_s$ ) (see data point values), and (b) feed forces, measured during machining with and without coated cutting tools ( $f = 0.2$ mm/rev and $a_p = 2$ mm)	96
5.3	(a) Cutting forces, and (b) feed forces, measured during machining with and without coated cutting tools at different cutting speeds and feed rates	97
5.4	Coefficient of friction calculated during machining with and without coated cutting tools at different cutting speeds ( $f = 0.2$ mm/rev and $a_p = 2$ mm)	99
5.5	Cutting temperatures measured during machining with and without coated cutting tools at different cutting speeds ( $f = 0.2$ mm/rev and $a_p = 2$ mm)	99
5.6	(a) Comparison of tool flank wear at different cutting speeds, and (b) wear growth at particular cutting speed (200 m/min) against cutting length in machining with and without coated cutting tools	101
5.7	Effect of cutting speed on the allowable wear limit and tool life at different cutting speeds when machining with uncoated cutting tool	102
5.8	Effect of cutting speed on the allowable wear limit and tool life at different cutting speeds when machining with EMSL coated cutting tool	102

5.9	Tool life comparison for both the uncoated and EMSL coated cutting tool at different cutting speeds	103
5.10	Built up edge (BUE) formation, tool flank wear and allowable wear land (wear criterion, $V_{b_k}$ ) on the cutting edge of uncoated tool at different cutting speeds: (a) 150 m/min, (b) 175 m/min, (c) 200 m/min, (d) 225 m/min, (e) 250 m/min, and (f) 300 m/min	104
5.11	(a) BUE formation on the tool cutting edge at 150 m/min speed, (b) flank wear on the tool surface at speed 200 m/min, (c) magnified view corresponding to (b), and (d) EDS chemical composition analysis on the worn surface corresponding to (c) during machining with EMSL coated cutting tools ( $f = 0.2$ mm/rev and $a_p = 2$ mm)	105
5.12	Comparison of chip shapes during machining of AA7075-T6 with and without coated cutting tools ( $f = 0.2$ mm/rev and $a_p = 2$ mm)	106
5.13	(a) Variation of shear angle to form a chip at different cutting speeds, and (b) chip formation showing shear deformation (shear angle, $\phi = 37.87^\circ$ ) corresponding to $v_c = 200$ m/min during machining with coated cutting tools ( $f = 0.2$ mm/rev and $a_p = 2$ mm)	107
5.14	A sample measure of surface finish on the machined workmaterial using surface profilometer (Taylor Hobson Surtronic S25)	108
5.15	Surface roughness as a function of cutting speed measured on machined workmaterial during machining with and without coated cutting tools ( $f = 0.2$ mm/rev and $a_p = 2$ mm)	109
5.16	Surface plots for effects of cutting conditions (cutting speed, feed and depth of cut) on average surface roughness of machined workmaterial: (a)-(c) during machining with uncoated cutting tool, and (d)-(f) during machining with EMSL coated cutting tool	115
5.17	Comparison of measured surface roughness on the machined work material under different cutting conditions: (a) during machining with uncoated tool, and (b) during machining with coated tool	116
5.18	Optical micrographs showing the quality of machined workmaterial at varying cutting conditions when machining with and without coated cutting tools	117



5.19	Normal probability plots for average surface roughness measured on the machined workmaterial: (a) during machining with uncoated cutting tool, and (b) during machining with coated cutting tool	120
6.1	Computer controlled UTM with high-temperature contact extensometer and three-zone resistance heating split furnace with a tensile test sample	126
6.2	Flow stress of AA7075-T6 workmaterial under various deformation temperatures at low strain rate ( $10^{-4} \text{ s}^{-1}$ )	126
6.3	Flow stress of AA7075-T6 workmaterial under various deformation temperatures at high strain rate ( $2.2 \times 10^4 \text{ s}^{-1}$ )	127
6.4	The two-dimensional FE cutting model used in machining simulations	134
6.5	Comparison of experimental and FE simulated cutting forces at low and high strain rate conditions with different constitutive models (cutting conditions: 250 m/min and 0.3 mm/rev)	136
6.6	Comparison of experimental and FE simulated results of cutting force during AA7075-T6 machining process with and without coated cutting tools at different cutting speeds ( $f = 0.3 \text{ mm/rev}$ )	139
6.7	Comparison of experimental and FE simulated results of cutting temperature during AA7075-T6 machining process with and without coated cutting tools at different cutting speeds ( $f = 0.3 \text{ mm/rev}$ )	139
6.8	FE predictions of cutting temperatures when simulating AA7075-T6 machining process: (a) with uncoated cutting tool, and (b) EMSL coated cutting tool (cutting conditions: 250 m/min and 0.3 mm/rev)	140
6.9	Experimental and FE simulated chip formation: (a) with coated tool, and (b) with uncoated tool (cutting conditions: 200 m/min and 0.3 mm/rev)	142
6.10	Experimental and FE simulated chip thicknesses during AA7075-T6 machining with and without coated tools at different cutting conditions	143
6.11	Comparison of experimental and FE simulated results of chip thickness ratio during AA7075-T6 machining process with and without coated cutting tools at different cutting speeds ( $f = 0.3 \text{ mm/rev}$ )	144
6.12	Comparison of experimental and FE simulated results of shear angle during AA7075-T6 machining process with and without coated cutting tools at different cutting speeds ( $f = 0.3 \text{ mm/rev}$ )	145

## LIST OF ABBREVIATIONS

---

AISI	American iron and steel institute
ALE	Arbitrary Lagrangian-Eulerian
Al <sub>2</sub> O <sub>3</sub>	Aluminum oxide
ANOVA	Analysis of Variance
APCVD	Atmospheric-pressure chemical vapor deposition
Arr	Arrhenius
ASTM	American society for testing and materials
BUE	Built up edge
CaF <sub>2</sub>	Calcium fluoride
CBN	Cubic boron nitride
Cr <sub>3</sub> C <sub>2</sub>	Chromium carbide
CrN	Chromium nitride
Cr <sub>2</sub> O <sub>3</sub>	Chromium oxide
CVD	Chemical vapor deposition
DC	Direct current
DLC	Diamond-like carbon
EDS	Energy dispersive spectroscopy
EMSL	Electrostatic micro-solid lubricant
FEM	Finite element method
HBN	Hexagonal boron nitride
H <sub>3</sub> BO <sub>3</sub>	Boric acid
HVOF	High velocity oxygen fuel
IBAD	Ion beam-assisted deposition
JC	Johnson-Cook

LPCVD	Low-pressure chemical vapor deposition
MEP	Main effect plot
MoS <sub>2</sub>	Molybdenum disulfide
NH	Norton-Hoff
NiCr	Nickel-Chromium
PECVD	Plasma-enhanced chemical vapor deposition
PTFE	Polytetrafluoroethylene
PVD	Physical vapor deposition
SAE	Society of automotive engineers
SEM	Scanning electron microscope
S/N	Signal to noise ratio
TiAlN	Titanium aluminum nitride
TiCN	Titanium carbo-nitride
TiN	Titanium nitride
UTM	Universal testing machine
WC-Co	Cemented tungsten carbide-cobalt
WS <sub>2</sub>	Tungsten disulfide
ZA	Zerilli-Armstrong
Zno	Zinc oxide
Zr	Zirconium

## LIST OF SYMBOLS

---

$\tau$	Shear stress
$\mu$	Coefficient of friction
$\sigma_n$	Normal stress
$F_c$	Cutting force
$F_f$	Feed force
$\gamma$	Rake angle
$\phi$	Shear angle
$f$	Feed
$v_c$	Cutting speed
$a_p$	Depth of cut
$R_a$	Average surface roughness
$V_b$	Flank wear
$\mu\text{m}$	Micrometer
$\text{kV}$	Kilovolt
$\text{\AA}$	Angstrom
$E, \epsilon_0, q, \epsilon_r$	Pauthenier's equation parameters
$\frac{q_{\max}}{m}$	Mean charge to mass ratio
$\rho$	Density
$\sigma$	Flow stress
$A, B, C, n, m$	Johnson-Cook flow stress equation constants
$\epsilon$	Plastic strain
$\dot{\epsilon}$	Strain rate
$\dot{\epsilon}_0$	Reference strain rate

$\dot{\epsilon}^*$	Dimensionless strain rate
T	Current absolute temperature
$T_r$	Reference temperature
$T_m$	Melting temperature
$C_0, C_1, C_3, C_4, C_5$	Zerilli-Armstrong flow stress equation constants
A, $\alpha$ , n, Q	Arrhenius type equation constants
Z	Zener-Hollomon parameter
K, m, n	Norton-Hoff flow stress equation constants
$R^2$	Coefficient of determination

# CHAPTER 1

## INTRODUCTION

---

In the current chapter, Section 1.1 presents a brief background to the metal cutting process, fundamental lubrication practices in cutting processes and the state of the art development in research. Motivation for this research work and research methodology is explained in Section 1.2. Aim and scope of the current research work and overall research objectives are presented in Section 1.3. Finally, Section 1.4 provides a complete organization of this dissertation – that is, a precursor of what is to come in each chapter of this research work.

### **1.1. Background**

Metal cutting processes are widely used to remove unwanted material and achieve desired surface finish of engineering components. In metal cutting processes, the unwanted material is removed by the cutting tool, which is significantly harder than the workpiece. During metal cutting operation, the cutting temperatures and forces on a cutting tool are typically high, which drastically decreases the tool life and affects quality of the products produced. Effective counter measures in control of the heat generation at cutting zone are strongly required to ensure simultaneous improvement of productivity and product quality. Hence, the use of proper lubrication approach in machining processes is critical to change in the contact conditions as a means of better control over frictional interaction at the tool-chip contact and mechanics of machining, thereby influencing the contact temperatures, tool life, cutting forces and energy consumption. Several technologies such as, flood cooling, minimum quantity lubrication/near dry machining, cryogenic cooling and solid lubricant assisted machining have been developed in recent years for controlling temperature in the

cutting zone and tool-chip contact frictional effects. Among them, cutting fluids and solid lubricants have been used by the researchers and manufacturers in the past for their ability to control above said parameters in order to improve the machining process performance.

Traditionally, cutting fluids are used to control high temperatures generated in cutting processes. Cutting fluids are also used to reduce the forces and energy consumption, control the friction coefficient between the tool and chip, wash away the chips and to protect the machined surfaces from environmental corrosion [1-2]. But the application of cutting fluids create several techno-environmental problems such as, environmental pollution due to chemical disassociation of cutting fluids at high cutting temperatures, biological problems to operators, water pollution and soil contamination during disposal [3-5]. Increasing consciousness for green manufacturing globally and consumer focus on environment friendly products has put increased pressure on manufacturers and researchers to eliminate or minimize the use of cutting fluids. Hence, as an alternative to cutting fluids, researchers experimented the use of solid lubricants with different strategies like, dispersing solid lubricants into the tool-workmaterial contact, forming a lubricating oxide film on the tool-chip interface through in-situ reaction by elevated cutting temperature and isolating the tool from workpiece with a lubricating layer on the cutting tool face [6-8]. Among these possible strategies, the use of self-lubricant layer/coating containing solid lubricants as one of the alternative materials onto contact surfaces have come a long way in recent years [9-12].

Self-lubricant layer/coating containing solid lubricant on cutting tools can provide excellent anti-friction and reasonable tool performances, and are now capable of controlling high heat generation during cutting processes. Advancement modern tribology has identified several solid lubricant materials such as molybdenum disulfide ( $\text{MoS}_2$ ), polytetrafluoroethylene (PTFE), Calcium fluoride ( $\text{CaF}_2$ ), diamond-like carbon (DLC), graphite, tungsten disulfide ( $\text{WS}_2$ ), etc. [13]. For any industrial application, it is very

important to find an effective approach being used to produce self-lubricant coatings. When choosing a solid lubricant coating deposition method, understanding of the coatings that used in a wide range of machining and tribological applications and factors influencing the performance of coatings material, such as coating thickness, substrate material, surface preparation, etc. are essential.

The common deposition techniques employed in tribological coatings include flotation process, electrochemical deposition, dispersion (dipping, brushing), burnishing, bonding, particulate deposition (thermal spray) and physical or chemical vapor deposition (PVD/CVD) [14]. Every technique has its distinctive advantages and its own application area, but, not all of them are suitable for tribological as well as machining applications due to their poor bonding strength, deposition rate, achievable coating thickness, cost, etc. These deposition methods allow us to prepare various adherent solid lubricant coatings on cutting tools from soft metal lamellar solids such as  $\text{MoS}_2$  and  $\text{WS}_2$  to hard metals like cubic boron nitride (CBN), titanium nitride (TiN) and DLC. The first-generation PVD coatings featured TiN as the hard coating and were applied in metal cutting processes. However, it is well known that hard coatings retain a high coefficient of friction and require lubricants. Sometimes, these properties render the hard coatings inappropriate when machining advanced engineering materials. Further, even if the diversified solid lubricant coatings can be achieved using above mentioned techniques, there are still some challenges connected to the deposition of micron-size/nano-size solid lubricant particles as they have an extremely high surface area to volume ratio, leading to diffusion at high temperatures, often results in aggregates and agglomerates rather than a single primary particle [15].

So, there is a need to concentrate efforts in this direction to overcome the above stated drawbacks and to look into new coating material and deposition methods to achieve sustainable machining system. Owing to its economic and simple in-house setup, high



transfer efficiency, and in especially easy depositing on large and complex geometrical surfaces with high deposition rate and coating thickness, researchers explored the application of electrostatic charging principle in depositing polymer and ceramic powders on different substrates to extend their wear and corrosive resistance. In near recent years, the application of this technique in using various solid lubricants like MoS<sub>2</sub>, Graphite, ZnO, etc. in machining applications makes researchers extremely attractive [16-18]. The researchers of the above work are successful in employing electrostatic charging principle in either depositing solid lubricant coating on cutting tools or dispersing solid lubricant mixture to tool-chip contact interface.

Study of tribological properties (friction and wear) of coatings play a vital role in comprehending their performance in machining applications. The purpose of tribology is to minimize the losses caused by friction and wear of components used in tribo-mechanical system. Practically, direct measurement of frictional effect and temperature at the sliding contact interfaces is very difficult due to the sliding movement and the small contact areas involved. In contrast, the laboratory based tribological tests can provide a quick and accurate prediction of sliding interaction of tribological components [19]. Accelerated laboratory wear tests using test machinery are common within the surface engineering research community. Different machinery can be used to understand the tribological behavior of material couples are: pin-on-disc, block-on-ring, micro-abrasion, ballon-plate impact and reciprocating-sliding wear tests [20]. These techniques are capable of providing reliable information to how materials or coatings react under different conditions and material couples used in a wide range of industrial applications include manufacturing, automobile, aerospace, positioning devices, and the like-require very stringent motion control.

In order to improve the efficiency and quality of machining process before resorting to costly and time consuming experimental trials, it is necessary to model and simulate the

metal cutting process by using finite element method (FEM). FEM employs a science-based approach in which the complete machining process can be simulated and optimized in understanding the physical cutting process variables such as, cutting force, cutting temperature, tool wear and to relate the same with practical conditions of machining process. Success and reliability of FE modelling of machining processes are heavily dependent upon the following attributes [21,22]: (i) the workmaterial flow stress model - should reasonably denote elastic, plastic and thermo-mechanical behavior of workmaterial deformations observed during cutting process, (ii) FE model should not require chip separation criteria - continuous remeshing and quality of the mesh is maintained throughout the chip formation, and (iii) friction parameters between the tool and workmaterial interfaces - should be modeled fairly enough to account the forces, stresses and temperature developments.

## **1.2. Motivation and research methodology**

The significance of solid lubricant-based coatings in enhancing process performance in current industrial applications quests for researchers and manufacturers a more sophisticated machining processes and methods being used to produce new and more effective coated cutting tools, which will be able to take sustainability into account as a significant parameter of the machining processes. Literature review emphasized that the concept of electrostatic charging and its importance exist in some industrial applications, to our knowledge, this technology is new in machining applications and the level of detail provided in machining applications is not enough for understanding the benefits of such concept in deposition of micron/nano-sized solid lubricant particles on cutting tools.

To this date, a literature search on the use of electrostatic charging principle in solid lubricant assisted machining yields a scarce amount of work, while to the our knowledge there is no data in the open literature for deposition of electrostatic solid lubricant coatings on

cutting tools, particularly to understand the tribological performance of electrostatic solid lubricant coatings and their machining performance in terms of cutting forces, cutting temperatures, tool wear and surface quality of machined workmaterial. Due to the limited work in the area of electrostatically deposited solid lubricant coated tools that could find use in machining processes, there is a motivation to investigate the electrostatically deposited solid lubricant coatings with a good machining as well as tribological performance.

Therefore, to focus in this direction and look into the feasibility of new coating materials and methods less expensive than the existing deposition techniques and thereby make the machining sustainable, the current research work contributes to the development of novel solid lubricant coated cutting tool, namely, electrostatic micro-solid lubricant (EMSL) coated carbide tool with molybdenum disulfide ( $\text{MoS}_2$ ) as a solid lubricant. To see the ability of coating adhesion to the substrate, coating strength was evaluated with the help of scratch tester by measuring the critical load required to remove the coating from the substrate. The tribological behavior of EMSL coatings in dry sliding conditions is evaluated using ASTM G99 standard pin-on-disc tribological testing method under various sliding speeds and applied loads. Comprehensive machining studies have been carried out in order to judge the performance of developed coated cutting tools during machining process. Further, relative comparison of process performance in terms of cutting temperature, cutting force, chip thickness and shear angle when machining with and without coated tool is presented.

In addition to the above, FE modelling of machining process has been carried out to comprehend the physical cutting process variables such as cutting temperature, cutting force, chip thickness and shear angle and to relate the same with practical conditions when machining with and without coated cutting tools. FE modelling of machining process by taking into account the frictional effects based on the combination of shear friction and

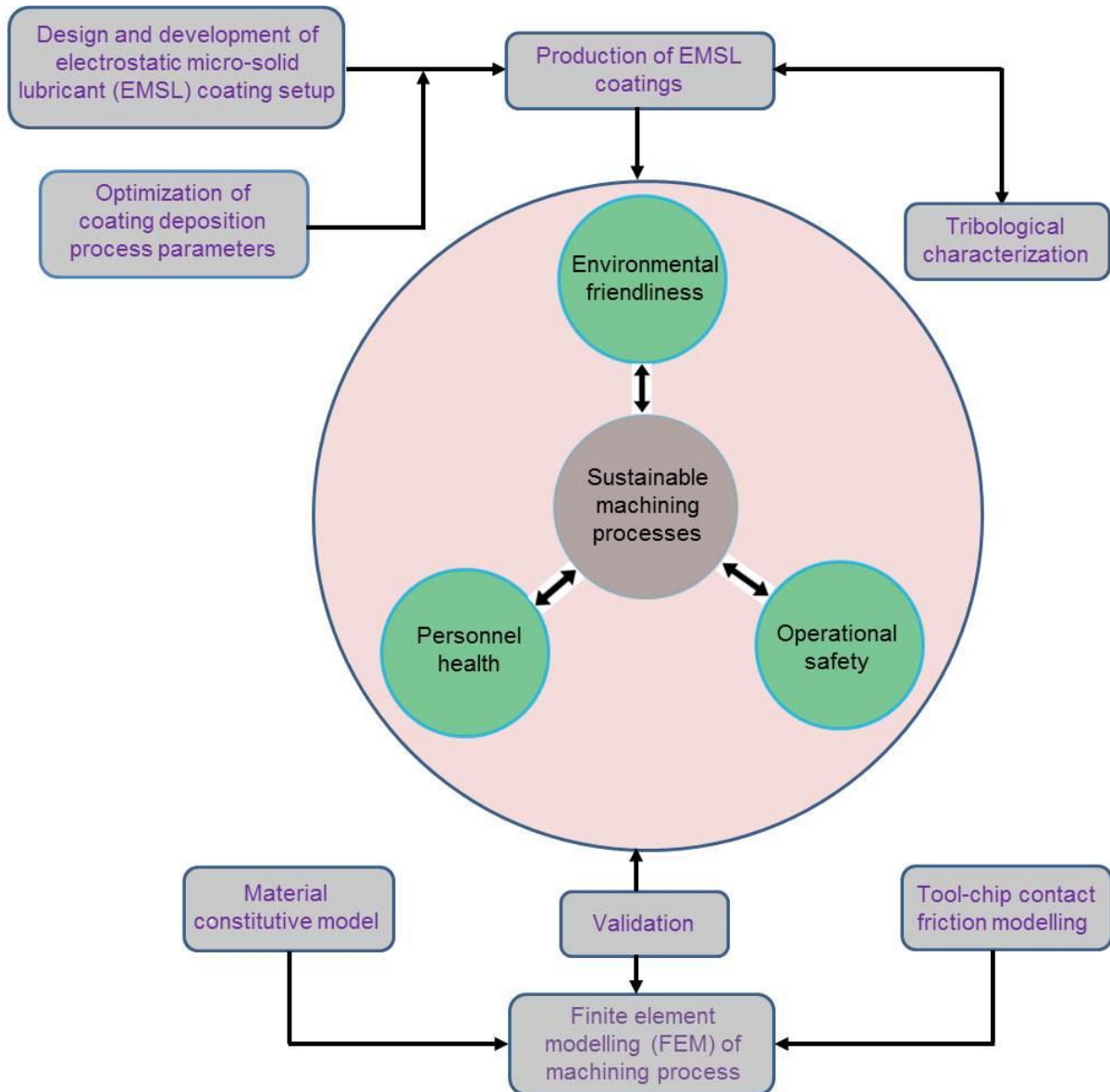
Coulomb friction and material flow behavior by formulated constitutive models was demonstrated with the help of numerical code, DEFORM<sup>TM</sup>.

### **1.3. Aim and scope of the current research**

Applications of cutting fluids improve the machinability and productivity by extending the cutting tool life because of its lubrication and cooling actions. However, due to the hazards posed by cutting fluids to ecology and health of the workers, there is a greater need to identify eco-friendly and user-friendly alternatives for sustainable machining. To realize this, the assistance of solid lubricant as one of the self-lubricating layer/coating on cutting tools in current metal cutting practices has received recent attention because the solid lubricant is a safe, clean and non-toxic that requires no expensive discard and can significantly enhance the machining process performance. Today, surface coating technology makes researches very attractive to use in preparation of solid lubricant coatings on cutting tools and tribological components. Surface coatings made of solid lubricant, exhibit good mechanical and tribological properties in several machining operations. Further, FE based simulations have the potential to provide a platform to design the machining process and virtually test the tool-work interaction and tool geometry selected. In response to input variables, FE simulations can offer very useful information of cutting process variables.

Therefore, the overall objective of this research (Fig. 1.1) is to achieve sustainability in machining system/technology (the quality of the machined part with regard to machined surface integrity and the societal demands, i.e., cleaner, healthier and safer machining) and contribute to the promotion of manufacturing sustainability research. This is through the development of novel electrostatic micro-solid lubricant (EMSL) coated cutting tool serving to meet the main challenge in the industry, i.e., making economical and environmentally compatible lubrication approach for machining as well as tribological operations. Further, the

current research work also aims to present FE modelling of machining process to comprehend the physical cutting process variables such as cutting force, cutting temperature, chip formation and shear angle.



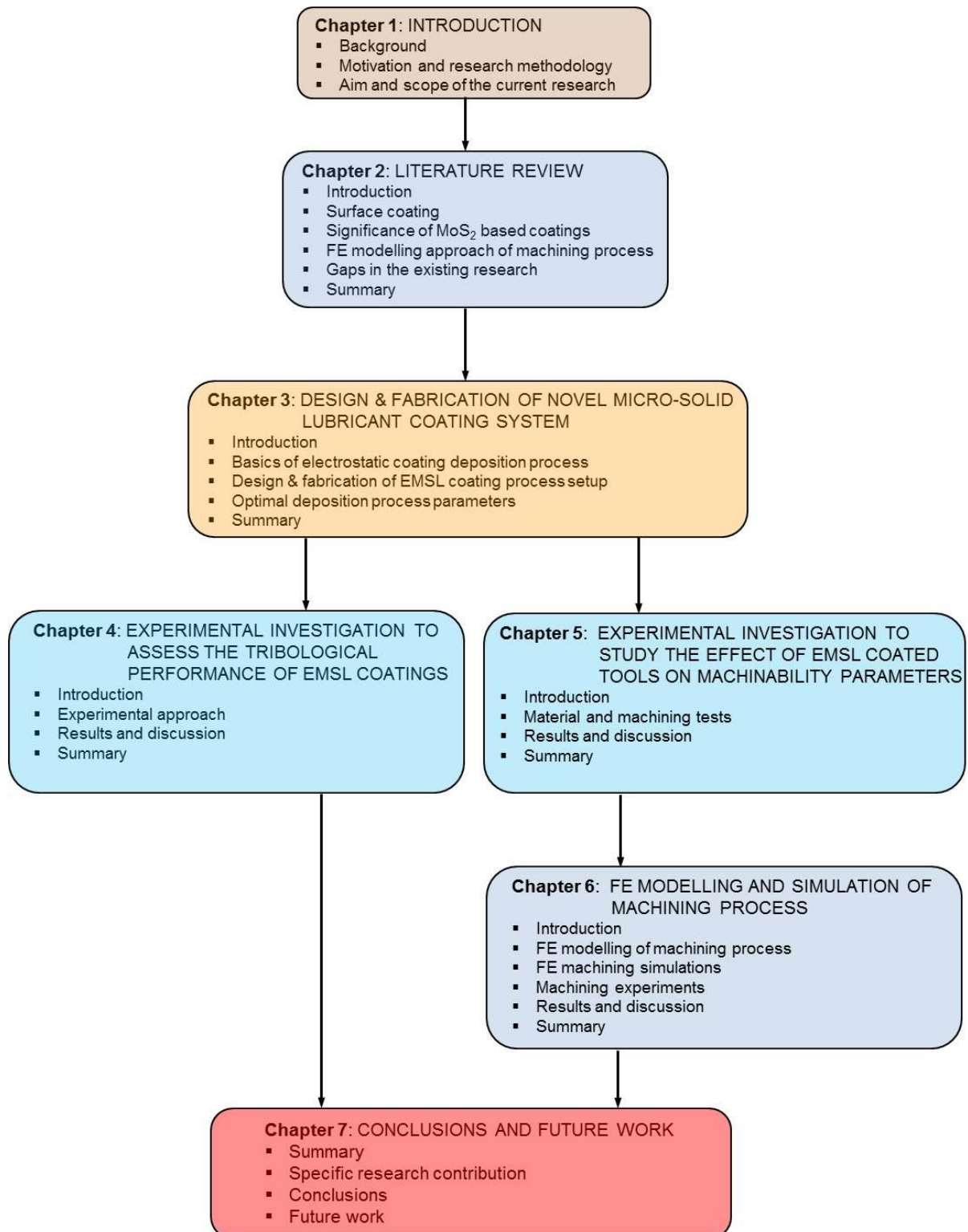
**Fig. 1.1.** The overall objectives of the research work.

The objectives in Fig. 1.1 can be described as follows:

1. To explore the development of low cost in-house surface coating method using electrostatic charging principle to facilitate the production of novel electrostatic micro-solid lubricant coating on cutting tools for sustainable machining process (green machining).
2. To optimize the coating deposition process parameters such as electric potential, solid lubricant feed pressure and distance between electrostatic nozzle tip to substrate from the point of view of coating thickness and comprehend their influence on the coating thickness.
3. To assess and compare the machining process performance of electrostatic micro-solid lubricant coated cutting tools in terms of cutting forces, cutting temperatures, tool wear, chip formation, shear angle and surface roughness of machined workmaterial with the uncoated cutting tools.
4. To characterize the tribological properties (friction and wear) of electrostatic micro-solid lubricant coatings under dry sliding conditions.
5. FE modelling of machining process to comprehend the physical cutting process variables such as cutting force, cutting temperature, chip thickness and shear angle during machining with coated and uncoated cutting tools and have the relative comparison of numerical predictions with experimental findings.

## 1.4. Organization of the dissertation

This dissertation is organized as presented in Fig. 1.2.



**Fig. 1.2.** Organization of the dissertation.

The *first chapter* of this dissertation is about the background of metal cutting processes and possible lubrication approaches, importance of tribology in current industrial practice and FE modeling of machining processes that sets the stage for research objectives and the methodology to be carried out for the current research work.

*Chapter 2* consists of an extensive literature survey from National and International Scientific Journals/Conferences in the area of metal machining operations. The purpose of this chapter is to well understand the background of machining processes in terms of present lubrication approaches, solid lubricant materials and the common coating deposition methods being used to produce solid lubricant coatings and its use in machining and tribological applications. Further, an extensive review of FE modelling of machining process has been carried out. Material constitutive modelling, chip formation process and tool-chip interfacial frictional modelling were discussed. Finally, existing research gaps and a framework that established to attempt in overcoming the existing research gaps were presented.

*Chapter 3* presents the basics of electrostatic coating process and its principle, design and development of experimental process setup to facilitate the production of EMSL coated cutting tools and related infrastructure. This chapter, also deals with the optimization of coating deposition process parameters such as electric potential, solid lubricant feed pressure and distance between nozzle tip to substrate from the point of view of coating thickness.

In *chapter 4*, coating strength of EMSL coatings was evaluated with the help of scratch tester by measuring the critical load required to remove the coating from the substrate. Tribological characterization of EMSL coatings was carried out using pin-on-disc wear testing machine under dry sliding conditions over a wide range of sliding speeds and normal loads. The results in terms of friction, wear volume and specific wear rate were compared with the uncoated tools under the similar operating environment.



The machining performance of EMSL coated cutting tools was discussed in *chapter 5*. A comprehensive experimental investigation and the efficacies of EMSL coated cutting tools in terms of cutting forces, cutting temperatures, tool wear, chip formation, and surface finish of machined workmaterial in comparison with the uncoated cutting tools in machining processes was presented in this chapter.

*Chapter 6* presents the FE evaluation of machining process with and without coated cutting tools and comparison of FE simulated results such as cutting force, cutting temperature, chip thickness and shear angle with the experimental results. FE modelling of machining process by taking into account the frictional effects based on the combination of shear friction and Coulomb friction and material flow behavior by formulated constitutive model, was demonstrated with the help of numerical code, DEFORM<sup>TM</sup>.

Finally, *chapter 7* presents the overall summary of the investigations carried out, specific contribution to the research and the conclusions drawn. It also suggests further recommendations for the future work.

# CHAPTER 2

## LITERATURE REVIEW

---

In previous chapter, the research goal and working approach are addressed. The current chapter consists of an extensive literature survey from highly rated National and International scientific Journals/Conferences on solid lubricants and their application in machining processes, research work done, concepts and methods to achieve proposed research objectives. It begins with the introduction (Section 2.1) by providing existing literature on conventional machining, solid lubricant assisted machining, dry machining and machining with self-lubricant coated tools. Section 2.2 presents the importance of surface coatings, classification of coating deposition methods and self-lubricating coating materials. Section 2.3 reviews the importance of MoS<sub>2</sub> based coatings in machining and tribological applications. Section 2.4 describes the FE modelling of machining process and fundamental aspects of metal cutting simulation with existing modelling approaches such as workmaterial modelling and friction modelling at tool-workmaterial interface. Section 2.5 highlights the existing research gaps in current machining technologies and establishes a framework to carry the current research work in order to overcome the research gaps. Finally, Section 2.6 presents the overall summary of this chapter.

### **2.1. Introduction**

Machining is a process of the removal of excess material from a component in order to impart the required dimension and finish. The importance of the machining process can be appreciated by the fact that nearly every component produced today has one or more machined surface or holes. Research into this field is mainly driven by the need to improve sustainability performance of cutting processes. The challenge of modern machining

industries has to fulfill increasingly high demands with regard to quality of machined workmaterial and productivity with a reduced environmental impact. Such goals are strongly affected by several elements, among them cutting fluid and cutting tool play a very important role in arresting the frictional influences, contact temperatures, tool wear and cutting forces during cutting process and ensuring them do not become unwarranted [23].

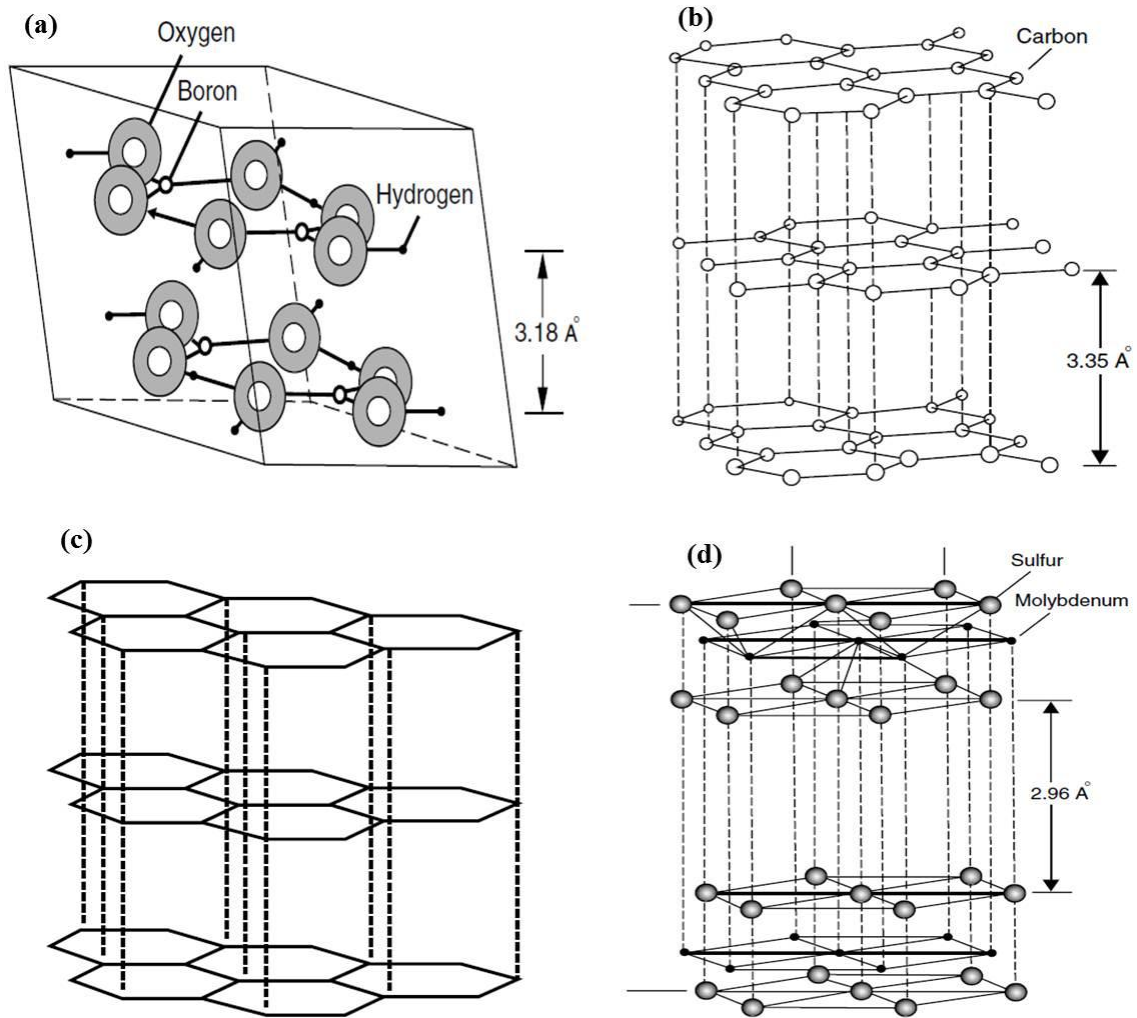
The friction arising during the machining operation and the wear on cutting tool are major loss factors. According to the German Society for Tribology [24], a loss of about 5% of gross social product arises annually in industrialized countries through the effects of friction and wear alone. Since, the cutting fluid application is not biological friendly, as the workers are continuously exposed to cutting fluids, they are mostly under the impact of toxic fluids, which cause severe health harms like genetic diseases, respiratory problems including occupational asthma and hypersensitive pneumonia [3,25], dermatological disorders such as irritation, oil acne and skin cancer [26]. In addition to these biological problems, the inappropriate use of cutting fluids destructs ground water, air, soil, agricultural products and food contaminations because of their toxic effects [5,27]. Further, consuming large quantities of cutting fluids in cutting process leads to not only above problems but also requires storage, disposal and maintenance. Increasing consciousness for green manufacturing globally and consumer focus on environment friendly products has put increased pressure on manufacturers and researchers to eliminate or minimize the use of cutting fluids.

Effective countermeasures without the use of cutting fluid (dry machining) are an important objective in manufacturing industry to control the above effects and reduce the environmental and production costs [28]. Dry machining consumes less power and produces fine surface of the machined workmaterial than conventional machining [29]. The advantages of dry cutting includes: non-pollution of the atmosphere or water; no residue on the swarf which will be reflected in reduced disposal and cleaning costs, no danger to health and

increased tool life by eliminating thermal shocks [28,30]. Dry machining is becoming more and more popular around the world. But, in dry machining, there will be more friction and adhesion between the tool and workpiece. This will result in increased tool wear and hence reduction in tool life. Thus, in reality, they are less effective when higher machining efficiency, better surface finish quality of machined workmaterial and severe cutting conditions are concerned.

Therefore, increasing the productivity in the machining industry through cost reduction by abandonment of the cutting fluid, saving the environment and at the same time improving machining properties is the main concern. In this direction, introduction of solid lubricants alternative to cutting fluids in machining processes is the best possible way of controlling the above said factors, if solid lubricant can be applied properly [31,32]. If the frictional effects at the tool-work interface can be minimized by providing effective lubrication, the heat generated in machining zone can be reduced to some extent [33]. Advancement modern tribology has identified many solid lubricant materials, which can allow minimum frictional effects and control heat generation between tool-work contact surfaces. If suitable lubricant can be successfully applied in the machining zone, it leads to process improvement.

The solid lubricants with a layered crystal structure are boric acid ( $H_3BO_3$ ), graphite, hexagonal boron nitride (HBN) and the transition-metal dichalcogenides  $MX_2$  (where M is molybdenum, tungsten, or niobium, and X is sulfur, selenium, or tellurium) are most commonly used in industrial applications [20]. Fig. 2.1 shows the layered crystal structure of these solid lubricants [34]. Several researchers investigated the possibility of using above solid lubricants in the form of dry powder or its suspension in oils in different applications such as turning [35-39], milling [40,41], drilling [17], grinding [42,43], sliding [44], forming [45], so on in order to reduce the heat generated at the tool-work contact interface.



**Fig. 2.1.** Schematic illustration of layered crystal structures of solid lubricants: **(a)**  $H_3BO_3$ , **(b)** graphite, **(c)** HBN, and **(d)**  $MoS_2$  [34].

Boric acid ( $H_3BO_3$ ) is a soft solid and an environmental friendly substance owes its lubricity primarily to its lamellar triclinic crystal structure (see Fig. 2.1) with closely packed and strongly bonded layers held together by weak Van der Waals forces [45]. Studies report that boric acid is a very promising solid lubricant material in industrial applications because of its relatively high load carrying capacity and low steady state friction coefficient [46,47]. Further, metal working fluids and vegetable oils with boric acid additives has shown very low wear and friction than the commercial fluids [48,49]. Boric acid has also been found to be an

effective lubricant in machining operations since it not only reduces the cutting forces and tool wear but also results in a improved surface finish [38,50]. In one such machining application [51], to control the tool-chip interface temperatures, the possibility of using boric acid mixed with SAE-40 oil as a minimum quantity lubricant is explored. In tribological applications, when combined with a commercial transmission fluid, the boric acid mixture proved to be highly effective in terms of both friction and wear performance. Further, boric acid exhibits the excellent wear behavior and was deemed to be potential natural lubricant alternative in some engineering applications [49]. Apart from these machining and tribological applications, boric acid also found to be a prospective lubricant in metal forming applications when compared with other conventional lubricants [52-54].

Graphite is a prominent solid lubricant used in all the industrial lubrication applications such as in machining, hot and cold forming, wire drawing, high-speed cutting tools and molding process. It is usually assumed that the low friction of graphite is due to the weak bonding between the layer lattice planes giving low shear strength [55]. The influence of graphite in dry powder form [40], mixture with cutting fluids and as a coating material in machining applications was successfully studied by many researchers [56,57]. All the above studies demonstrate that the presence of graphite in machining processes found to be effective in reducing surface roughness of machined workmaterial when compared to machining with cutting fluids. The lower frictional results are due to its hexagonal layer lattice structure (see Fig. 2.1) with weak bonding between the layer lattice planes [58].

Studies have shown that among various types of the soft-layered lamellar solid lubricants, molybdenum disulfide ( $\text{MoS}_2$ ) is the most commonly used solid lubricant in machining as well as tribological applications because it offers very low coefficient of friction, relatively high wear resistance and ability to withstand reasonable loads [59-63]. In terms of tribological characterization, it is worth to mention that the effect of  $\text{MoS}_2$  solid

lubricant on bearing applications have been studied [64] due to its lamellar structure and self-lubricating mechanism. A study [65] on the tribological properties of shaft surfaces were successfully envisaged under different conditions using MoS<sub>2</sub> coatings on shaft surfaces of foil air bearings to prevent wear and reduce friction in an oil-free air craft engine. In addition, the application of MoS<sub>2</sub> solid lubricant in machining operations found to be one of the greatest among several lamellar structured materials due to its ability in controlling frictional effects and taking away the heat generated from machining zone [32,66].

DN Rao et al. [35] has investigated the influence of solid lubricant on machining parameters in turning by supplying solid lubricant in dry powder form to tool-work cutting interface under constant cutting conditions. The substantial reduction in flank wear is observed due to the low coefficient of friction and sliding action. Particles of varying size of graphite and boric acid are employed and it is observed that the 50 µm particle size of boric acid improves the process performance by reducing cutting forces and tool flank wear. The experimental results reveal that the use of the solid lubricant is advantageous with regard to cutting forces, tool wear and surface finish and noticeably superior to machining with conventional cutting fluids and dry machining without presence of solid lubricant. In another study [38], authors investigated the process performance by supply of graphite and boric acid dry powder with mixture of SAE 40 oil to the machining zone. The solid lubricant mixture creates a thin lubricating film on the workpiece and causes reduction of flank wear. Low coefficient of friction, sliding action and low shear resistance within the contact interface are the reasons for reduction of flank wear with solid lubricants.

In order to improve the surface quality of machined workmaterial, Deep et al. [32] introduced MoS<sub>2</sub> in dry powder form at tool-work interface during turning of AISI 1040 steel. The use of solid lubricant has been successful in improving surface quality of workmaterial about 5 to 30% during MoS<sub>2</sub> assisted machining when compared to wet

machining. In addition to this, the improved machinability was observed without affecting the quality of machined workmaterial in solid lubricant assisted machining due to lower frictional characteristics of MoS<sub>2</sub> and effective removal of heat from the cutting zone.

Another study focused on the supply of solid lubricant powder (graphite, MoS<sub>2</sub>) to cutting zone with specially developed experimental setup while machining of AISI 1045 steel [40]. Graphite and MoS<sub>2</sub> assisted end milling process has shown considerable improvement in the process performance as compared to that of machining with cutting fluid in terms of cutting forces, surface quality and specific energy. This work also emphasizes that proper selection of solid lubricant is essential for making it an interesting alternative to eliminate cutting fluids in metal cutting and hence making the machining environmental friendly. In another study, Reddy et al. [17] developed electrostatic solid lubrication setup to supply constant and defined amount of solid lubricant mixture to the machining zone during drilling of AISI 4340 steel. SAE 40 oil is chosen as the mixing medium with graphite solid lubricant. A comparative performance analysis of the novel method of machining with wet and dry machining conditions was conducted. Results demonstrate that the tool life improved dramatically due to the fact that solid lubricant mixture is able to penetrate the chip–tool interface and perform both lubrication and cooling functions satisfactorily.

Shaji et al. [56] investigated the effect of graphite in surface grinding. The results revealed that the lower tangential force and subsequent specific cutting energy are due to lower frictional forces. Further, improvement in surface finish is reported with the application of solid lubricant. During the machining of thoroughly hardened AISI 52100 steel with ceramic inserts by using solid lubricants like graphite and MoS<sub>2</sub>, it was observed that at high cutting speed range, the solid lubricants were more effective [39]. Solid lubricant assisted hard turning produced low value of surface roughness as compared to the dry hard turning. The decrease in surface roughness due to solid lubricants can be attributed to the inherent



lubricating properties of the solid lubricants even at extreme temperatures. This is due to the layered lattice structure of solid lubricants. Also, there is a decrease in surface roughness value by 8 – 10% due to graphite and by 13 – 15% due to MoS<sub>2</sub> solid lubricant. The lower values of surface roughness produced by MoS<sub>2</sub> can be attributed to its strong adhesion as compared to graphite.

Lovell et al. [45] utilized an environmentally friendly lubricant, blend of canola oil and boric acid, as forming lubricant in steel deep drawing operation. A strip tensile friction simulator is employed to evaluate the interfacial friction characteristics. It is reported that the boric acid and canola oil combination had a steady state friction value and it was 54% lower than the unlubricated condition and 44% less than the transmission commercial transmission fluid case. Similarly, surface roughness values of the sheet under this combination of lubrication, were better than that of commercial fluid.

In spite of well accepted fact that the use of lamellar structured solid lubricants alternative to liquid lubricants have come a long way in recent years, literature review emphasized that the questionability on achieving sustainable manufacturing objectives is still remain unsolved. Studies on use of solid lubricants in dry powder form or in oil suspension form in machining processes show benefits in controlling the heat and frictional effects at cutting zone, however, there are still some challenges connected to the use of such lubricants in powder or mixture form as they have an extremely high harmful to the environment due to improper disposal of these used lubricants, leading to health and safety problems. Further, inappropriate use of dry powder at machining contact would navigate micron-sized particles into the atmosphere polluting the working environment. It is thought that a reduction in these problems could be achieved by self-lubricating cutting tools. The possible strategies involved here: (i) dispersing solid lubricants into the tool materials [7], (ii) forming a lubricating oxide film on the tool-chip interface through in-situ reaction by elevated cutting temperature [8,10]

and (iii) isolating the tool from the workpiece with a lubricating layer on the cutting tool face [11,12]. Among these possible strategies, the assistance of solid lubricant as one of the self-lubricating coating material on cutting tools has received recent attention because of its excellent inherent lubricating properties which can control heat generated and frictional effects during machining process [12,16]. In addition to this, solid lubricant coatings are now capable of providing extremely low friction and wear values in tribological applications [67-77]. Thus, surface coating place a vital role in machining as well as tribological operations.

## **2.2. Surface coating**

Surface coating is one of the most efficient way of enhancing the durability of the tools and components used in machining and tribological operations. Selection of coating deposition methods and self-lubricating coating materials plays a significant role as far as improvement of process performance is affected directly. As a result, in the last few years, advancement of surface coating technology opens up the possibility of producing some new coating deposition methods, which gives the possibility of depositing coatings with high performance with respect to hardness, coating strength and low friction coefficients that was previously unattainable [78]. However, with the advancement of surface coating technology, there are several issues. It is very difficult to deposit coatings with all of the desired properties, such as low shear strength, high hardness, good bonding strength, high toughness, etc. because some of them are in conflict with each other. For example, high hardness will sacrifice toughness and bonding strength. Therefore, we need to select the most suitable one from hundreds of thousands of coatings for a specific application. The use of coatings is a very complex situation, and there is no general rule to help the selection of coatings for various tribological applications. However, irrespective of the application whether it is a tribological operation or machining operation, the minimum requirements that are expected

from coatings are: (i) excellent tribological and mechanical properties and (ii) high coating strength.

### **2.2.1. Classification of coating deposition methods**

In the field of surface engineering, coating deposition techniques used for industrial applications rapidly increase since the successful application of decorative coatings [79]. According to Bunshah [14] deposition methods are divided based on the dimensions of the depositing geometry, e.g., whether it is atoms/molecules, particles, liquid droplets or bulk quantities, as shown in Table 2.1.

Though there are many coating deposition methods available (Table 2.1), but not all of them are suitable for tribological applications due to their poor bonding strength, achievable coating thickness, etc. Some of them are developed for electronic, optical or decorative applications. The most commonly used coating deposition methods for tribological and machining applications are as follows: PVD/CVD [12,13], thermal spray [70], flotation process [80], electrochemical deposition [81], bonding [82], etc.

Nowadays, PVD coatings have become an extremely important technological material and are frequently used in machine elements, cutting and forming tools to improve their mechanical properties, tribological behavior and corrosion resistance [83-86]. PVD coatings can provide to achieve nano-structured composite coatings of high hardness above 50 GPa [87]. Evaporation, sputtering and ion plating are the most commonly used PVD techniques for depositing thin film coatings. Typically, PVD process is used to deposit films of elements, alloy materials and composites with film thickness in the range of a few nanometers to several microns [88]. The substrates can range in shape from flat to complex geometries such as watchbands and tool bits. Typical PVD deposition rates are 10-100Å (1-10 nanometers) per second. The limit of PVD process is its achievable coating thickness, usually lower than

10 μm. PVD coatings have been used in many industrial applications, such as aerospace, automotive, surgical/medical, dies and moulds, cutting tools and semiconductors.

**Table 2.1.** Methods of fabricating coatings [14].

<b>Atomistic deposition</b>	<b>Particulate deposition</b>	<b>Bulk coating</b>	<b>Surface modification</b>
<p><b><i>Electrolytic environment</i></b></p> <ul style="list-style-type: none"> <li>- Electroplating</li> <li>- Electroless plating</li> <li>- Fused salt electrolysis</li> <li>- Chemical displacement</li> </ul> <p><b><i>Vacuum environment</i></b></p> <ul style="list-style-type: none"> <li>- Vacuum evaporation</li> <li>- Ion beam deposition</li> <li>- Molecular beam epitaxy</li> </ul> <p><b><i>Plasma environment</i></b></p> <ul style="list-style-type: none"> <li>- Sputter deposition</li> <li>- Activated reactive evaporation</li> <li>- Plasma polymerization</li> <li>- Ion plating</li> </ul> <p><b><i>Chemical vapor environment</i></b></p> <ul style="list-style-type: none"> <li>- Chemical vapor deposition</li> <li>- Reduction</li> <li>- Decomposition</li> <li>- Plasma enhanced</li> <li>- Spray pyrolysis</li> </ul> <p><b><i>Liquid phase epitaxy</i></b></p>	<p><b><i>Thermal spraying</i></b></p> <ul style="list-style-type: none"> <li>- Plasma spraying</li> <li>- D-gun</li> <li>- Flame spraying</li> </ul> <p><b><i>Fusion coatings</i></b></p> <ul style="list-style-type: none"> <li>- Thick film ink</li> <li>- Enameling</li> <li>- Electrophoretic</li> </ul> <p><b><i>Impact plating</i></b></p>	<p><b><i>Wetting process</i></b></p> <ul style="list-style-type: none"> <li>- Painting</li> <li>- Dip coating</li> </ul> <p><b><i>Electrostatic spraying</i></b></p> <ul style="list-style-type: none"> <li>- Printing</li> <li>- Spin coating</li> </ul> <p><b><i>Cladding</i></b></p> <ul style="list-style-type: none"> <li>- Explosive</li> <li>- Roll bonding</li> </ul> <p><b><i>Overlaying</i></b></p> <ul style="list-style-type: none"> <li>- Weld coating</li> </ul>	<p><b><i>Chemical conversion</i></b></p> <ul style="list-style-type: none"> <li>- Electrolytic anodization</li> <li>- Fused salts</li> </ul> <p><b><i>Chemical-liquid</i></b></p> <p><b><i>Chemical vapor</i></b></p> <ul style="list-style-type: none"> <li>- Thermal</li> <li>- Plasma</li> </ul> <p><b><i>Leaching Mechanical</i></b></p> <ul style="list-style-type: none"> <li>- Shot peening</li> </ul> <p><b><i>Thermal surface enrichment</i></b></p> <ul style="list-style-type: none"> <li>- Diffusion from bulk</li> </ul> <p><b><i>Sputtering ion implantation</i></b></p>

CVD process is used to deposit coatings of metals, nonmetallic elements (such as carbon and silicon), compounds (such as carbides, nitrides and oxides), intermetallics, as well as many other materials. The high hardness and strength and superior mechanical properties of

CVD coatings have led to it being used in nuclear, aircraft, missile, defense and machine tooling applications [89-91]. The diamond coated tungsten carbide tools are attractive for cutting processes due to their high hardness, low friction coefficient, excellent wear resistance and chemical inertness [92]. The application of diamond coatings on cemented tungsten carbide (WC-Co) tools was the subject of much attention in recent years in order to improve the cutting performance and cutting tool life. Coatings made with these techniques are relatively thick coatings and are usually in the thickness range of 4 - 20  $\mu\text{m}$ . According to the operating pressure and environment, CVD can be classified as atmospheric pressure CVD (APCVD), low-pressure CVD (LPCVD) and plasma-enhanced CVD (PECVD).

Thermal spraying is a type of a surface engineering method which is widely employed in many industrial applications [93-95]. Recently many kinds of thermal spraying techniques have been developed, such as flame spraying, electric arc spraying, plasma spraying, detonation gun spraying and high-velocity oxy-fuel (HVOF) spraying [96-98]. The materials used in thermal spraying processes are extremely wide, ranging from soft metals to hard metal alloys to refractory ceramics and cermets such as, WC/Co,  $\text{Cr}_3\text{C}_2/\text{NiCr}$ ,  $\text{Cr}_2\text{O}_3$ , and  $\text{Al}_2\text{O}_3$ . Thermal spraying technique is suitable to improve the surface property, i.e. to resist all forms of wear, including abrasion, erosion, and adhesion, but has no significant effect on the substrate [99]. The main disadvantage of thermal spraying process is its line of sight nature, which results that the process is may not suitable for geometrically complex-shaped substrates.

Electrochemical deposition, also called electroplating, is generally used to modify the characteristics of a surface so as to provide enhanced surface performance (e.g. abrasion and wear resistance, corrosion protection, lubricity, etc.) or other desired properties or a combination of them through depositing a layer of material to a surface [100]. There has been a rapid increase in the use of electroplating in manufacturing applications (e.g. surface

finishing, thickness maintaining, avoiding oxidizing, aesthetic, etc.) due to its ability to repair worn parts and to make them rework with a less expensive cost [101]. The selection of the electroplating to suit a particular application is mainly depend upon various parameters/attributes such as handling behavior, finishing, quality, aesthetic, expected service life, time of electroplating, metal substrate, cost, etc. [102].

Bonding is the process in which self-lubricating material particles are mixed into organic or inorganic binding agents, and then the liquid mixture is applied on the substrate surface by immersion, brushing, or spraying, etc. They are commonly used on tribological components, where the contacting surfaces cannot be re-lubricated or liquid lubricants are ineffective and undesirable [82,103]. This use is growing rapidly in space mechanisms and in nuclear power plants, which deemed to have the extreme environments and weight limitations [104]. Among bonded MoS<sub>2</sub>, bonded graphite and bonded PTFE coatings, bonded MoS<sub>2</sub> solid lubricant coating is the most widely used due to its highest load carrying capability with a corresponding low friction coefficient and easy shearing action between contact surfaces [103,105]. Intrinsically, both graphite and MoS<sub>2</sub> have lamellar crystal structure, but the extent of their lubricity and durability is largely depend upon extrinsic factors such as the presence or absence of vapors or gaseous species in the test conditions [34]. Graphite functions best in humid air, while MoS<sub>2</sub> lubricates best in dry and vacuum conditions. In addition, weak Van der Waals interaction between the layers characteristic of MoS<sub>2</sub> and ecological friendliness makes bonded MoS<sub>2</sub> coating one of the most promising self-lubricating material in dry environment.

In practical applications, selecting the appropriate coating deposition method for a given application is still difficult and complicated because the tribological response of a coating system depends on many factors including, coating material, bonding strength, coating mechanical properties, processing temperature, counterpart, substrate, interface and testing

conditions. Further, even if the above said deposition methods can be used in preparation of several solid lubricant coatings, but, there are still some challenges connected to the deposition of micron-sized/nano-sized solid lubricant particles as they have an extremely high surface area to volume ratio, leading to diffusion at high temperatures, often results in aggregates and agglomerates rather than a single primary particle. Also, these deposition methods may not be suitable when depositing on large and complex geometrical surfaces with high deposition rate and coating thickness.

### **2.2.2. Classification of coating materials**

Advancement modern tribology has identified several self-lubricating or solid lubricant materials such as MoS<sub>2</sub>, WS<sub>2</sub>, CaF<sub>2</sub>, graphite, H<sub>3</sub>BO<sub>3</sub>, DLC, HBN, and PTFE, etc., which can allow minimum frictional effects and control heat generation between rubbing surfaces [13]. Table 2.2 lists some of the coating materials based on soft and hard category.

In order to provide the optimum wear protection for rubbing surfaces of tribological components, it is necessary to use a solid lubricant material as one of the self-lubricating coating with low friction and the ability to protect the opposing surface and to provide a transfer film on the opposing surface. Transition metal dichalcogenides such as MoS<sub>2</sub> and WS<sub>2</sub> are among the most available and widely studied self-lubricant materials owing to their excellent lubricity and layered crystal structure [59,106]. The low friction characteristics of these solid lubricant materials have been attributed to their anisotropic hexagonal layered structure with strong covalent bonds between M and X atoms (M = Mo, W; X = S) within a lamella, while adjacent lamella interact through relatively weak Van der Waals forces [107,108]. This feature, MoS<sub>2</sub> basal layer sliding and its weak Van der Waals forces interaction along the 002 plane, makes MoS<sub>2</sub> solid lubricant one of the most promising self-lubricant materials.

**Table 2.2.** Classification of tribological coatings, depending on the nature of the constituting material [13].

<b>Hard coatings</b>	<b>Soft coatings</b>
<i>Nitrides</i> TiN, CrN, ZrN, BN, BaSO <sub>4</sub>	<i>Soft metals</i> Ag, Pb, Au, In, Sn, Cr, Ni, Cu
<i>Carbides</i> TiC, WC, CrC	<i>Lamellar solids</i> MoS <sub>2</sub> , WS <sub>2</sub> , Graphite H <sub>3</sub> BO <sub>3</sub> , HBN, GaS, GaSe
<i>Oxides</i> Al <sub>2</sub> O <sub>3</sub> , Cr <sub>2</sub> O <sub>3</sub> , TiO <sub>2</sub> , ZnO, CdO, Cs <sub>2</sub> O, PbO, Re <sub>2</sub> O <sub>7</sub>	<i>Halides sulfates, sulfur</i> CaF <sub>2</sub> , BaF <sub>2</sub> , PbS, CaSO <sub>4</sub> , BaSO <sub>4</sub>
<i>Borides</i> TiB <sub>2</sub>	<i>Polymers</i> PTFE, PE, Polyimide Polymerlike DLC
<i>DLC &amp; Diamond</i> a-C, ta-C, a-C:H, ta-C:H, CN <sub>x</sub> a-C:X(:H), (nc-) diamond	

DLC = diamondlike carbon

a = amorphous

ta = tetrahedral amorphous

X = a metal

nc = nanocrystalline

PTFE = polytetrafluorethylene

PE = polyethylene

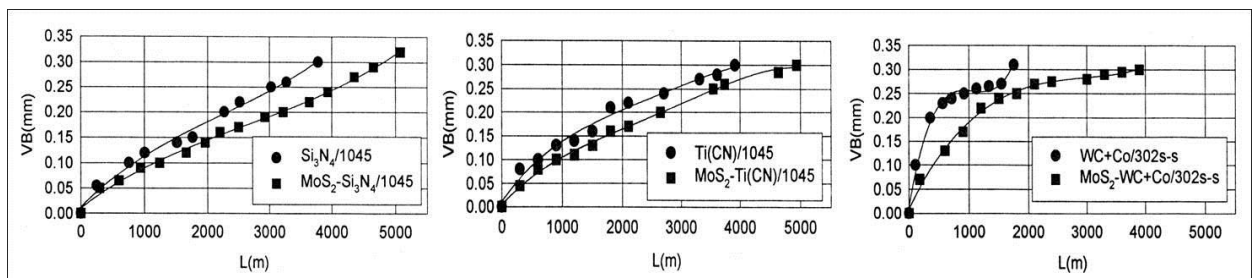
### 2.3. Significance of MoS<sub>2</sub> based coatings

Quite a lot of researchers studied the effectiveness of use of MoS<sub>2</sub> as a solid lubricant in tribological and machining applications and state that the process performance can be improved to a greater extent satisfying the societal demands (cleaner, healthier and safer



machining). All of these studies show a benefit of MoS<sub>2</sub> solid lubricant presence in reducing coefficient of friction and contact temperatures. Such improvement may be attributed to the presence of soft lamella structured MoS<sub>2</sub> solid lubricant and its interaction through weak Van der Waals forces which allows for easy shear to occur at the interface between MoS<sub>2</sub> basal planes.

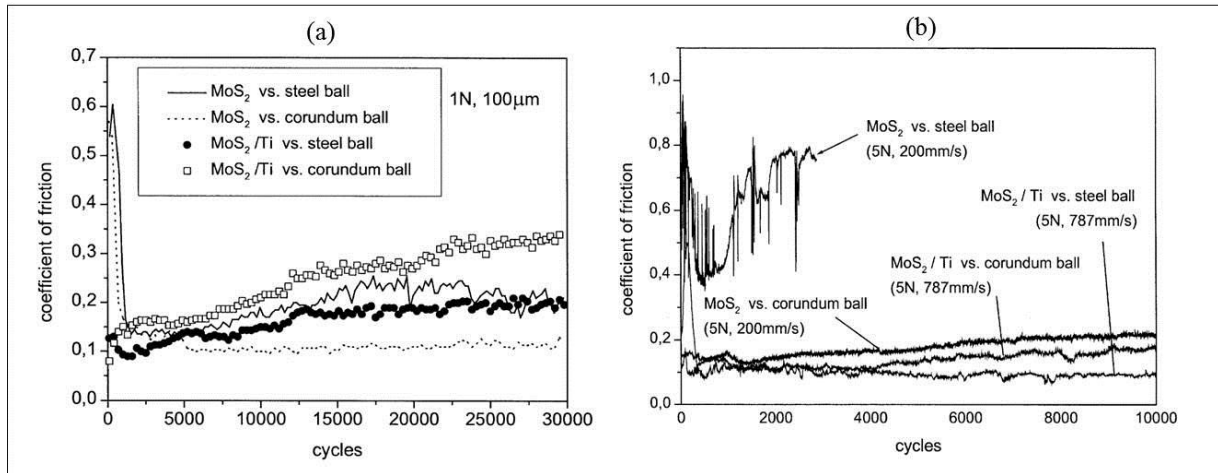
You-Rong Liu et al [12] studied the cutting performance of MoS<sub>2</sub> coated cutting tools and compared the wear resistance and wear life of cutting tools with and without presence of MoS<sub>2</sub> on cutting tools (Fig. 2.2). Results demonstrate that MoS<sub>2</sub> coating extended the tool life when cutting 1045 carbon steel, while MoS<sub>2</sub> coated tools are may not effective in cutting of 302 stainless steel workmaterial due to differences in cutting temperatures and cutting forces. Further, flank wear values of the cutting tools with the coating decrease at all cutting distances with significant increase of tool life. The positive benefits could be due to the existence of MoS<sub>2</sub> coating prevented effectively the adhesion of elements from workpiece to the surface of cutting tool.



**Fig. 2.2.** The life curves of tools with and without MoS<sub>2</sub> [12].

Xiaodong Zhu et al. [72] compared the tribological behavior of sputtered MoS<sub>2</sub> coatings in fretting and pin-on disk tests under different conditions (Fig. 2.3). The coefficient of friction of the MoS<sub>2</sub>/Ti coating is higher than that of the MoS<sub>2</sub> coating when a corundum ball is used, but it is comparable in case of a steel ball. Opposite to the MoS<sub>2</sub> coating, the friction

of MoS<sub>2</sub>/Ti with a steel ball is lower than with a corundum ball. The results show the trend that the wear rate in the fretting test is higher than that in the pin-on-disk test, except the MoS<sub>2</sub> coating tested in pin-on-disk conditions against the steel counterbody.

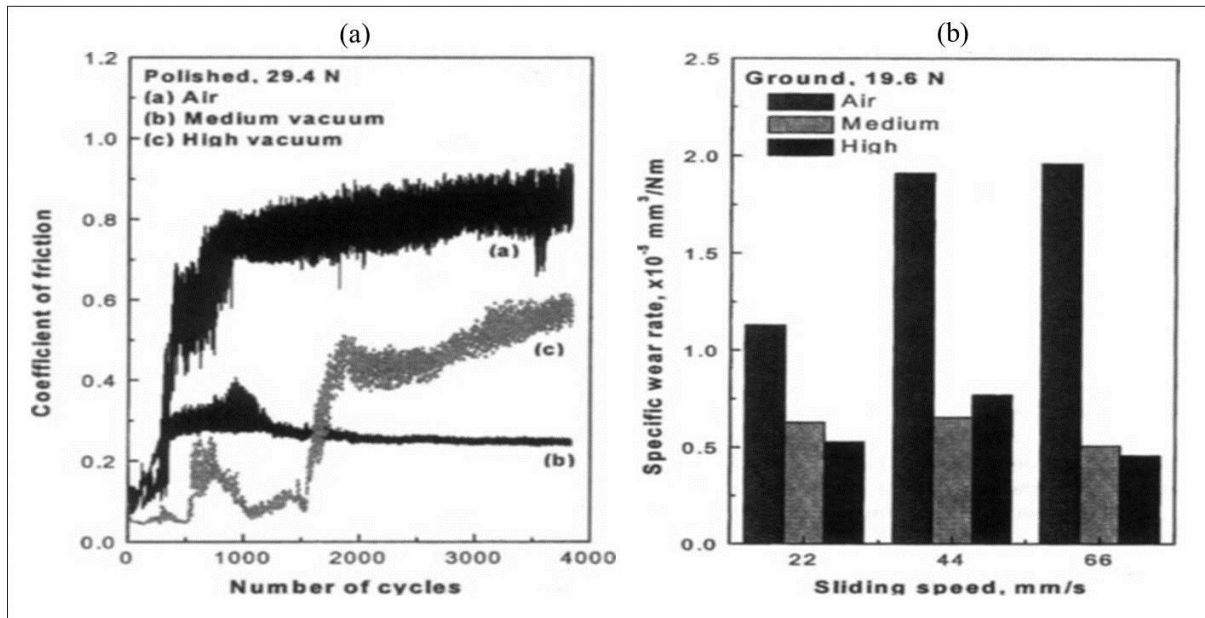


**Fig. 2.3.** Coefficient of friction of MoS<sub>2</sub> and MoS<sub>2</sub>/Ti coatings: (a) in fretting test, and (b) in pin-on-disk test [72].

Singer et al. [73] investigated the tribological performance of triode-sputtered MoS<sub>2</sub> solid lubricant coatings in dry sliding conditions. This study has demonstrated that DC triode sputtered MoS<sub>2</sub> solid lubricant coatings have the same wear and failure modes as burnished or bonded coatings in dry air and dry argon. In all cases, run-in leads to a thinning and compaction of MoS<sub>2</sub> particles, and wear is controlled by the chemical and time dependent (fatigue) mechanical processes. In air, the lifetime of MoS<sub>2</sub> coatings is limited due to oxidation, while the longer lifetime can be seen in argon atmosphere due to the mechanical blister wear mode.

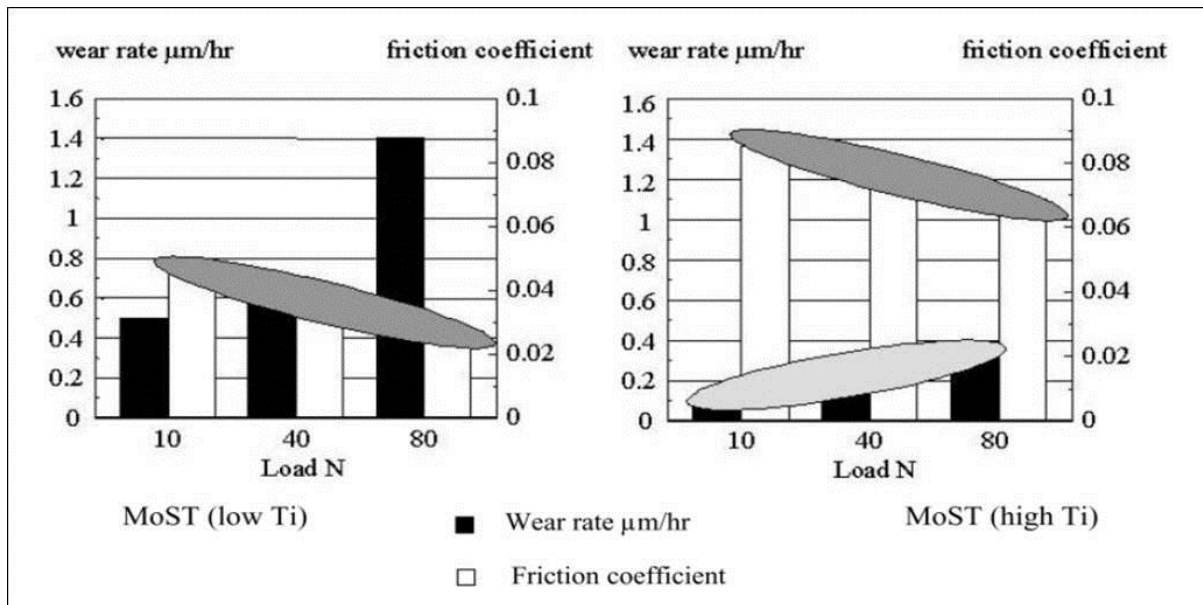
Kim et al. [74] evaluated the friction and wear behaviors of magnetron sputtered MoS<sub>2</sub> solid lubricant coatings in various atmospheric conditions (Fig. 2.4). Results show that the low friction values with MoS<sub>2</sub> coatings was most obvious in high vacuum and the MoS<sub>2</sub>

coatings could not work well as an effective solid lubricant in air due to severe oxidation. Specific wear rate in air was very high but decreased sharply as the environment was changed to high vacuum owing to the inherent low shear strength of MoS<sub>2</sub> coatings and the formation of transfer film.



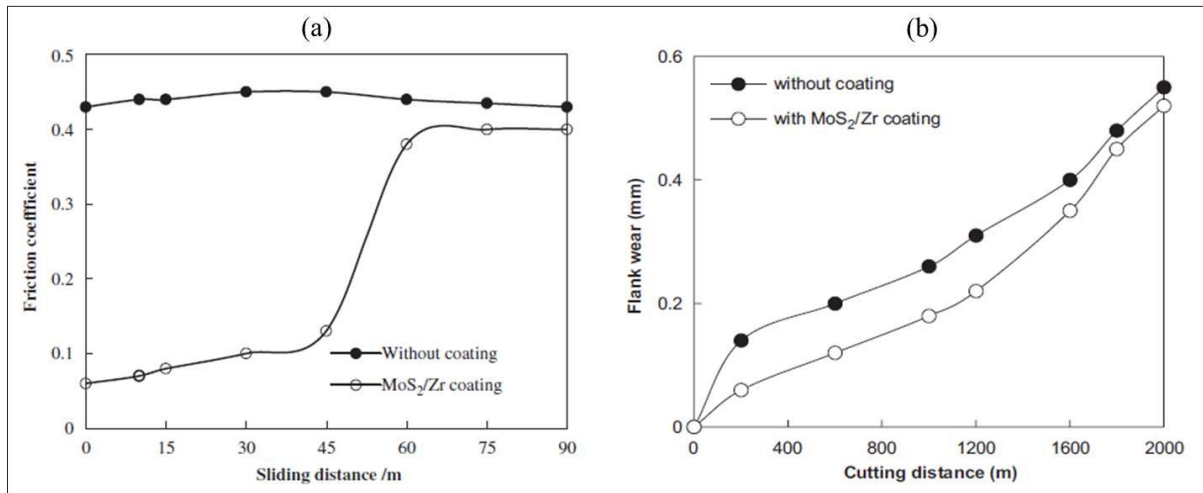
**Fig. 2.4.** (a) Coefficient of friction in different atmospheric conditions at sliding speed of 66 mm/s, and (b) specific wear rate of coatings after 4000 cycles [74].

Renevier et al. [76] developed new metal coatings based on MoS<sub>2</sub> solid lubricant. The coatings have found application in improving the tribological performance of cutting and forming tools, and also make high-speed machining possible (Fig. 2.5). The advantages offered by the use of such solid lubricant based coatings in non-lubricated conditions for many mechanical components have been demonstrated. The MoS<sub>2</sub>/metal coatings act as solid lubricants, providing protection for both the coated surface and any opposing uncoated surface. These coatings retain above desirable properties in humid atmospheres and are suitable for terrestrial applications.



**Fig. 2.5.** Results from pin-on-disc testing at 10, 40 and 80 N loads showing friction coefficient and wear rates for low and high-Ti MoST coatings [76].

Jianxin et al. [77] deposited PVD MoS<sub>2</sub>/Zr composite coatings on the surface of carbide cutting tools by medium-frequency magnetron sputtering together with multi-arc ion plating. MoS<sub>2</sub>/Zr composite coatings onto the cemented carbide tool substrate show higher hardness and better adhesion with the substrate in comparison with the pure MoS<sub>2</sub> solid lubricant coatings. The MoS<sub>2</sub>/Zr composite coatings exhibit decreased friction coefficient to that of the uncoated carbide in sliding wear tests. Cutting speeds were found to have a significant effect on the wear behaviors of MoS<sub>2</sub>/Zr-coated tools. In case of low-speed cutting, the MoS<sub>2</sub>/Zr-coated tools showed much better cutting performance compared to the uncoated cutting tools, the MoS<sub>2</sub>/Zr coating on the tool rake face can be acted as a lubricating additive between the tool–chip sliding couple during machining processes, and contribute to the decrease of the tool wear (Fig. 2.6).



**Fig. 2.6. (a)** Friction coefficient with sliding distance of the specimens when sliding against a hard steel ring at sliding speed of 200 r/min, load of 20 N, and **(b)** Flank wear of the inserts in dry cutting of the hard steel [77].

Solid lubricants in the form of bonded coatings are used in a wide variety of applications than those in any other forms, for example, burnishing, sputtering, ion deposition, and mechanical impingement. Bonded films of MoS<sub>2</sub> generally have better friction and wear characteristics than bonded films of other solid lubricants [109]. There have been some investigations [103,105,110,111] concerning the performance of bonded coatings under fretting conditions. All these studies show that the application of bonded coatings can efficiently improve wear-resistant performance. Due to excellent combination of wear life and friction, bonded films of MoS<sub>2</sub> are used in many industrial, automotive applications, space mechanisms and in nuclear power plants where extreme environments and weight limitations are encountered [104].

## 2.4. Finite element (FE) modelling approach of machining process

Cutting operations are performed to modify shape, dimension and achieve desired surface finish of engineering components. Theory of deformation process causing chip

formation and tribological aspects of tool–chip contact and very high rates of plastic deformation in cutting operation are quite complex as it involves material, physical and thermo-mechanical issues. Clear understanding of physical phenomenon of cutting process needs a simplified machining model. In the recent years, FE based modeling and simulation of cutting operations is continuously attracting researchers for better understanding the chip formation mechanisms [112,113], heat generation in cutting zones [114-116], tool-chip interfacial frictional characteristics and integrity on the machined surfaces [117-120]. Predictions of the physical parameters such as, cutting force, cutting temperature, chip formation, stresses, etc. accurately play a pivotal role for predictive process engineering of machining processes. Therefore, FEM tool can help in modelling metal cutting process to understand the cutting conditions, tool wear mechanisms, tool-chip temperature, residual stresses, etc., which cannot be measured directly. The mainly simulated cutting types include turning, milling, drilling and microscopic cutting of single abrasive grain in grinding.

Orthogonal cutting or two dimensional cutting is the most frequently simulated cutting type. Usui and Shirakashi [121] proposed the first two dimensional FE cutting simulation by using a special method of computation called the iterative convergence method to obtain solutions for steady state cutting. Later, several researchers [122-124], introduced two dimensional and three dimensional FE techniques to machining processes to investigate the chip geometry, residual stresses in the machined surface, temperature distributions in the chip, cutting forces, etc. Orthogonal cutting is a restrictive approach from an industrial point of view, but it is considered accurate enough to make a sensitivity analysis in order to validate numerical results [125-127]. Furthermore, it reduces significantly the computational time [128,129].

In modelling and simulation of machining process, the choice of FEM package is very important because different packages have different capabilities and it is critical to select the

package with the appropriate feature set. The most common commercial FE codes used in machining simulation are: DEFORM<sup>TM</sup>, Abaqus<sup>TM</sup>, FORGE<sup>R</sup>, LS DYNA<sup>TM</sup> and AdvantEdge<sup>TM</sup>, etc. Irrespective of these FE codes, success and reliability of numerical simulation of cutting process are heavily dependent upon the following attributes [22,130-132]: (i) the workmaterial flow stress model should reasonably denote elastic, plastic and thermo-mechanical behavior of workmaterial deformations observed during cutting process, (ii) FE model should not require chip separation criteria- continuous remeshing and quality of the mesh is maintained throughout the chip formation, and (iii) friction parameters between the tool and workmaterial interfaces should be modeled fairly enough to account the forces, stresses and temperatures developments.

#### **2.4.1. Modelling of chip formation process**

Chip formation and heat transfer analysis are the essential phenomenon in the cutting process. It is the basic of the cutting process simulation to predict process variables like, cutting force, cutting temperature, tool wear, chip curling and chip breakage. In fact, there is no general predictive chip formation model, because the physical phenomena associated with the cutting process are extremely complex [133]. Chip formation and separation from the workpiece is one of the main concerns in simulation which was first attempted by Strenkowski and Carroll [134]. A comparison of different conditions used in FE modeling has been reported by Bil et al. [135], who used commercial implicit FE codes MSC. Marc, DEFORM 2D and the explicit code ThirdWave AdvantEdge to study the chip formation, effect of friction and material data. Further, compared to empirical and analytical methods, FE methods used in the analysis of chip formation has advantages in several aspects [136-139]: (i) workmaterial properties can be handled as functions of strain, strain rate and temperature, (ii) the frictional interaction between the tool rake face and chip can be

modelled as sticking and sliding, (iii) non-linear geometric boundaries such as the free surface of the chip can be represented and used, and (iv) in addition to the global variables such as cutting force, feed force and chip geometry, the local stress, temperature distributions, etc. can also be obtained.

#### **2.4.2. Material constitutive modelling**

Material constitutive model is highly essential for the FE analysis of metal cutting simulation to denote elastic, plastic and thermo-mechanical behavior of workmaterial under various strain rate deformation conditions. Several researchers are making efforts to establish such material constitutive models for different workpiece materials through experimental, analytical or simulation methods [140-142]. Success and reliability of numerical models are heavily dependent upon how accurately the thermal-mechanical behavior of the material is being represented by the constitutive equations [143,144].

There have been many developments exists in the open literature in constitutive modelling on a wide variety of engineering materials, including stainless steel, carbon and alloy steels, aluminum alloys with different chemical compositions and heat treatment conditions, magnesium alloys, copper and copper alloys, iron, nickel, titanium, and tungsten alloys [140,145]. These studies present flow behavior of workmaterial against different process parameters through the empirical, semi empirical and physically based constitutive models. The common constitutive models include, Johnson-Cook (JC) model [145], Oxley model [146], Zerilli-Armstrong model [147], and Maekawa et al. models [148]. Every constitutive model has its distinctive advantages and its own application area, but, not all of them are suitable for all cases, due to their applicability range, working domain, accuracy needed, computational time required and the amount of data required to evaluate the material constants, etc. Due to its simplicity and less number of material constants, JC model is one of



the most widely used in a wide variety of areas, such as applied mechanics, engineering materials, machining and in all other manufacturing processes and a benchmark for comparison of different models.

### 2.4.3. Tool-chip interfacial friction modelling

In metal cutting process, friction between chip and tool contact interface determines not only the cutting power and machining quality, but also plays a significant role on important process variables such as cutting temperatures, cutting forces, tool wear, etc. [131,143]. According to Zorev model [149], in cutting process, along the tool-chip contact area near the cutting edge a sticking region forms and frictional shear stress, ' $\tau$ ' (N/mm<sup>2</sup>), can be determined using Eq.2.1 and over the remainder of the tool-chip contact area (Eq.2.2) a sliding region forms and the frictional stress can be determined using a coefficient of friction ( $\mu$ ) as illustrated in Fig. 2.7.

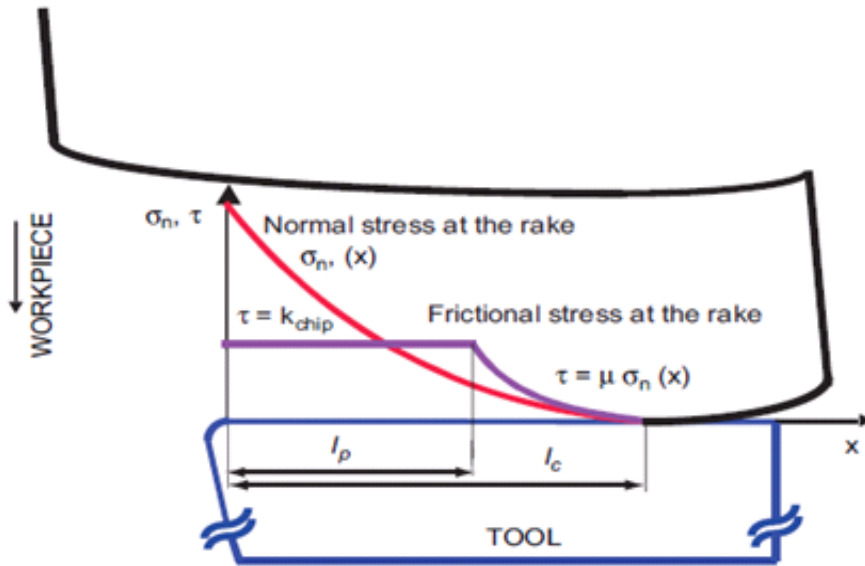
$$\tau(x) = k_{chip} \quad (2.1)$$

when  $\mu \sigma_n(x) \geq m k$  and  $0 < x \leq l_p$

$$\tau = \mu \sigma_n(x) \quad (2.2)$$

when  $\mu \sigma_n(x) < m k$  and  $l_p < x \leq l_c$

where, ' $k_{chip}$ ' is the average shear flow stress at tool-chip interface in the chip (N/mm<sup>2</sup>), ' $\sigma_n$ ' is the normal stress distribution over the rake face (N/mm<sup>2</sup>), ' $m$ ' is the shear friction factor, ' $l_p$ ' is the length of the sticking region (mm) and ' $l_c$ ' is the chip-tool contact length (mm).



**Fig. 2.7.** Stress distribution on tool-chip interface [149].

In the FE modelling of metal cutting processes, several approaches are used in the modelling of friction. Constant coefficient of friction based on Coulomb's friction law is used in most cases. From the assumptions of orthogonal cutting force as explained by Merchant's force circle approach [150], the coefficient of friction ( $\mu$ ) as the function of the forces is represented with Eq.2.3.

$$\mu = \frac{F_f + F_c \tan \gamma}{F_c - F_f \tan \gamma} \quad (2.3)$$

where, ' $F_c$ ' is the cutting force (N), ' $F_f$ ' is the feed force (N) and ' $\gamma$ ' is the tool rake angle.

Ng et al. [151] performed orthogonal cutting tests under different cutting conditions to establish a linear relation between the coefficient of friction ' $\mu$ ', cutting speed ' $v_c$ ' (m/min), rake angle ' $\gamma$ ', and feed ' $f$ ' (mm/rev), given by Eq.2.4, by using regression analysis.

$$\mu = 1.034 - 0.00446 \gamma - 3.888 f - 0.0002 v_c \quad (2.4)$$

Filice et al. [131], investigated the effectiveness of the most friction models such as simple Coulomb's law, constant shear model, Zorev, Usui and Childs model in comparing with numerical predictions with experimental measurements, namely cutting forces, contact length, chip thickness and shear angle. Results indicate that apart from small differences, the main mechanical results (i.e. forces, contact length and so on) are practically not sensitive to friction model.

Based on Zorev's model, Usui et al. [152,153] derived an empirical stress characteristic relation (Eq.2.5) as a friction model, which relates the different stresses at tool-chip interface.

$$\tau = k \left[ 1 - e^{-\left(\frac{\mu \sigma_n}{k}\right)} \right] \quad (2.5)$$

where, ' $\tau$ ' is frictional shear stress (N/mm<sup>2</sup>), ' $\sigma_n$ ' is the normal stress (N/mm<sup>2</sup>), ' $k$ ' is the shear flow stress of the workpiece material (N/mm<sup>2</sup>) and ' $\mu$ ' is the friction coefficient experimentally obtained for different workpiece-tool material combination.

Childs et al. [154] modified the above model to by multiplying shear flow stress of the workpiece ' $k$ ' with a friction factor ' $m$ ', as represented by Eq.2.6.

$$\tau = m k \left[ 1 - e^{-\left(\frac{\mu \sigma_n}{m k}\right)} \right] \quad (2.6)$$

where  $0 < m < 1$

In order to let the high frictional stresses in the sticking zone be other than the shear strength, ' $k$ ', Childs et al. [155,156] made a further modification to this model by introducing an exponent ' $n$ ', as represented by Eq.2.7.

$$\tau = m k [1 - \exp(-(\frac{\mu \sigma_n}{m k})^n)]^{1/n} \quad (2.7)$$

where, ‘ $m$ ’ and ‘ $n$ ’ are correction factors. ‘ $m$ ’ ensures that at high normal stresses, the friction stress does not exceed the shear flow stress of the material, namely that if  $\sigma_n \rightarrow \infty$ , then  $T_f \rightarrow mk$ , and ‘ $n$ ’ controls the transition from the sticking to the sliding region.

Though researchers explored above friction modelling techniques in several machining studies, but, implementation of such models into FE cutting simulations is still not exploited as evident from the many studies reporting uses of a mean friction coefficient. Further, friction with stick-slip behavior is vastly ignored in FE cutting simulations due to unavailability of such friction models in most commercially available FE codes [130]. On the other hand, in most studies [131,157], friction models were carried out comparing the numerical predictions with experimental measurements, such as cutting force, chip contact length, chip thickness, chip-tool rake contact temperature and shear angle.

## 2.5. Gaps in the existing research

The literature study from highly rated National and International scientific Journals/Conferences in the area of solid lubricant assistance machining, surface coating, coating deposition methods, coating materials, MoS<sub>2</sub> based coatings in tribological and machining applications and FE modelling of machining process and state of the art development in research to achieve proposed objectives establishes a framework for carrying this research work. The literature review summarizes the key gaps as follows.

1. Consuming large quantities of cutting fluids in metal cutting process leads to not only environmental problems but also requires storage, disposal and maintenance. In addition, cutting fluid related costs and health concerns associated with exposure to

cutting fluid mist and a growing desire to achieve environmental sustainability in manufacturing have caused industry and academia to re-examine the role of cutting fluids and quantify their benefits.

2. The supply of solid lubricants in dry powder form or its mixture with cutting fluids to tool-workpiece interface alternative to cutting fluids have come a long way in recent years, literature review emphasized that the questionability on achieving sustainable machining objectives is still remain unsolved. Studies on the use of solid lubricants in dry powder form or in oil suspension form in machining processes show benefits in controlling the heat and frictional effects on machining zone, however, there are still some risks connected to the use of solid lubricants in powder or mixture form as they lead to environment, health and safety problems when mixed with atmosphere.
3. Literature review on coating deposition methods reveal that each deposition process shows its own advantages and disadvantages. In actual applications, it is difficult for a single deposition process to meet the desired levels such as bonding strength, deposition rate, substrate temperature, achievable coating thickness, cost, etc. Though, PVD, CVD and their combination techniques able to produce coatings being used for industrial components, but, there are still some challenges connected to the deposition of micron-size/nano-size particles as they have an extremely high surface area to volume ratio, leading to diffusion at high temperatures, often results in aggregates and agglomerates rather than a single primary particle.
4. Literature survey indicates that in spite of well accepted fact that electrostatic charging principle is very effective in depositing powder coatings on several engineering parts as well as on parts used for domestic purpose, but, this principle is new in machining applications and hardly any efforts are put to explore the potential

of electrostatic charging principle especially in deposition of self-lubricating materials on cutting tools.

5. The complexity in accounting the flow behavior of the workmaterial and friction between tool-chip in the FE modeling and simulation of cutting process strongly affects the machining process performance. This could be one of the reasons that the numerical values differ from the experimental values.

The above research gaps motivates the researchers and manufacturers quest for a more sophisticated machining processes and methods being used to produce new and more effective cutting tools, which will be able to take sustainability into account as a significant parameter of the machining processes. In this direction, the current research work contributes to the development of first-ever solid lubricant coated cutting tool, namely, electrostatic micro-solid lubricant (EMSL) coated carbide tool with molybdenum disulfide as a solid lubricant. To assess the coating strength of EMSL coating, scratch testing is conducted on the coated surface using ASTM standard commercial scratch tester. In order to evaluate the tribological performance of EMSL coated tools and comprehend its influence in dry sliding conditions, tribological tests were carried out using pin-on-disc wear and friction tribometer. Friction coefficient, wear volume and wear rate of coated specimen were compared with that of uncoated tools. To support in understanding the wear mechanisms of contact surfaces with and without the presence of solid lubricant, worn surfaces were examined using scanning electron microscopy and optical microscopy. To distinguish the effectiveness of EMSL coated tools on the machining performance, the results in terms of cutting force, cutting temperature, chip formation, shear angle and surface quality of machined workmaterial obtained during machining of workmaterial with EMSL coated tools were compared with those results found in machining with uncoated tools. Further, to identify the wear

mechanisms of worn surfaces, microscopic examinations were conducted. In addition, FE modelling of machining process has been carried out to comprehend the physical cutting process variables such as cutting temperature, cutting forces, chip thickness and shear angle and to relate the same with practical conditions when machining with and without coated cutting tools. FE modelling of machining process by taking into account the frictional effects based on combination of shear friction and Coulomb friction and material flow behavior by formulated constitutive model was demonstrated with the help of numerical code, DEFORM™.

## **2.6. Summary**

Comprehensive literature review on machining processes and typical lubrication approaches used in machining operations is presented. The literature review has provided an insight into the performance of different solid lubricant materials and how and where their use is appropriate. Several strategies in using solid lubricants in machining operations are explored. Among all strategies, the assistance of solid lubricant as one of the self-lubricating alternative materials on cutting tools in current metal cutting practices has received recent attention. The importance of the surface engineering in preparation of self-lubricating coatings is highlighted. The review has provided a clear understanding on most commonly used self-lubricating coating materials and coating deposition methods commonly used in tribological and machining applications. Among different solid lubricant materials highlighted in the review, MoS<sub>2</sub> is the most widely used solid lubricant due to its highest load carrying capability with a corresponding low friction coefficient and easy shearing action between contact surfaces. An understanding of the importance of MoS<sub>2</sub> based coatings for tribological as well as machining applications and their effect on process performance has also been gained. Further, FE modelling and fundamental aspects of metal cutting simulations

with existing constitutive material models and tool-chip contact friction modelling were discussed. The literature review provides the specific issues for future investigation within the focused areas, including research gaps in the evidence and promising areas for current research work provided a platform from which to develop a sustainable machining technology. Finally, the literature review on the state of the art developments in research identifies and summarizes the research gaps and thereby highlighting a framework to carry the current work in order to overcome the existing research gaps.



# **CHAPTER 3**

## **DESIGN & FABRICATION OF NOVEL MICRO-SOLID LUBRICANT COATING SYSTEM**

---

The set objective of current research and impetus to overcome the research gaps in the existing literature (see chapter 2) establishes a framework to design and fabricate a novel coating technology to facilitate the deposition of solid lubricant coating on cutting tools for sustainable machining (green machining). To realize this objective, the current research work introduces a novel coating deposition technique, namely, electrostatic micro-solid lubricant (EMSL) coating system. This chapter is organized as follows: Section 3.1 presents the brief information about electrostatic coating history and its application. Section 3.2 explains the basics of electrostatic principle used in powder coating deposition. In Section 3.3, design and development of EMSL coating experimental setup is presented. Section 3.4 presents the selection of optimal process parameters used in coating deposition experiments. Finally, Section 3.5 presents the overall summary of this chapter.

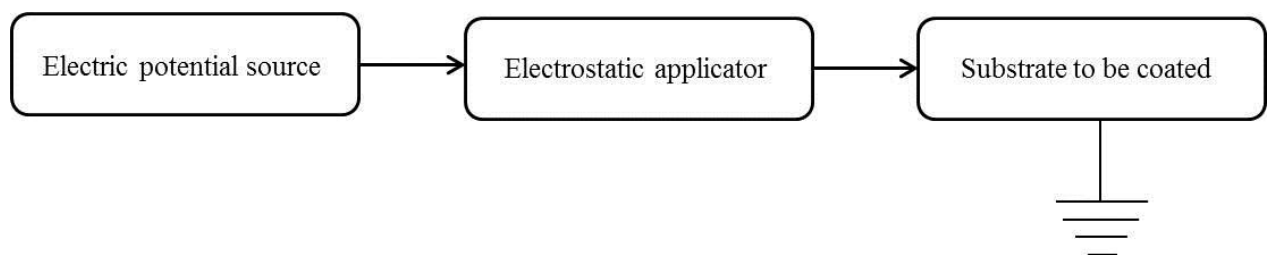
### **3.1. Introduction**

Electrostatic coating deposition process is widely used method in powder coating industry for applying polymer coatings either to protect the surface or promote aesthetics. Electrostatic charging in industrial coating applications was first introduced to the finishing industry in Europe countries in early 1950s. It complemented the existing electrostatic powder coating industry but offered important advantages, especially, the powder coating process did not utilize solvents and so was attractive from the environmental point of view as over sprayed powder particle could, in principle, be collected and recycled so that product utilization could approach 100% [158]. Nowadays, the concept of electrostatic charging

principle exist almost in all powder coating industries for applying coatings on several engineering parts as well as on parts used for domestic purpose, for example, washer tops and lids, dryer drums, electrical panels, water heaters, refrigerator panels, racks and cavities of microwave ovens, etc.

### 3.2. Basics of electrostatic coating deposition process

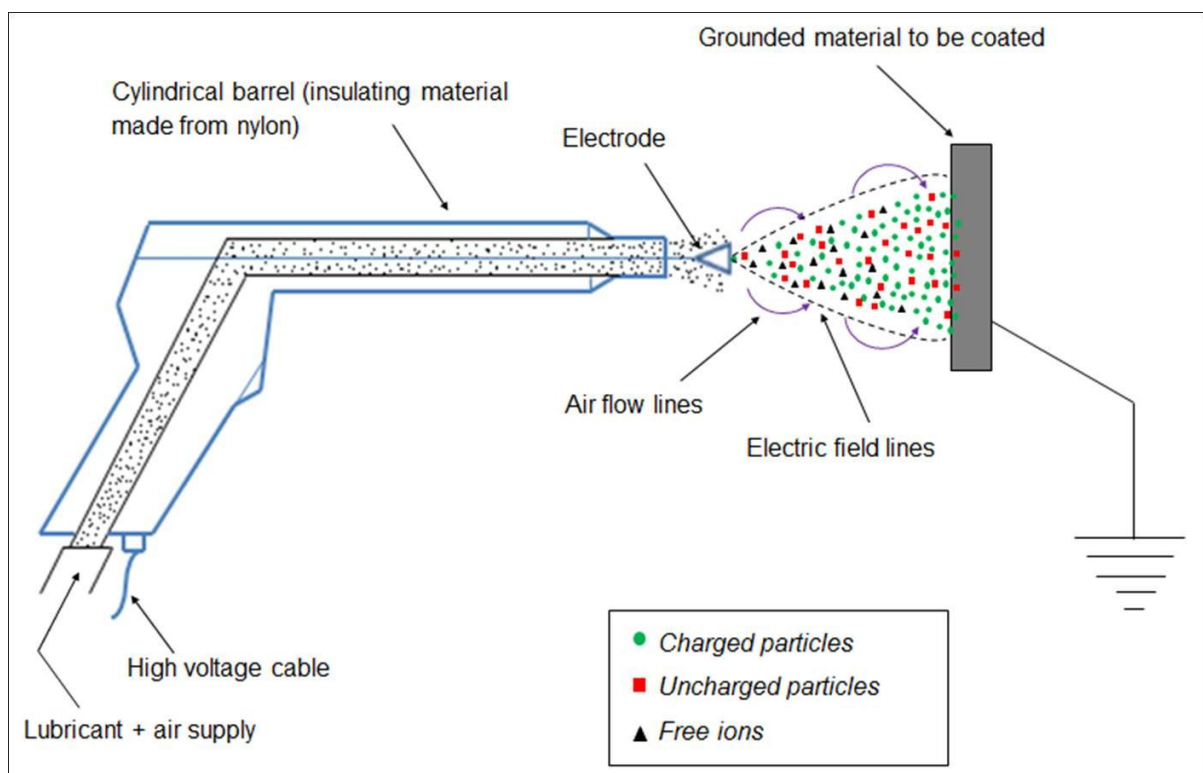
Triboelectric and corona charging are two methods widely used in commercial electrostatic powder coating system. In the triboelectric charging, fluidized powder is carried vigorously through the barrel, which consists of a carefully chosen material to maximize triboelectric charging, and then emerges charged and is pushed towards the workpiece to be coated. The alternative and more common method in electrostatic powder coating is the process of corona charging (principle of low amperage field) [158], which is comprised of three main components (Fig. 3.1), charges powder particles by ensuring that they pass through a corona discharge in the powder exit region.



**Fig. 3.1.** The most common components of electrostatic coating equipment.

The schematic procedure of electrostatic charging principle by using corona charging in deposition of powder coatings is explained in Fig. 3.2. In corona charging system, a cylindrical barrel at the end of which is one or more sharply pointed electrodes held at a very high negative potential, requiring a power supply rated from 0 - 100 kV. The process

disperses finely ground powder into an air stream, producing a cloud as it exits the nozzle. The particles pass through a highly charged and ionized corona field at the nozzle tip applying a strong negative charge to each particle. This process can apply coatings between one to several hundred microns in thickness. The electric field lines shown are said to describe both the trajectories of charged particles and the way in which coating of the area, of the workpiece becomes possible as a result of wrap-around.



**Fig. 3.2.** Schematic of experimental process used in corona charging EMSL coating deposition system.

The movement of ions onto the surface will cease when the potential of the particle equals that of its surroundings. An electric field, 'E', will be created as a result of this surface charge, and will be the field at the interface between the particle and its surroundings. In electrostatically deposited coatings, the process of particle surface charging in the electric

field of corona discharge is governed by Pauthenier's Eq.3.1 [158]. With continued increase in charge collection, 'E' will increase until a value is reached which corresponds to a situation where no further transport of ions onto the particle will be possible. If particles are exposed to field charging for a time 't' significantly greater than the charging time constant 'τ' then, this limit, the Pauthenier limit, is given by Eq.3.2.

$$q = A \varepsilon_o \left[ 1 + 2 \left( \frac{\varepsilon_r - 1}{\varepsilon_r + 2} \right) \right] E \frac{t}{(t + \tau)} \quad (3.1)$$

$$q = A \varepsilon_o \left[ 1 + 2 \left( \frac{\varepsilon_r - 1}{\varepsilon_r + 2} \right) \right] E \quad (3.2)$$

The ability of particle surface charging depends on the term  $\left( \frac{\varepsilon_r - 1}{\varepsilon_r + 2} \right)$ , which for particles of 'ε<sub>r</sub>' >> 1, i.e. metallic particles, the surface charging on particle defined by the Pauthenier limit is expressed with Eq.3.3.

$$q_{max} = 12 \pi r^2 \varepsilon_o E \quad (3.3)$$

where,

*q* is the charging acquired by the particle (Coulombs)

*A* is the surface area of the particle (mm<sup>2</sup>)

ε<sub>o</sub> is the permittivity of the free space (Coulomb/Volts)

ε<sub>r</sub> is the ratio of the permittivities of particles to that of free space (Coulomb/Volts)

*E* is the strength of the electric field (Newtons/Coulomb)

*r* is the radius of the particle (μm)

*m* is the mass of the particle (g)

ρ is the density of the particle (g/cc)

In electrostatic charging deposition process, the amount of surface charge acquired by the powder particles not only determines their trajectories but also their adherence tendency to the metal substrate [159,160]. The studies explained that the particle adherence tendency is the function of the mean surface charge to mass ratio ( $\frac{q_{max}}{m}$ ) of the particles (Eq.3.4).

$$\frac{q_{max}}{m} = \frac{12 \pi r^2 \epsilon_0 E}{\left(\frac{4}{3}\right) \pi r^3 \rho} \quad (3.4)$$

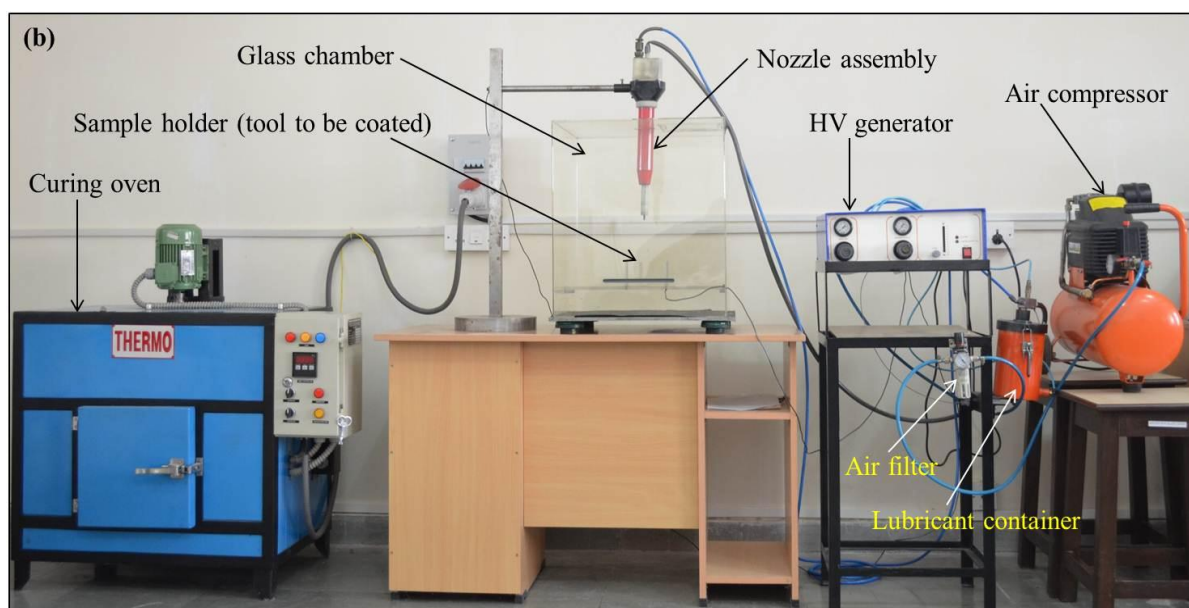
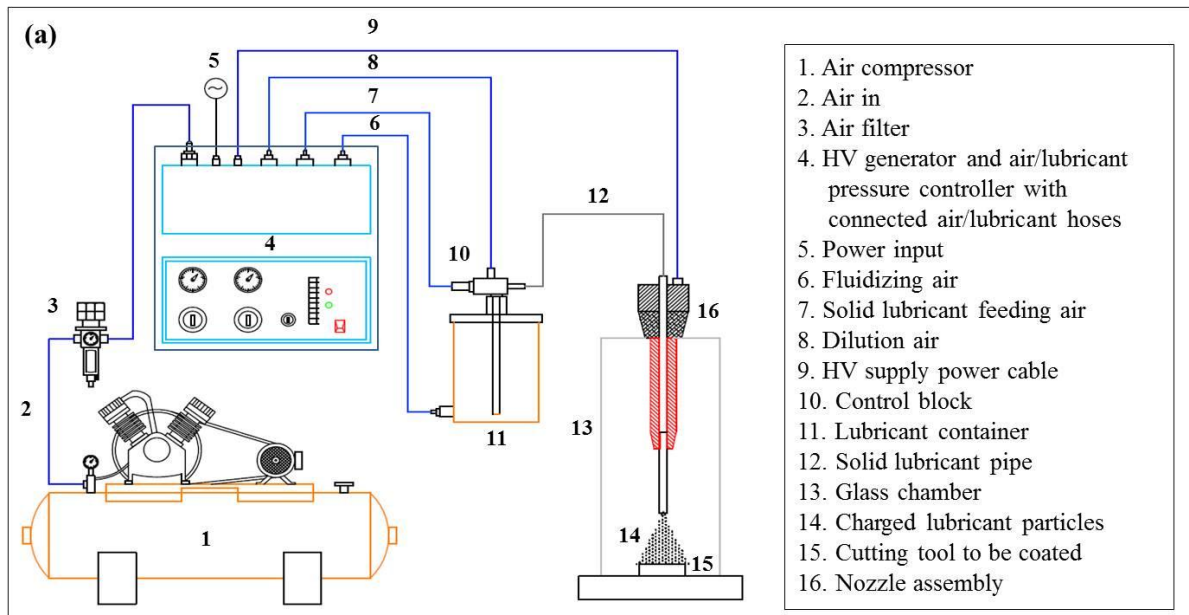
Measurement of this mean surface charge to mass ratio is very helpful in electrostatic powder coating process as it provides an indication of how well a particular coating experimental setup is working, which in turn may be used to evaluate the transfer efficiency of the system. Therefore, in order to maximize the adhering tendency, appropriate mean surface charge to mass ratio (minimum of  $2 \times 10^{-4}$  to  $5 \times 10^{-4}$  Coulomb/kg) is functionally important before the particles adhere to any grounded workpiece [159,160].

### **3.3. Design and fabrication of EMSL coating deposition process setup**

The EMSL coating process experimental setup has been developed in order to achieve solid lubricant coating on cutting tools. The complete EMSL coating deposition experimental setup developed for the investigation comprises a high voltage (HV) power supply and pressure controls, electrostatic spray nozzle assembly with height adjustment facility, air compressor, solid lubricant container, glass chamber and convection curing oven. These components are connected by hoses, cables, all the necessary regulators and fittings. The detailed explanation about EMSL coating experimental system, nozzle design and selection of optimal coating deposition parameters such as electric potential, solid lubricant feed pressure and distance between nozzle tip to substrate are presented in forthcoming sections.

### 3.3.1. EMSL coating system

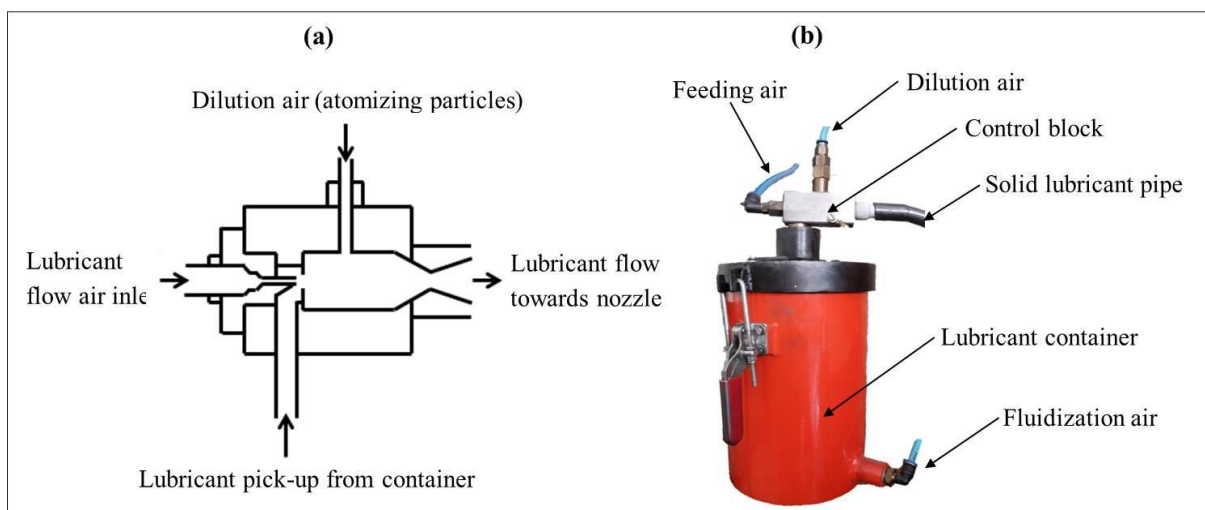
A schematic line diagram and photograph of the developed EMSL coating deposition experimental setup is shown in Fig. 3.3. The purpose of air compressor is to fluidize the particles by passing air through the porous membrane located at bottom of the solid lubricant



**Fig. 3.3.** Electrostatic micro-solid lubricant (EMSL) coating deposition system: (a) schematic view, and (b) photograph of the developed EMSL coating experimental setup.

container and then to transport the same to the electrostatic spray nozzle assembly. A second line of air is introduced through a control block (see Fig. 3.4) that creates a vacuum in the control chamber by way of the Venturi effect. Then, the powder passes through an electrostatic zone where fluidized powder become charged with the help of supplied potential to the tip of the electrode and moves, along with free ions, in a powder cloud toward the grounded part.

A HV charging in the range of 0-100 kV in a low amperage field (corona charging) was employed and connected by the cable to the tip of EMSL coating nozzle assembly. The electrostatic field created at the tip of the nozzle, serves to ensure the charging of lubricant particles owing to ionized air flow in the stream, and, consequently, the in-line air supply through nozzle provides easy transfer of powder particles towards the grounded tool specimens. When the powder particles come close to the grounded part, an electrostatic attraction between the charged powder particles makes them to temporarily adhere to the grounded part. The powder flow is regulated by controlling the air supplied to the lubricant container.



**Fig. 3.4.** Details of control block: (a) working schematic view, and (b) photograph of the control block.

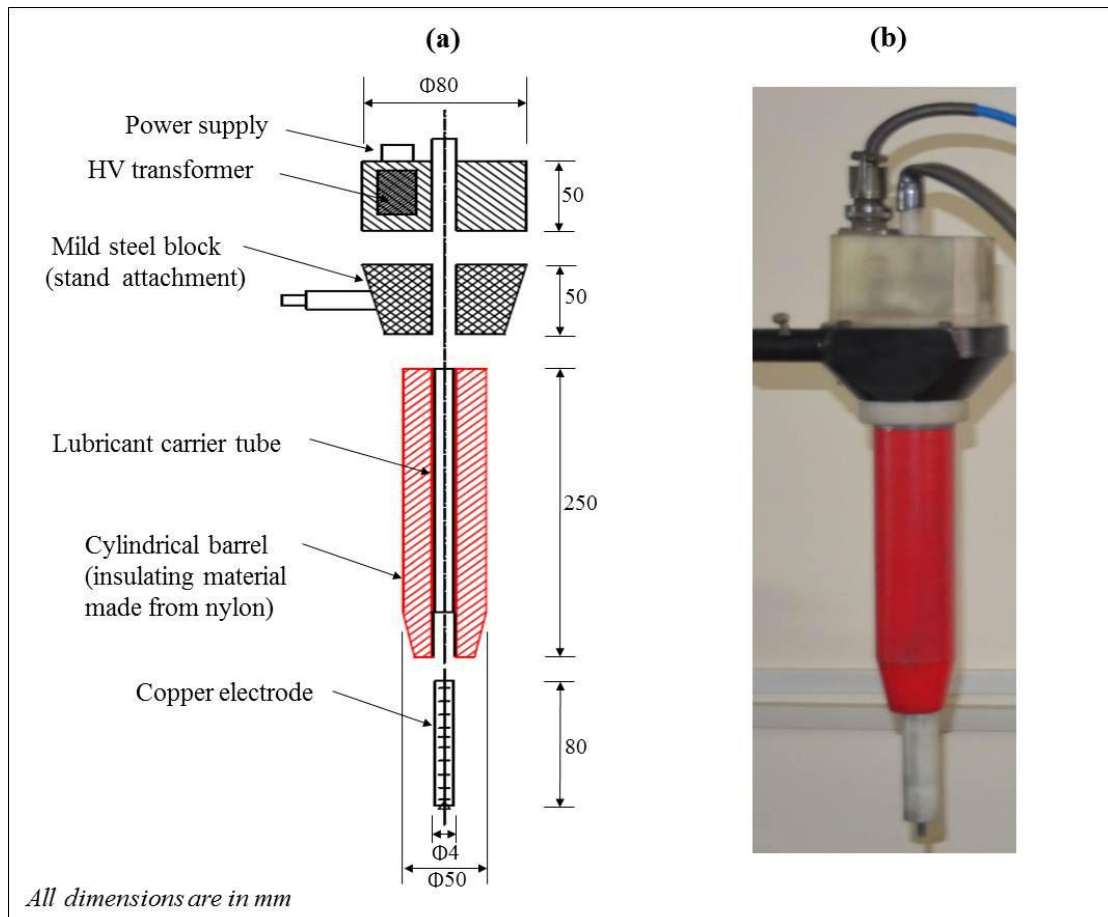
The function of HV supply is to generate the necessary electrostatic charge within the sprayed particles and facilitate them to adhere to the cutting tool inserts (also called as substrate). The strength of the electric field required to move the particles towards the grounded workpiece is evaluated by calculating mean charge to mass ratio ( $q_{max}/m$ ) of the particles. The calculated particle mean charge to mass ratio and transfer efficiency of the developed coating deposition system are presented in Appendix A. The position and direction of the nozzle in conjunction with spray pattern, which depends on the nozzle size, play crucial role in achieving uniform coatings. The distance between nozzle and workpiece is another important parameter in deciding the supply of electrostatic charge and deposition quality. Hence, a height adjustment to the nozzle is provided to facilitate the required distance between the nozzle and workpiece. To avoid solid lubricant particles to mix with air, the coating deposition system is enclosed in a glass chamber. After the deposition of solid lubricant particles on to substrates, a convective oven was employed to cure the temporarily adhered powder particles and to form continuous films that permanently adhered to the substrate.

### **3.3.2. Nozzle assembly**

There have been many developments in electrostatic corona charging device designs over the years for example special air-ventilated deflector plates, flat fan jets and single jets. Keeping its basic principle in imparting electrostatic charges, in the present work, a simple electrostatic spray nozzle based on modularized design with commercially available electrical components and materials and industrial manufacturing standard was built. The electrostatic spray nozzle is the most important component of the EMSL coating system. Its structure design decides directly the effects of spraying transfer efficiency. The main function of nozzle is to shape and direct the flow of powder particles with electrostatic charge. The



schematic diagram of nozzle assembly along with dimensions considered in fabrication is shown in Fig. 3.5. It comprises of HV cascade that is cast into a cylindrical barrel made from insulating material, nylon, in connect with a HV transformer, and a delivery tube is put inside which carries electrical component parts of the HV cascade. The technical specifications of the HV transformer are as follows: input voltage = 60 V AC  $\pm$  10%, input current = 60 mA, output voltage = 100 kV (max), output current = 100  $\mu$ A (max), polarity = negative and frequency = 50 KHz  $\pm$  10%. The inside bore of the delivery tube can serve as a holder for the HV stranded electrode conductor. The system makes use of a corona charging principle to impart the electrostatic charge to the powder particles passing through comb-like corona charging device, located at the tip of the nozzle.



**Fig. 3.5.** EMSL coating nozzle assembly: (a) schematic view of the nozzle assembly, and (b) photograph of the fabricated nozzle assembly.

### **3.3.3. EMSL coating process operating parameters**

#### **3.3.3.1. Air pressure**

Accurate setting of air pressure is very essential as it determines the powder outflow pattern. The main air coming out from the compressor is regulated and distributed inside the spray nozzle control block for uniform flow. The main air pressure is responsible for the powder fluidization and travel of particles from the powder container, through the powder control block and out to the electrostatic spray nozzle. The detailed function of control block unit can be seen from the Fig. 3.4. Supply of proper pressure for lubricant feed and fluidization is important aspect in achieving the uniform coating. Lower pressure doesn't make the powder particles free and therefore fluctuation may occur in the powder outflow. On the other hand, if the pressure is too high formation of air bubbles takes place due to which again fluctuation in the powder outflow occurs. Therefore, the lubricant feed and fluidization pressure should be maintained at value so as to cause smooth flow of powder from the powder feed pump to spray nozzle. However, there is no standardized flow pressure for all powders as the bulk density of each type of powder varies. The optimization of powder feed air pressure is essential in order to achieve desired coating thickness.

#### **3.3.3.2. Electric potential**

Electric potential (or voltage) is very important factor in the electrostatic coating process as it directly decides the charging of the powder particles and affecting the coating thickness and transfer efficiency. In corona-charging systems, a sharply non-uniform electric field is created between a nozzle and substrate by applying high (usually negative) voltage potential to a pointed electrode resulting in the formation of ions due to electrical breakdown of air (see Fig. 3.2). If an electron passes through a strong electric field, it will start moving in this field along the field lines and be accelerated by the field force. As the electron accelerates

along the field lines, it will ultimately run into an air molecule. If the field strength is adequate and the electron has gathered sufficient kinetic energy while traveling along the field lines, its impact on the air molecule will be strong enough to split that molecule to form two secondary electrons and one positive ion (the remainder of the molecule). Secondary electrons will instantly be accelerated in the electric field. Moving along the field lines, they will split new molecules and create more ions and electrons.

In order to optimize powder charging in a corona-charged system, the choice of voltage will almost always necessitate a compromise between an acceptable level of coating quality and charging efficiency in terms of layer disruption from back-ionization. The best approach in this situation is to set up the equipment such that powder flow pattern appears visually acceptable. At the chosen voltage, a check on particle charge-to-mass ratio will then confirm whether, electrostatically, the system is close to optimum performance. If the particle mean surface charge-to-mass ratio falls to the order of  $10^{-4}$  Coulomb/kg, then charging efficiency will be poor, leading in turn to poor deposition efficiency. Hence, in terms of coating performance and efficiency of deposition, this will be one of the critical parameter.

### **3.3.3.3. Nozzle tip to substrate distance**

The distance between the parts that are coating and the tip of the nozzle will affect coating thickness. Normally, the distance between the spray nozzle and work-piece increases, the film thickness decreases. This is in accordance with the fact that the attractive force between charged particles and workpiece decreases with the square of the distance between the spray nozzle and workpiece. For a smaller distance of separation, the resistance of the surrounding air is seen by the applied nozzle potential is less, which leads to the increase in the discharge current for the nozzle electrode. When the discharge current is high, the

discharge voltage will be low, which, in turn, affects the effective charging of the particles. Hence, an optimal separation distance between nozzle and workpiece is preferred.

### 3.4. Optimal deposition process parameters

The focus here in this coating is to identify the most important parameters, electric potential, lubricant feed pressure and distance between nozzle tip to substrate, that affecting the coating thickness, and to choose optimum deposition process parameters for EMSL coating deposition. To relate the actual industrial coating deposition testing conditions, the selected trial domain is as follows: electric potential (50, 70, 90 kV), solid lubricant powder feed pressure (0.5, 1, 1.5 bar) and distance between nozzle tip to substrate (140, 160, 180 mm). For all the coating deposition experimental trials, appropriate powder fluidization pressure was selected by adjusting powder output level to achieve the desired powder flow pattern. Table 3.1 presents some of the other conditions adopted in EMSL coating deposition process.

**Table 3.1.** The EMSL coating deposition conditions.

Corona charging ( $\mu\text{A}$ )	Powder fluidization pressure (bar)	Coating time (s)	Curing time (min)	Curing temperature ( $^{\circ}\text{C}$ )
0-100	0.4	10-15	10	260

#### 3.4.1. Material and tool substrate

$\text{MoS}_2$  solid lubricant material used in the EMSL coating deposition process was obtained from Dow Corning Corp., U.K. The physical properties of  $\text{MoS}_2$  are as follows: mean particle size is 0.7  $\mu\text{m}$ , theoretical density is 4.8 g/cc and purity is about 98%. To enhance the coating

adhesion to cutting tool substrate, the pure modified micron-sized phenolic novolac resin powder was used as binding agent in composition with the solid lubricant. The physical properties of resin is as follows: mean particle size is 2  $\mu\text{m}$  and approximate density is 0.36 g/cc. Substrates to be coated are as follows: (i) cemented tungsten carbide-cobalt alloy (WC-Co) pin with the composition of 94% WC and 6% Co and (ii) carbide cutting tool inserts. The coated pin and coated tool insert are used in tribological and machining tests respectively.

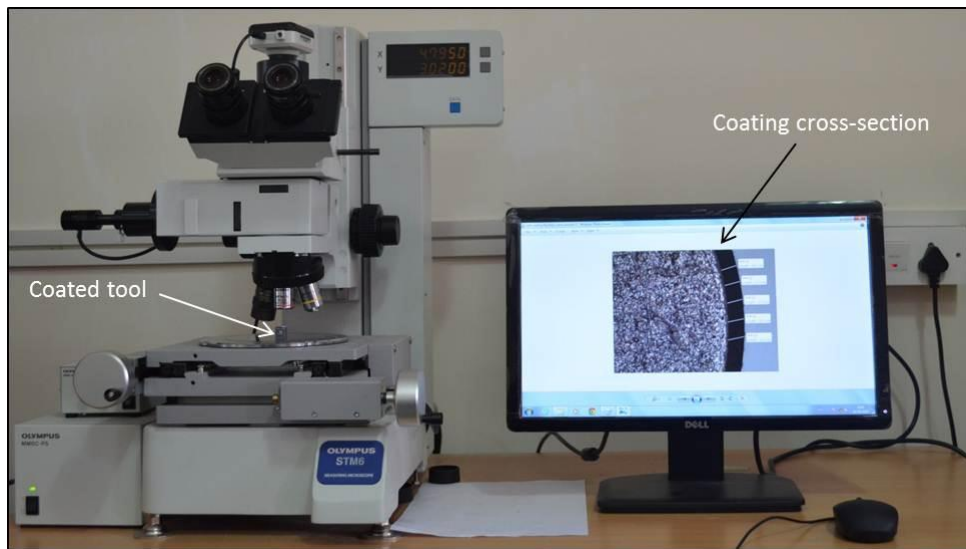
### 3.4.2. Plan of EMSL coating experiments

As explained in Section 3.3.3, the coating deposition process parameters, air pressure, electric potential and nozzle tip to substrate distance plays a vital role in achieving desired level of coating thickness and transfer efficiency of the coating system. Hence, in order to investigate the optimal deposition process parameters and comprehend their significance on its overall thickness of the coatings, Taguchi design approach and the Analysis of Variance (ANOVA) are employed in experimental plan. Taguchi design approach and ANOVA allow optimizing and analyzing the data in a controlled way before and after the experiments. The obtained results were analyzed using Minitab-16, statistical analysis software. The number of trial experiments conducted with the three levels for each identified control factors solid lubricant powder feed pressure, electric potential and distance between nozzle tip to substrate is illustrated in Table 3.2.

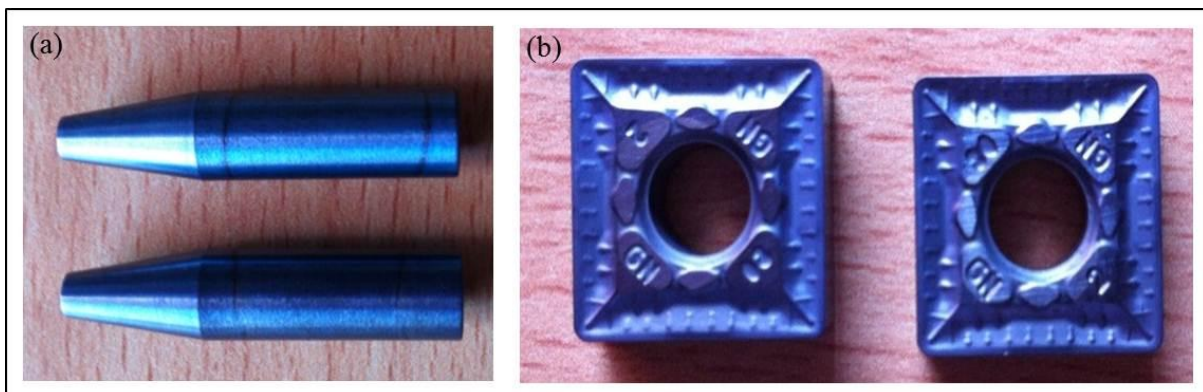
**Table 3.2.** Assignment of levels to the factors used in experiments.

Control factors	Levels		
	1	2	3
Electric potential (kV)	50	70	90
Solid lubricant powder feed pressure (bar)	0.5	1.0	1.5
Distance between nozzle tip to substrate (mm)	140	160	180

Taguchi orthogonal array ( $L_{27}$ ) is selected for conducting experiments, which is having 27 rows corresponding to the number of experiments. To ensure the repeatability and minimum error, each experiment was repeated for three times. The deposited samples were characterized for coating thickness using tool maker's microscope (Olympus, STM6) as shown in Fig. 3.6. Photographs of EMSL coated tool substrates are presented in Fig. 3.7. The detailed studies on EMSL coated tools in tribological and machining applications are explained in chapter 4 and chapter 5 respectively.



**Fig. 3.6.** Coating thickness measurement using tool measuring microscope (Olympus STM6).



**Fig. 3.7.** Photographs of EMSL coated carbide substrates: (a) pin specimens used in tribological pin-on-disc tests, and (b) cutting tool inserts used in machining experiments.

### 3.4.3. Experimental results

The coating thickness results are presented in Table 3.3. The relation between the deposition parameters such as, electric potential, solid lubricant powder feed pressure and distance between the nozzle tip to substrate play important roles in achieving uniform coatings. Fig. 3.8 shows the SEM and microscopic images of the coated surfaces at various coating process conditions. Table 3.4 shows the results of the ANOVA for the coating thickness. This analysis is carried out for a level of confidence of 95%. The last column of the ANOVA table indicates the percentage of contribution ( $P$ ) of each process parameter on the total variation indicating then, the degree of influence on the response of the coatings.

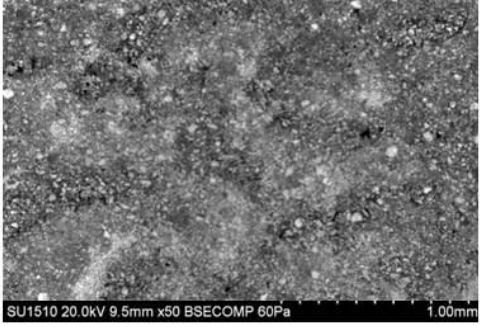
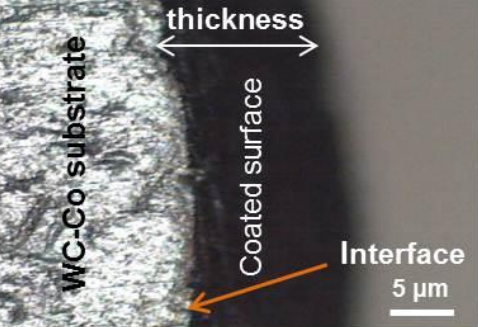
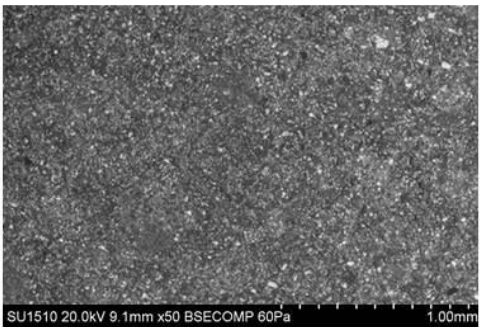
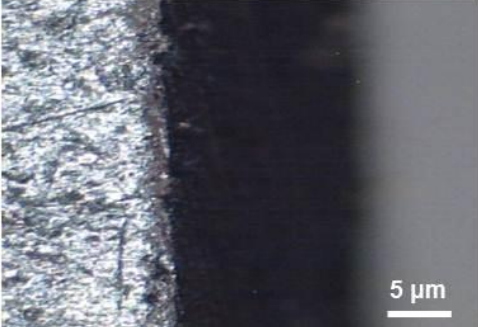
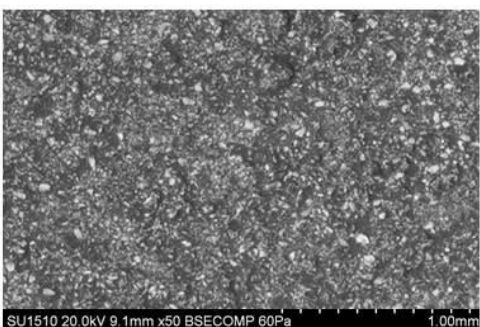
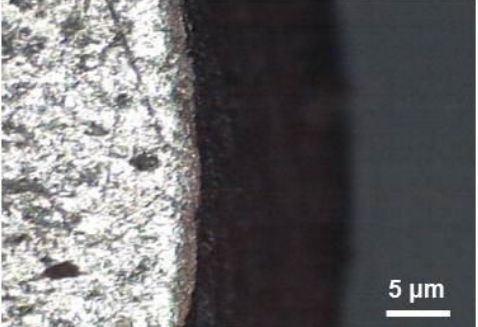
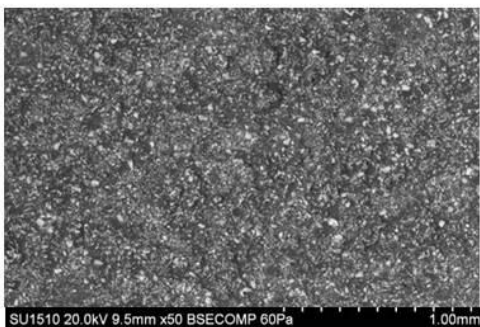
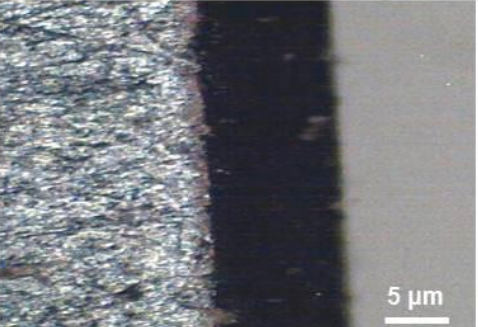
From the analysis of Table 3.3, we can observe that electric potential factor has significant influence on the variation of coating thickness followed by powder feed pressure and distance between nozzle tip to substrate. The percent contribution of each factor on the overall thickness of coatings is as follows: electric potential factors (50.33%), powder feed pressure factors (17.73%) and distance between the nozzle tip to substrate factors (13.81%).

Fig. 3.9 presents the Taguchi statistical approach with the use of S/N ratio to interpret the experimental results and shows the main effect plot (MEP) of S/N ratios for the preliminary experimental plan. In general, among all available quality characteristics in the analysis of the S/N ratio, a greater S/N ratio corresponds to the better quality characteristics. Therefore, from the Fig. 3.9, the optimal deposition process parameters for coating thickness were the electrical potential at level 2, powder feed pressure at level 2, and the distance between the nozzle tip to substrate at level 3. The optimum values of deposition parameters are shown in Table 3.5. Furthermore, it can be seen from the analysis of results, among all the deposition process parameters tested, electric potential has the most significant main effect on the coating thickness. Thus, the line related to electric potential on the MEP has a steeper slope than the line connecting S/N ratios with other two process parameters.

**Table 3.3.** Selected electrostatic coating deposition process parameters and measured coating thickness.

Exp. No.	Electric potential	Powder feed pressure	Distance between nozzle tip to substrate	Coating thickness ( $\mu\text{m}$ )	S/N ratio
1	1	1	1	12.23	21.7485
2	1	1	2	14.2	23.0458
3	1	1	3	15.6	23.8625
4	1	2	1	13.07	22.3255
5	1	2	2	15.2	23.6369
6	1	2	3	16.45	24.3233
7	1	3	1	12.79	22.1374
8	1	3	2	13.77	22.7787
9	1	3	3	14.08	22.9721
10	2	1	1	16.4	24.2969
11	2	1	2	15.3	23.6938
12	2	1	3	14.9	23.4637
13	2	2	1	17.9	25.0571
14	2	2	2	19	25.5751
15	2	2	3	20.1	26.0639
16	2	3	1	17	24.6090
17	2	3	2	18.21	25.2062
18	2	3	3	18.86	25.5108
19	3	1	1	14.5	23.2274
20	3	1	2	16.12	24.1473
21	3	1	3	14.76	23.3817
22	3	2	1	15.8	23.9731
23	3	2	2	17.12	24.6701
24	3	2	3	18.24	25.2205
25	3	3	1	15.1	23.5795
26	3	3	2	16.4	24.2969
27	3	3	3	17.2	24.7106

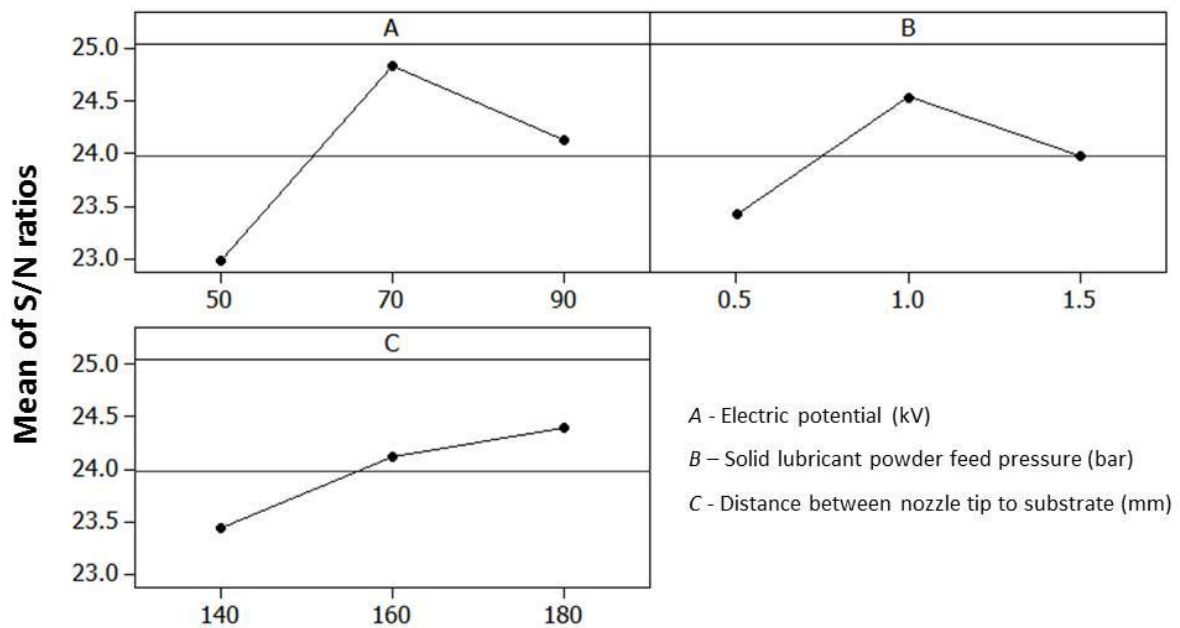


Coating process parameters	Uniformity of coatings (SEM images)	Coating cross-sections (microscopic images)
50 kV 1 bar 180 mm		
70 kV 1 bar 180 mm		
90 kV 1 bar 180 mm		
70 kV 1.5 bar 180 mm		

**Fig. 3.8.** (a) SEM images, and (b) microscopic images, showing the uniformity and cross-sectional views of coatings at different process conditions.

**Table 3.4.** ANOVA results for coating thickness.

Factors	Sum of square	Degree of freedom	Variance	Test F	F <sub>table</sub>	Percentage of contribution P (%)
Electric potential	15.70	2	7.85	43.61	4.46	50.33
Lubricant feed pressure	5.53	2	2.76	15.33	4.46	17.73
Distance between nozzle tip to substrate	4.31	2	2.15	11.94	4.46	13.81
Electric potential x Lubricant feed pressure	2.02	4	0.50	2.77	-	6.47
Electric potential x Distance between nozzle tip to substrate	1.41	4	0.35	1.94	-	4.52
Lubricant feed pressure x Distance between nozzle tip to substrate	0.69	4	0.17	0.94	-	2.21
Error	1.51	8	0.18	-	-	4.84
Total	31.19	26	-	-	-	100.00

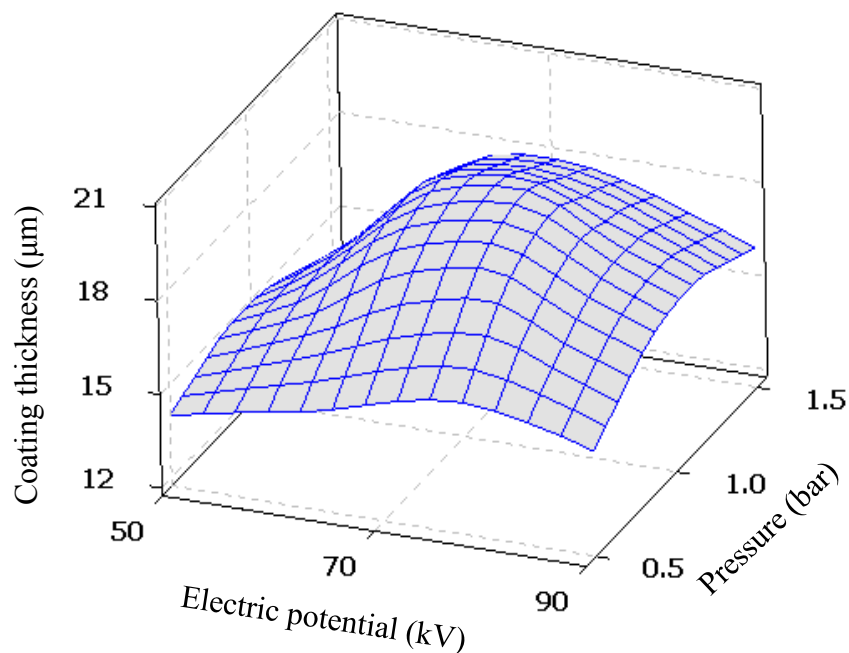


**Fig. 3.9.** MEP of experimental plan for coating thickness.

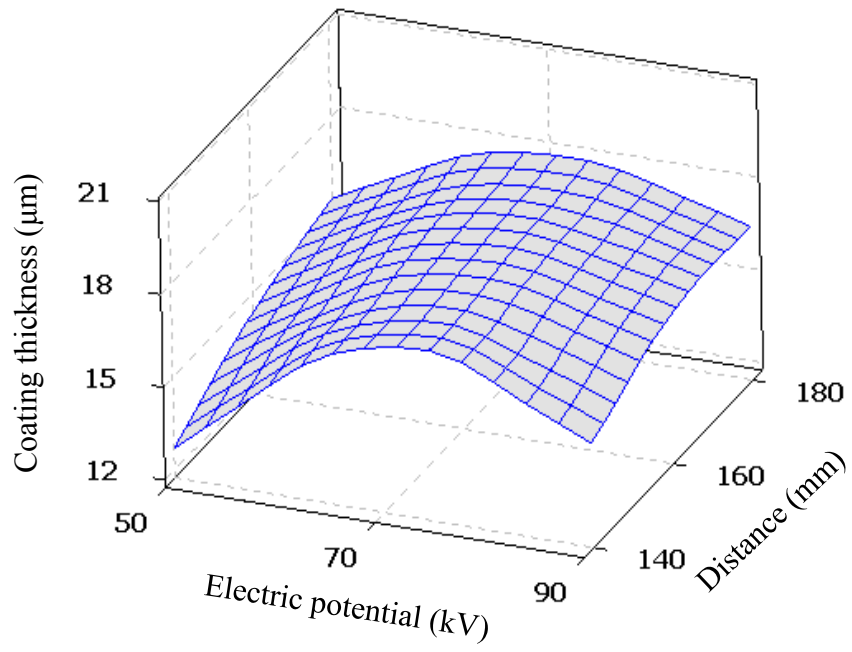
**Table 3.5.** The optimum values of EMSL coating deposition process parameters.

Electric potential (kV)	Powder feed pressure (bar)	Source to substrate distance (mm)
70	1	180

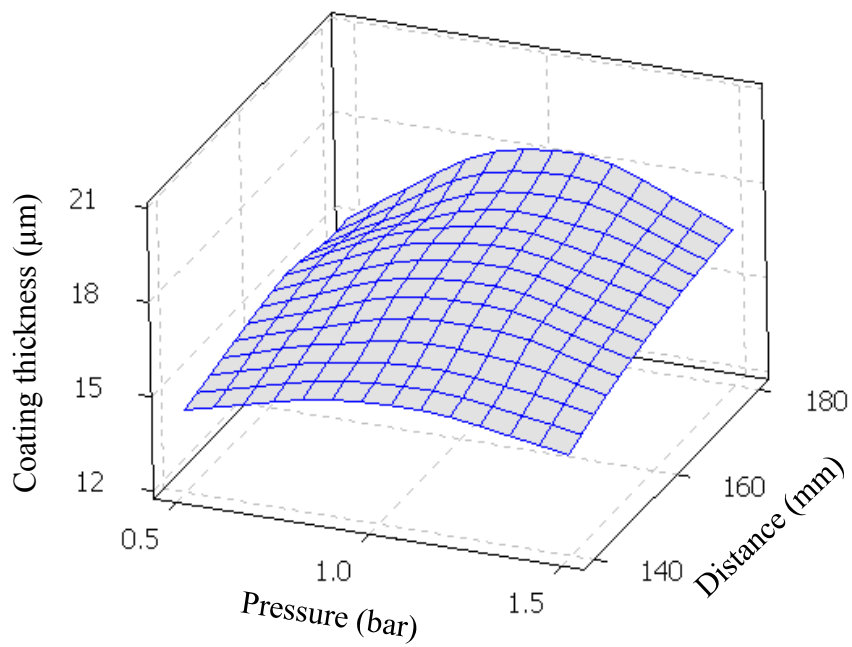
Fig. 3.10 to 3.12 shows 3D plots of the electrostatic coating experimental response versus all the operational variables. The influence of varying the deposition process parameters on the coating thickness is presented. From these figures, it can be seen that the trend in coating thickness was greatly influenced by the electrical potential. An increase in coating thickness values were observed when the voltage changes from 50 to 70 kV and when electric potential changes from 70 to 90 kV there is moderate reduction in coating thickness was observed. This was related to the increase in electrostatic forces, which could largely influence the powder action.



**Fig. 3.10.** Surface plot for electric potential and powder feed pressure effects on coating thickness.



**Fig. 3.11.** Surface plot for electric potential and source to substrate distance effects on coating thickness.



**Fig. 3.12.** Surface plot for powder feed pressure and source to substrate distance effects on coating thickness.

Further, when the electric potential increases the formation of electric field around powder cloud would be expected to increase. This indicates that, as the electric potential increases the more number of charged powder particles pass through the electric field and pushed towards grounded metal substrate. As the number of charged particles push from nozzle tip to substrate increases, transfer efficiency of electrostatic spray deposition would be expected to increase. In addition to the above, change in powder feeding pressure also influences the thickness of coatings. On the other hand, change in the distance between the nozzle tip to substrate caused little variation in the thickness of coatings. This could be mainly due to the electrical field force, which is determined from the electric potential set. The, effect of gravitational force on particle movement is neglected because the effect of electrostatic forces on particle is more than the gravitational effects.

#### **3.4.4. Correlations and confirmations**

In previous section the influence of coating deposition process parameters on coating thickness is presented. In continuation to the above and comprehend the coating thickness at different process parameter conditions, the correlation between the coating deposition process parameters and measured coating thickness is determined from the multiple linear regression model (Eq.3.5). The coefficient of determination ( $R^2$ ) value of developed model has very good correlation between the experimental and predicted values of coating thickness. The adequacy of the model was tested using the ANOVA technique and the calculated value of the F-test of the model does not exceed the standard tabulated value of F-table for a desired confidence level of 95%. The 95% prediction interval is the range in which we can expect any individual value to fall into 95% of the time. From Table 3.4, it is evident that the model is adequate at 95% confidence level.

$$\text{Coating thickness} = - 48.7228 + 0.9488A + 6.7325B + 0.3156C - 0.0059A^2 - 6.2978B^2 - 0.0008C^2 + 0.0393A*B - 0.0007A*C + 0.0260B*C \quad (R^2 = 94.1\%) \quad (3.5)$$

where,

A = electric potential (kV)

B = solid lubricant powder feed pressure (bar)

C = distance between nozzle and substrate (mm)

In order to verify the adequacy of the linear regression model developed, three confirmation trial experiments, consisting of combination of input process parameters which do not belong to the original plan of experimental domain were performed. The process parameters such as electric potential, powder feed pressure and distance from nozzle to substrate used in confirmation tests and comparison of measured and predicted results of coating thickness are illustrated in Table 3.6. The predicted coating thickness value from the developed model and the actual experimental value were compared and the percentage error is calculated.

**Table 3.6.** Input process parameters employed in confirmation tests and comparison of measured and predicted results.

Experimental runs	Electric potential (kV)	Powder feed pressure (bar)	Distance from nozzle to substrate (mm)	Measured thickness (μm)	Predicted thickness (μm)	Error (%)
1	50	1.5	160	14.16	13.49	4.73
2	60	1.5	180	15.85	16.77	5.80
3	80	1.25	170	18.14	18.46	1.76

From the results presented in Table 3.6, it was observed that the calculated error for coating thickness: maximum value 5.8% and minimum 1.76%. The Table 3.6 shows the validation of experimental results for the coating thickness. The developed model correlates the relationship of the coating thickness with the process parameters and can be effectively used for the prediction of coating thickness.

### **3.5. Summary**

In this chapter, the fundamental aspects of electrostatic coating process and importance of process parameters such as electric potential, powder feeding pressure and the distance between the nozzle tip to substrate on coating thickness have been explained. The design and fabrication of coating deposition experimental setup for deposition of electrostatic micro-solid lubricant coatings on cutting tools has been built. To realize the success and completion of EMSL coating deposition experimental setup, micron-sized molybdenum disulfide solid lubricant powder particles in composition with phenolic novolac resin were deposited onto the carbide tool substrates. Taguchi design and ANOVA statistical approach is employed in coating experimental trials to identify the optimum process parameters and comprehend their influence on the coating thickness. From the experimental results, it is noticed that the optimal deposition process parameters for coating thickness were the electrical potential at level 2 (70 kV), powder feed pressure at level 2 (1 bar), and the distance between the nozzle tip to substrate at level 3 (180 mm). Further, among all the coating process parameters, electric potential was found to have a significant effect on the coating thickness.

To assess the performance of EMSL coatings, tribological and machining studies have been carried out over a wide range of industrial test conditions and experimental investigations were presented in chapter 4 and chapter 5 respectively.

# CHAPTER 4

## EXPERIMENTAL INVESTIGATION TO ASSESS THE TRIBOLOGICAL PERFORMANCE OF EMSL COATINGS

---

The current chapter investigates the tribological performance of EMSL coatings by conducting pin-on-disc tribological tests over a wide range of sliding speeds and applied loads. To support in understanding the tribological performance (friction and wear) of coatings, this study also analyzes the coating characteristics in terms of coating thickness, coating strength, coating hardness and elastic modulus. The current chapter is organized as follows: Section 4.1 presents the brief information about importance of MoS<sub>2</sub> solid lubricant in tribological application. Section 4.2 deal with the material and test condition used in dry sliding experiments. Section 4.3 presents the friction and wears performances of EMSL coatings. Finally, Section 4.4 presents the summary of this chapter.

### 4.1. Introduction

In industrial applications, MoS<sub>2</sub> based coatings have been applied to improve tribological performances of machine components in some special conditions such as highly clean environment, severe load, slow relative velocity between mating surfaces, high working temperature, and so on where liquid lubricant cannot be used. Furthermore, the use of MoS<sub>2</sub> based solid lubricant coatings is very common in all kinds of applications, such as machine tools, cams and followers, piston rings and bearings subjected to rolling, sliding and rolling-sliding conditions. However, it is often difficult to choose an appropriate solid lubricant coating for a given tribological application without conducting tribological tests. The level of success of any novel coating materials that are used in industrial applications is often evaluated by one or more of the following tribological tests: pin-on-disc, rubber-wheel



abrasion, block-on-ring, micro-abrasion, ballon-plate impact and reciprocating-sliding wear tests.

In current research work, pin-on-disc testing as per ASTM G99 standard is conducted in order to assess the friction and wear behavior of developed EMSL coatings ( $\text{MoS}_2$  is used as solid lubricant) in dry sliding conditions. Coating strength was evaluated by conducting scratch testing on the coated surface. To support in understanding the tribological characteristics, a relative comparison is made between the process performances of EMSL coated specimen and uncoated specimen when slid against a disc material. Bonded  $\text{MoS}_2$  coatings were prepared with the help of electrostatic coating deposition process as explained in chapter 3. Dry sliding behavior of contact surfaces were analyzed over a wide range of experimental conditions. The experimental results of this research work are very promising and will be useful for tribology designers to implement and promote EMSL bonded  $\text{MoS}_2$  coatings for process enhancement.

## **4.2. Experimental approach**

### **4.2.1. Materials**

The detailed information about material used in preparation of EMSL coating is explained in chapter 3 (section 3.4.1). In tribological tests, the disc material used was a titanium alloy (Ti-6Al-4V) with the chemical composition of 88.76% Ti, 6.29% Al and 4.95% V. The pin specimen material is cemented tungsten carbide-cobalt alloy (WC-Co) with the composition of 94% WC and 6% Co.

### **4.2.2. Preparation of EMSL coatings**

$\text{MoS}_2$  bonded solid lubricant coating on carbide tool specimens were prepared by means of the developed EMSL coating deposition system (Fig. 3.3, chapter 3). Before coating

deposition, uncoated WC-Co specimens were preheated in a curing oven at about 200 °C temperature for about 10 to 15 min to remove any contaminant and to achieve uniform coating. Then, the micron sized MoS<sub>2</sub> solid lubricant particles mixed with phenolic novalac resin powder particles were deposited onto the specimens. All the deposition conditions are listed in Table 4.1.

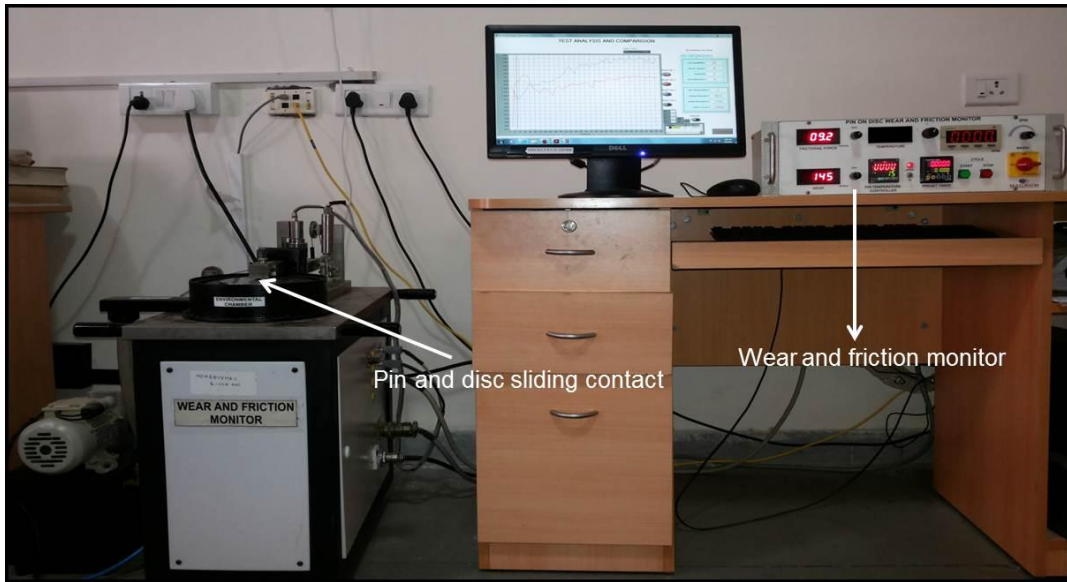
**Table 4.1.** The MoS<sub>2</sub> coating deposition conditions.

Corona charging (μA)	Electric potential (kV)	Powder feeding pressure (bar)	Source to substrate distance (mm)	Fluidization pressure (bar)	Coating time (s)	Curing time (min)	Curing temperature (°C)
0-100	70	1	180	0.4	10-15	10	260

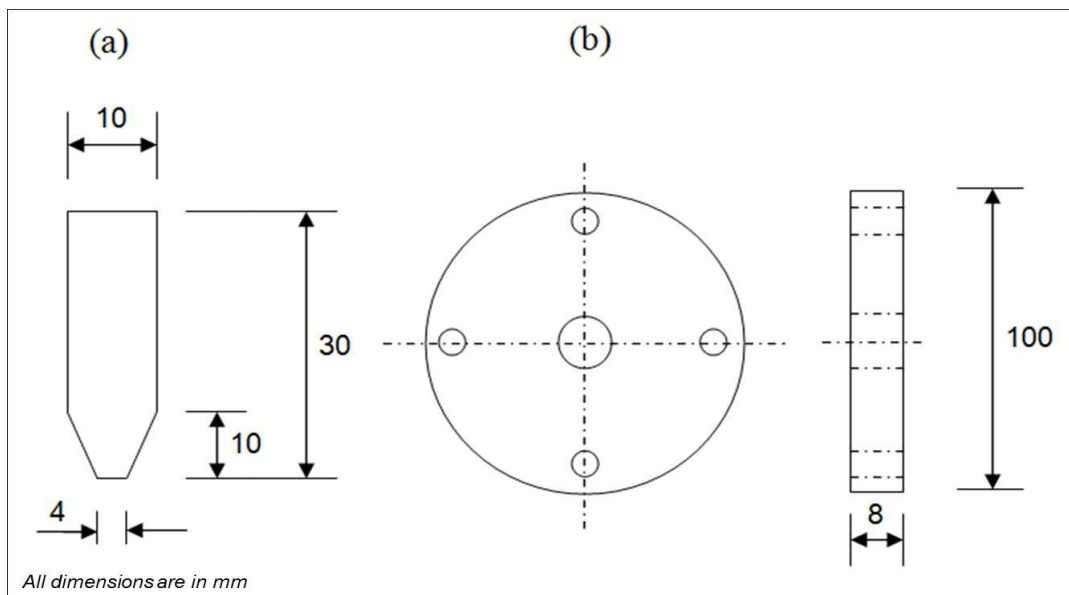
### 4.2.3. Sliding wear tests

Using ASTM G99 standard pin-on-disc tribometer (Fig. 4.1), dry sliding wear tests were performed on Ti-6Al-4V alloy and WC-Co alloy tribological pair. The tribometer consists of a rotating disc (Ti-6Al-4V), a stationary pin (WC-Co) fixed at a specified location, loading system with a normal load applied by attaching weights along the pin's support arm, and friction and temperature measurement systems.

Two different combinations of pin specimen and disc material used in dry sliding wear tests are: (i) uncoated WC-Co specimen sliding against Ti-6Al-4V alloy disc (tribopair-1), and (ii) EMSL coated WC-Co specimen sliding against Ti-6Al-4V alloy disc (tribopair-2). The flat end specimen and circular disc were prepared as per Fig. 4.2. The size of the pin specimen is 10 mm in diameter and 30 mm in length with a conical shape at one end with 4 mm diameter is in contact with the counterpart (disc) of size 100 mm in diameter and 8 mm in thickness.



**Fig. 4.1.** Pin-on-disc tribological testing setup used in tribological tests.

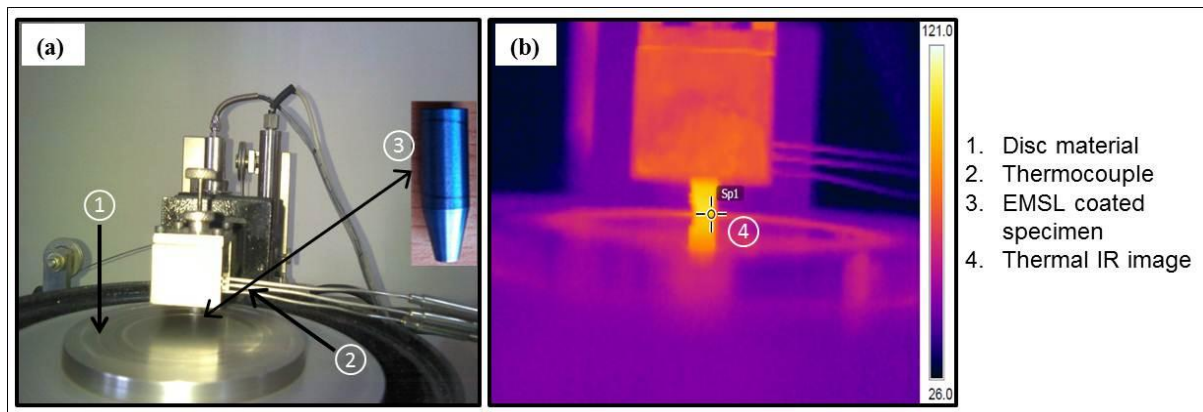


**Fig. 4.2.** Schematic of tribological pair designs: (a) WC-Co alloy specimen, and (b) Ti-6Al-4V alloy counter material.

Tribological tests were performed in two different sliding conditions (tribopair-1 and tribopair-2) at different sliding speeds of 50, 100, 150, 200 and 250 m/min under varying loads of 40, 60 and 80 N. The sliding duration of each test was 10 min. The corresponding

sliding distance for each test was found to be enough to attain steady state sliding conditions. From experiments, results of pin wear rate and coefficient of friction in two tribopairs were measured and compared in similar sliding conditions.

Temperature generated in the specimen during sliding test was measured using K-type chromel–alumel thermocouple inserted into the pin holder hole and touches the pin surface at 5 mm above from pin-disc contact point. Further, to ensure and measure actual contact temperatures, a thermal infrared camera (FLIR E60) with 320 x 240 pixels with thermal sensitivity less than 0.05°C at 30°C was employed. Magnified view of the pin-disc contact and a sample measure of temperatures in the pin specimen is presented in Fig. 4.3. Using Mitutoya digimatic caliper (CD-6” CSX), the pin height loss was measured before and after each sliding test.

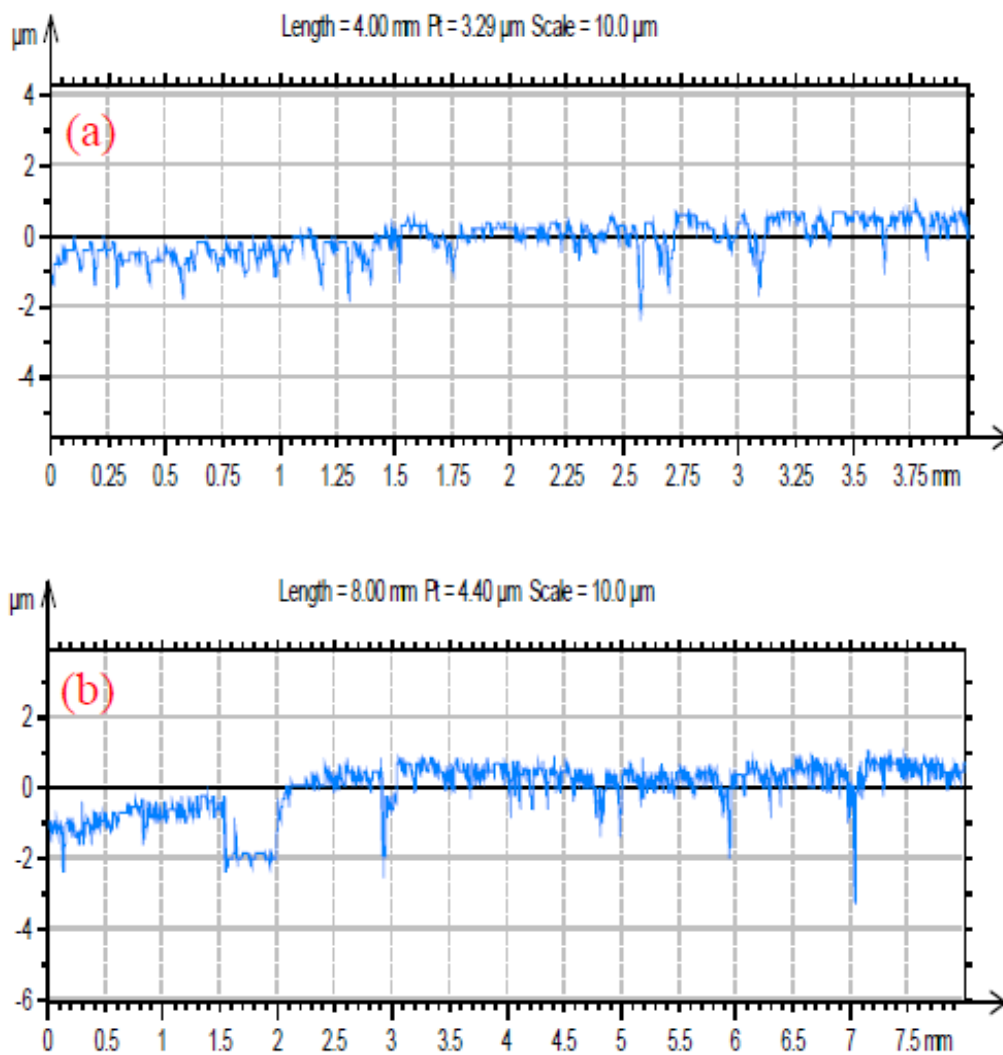


**Fig. 4.3.** (a) Magnified view of pin and disc used in tribological tests, and (b) a sample of thermal infrared image captured at tribopair contact.

To ensure the consistency of test data, every test was repeated for three times on each of new specimens and the average values were recorded as wear loss. Before the start of each sliding test, the disc surface was cleaned with acetone and mechanically ground to maintain

the desired level of quality of surface finish. The disc and pin surface finish values were consistently maintained in all sliding tests as per the Fig. 4.4.

Conformity of the identical contact conditions between mating parts was achieved by rotating the pin specimen on the disc surface so that contact did not occur along the same region of the pin more than once. In order to elucidate the wear process, the surfaces of the wear samples were examined under scanning electron microscope (SEM) equipped with energy dispersive spectroscopy (EDS) (Hitachi, SU-1510) and optical microscopy (Olympus STM6).



**Fig. 4.4.** Surface roughness profiles: (a) disc ( $R_a = 0.256 \mu\text{m}$ ), and (b) pin ( $R_a = 0.24 \mu\text{m}$ ).

## 4.2.4. Analysis of the EMSL coatings

### 4.2.4.1. Mechanical properties of coatings

To comprehend the adhering tendency of deposited powder particles onto grounded tool specimens, the limiting value of powder particle mean surface charge to mass ratio ( $q_{max}/m$ ) as a result of applied electric field is evaluated. The procedure of ' $q_{max}/m$ ' calculation is presented in Appendix A. The EMSL coated specimens were characterized by measuring the coating thickness with the help of measuring microscope (Olympus STM6) (see Fig. 3.6 in chapter 3).

Micro-hardness tests over the load range 10 - 1000 gf were conducted in air at room temperature with the dwell time of 15 s using micro-Vickers hardness tester (CV-400DTS, CV instruments, Europe). The microindentations were applied near the centerline of coating cross-sections. To minimize stress-field effects, the distance between indentations was kept three times greater than the diagonal length of the indentation. The average of 10 indentations was used to represent the micro-hardness of the coatings. The hardness (HV) and elastic modulus (E) of the coatings are determined according to the standard procedure [161] using Eq.4.1 and Eq.4.2 respectively.

$$HV = \frac{P_{max}}{A} \quad (4.1)$$

$$E = \frac{\sqrt{\pi}}{2} \frac{S_{max}}{A} \quad (4.2)$$

where, ' $P_{max}$ ' is the test load (gf), ' $A$ ' is the effective contact surface area ( $\text{mm}^2$ ) of the indentation after the indenter has been withdrawn. The area is computed from the mean diagonal of the two measured diagonals of indentation. ' $S_{max}$ ' is the slope of the unloading curve for maximum load.

#### 4.2.4.2. Coating strength

Scratch test was performed using a commercial microscratch tester (DUCOM, TR104, India) as shown in Fig. 4.5 to evaluate the scratch resistance of the coatings. A spherical Rockwell C diamond stylus of 100  $\mu\text{m}$  radius was used to produce the scratch. Standard scratch parameters were used. The test was carried out with the load ranging from 20 N to 200 N. The loading rate is 100 N/min and scratching speed is 10 mm/min. The coating failure and critical load were analyzed by inspection of the scratch track under a light microscope.



**Fig. 4.5.** Coating strength test using standard scratch tester (Ducom Instruments).

#### 4.2.5. Dry sliding behavior

Dry sliding wear tests are carried out under different speeds and normal loads to evaluate the performance of EMSL coatings. Specimen wear volume and wear rate were calculated according to following equations (Eq.4.3 and Eq.4.4) [162].

$$WV = \frac{\pi}{24} (D_2 - D_1) (D_1^2 + D_2^2 + D_1 D_2) \quad (4.3)$$

$$WR = \frac{WV}{F_n L} \quad (4.4)$$

where, 'WV' is the pin wear volume (mm<sup>3</sup>), 'WR' is the pin wear rate (mm<sup>3</sup>/(N.m)), 'D<sub>1</sub>' and 'D<sub>2</sub>' respectively the mean value of an initial diameter and of the final diameter of the pin contact surface (mm), 'F<sub>n</sub>' is the normal load (N), and 'L' is the sliding distance (m).

The mechanical energy dissipated in the sliding contact was calculated as the work of the friction force. For each time interval, the dissipated energy is calculated using Eq.4.5 [163]. Further, using simplified Eq.4.6, considering the mean value of the friction with constant sliding speed, dissipated energy is calculated. The results, wear volume, wear rate and energy dissipated in two tested tribological contacts corresponding to applied load and sliding speed are presented in Appendix B.

$$\Delta E = \int_0^{\Delta t} F dx = \int_0^{\Delta t} F V dt \quad (4.5)$$

$$\Delta E = \bar{F} V \Delta t \quad (4.6)$$

where, 'ΔE' is the dissipated energy (J), 'F' is the frictional force (N), 'V' is the sliding speed (m/min), 'F̄' is the average value of frictional force (N) calculated from the acquired friction force data and 'Δt' is the sliding duration (min).

### 4.3. Results and discussion

#### 4.3.1. Particle surface charge to mass ratio, coating thickness, hardness, elastic modulus and coating strength

In electrostatically deposited coatings, particle surface charging in the electric field of corona discharge is governed by Pauthenier's Eq.4.7 [158]. For metallic particles ( $\epsilon_r \rightarrow \infty$ ), the Pauthenier limit is expressed with Eq.4.8. The amount of charge acquired by the particles



not only determines their trajectories but also their adherence tendency to the substrate [159,160]. These studies explained that the particle adherence tendency is the function of the surface charge to mass ratio ( $q_{max}/m$ ) of the particles (Eq.4.9).

$$q = A \varepsilon_o \left[ 1 + 2 \left( \frac{\varepsilon_r - 1}{\varepsilon_r + 2} \right) \right] E \quad (4.7)$$

$$q_{max} = 12 \pi r^2 \varepsilon_o E \quad (4.8)$$

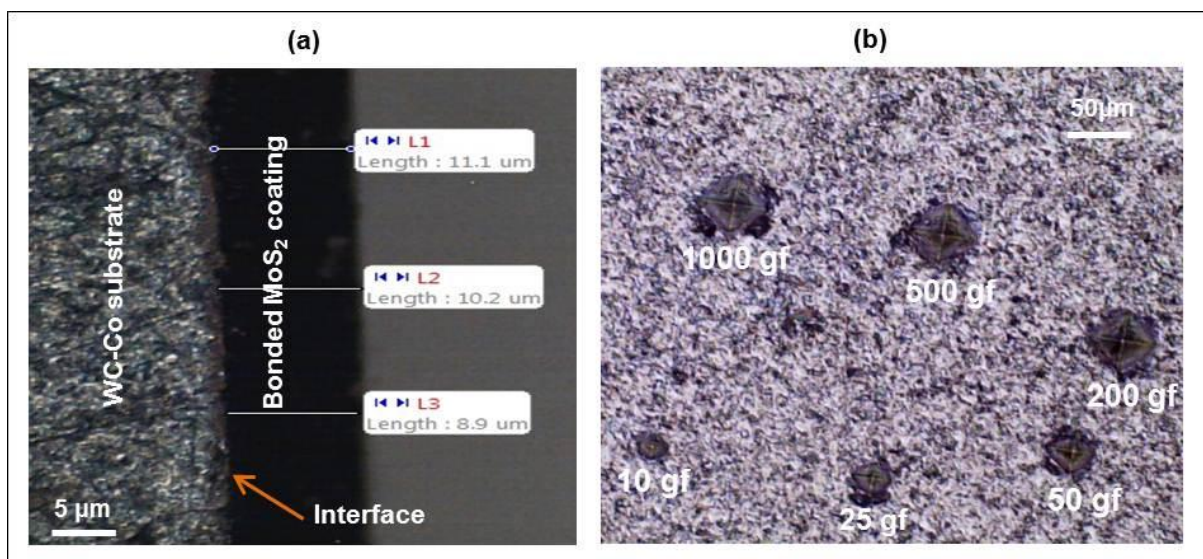
$$\frac{q_{max}}{m} = \frac{12 \pi r^2 \varepsilon_o E}{\left( \frac{4}{3} \right) \pi r^3 \rho} \quad (4.9)$$

where, 'A' is the surface area of the particle ( $\text{mm}^2$ ), ' $\varepsilon_o$ ' is the permittivity of the free space ( $8.85 \times 10^{-12}$  Coulomb/Volt), ' $\varepsilon_r$ ' is the ratio of the permittivities of particles to that of free space, ' $E$ ' is the strength of the electric field (assumed to be  $3 \times 10^5$  Newton/Coulomb), ' $r$ ' is the radius of the particle ( $\mu\text{m}$ ), ' $m$ ' is the mass of the particle (g) and ' $\rho$ ' is the density of the particle (g/cc).

In the electric field of corona discharge, appropriate particle surface charge to mass ratio (minimum of  $2 \times 10^{-4}$  to  $5 \times 10^{-4}$  Coulomb/kg) is functionally important before the particles adhere to any grounded workpiece. Therefore, in order to maximize the particle adhering tendency to the grounded metallic substrate, it is very important that the particles are charged consistently with a sufficient charge during the electrostatic coating process. In the current research work, the calculated particle surface charge to mass ratio is about  $142.2 \times 10^{-4}$  Coulomb/kg, which is many times more than the usually required particle charge to mass ratio in any deposition using electrostatic charging principle. This indicates that the EMSL coating process can be used successfully in achieving high adhering tendency of particles to

the metal substrate. The calculated particle mean charge to mass ratio and transfer efficiency of the coating deposition system are presented in Appendix A.

The optical micrograph of the EMSL coating cross-sectional view and typical Vicker's indentations at different loads are presented in Fig. 4.6. From Fig. 4.6, it is observed that the coated surface seen to be quite uniform throughout the microstructure. Further, EMSL coatings possess a higher crack resistance within the applied indentation load range. This can be seen from Fig. 4.6 (b) as there are no visible cracks under different applied loads. This indicates that the electrostatic charging principle works quite satisfactorily in depositing solid lubricant coatings. The thickness of EMSL coating is on average about 10  $\mu\text{m}$  (see Fig. 4.6 (a)). In the current study, the hardness and elastic modulus of the electrostatically deposited  $\text{MoS}_2$  coatings are found to be approximately 3.9 GPa and 85 GPa respectively. These results are somewhat differ the existing results of conventional  $\text{MoS}_2$  coatings [72,73] and  $\text{MoS}_2$  - based coatings [75,76] prepared by sputtering deposition. The differences in hardness and elastic modulus of EMSL coatings with existing coatings are possibly due to the coating composition, coating thickness and coating deposition method employed.

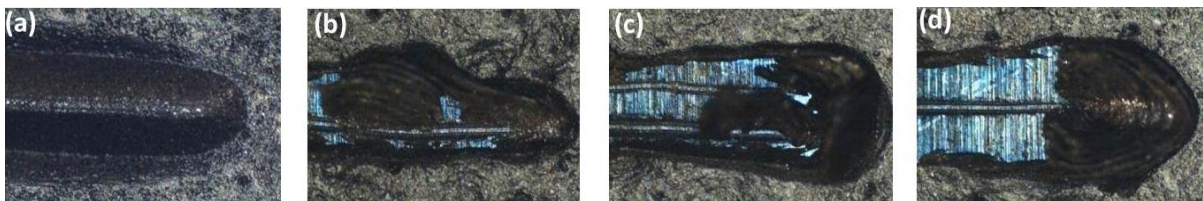


**Fig. 4.6.** Optical micrographs: (a) EMSL coated surface, and (b) typical microindentations on the coated surface at various loads.

In addition to the above, coating strength was evaluated by measuring the critical load required to remove the coating from the substrate using scratch tester. Table 4.2 presents the critical loads corresponding to a coating failure shown in Fig. 4.7. From Fig. 4.7, the following trends can be observed: (i) minor damage of coating corresponding to load 52 N, (ii) coating film began to fail corresponding to 61 N, and (iii) coating debonds completely when load reaches to 69 N, indicating the scratch groove was much deeper with a larger width and full deformation. The highest critical load of bonded MoS<sub>2</sub> coating is about 64 N, indicating that electrostatically deposited MoS<sub>2</sub> coating has quite reasonable coating strength and compared favorably with a reported critical load of about 80 N measured by scratch testing for conventional MoS<sub>2</sub> and MoS<sub>2</sub>/metal based coatings prepared by sputtering deposition process [72].

**Table 4.2.** Critical load of EMSL coatings.

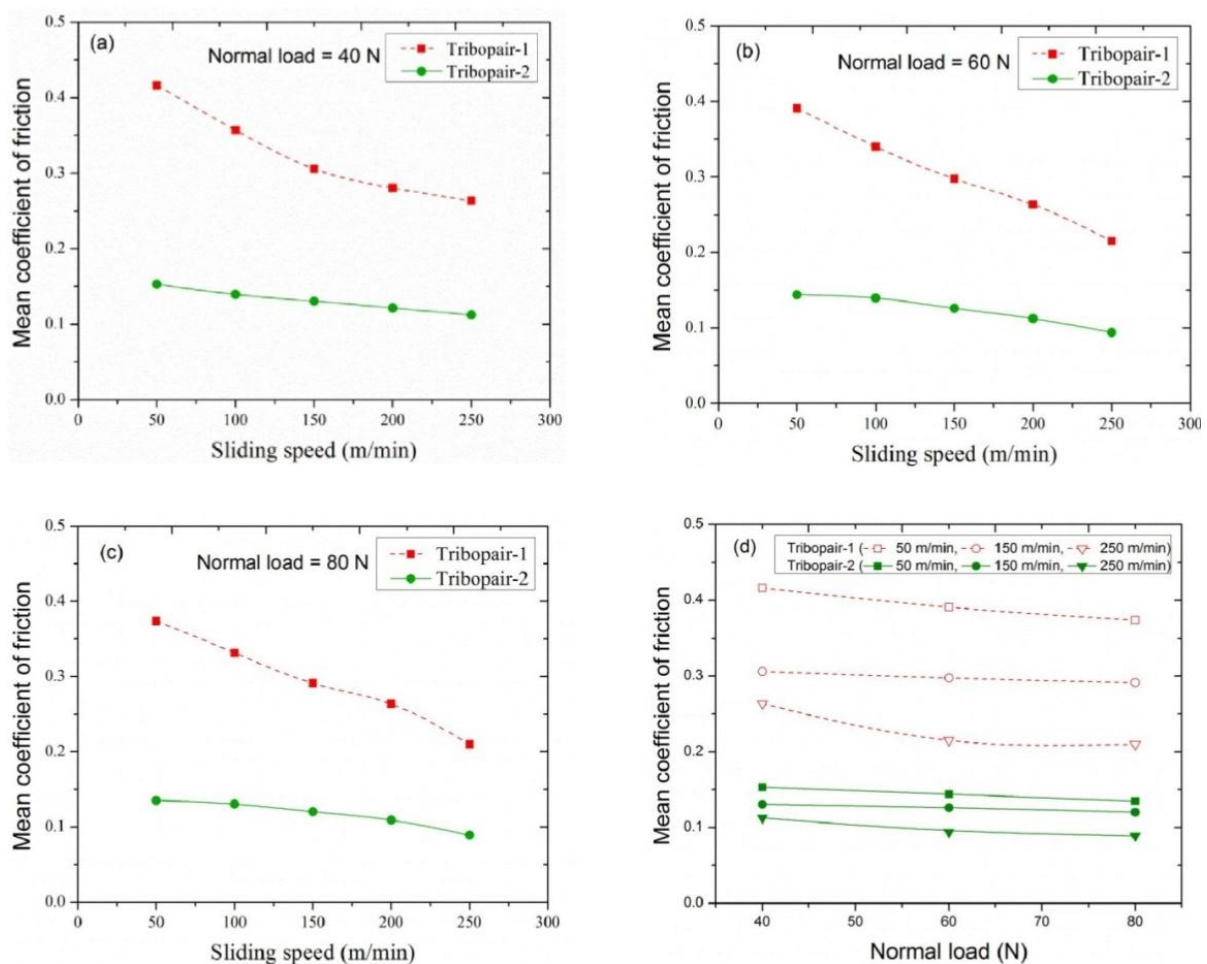
Scratch test conditions	Critical load (N)		
	(L <sub>c1</sub> )	(L <sub>c2</sub> )	(L <sub>c3</sub> )
Rock well C diamond stylus - 100 μm, Load rate - 100 N/min Scratch speed - 10 mm/min	52	61	69



**Fig. 4.7.** Scratch images on the coated surface: (a) no failure in the coating, (b) corresponding to a load of 52 N, (c) corresponding to a load of 61 N, and (d) corresponding to a load of 69 N.

### 4.3.2. Friction and wear behavior

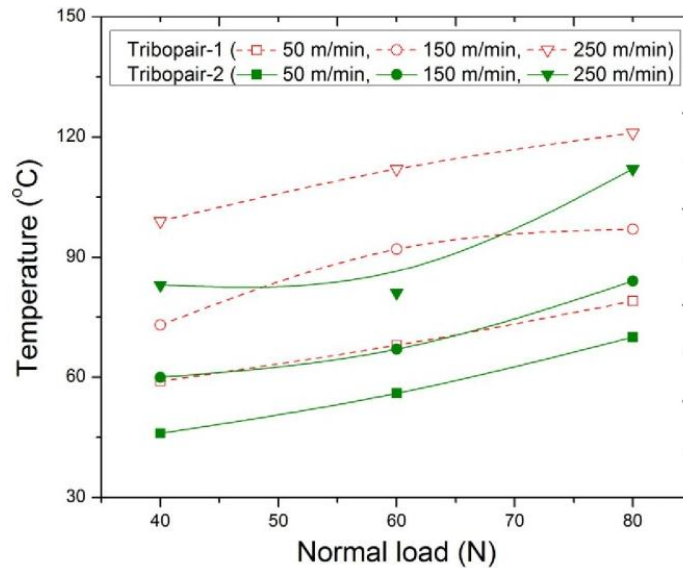
At the start of each sliding test, the instantaneous coefficient of friction between pin and disc contact surface is increases up to a certain maximum value and thereafter remains stable and attains a steady state condition. Then, the mean value of friction coefficient was calculated from acquired test results. Fig. 4.8 depicts the influence of sliding speeds on the mean coefficient of friction under different normal loads in two tested tribological pairs.



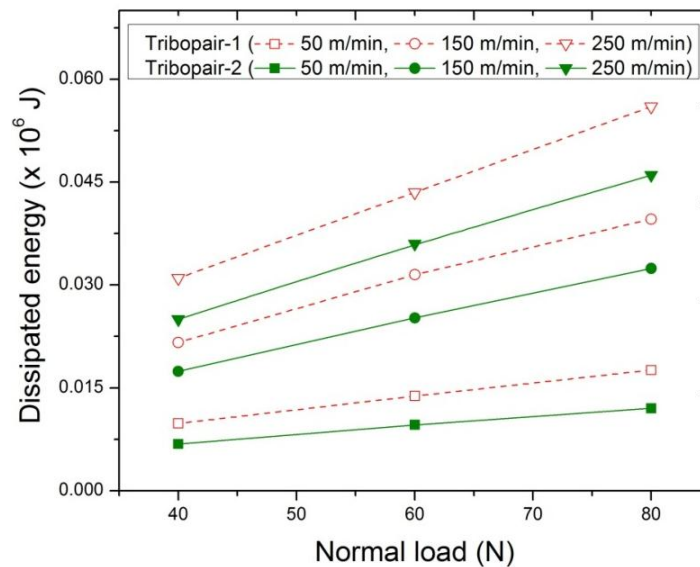
**Fig. 4.8.** Mean coefficient of friction ( $\mu$ ) against sliding speed ( $V$ ) at different applied loads: (a) 40 N, (b) 60 N, (c) 80 N, and (d) all loads corresponding to (a), (b) and (c).

The general trend observed in all the tested cases is the decrease of the coefficient of friction with the increase of the normal load and sliding speed. This could be due to the

increase in contact temperatures (Fig. 4.9) and energy dissipated by the friction in the sliding contact (Fig. 4.10). The temperature distribution at contact surfaces is directly dependent on the mechanical energy dissipated into the sliding contact and the presence of self-lubricating film, MoS<sub>2</sub>.



**Fig. 4.9.** Pin contact temperatures as the function of normal load at different sliding speeds for two tested tribological pairs.

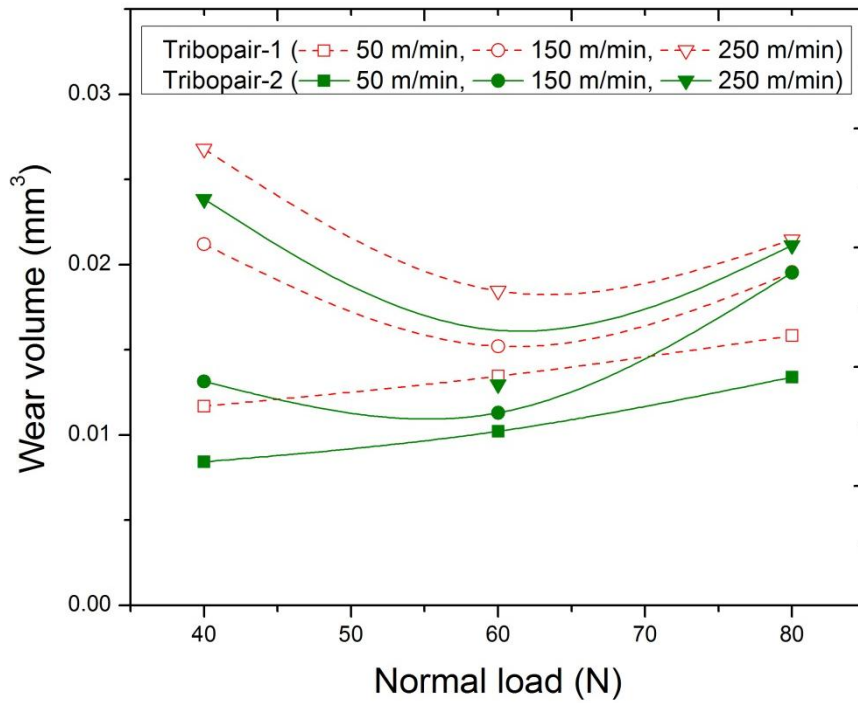


**Fig. 4.10.** Dissipated energy ( $\Delta E$ ) in the sliding contact as the function of normal load at different sliding speeds for two tested tribological pairs.

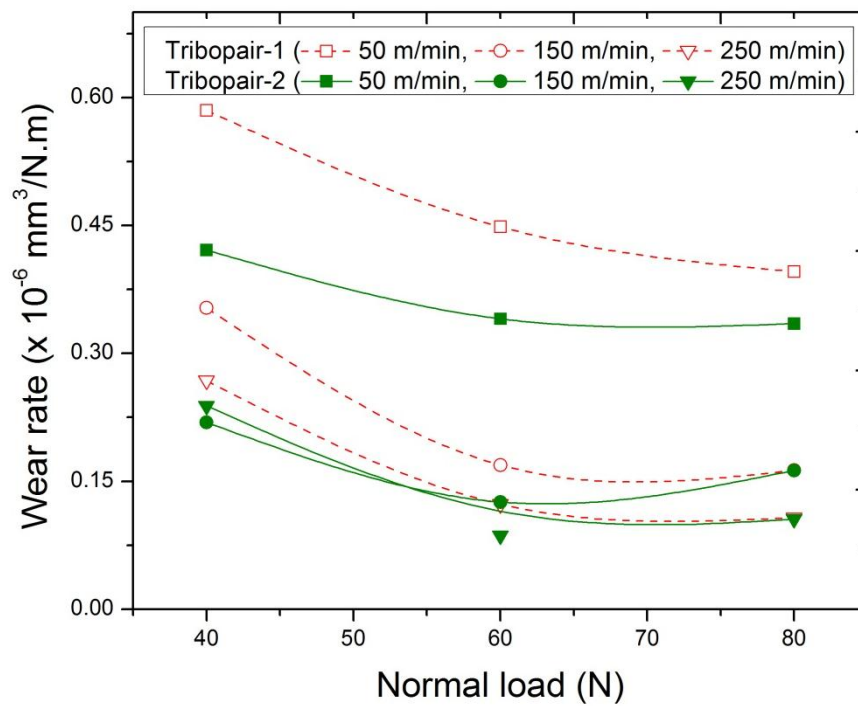
Further, from Fig. 4.8, the following trends can be observed. The first noticeable trend shows that, at all sliding speeds under applied loads, EMSL coatings markedly reduce the coefficient of friction down to 50%. A second noticeable trend reveals that the friction of these coatings decreases with applied load. This observation is very common as the transition metal dichalcogenide coatings are violating classical Amonton law i.e. the frictional force is directly proportional to applied load [59]. The third observation is that the effect of coatings on the friction coefficient was more dependent on the sliding speeds than the applied loads. The lower frictional values with EMSL coatings are could be due to the MoS<sub>2</sub> solid lubricant easy shearing action between rubbing parts, which may contribute to the decrease of frictional forces.

The trend in wear volume of pin specimen in both the tribological pairs under tested conditions is presented in Fig. 4.11. It can be seen that, at lower normal loads, the wear loss with tribopair-2 is quite low and the difference in wear volumes recorded for specimens in both the tribological pairs was relatively very high when compared to that of one at higher loads. In both the tribopairs, at higher loads with regardless of selected speed, there is no much variation in recorded wear volume of specimens, which can directly depend on the dissipated energy by friction in the sliding contact. It can be seen from Eq.(4.4) and Eq.(4.6), the wear volume ( $WV$ ) seems to be directly proportional to the product of frictional force ( $\bar{F}$ ) and sliding distance ( $L$ ).

Specimen wear rate results in both the tribological pairs were presented in Fig. 4.12. Examinations of Fig. 4.12 reveal that the pin wear rate in tribopair-1 decreases with increasing normal load, while the normal load progresses, the change in wear rate with the pin specimen of tribopair-2 is very much less as compared to pin results of tribopair1. This trend is more evident at lower sliding speeds, while at higher sliding speeds, there is no much considerable change in the recorded wear rates of specimens in both the tribopairs.



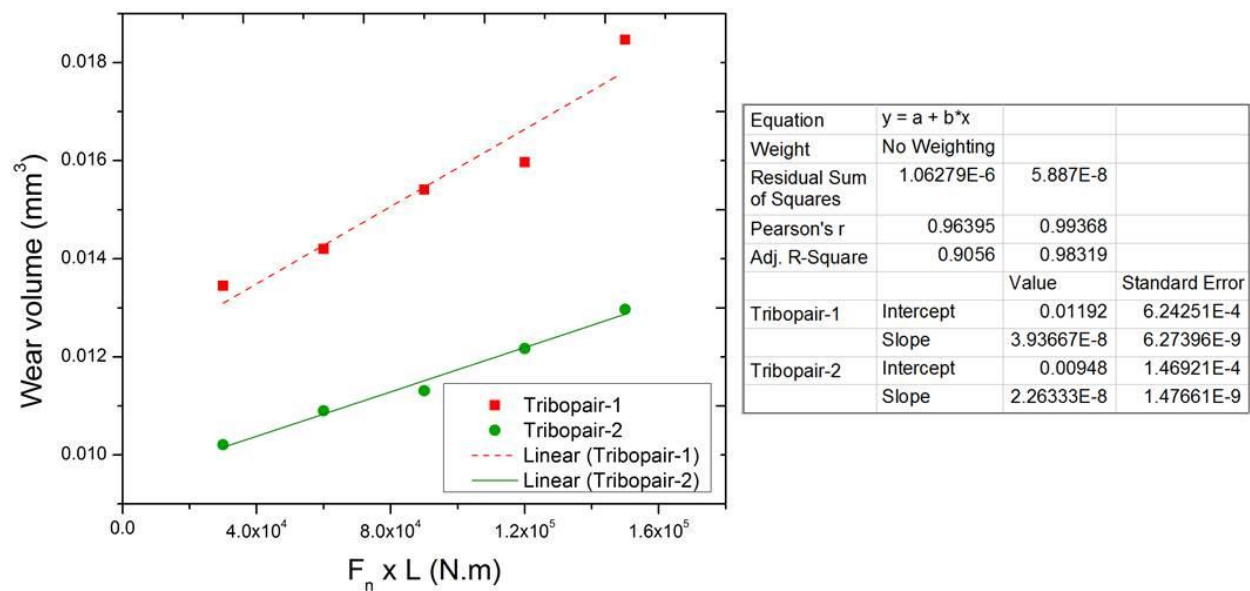
**Fig. 4.11.** Specimen wear volume (*WV*) as the function of normal load at different sliding speeds for two tested tribological pairs.



**Fig. 4.12.** Specimen wear rates (*WR*) as the function of normal load at different sliding speeds for two tested tribological pairs.



In order to see the influence of MoS<sub>2</sub> solid lubricant presence in lubricating and preventing wear of the pin specimen, results were analyzed by means of the classical approach (Archard's wear law) and wear volume as the function of mechanical energy is presented in Fig. 4.13. From Fig. 4.13, it can be seen that the wear volume of pin in both the tribological pairs under tested sliding conditions is continuously increasing and directly dependent on the function of product of sliding distance and normal load. Further, it is clear that the specific wear rate, i.e., the slope of the curve, with the tribopair-2 ( $2.26 \times 10^{-8}$  mm<sup>3</sup>/N.m) is very much low (42% less) when compared to that of tribopair-1 ( $3.93 \times 10^{-8}$  mm<sup>3</sup>/N.m).



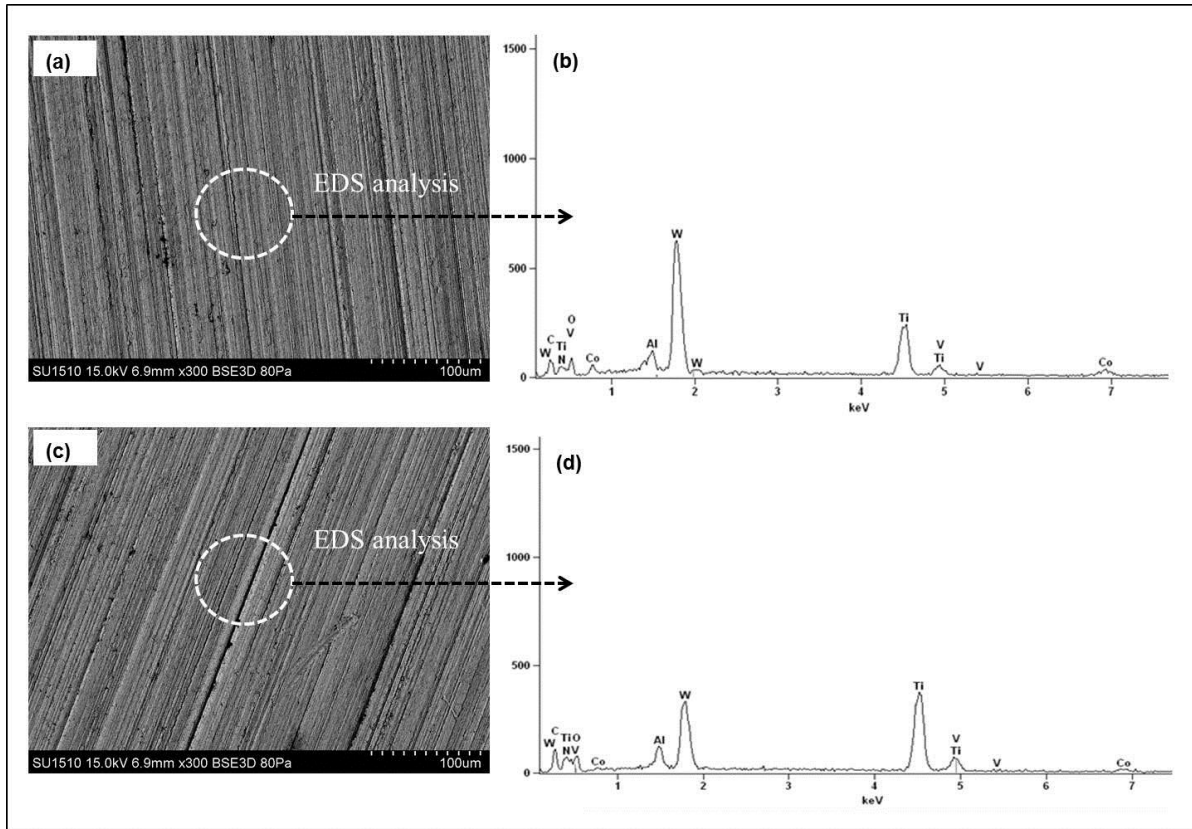
**Fig. 4.13.** Specimen wear volume ( $WV$ ) against mechanical energy ( $F_n * L$ ) in the sliding contact for the two tested tribological pairs at normal load of 60 N (Archard's approach).

Specific wear rate of EMSL coatings are found to be in the same trend as it can be seen in previous studies with magnetron sputtered MoS<sub>2</sub> coatings [72,74] and MoS<sub>2</sub>/metal coatings [76,164]. The observed differences in wear rate values and friction coefficients could be due to the presence of MoS<sub>2</sub> as a solid lubricant on the wear track, and, it is dependent on the



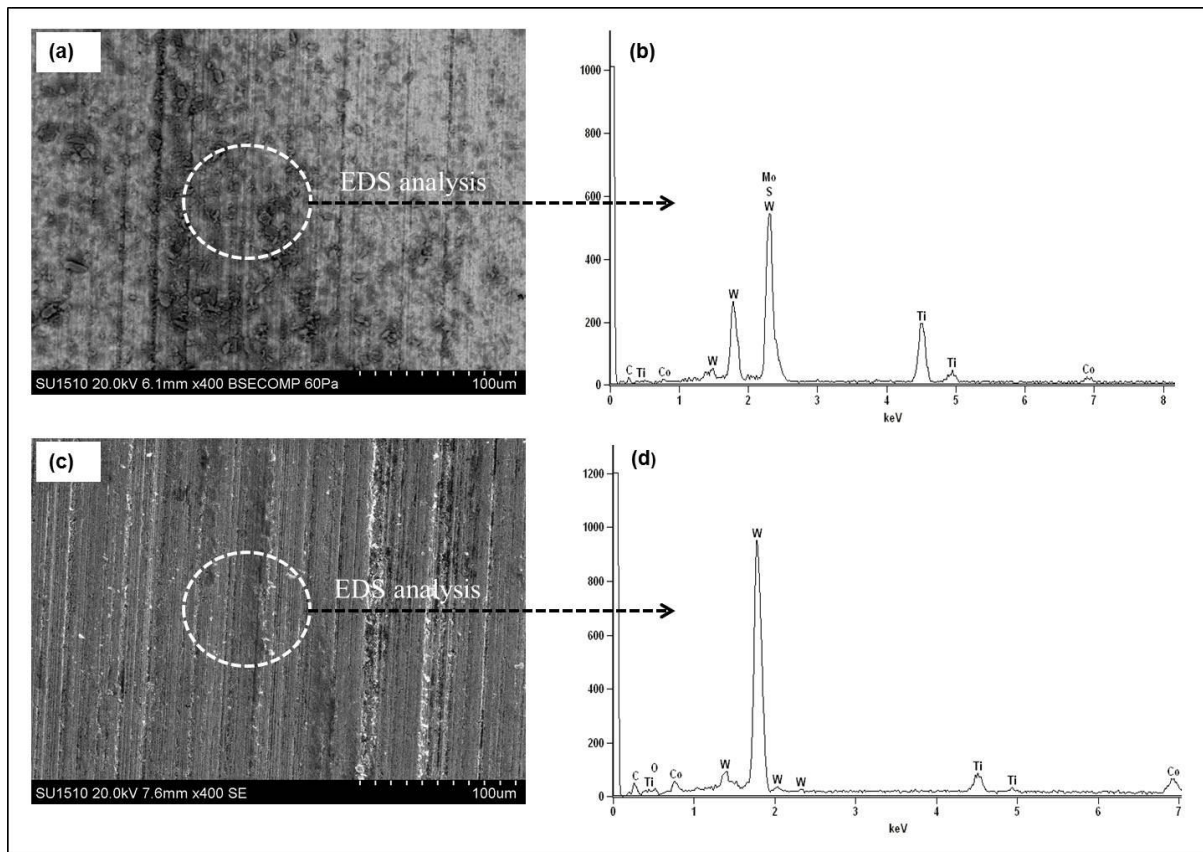
sliding conditions, testing environments, specimen coating thickness and coating deposition methods employed. Further, in this study, results prove that the specimen wear volume is linear against the product of normal load applied and sliding distance satisfying Archard's approach, i.e., mechanism of wear loss can be considered as linear as the function of mechanical energy given into sliding contact. The lower wear rate with tribopair-2 is possibly due to the existence of MoS<sub>2</sub> coating on the specimen, which plays as lubricating additive between rubbing parts and can control the adhesion of workmaterial to specimen thereby reduce wear as a result of lesser frictional forces.

The wear characteristics of the samples have been substantiated through the observed features of worn surfaces. SEM and EDS results of the pin contact surfaces in tribopair-1 during specified normal load are shown in Fig. 4.14. From Fig. 4.14 (a), it is seen that there are a number of abrasive scratches present due to mechanical plowing on the contact surface. From EDS examinations (Fig. 4.14 (b)), at low sliding speeds, wear particle transfer from disc material to pin contact surface was found to be about 21.6% by weight, while at high sliding speeds more particle transfer about 36.97% by weight is seen (Fig. 4.14 (d)). The increased in the wear growth is related to the production rate of the wear particles from disc material and centrifugal force acting on them. The sliding speed increases, the transfer rate of the wear particles would be expected to increase and the number of wear particles pass through the contacting surfaces increases. As the number of wear particles increases, the effect of frictional force in dry sliding can be attributed to the corresponding contact of the asperities which can largely influence the frictional results. This explanation is consistent with the EDS observations made on the pin worn surfaces which indicate that at higher sliding speeds the transfer of wear particles is more toward the pin contact surface. Therefore, more energy dissipated by friction (about 35%, see Fig. 4.10) in the sliding contact was seen, which resulted in abrasion of pin contact surfaces (Fig. 4.14 (c)).



**Fig. 4.14.** SEM images and EDS observations on the specimen surfaces in tribopair-1 at applied load of 60 N: **(a)** worn surface at sliding speed of 100 m/min, **(b)** EDS chemical composition on the worn surface corresponding to (a), **(c)** worn surface at sliding speed of 200 m/min, and **(d)** EDS chemical composition on the worn surface corresponding to (c).

The SEM and EDS observations of the worn surface of EMSL coated specimen in tribopair-2 at particular applied load are presented in Fig. 4.15. At lower sliding speeds, the damage is seen as mild abrasive wear (Fig. 4.15 (a)) due to the presence of MoS<sub>2</sub> solid lubricant particles on the specimen, which has almost transferred to sliding contact and acted as the lubricant in preventing the wear of the contact surfaces. The EDS chemical composition analysis on the specimen worn surface (Fig. 4.15 (b)) confirms Mo and S elements (40% by weight) and W, C and Co elements (35% by weight) and the adhered Ti elements (25% by weight).

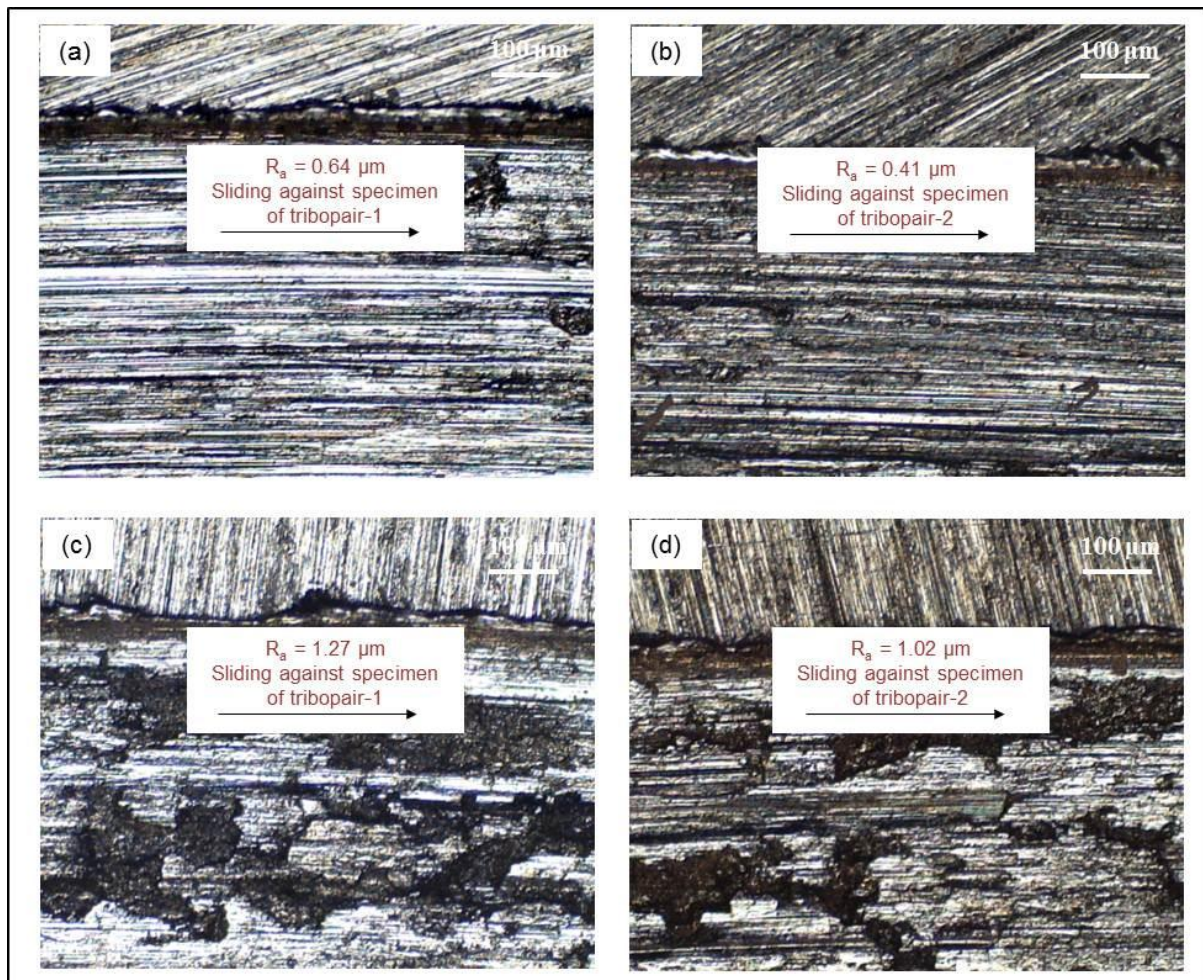


**Fig. 4.15.** SEM images and EDS observations on the specimen surfaces in tribopair-2 at applied load of 60 N: **(a)** worn surface at sliding speed of 100 m/min, **(b)** EDS chemical composition on the worn surface corresponding to (a), **(c)** worn surface at sliding speed of 200 m/min, and **(d)** EDS chemical composition on the worn surface corresponding to (c).

The presence of coating elements on the contact surfaces was responsible for lower frictional values as shown in Fig. 4.8. At higher sliding speeds, the deposited solid lubricant coating has entirely wiped out from the specimen, and the sliding wear appears to occur on the specimen (Fig. 4.15 (c)). The EDS chemical composition analysis on the worn surface of specimen (Fig. 4.15 (d)) confirms W, C and Co elements (90% by weight) and the adhered Ti elements (10% by weight), while Mo and S elements of the coating were not seen on the worn surface. In these conditions, there is no much considerable difference in observed wear mechanisms.

To assess the influence of applied load on the surface roughness of counter material, surface profiles of the worn surfaces were examined by using optical microscopy. The microscopic examination on the worn surfaces Ti-6Al-4V alloy disc under different normal loads is shown in Fig. 4.16. Results indicate that the quality of surface finish ( $R_a$ ) values on the disc surface differ greatly in tribopair-1 as compared to that of tribopair-2. It can be seen that at lower loads, contact of the asperities is less and results in plowing, thus increasing the coefficient of friction, while  $\text{MoS}_2$  solid lubricant presence on the specimen reduces it to further extent. When the normal load progresses, surface roughing and a large quantity of wear debris generated on the contact surfaces reduces the severity of the plowing, which results in marginal changes in the coefficient of friction, while  $\text{MoS}_2$  solid lubricant reduces it to further level. This is evident from the observation of depth of wear tracks on worn Ti-6Al-4V alloy discs in two tested tribopairs.

From Fig. 4.16 it was observed that the wear scar depths on the counter material surface produced during sliding against EMSL coated and uncoated specimens show that the damage of the counter material surface in tribopair-2 was the lowest, while the largest wear scars were present on the counter material surface in the case of tribopair-1. The maximum wear scars in tribopair-1 counter material surface is related to the increase of scratches as the result of mechanical plowing action since as there is no lubricating film to protect the contact surfaces from the wear loss.



**Fig. 4.16.** Wear tracks and surface finish on counterpart against uncoated and EMSL coated specimens at sliding speed of 150 m/min at different loads: **(a)-(b)** 40 N, and **(c)-(d)** 80 N.

#### 4.4. Summary

The performance of EMSL coating, MoS<sub>2</sub> as a potential solid lubricant onto tribological components, was investigated over a wide range of sliding conditions. EMSL coatings have a high tendency in adhering to the tool substrate and demonstrate the benefits in curtailing the contact frictional effects, enhancing wear resistance and contribute to the favorable control of heat generation at the sliding contact. The critical load on the electrostatically deposited MoS<sub>2</sub> coating found to be quite favorable with a reported critical contact pressure of existing MoS<sub>2</sub> coatings prepared by sputtering deposition process. Further, SEM and optical

microscopy analysis were conducted in order to see the wear behavior of worn surfaces. The results confirm that the specimens in tribopair-2 reveal the superior friction behavior to that of tribopair-1 under the same tested conditions. The positive results of tribopair-2 are owing to the inherent low shear strength of lamellar structured MoS<sub>2</sub> solid lubricant, which can transfer to the track on the disc surface during sliding and contribute to the lower frictional forces. In both the tribological pairs, the wear volume of the specimen is linear and satisfying the Archard's wear law and directly dependent on the mechanical energy dissipated in the sliding contact. Wear rate values of the EMSL coatings in this study are in reasonable agreement with the results presented in previous studies. The high material removal from the disc surface in tribopair-1 is attributed to mechanical plowing action which resulted in high friction between the opposing surfaces and considerable plastic deformation of asperities caused during sliding motion.

Apart from the tribological performance assessment, the level of success of MoS<sub>2</sub> solid lubricant coating prepared by electrostatic deposition process was also analyzed by carrying machining studies over a large cutting condition. The performance of EMSL coated cutting tool on machinability parameters like cutting force, cutting temperature, tool wear, shear angle and quality of machined surface during machining process was comprehensively presented in chapter 5.



# CHAPTER 5

## EXPERIMENTAL INVESTIGATION TO STUDY THE EFFECT OF EMSL COATED TOOLS ON MACHINABILITY PARAMETERS

---

As described in chapter 4, the experimental findings from tribological tests could herald widespread advantages of EMSL coatings within the practical experimental domain. In order to implement and find EMSL coating use in machining applications, studies must be done on these coatings with the requirements and limits of a specific machining process. Hence, in the current chapter, a comprehensive experimental investigation has been carried out to exploit the efficacies of EMSL coated cutting tools on machinability parameters in comparison with the uncoated cutting tools during turning process. Chapter 5 is organized as follows: Section 5.1 presents the brief information about metal machining process. Section 5.2 presents the materials and cutting conditions used in machining experiments. Section 5.3 presents the machining performance of EMSL coated cutting tools in terms of cutting forces, tool wear, chip formation and surface finish of machined workmaterial over a broad experimental domain. Finally, Section 5.4 presents the overall summary of this chapter.

### 5.1. Introduction

Machining operation is one of the most important and widely used material removal techniques in manufacturing industries. Machining performance through improved machinability parameters has long been recognized as they have considerable impact on the productivity, product quality and overall economy. Machinability of a material provides an indication of its adaptability to be manufactured by a machining process. The influence of heat generation and frictional effects on contact surfaces during machining process becomes subject of concern due to its influence on machining efficiency and quality of machined

workmaterial. Effective lubrication in machining is essential to safeguard friction and temperature levels do not become excessive. Cutting fluids have extensively been used for controlling the above effects in conventional machining processes, raising however, severe environmental and economic panics [1,2,165]. Further, the cutting fluid application is not biological friendly and also its negative effect which it destructs environment. As a result, the growing demand to achieve sustainable machining objectives, i.e., societal demands (cleaner, healthier and safer machining) is going to entail the use of alternative machining approaches to avoid or limit the consumption rates of cutting fluids [28,166-169].

Effective countermeasures without the use of cutting fluid (dry cutting) in control of the frictional and temperature effects at tool-work contact are strongly required. It is believed that any change in the contact conditions, as a means of better control over frictional interaction, result in a change in the tool-chip contact and mechanics of machining, thereby influencing the contact temperatures, tool wear, cutting forces and energy consumption [1,165]. This change is coupled with the requirement of improvement in cutting tool designs and tribological properties. Such improvement on cutting tools can be achieved in three different routes: (i) by using new cutting tool materials, (ii) by adapting new cutting tool geometries, and (iii) by applying hard and/or soft lubricant material coatings on cutting tools. Among these possible strategies, the assistance of solid lubricant as one of the self-lubricating alternative materials on cutting tool in current metal cutting practices has received recent attention because the solid lubricant is a safe, clean and non-toxic that requires no expensive discard and can significantly enhance the machining process performance.

In this context, in search of economical and environmentally compatible lubrication approach for machining operation, and to look into the feasibility of new coating materials and methods, the current research work introduces a new approach, i.e. machining with novel coated cutting tool, namely, electrostatic micro-solid lubricant (EMSL) coated cutting tool



(MoS<sub>2</sub> as solid lubricant). To endorse the performance of developed coated cutting tools, turning experiments were conducted at different cutting conditions and results in terms of cutting forces, tool wear, chip formation and surface finish of machined workmaterial are compared with that of uncoated cutting tools.

## **5.2. Material and machining tests**

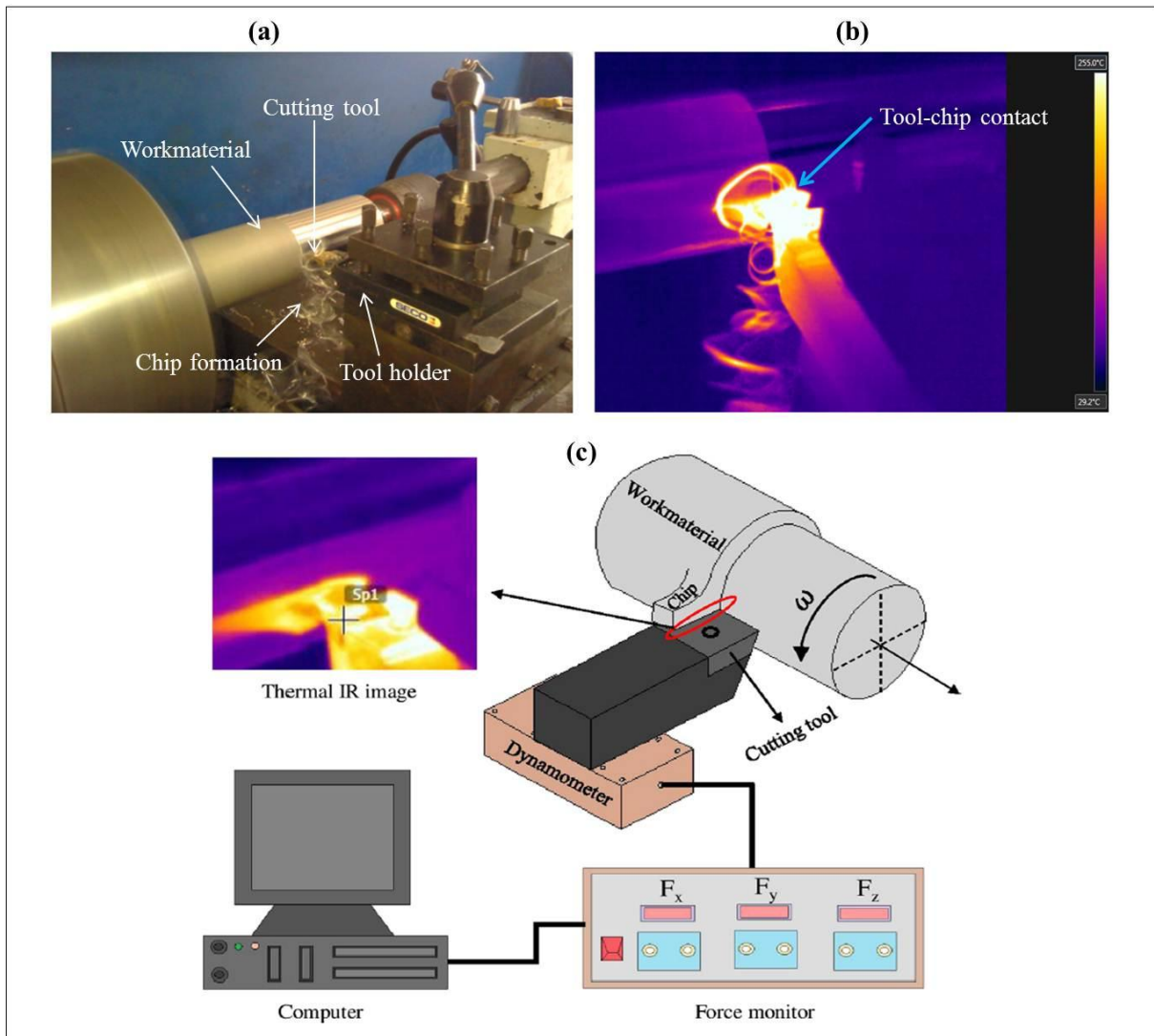
The material and experimental condition used in turning tests are presented in Table 5.1. The workmaterial chosen in the current study is high strength aluminum alloy, AA7075-T6. This material has drawn a great attention in the fabrication of structural components used in transport applications including marine, automotive and aviation due to its low cost and outstanding physical and mechanical properties. Further, low density, good plasticity, resistance to corrosion, heat-treatable properties, high strength-to-weight ratio and machinability comparable to many metals makes AA7075-T6 very attractive to use by manufacturers, engineers and researchers. The composition and element limits for the material was chosen according to the requirements of standards.

The turning experiments were performed on a commercial high precision lathe machine. Two different machining test environments were chosen are as follows: (i) machining with EMSL coated cutting tools (MoS<sub>2</sub> as solid lubricant), and (ii) machining with uncoated cutting tools. Each experiment was repeated for three times at every cutting condition and the average of three measurements was used to represent the performance parameters such as cutting forces, tool wear, chip thickness and surface finish of machined workmaterial. After completion of each experiment under specified cutting condition, surface finish on the machined workmaterial was measured using a surface profilometer (Taylor Hobson Surtronic S25). The cutting force and feed force were measured with the help of strain gauge dynamometer. The chip thickness and tool wear of cutting tools were analyzed using tool

maker's microscope (Olympus STM6) and scanning electron microscope (SEM) (Hitachi, SU-1510). Cutting temperatures at the tool-chip interface were measured with the help of a thermal infrared (IR) imaging camera (FLIR E60) with 320 x 240 pixels having thermal sensitivity less than 0.05°C at 30°C. A photograph and a schematic view of the experimental setup used for measuring cutting force and cutting temperature are shown in Fig. 5.1.

**Table 5.1.** Material and experimental conditions adopted in machining tests.

<p><i>Workmaterial:</i> AA7075-T6 aluminum alloy</p>
<p><i>Workmaterial size:</i> Diameter = 50 to 65 mm and length = 500 to 600 mm</p>
<p><i>Cutting conditions:</i> Series 1: Cutting speed (<math>v_c</math>) = 150, 175, 200, 225, 250 m/min, feed (<math>f</math>) = 0.2 mm/rev and depth of cut (<math>a_p</math>) = 2 mm Series 2: Varying cutting speed, feed and depth of cut Machining time for each test = 15 min</p>
<p><i>Machining test environments:</i> (i) Machining with EMSL coated cutting tools, and (ii) Machining with uncoated cutting tools</p>
<p><i>Cutting tool and tool geometry:</i> Carbide tool (P-30 grade, grain size 1.4 <math>\mu</math>m), rake angle (<math>\gamma</math>) = -6°, clearance angle (<math>\alpha</math>) = 6°, and nose radius (<math>r_e</math>) = 0.8 mm</p>
<p><i>Cutting force measurement:</i> Strain gauge dynamometer</p>
<p><i>Cutting temperatures (at the tool-chip interface) measurement:</i> Thermal infrared (IR) imaging camera</p>
<p><i>Chip thickness and tool wear measurement:</i> Tool maker's microscope (Olympus STM6) and Scanning electron microscope (SEM) equipped with energy dispersive spectroscopy (EDS) (Hitachi, SU-1510)</p>
<p><i>Surface roughness measurement:</i> Surface profilometer (Taylor Hobson Surtronic S25)</p>



**Fig. 5.1.** (a) Turning experiments using a high precision lathe, (b) a sample of thermal infrared image captured at tool-chip contact, and (c) a schematic view of the experimental setup.

### 5.3. Results and discussion

Machining process efficiency directly relies on the ability of cutting tool in arresting the frictional influences, cutting temperature, tool wear, cutting force and energy consumption during cutting process and ensuring them do not become unwarranted. Further, these parameters are very important as an indicator in order to verify the predictive capability of the FE machining model (detailed explanation is presented in chapter 6), and suggest how to

modify the model if the predictions are not accurate. Thus, in order to assess the performance of the EMSL coated cutting tool, an attempt has been made in comprehending the above said parameters during turning process.

### **5.3.1. Cutting forces**

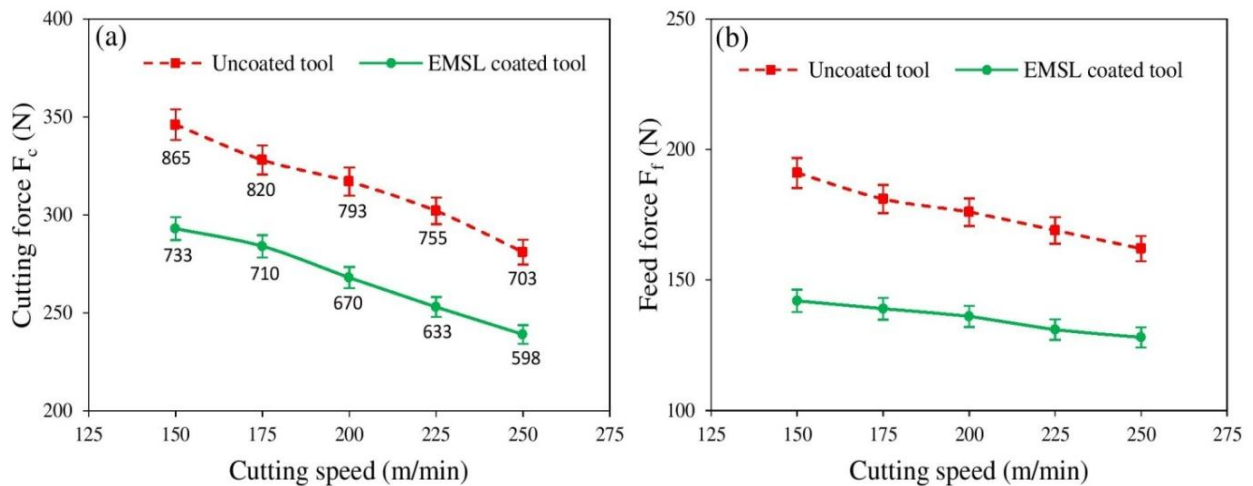
The compressive and frictional contact stresses on the cutting tool result in a substantial cutting force. Knowledge of the cutting force is essential as it has a great effect on the dynamics of the machining process. Further, compared with other machinability parameters, study of cutting force in machining process is essential in design of mechanical structure of cutting machine, estimation of power consumed during machining process, selection of cutting parameters to avoid an excessive distortion of the workpiece, to predict the cutting tool life and enhance the productivity.

There are several parameters which affect the cutting forces. These include cutting tool variables (tool geometry and tool material), workmaterial variables (hardness and mechanical properties), cutting conditions (speed, feed and depth of cut) and the type of lubrication (cutting fluids and solid lubricants). Further, the heat generation at tool-work interface during machining process depends upon this cutting force and it is fundamentally important as far as the cutting temperature and surface quality of the products are concerned.

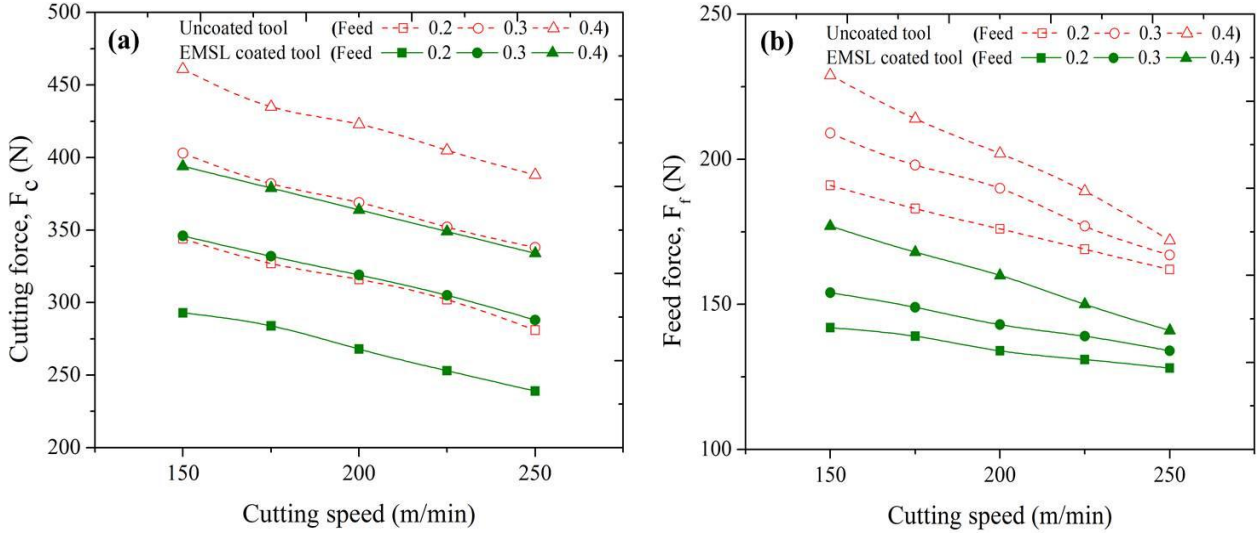
In the present work, during the machining process the cutting force ( $F_c$ ) and feed force ( $F_f$ ) are measured in the direction parallel and perpendicular to the relative velocity of the cutting tool and workmaterial. In both the machining environments, the effect of cutting speed on cutting force and feed force in turning of AA7075-T6 workmaterial with and without coated cutting tools at different cutting speeds was presented in Fig. 5.2.

The effect of cutting speed on cutting forces and feed forces under varying feed conditions is presented in Fig. 5.3. For a given value of cutting speed, cutting and feed force

increases with increasing feed. For a given feed rate, cutting and the feed forces are decreases with increasing cutting speed. Further, it was observed that the cutting speeds were found to have a significant effect on the forces. In both the machining, i.e. machining with coated tool and machining with uncoated tool, forces decreases when the cutting speed increases; while variation in these forces during machining with EMSL coated cutting tools seems to be quite steady and is lesser as compared to those forces found during machining with uncoated cutting tools. The performance of the EMSL coated cutting tool is the most obvious and was reduced the cutting forces by on average of about 15-18% in all tested cutting conditions. This is due to the fact that as the presence of MoS<sub>2</sub> solid lubricant in EMSL coating exists on cutting tool face, the friction on the tool-chip interface zone is reduced and thus the cutting force is reduced.



**Fig. 5.2.** (a) Cutting forces with induced specific cutting energy, ' $u_s$ ' (N/mm<sup>2</sup>) (see data point values), and (b) feed forces, measured during machining with and without coated cutting tools ( $f = 0.2$  mm/rev and  $a_p = 2$  mm).



**Fig. 5.3.** (a) Cutting forces, and (b) feed forces, measured during machining with and without coated cutting tools at different cutting speeds and feed rates ( $a_p = 2$  mm).

Measured horizontal force (cutting force) and vertical force (feed force) on the tool rake face are usually transformed in the direction of primary motion and feed motion, i.e. to the normal force ( $N$ ) and friction force ( $F$ ) in orthogonal cutting. Based on the geometric parameters of orthogonal cutting, the average coefficient of friction ( $\mu$ ) between the tool and chip is calculated using the following Eq.5.1.

$$\mu = \frac{F}{N} = \tan\beta = \frac{F_f + F_c \tan\gamma}{F_c - F_f \tan\gamma} \quad (5.1)$$

where, ' $F_c$ ' is the cutting force (N), ' $F_f$ ' is the feed force (N) ' $\beta$ ' is the friction angle, and ' $\gamma$ ' is the rake angle.

The specific cutting energy, ' $u_s$ ' (N/mm<sup>2</sup>), which represents the energy consumed in removing a unit volume of workmaterial, is calculated from the following relation (Eq.5.2).

$$u_s = \frac{F_c}{a_p \times f} \quad (5.2)$$

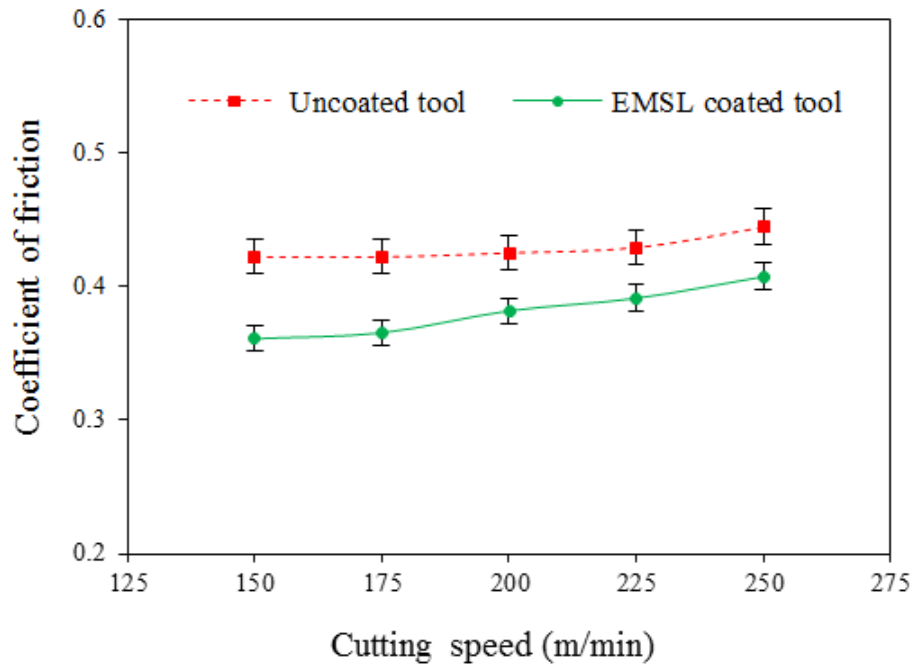
where,

$F_c$  = Cutting force (N)

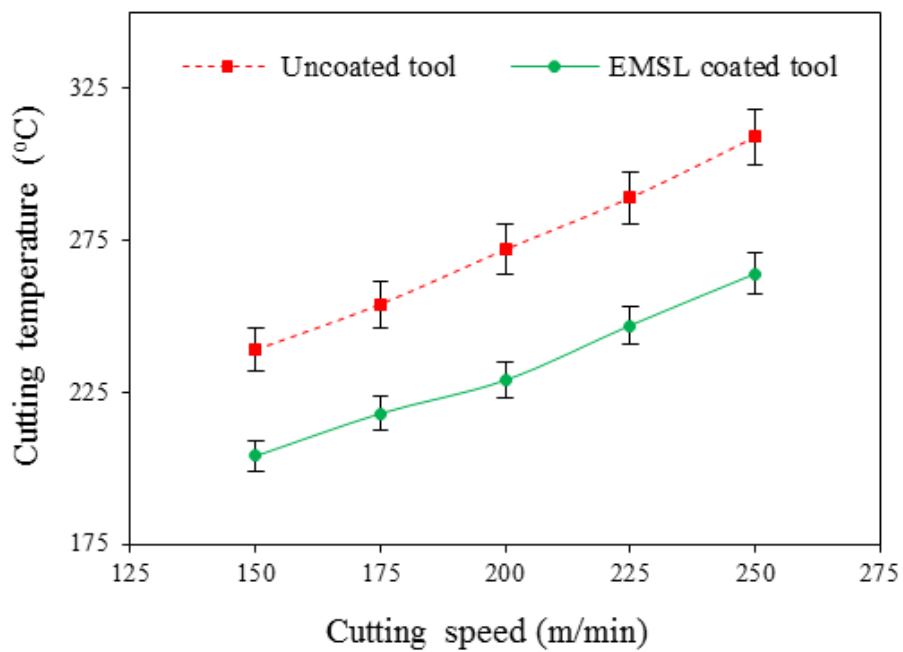
$f$  = Feed (mm/rev)

$a_p$  = Depth of cut (mm)

The effectiveness of EMSL coated cutting tool in minimizing the frictional effects at the tool-chip interface is evident from Fig. 5.4. The lower values of coefficient of friction (reduction by 14-16%) during machining with EMSL coated cutting tools in all the tested cutting conditions could be related to the two phenomena: (i) decrease in specific cutting energy in the tool-work interface (see Fig. 5.2 (a)), and (ii) lower tool-work contact cutting temperatures (Fig. 5.5) due to presence of MoS<sub>2</sub> solid lubricant in EMSL coating. In the first case, one can see that the reduction in the specific cutting energy induces the lower cutting forces with EMSL coatings due to the existence of MoS<sub>2</sub> solid lubricant on cutting tool face and its easy shearing action between chip-tool rake face, which may contribute to the decrease of the coefficient of friction. In both the machining environments, i.e. when machining with uncoated cutting tool and machining with coated cutting tool at given feed, cutting temperature increases with increasing cutting speed. Further, the decrease in cutting temperatures (reduction by 14-18%) at all cutting speeds when the EMSL coated cutting tool is used is directly dependent on the presence of self-lubricant MoS<sub>2</sub> coating on cutting tools, which was transferred and acted as lubricating additive between the tool-chip-work interfaces.



**Fig. 5.4.** Coefficient of friction calculated during machining with and without coated cutting tools at different cutting speeds ( $f = 0.2$  mm/rev and  $a_p = 2$  mm).



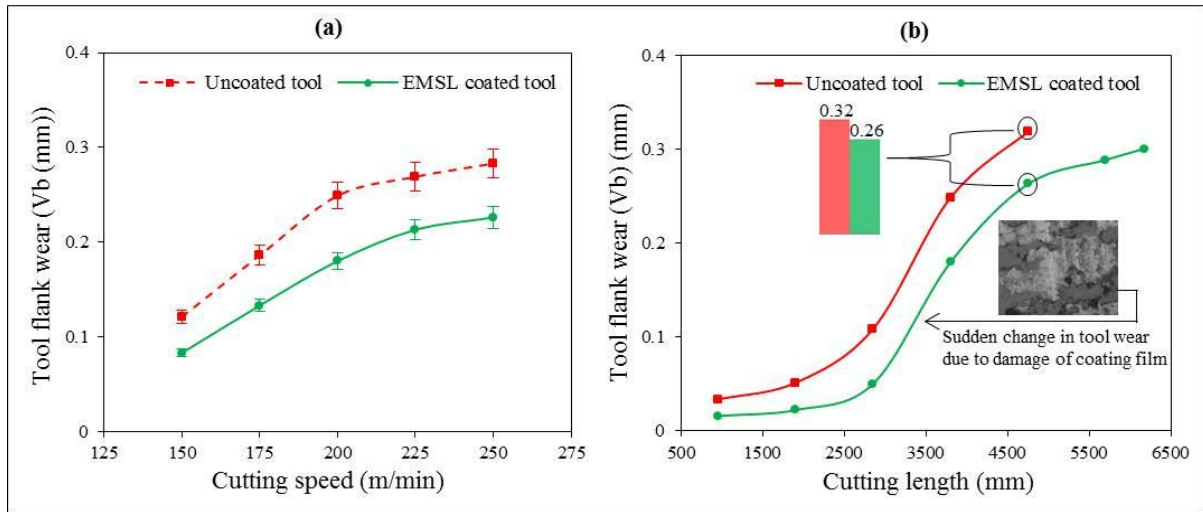
**Fig. 5.5.** Cutting temperatures measured during machining with and without coated cutting tools at different cutting speeds ( $f = 0.2$  mm/rev and  $a_p = 2$  mm).



### 5.3.2. Tool flank wear

Flank wear occurs on the cutting tool flank face as a result of rubbing of the cutting tool with workpiece at the tool-work contact interface. Tool flank wear appears in the form of wear land and is measured by the width of this wear land,  $V_b$ . Tool flank wear is a time dependent process. In the present work, the flank wear of cutting tools in both the machining i.e. machining with uncoated cutting tool and machining with coated cutting tool at different cutting speeds and wear growth at particular cutting condition as the function of cutting length is shown in Fig. 5.6. From results, it is indicated that the tool flank wear of both coated and uncoated cutting tool was increased steadily with increase in cutting speed at all tested conditions (Fig. 5.6 (a)). However, EMSL coated cutting tools exhibited much superior ability in maintaining the wear resistance during the entire tool life than that of the uncoated cutting tool (Fig. 5.6 (b)).

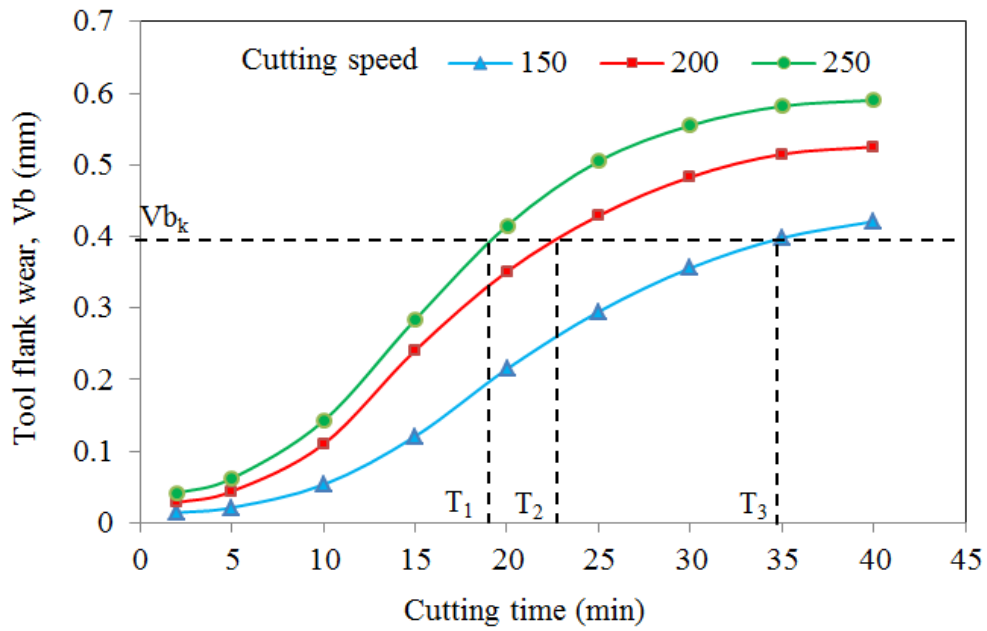
Results reveal that within the tested experimental conditions, it is almost on average of about 25% less tool flank wear occurred with EMSL coated cutting tools when compared to that of uncoated cutting tools. This can be due to the following tendency: (i) decrease in the specific cutting energy on average of about 15% (Fig. 5.2 (a)) due to the presence of  $\text{MoS}_2$  solid lubricant film on the tool face, and (ii) decrease in tool-work contact cutting temperatures on average by 14-18% (Fig. 5.5) in all tested conditions owing to transfer of self-lubricant,  $\text{MoS}_2$  film to the tool-work interface. Therefore, it implies that EMSL coated cutting tool with  $\text{MoS}_2$  as a solid lubricant can work effectively as a self-lubricating cutting tool in machining process. In this study, the flank wear results on the uncoated carbide tool insert found to be more or less nearer to the results found in previous studies [170]. The observed differences in tool flank wear values could be due to the differences in selected cutting conditions and testing environments.



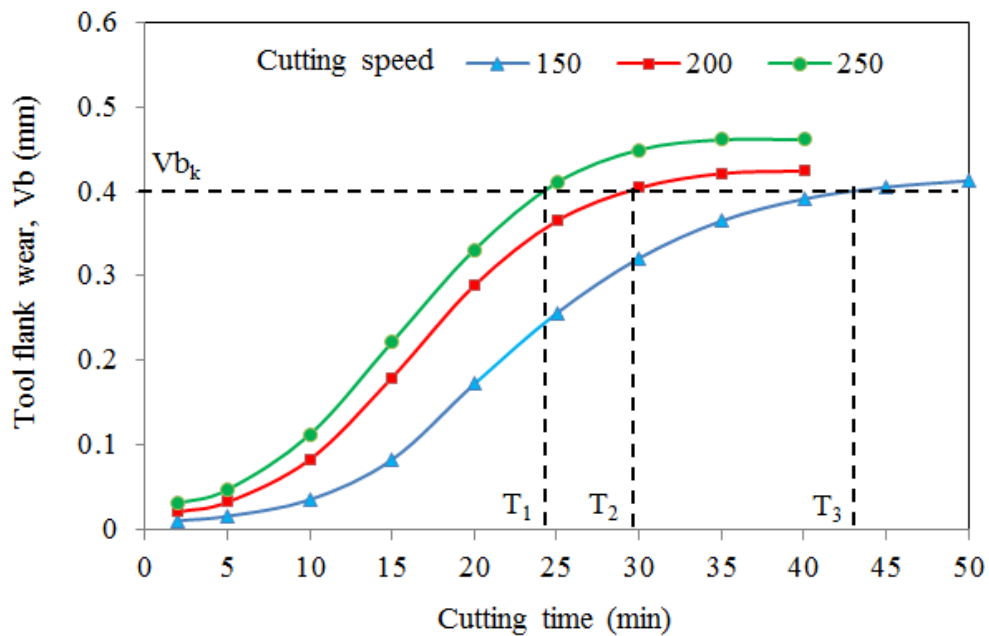
**Fig. 5.6.** (a) Comparison of tool flank wear at different cutting speeds, and (b) wear growth at particular cutting speed (200 m/min) against cutting length in machining with and without coated cutting tools.

Generally, in machining process as the cutting speed increases, the amount of tool wear increases gradually. But the tool wear must not be allowed to reach beyond a certain level in order to avoid tool failure. If the amount of tool flank wear exceeds some critical level ( $V_b > 0.3\sim 0.5$  mm), the excessive cutting force may cause the tool failure. The safe level of this value is referred to as allowable wear land (wear criterion),  $V_{b_k}$ . The cutting time required for the cutting tool to reach a flank wear land of width  $V_{b_k}$  is called tool life,  $T$ , a vital parameter in understanding machining process performance [171].

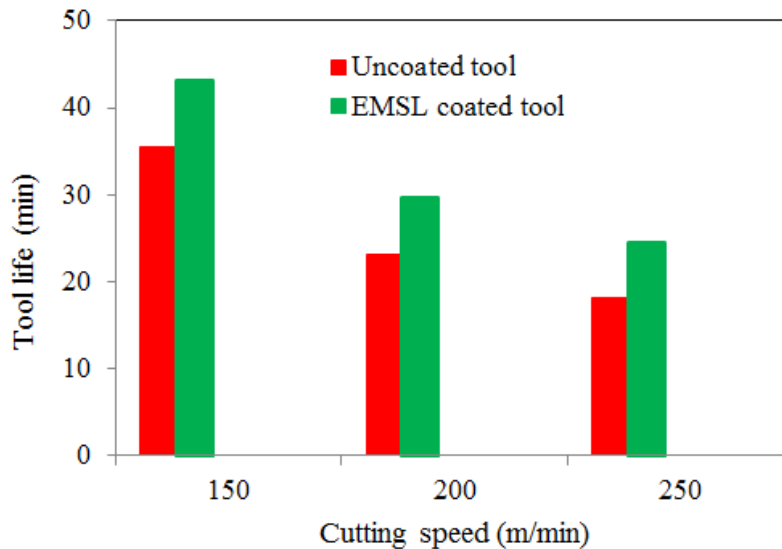
In the present study, from the experimental results it is noticed that the cutting speed is the most important parameter in evaluating the cutting tool life. As the cutting speed is increased, tool wear increases and wear criterion is reached, i.e., tool life decreases with cutting speed. This can be clearly seen for both the uncoated and EMSL coated cutting tools from the Fig. 5.7 and Fig. 5.8 respectively. It has been observed from these figures that the tool life can be greatly enhanced (25-30%) with EMSL coated cutting tool when compared to that of uncoated one (Fig. 5.9) due to the presence of  $\text{MoS}_2$  solid lubricant on cutting tool.



**Fig. 5.7.** Effect of cutting speed on the allowable wear limit and tool life at different cutting speeds when machining with uncoated cutting tool.



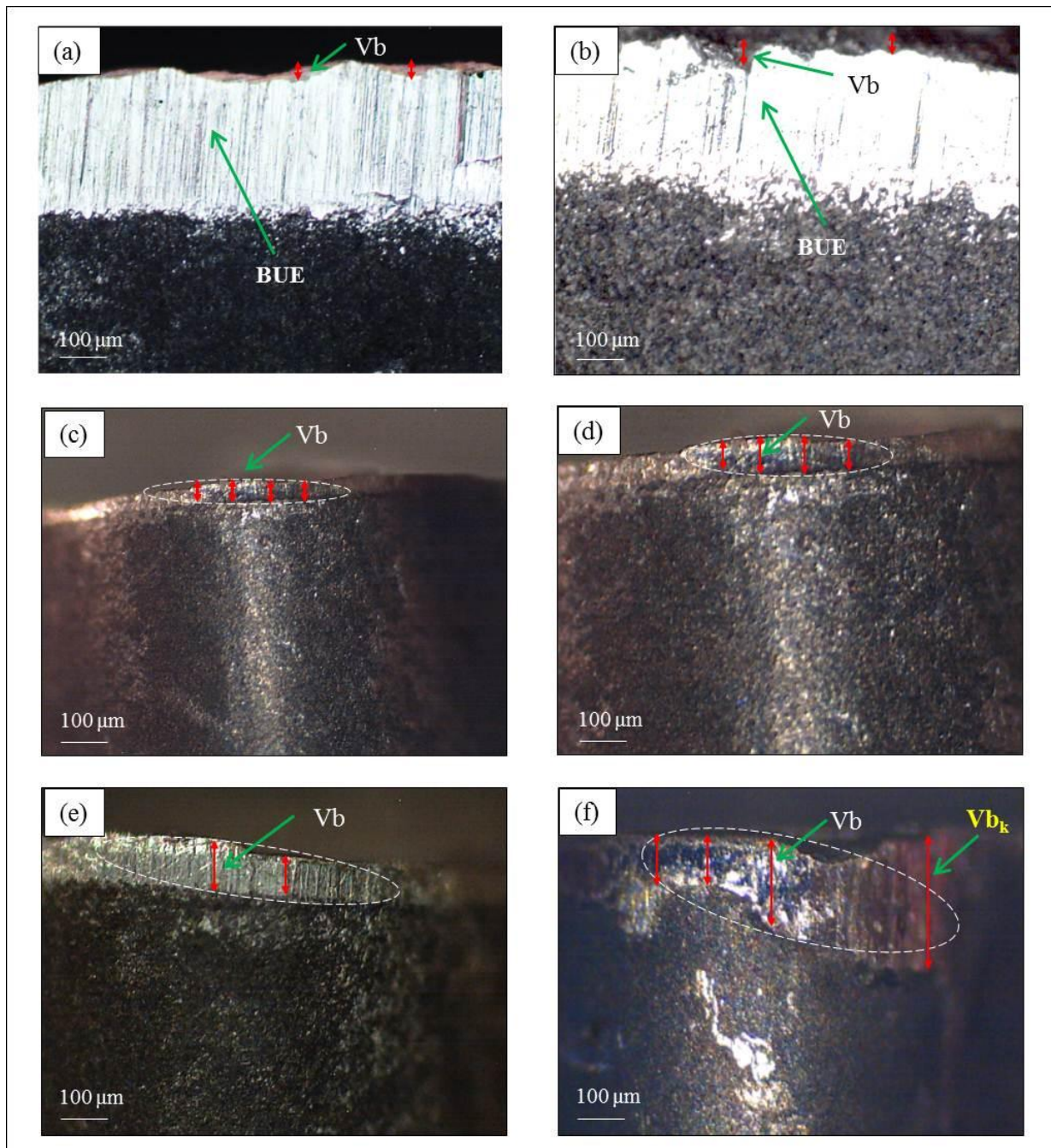
**Fig. 5.8.** Effect of cutting speed on the allowable wear limit and tool life at different cutting speeds when machining with EMSL coated cutting tool.



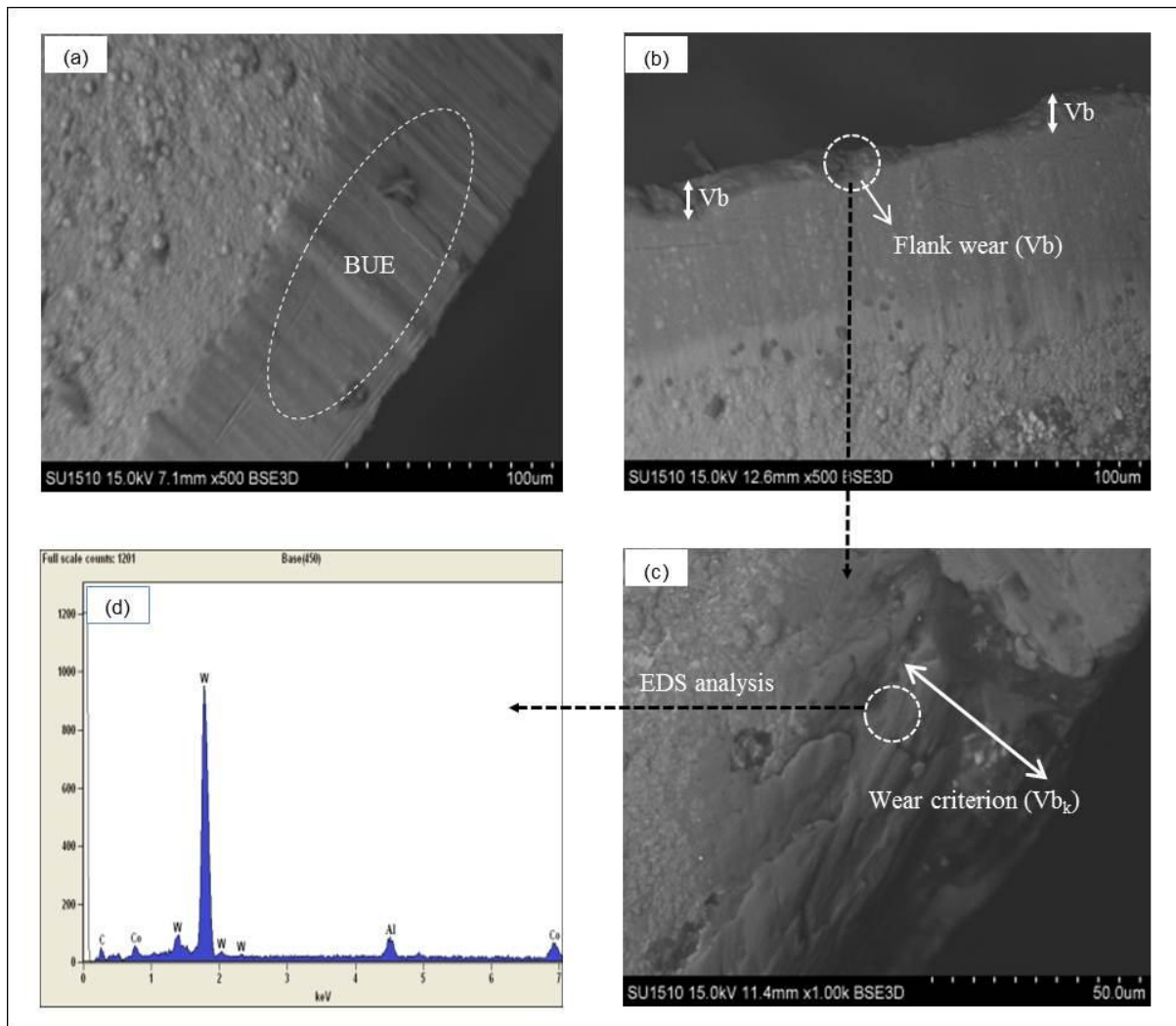
**Fig. 5.9.** Tool life comparison for both the uncoated and EMSL coated cutting tool at different cutting speeds.

The wear characteristics of the cutting tools have been substantiated and scientifically observed through the features of worn surfaces. Fig. 5.10 shows the optical micrograph of wear surfaces of the uncoated cutting tools used in turning of workmaterial at different cutting speeds. Fig. 5.11 presents the SEM micrographs of worn surfaces of coated cutting tools used in turning of workmaterial at particular cutting conditions. Examinations of the worn surfaces of both uncoated and coated cutting tools revealed that the built up edge (BUE) on the cutting edge was predominant at lower cutting speeds. This could be mainly due to adhesion of the machined workmaterial on the cutting tool surface. With high plastic deformability due to large shear strains within the primary shear zone, aluminum alloy has a high tendency to adhere with the cutting tool material and result in high BUE. The presence of MoS<sub>2</sub> solid lubricant in EMSL coating on cutting tool further lowers the tool-work contact cutting temperatures and as a result in very less BUE. The EDS chemical composition analysis on the worn surface of the coated cutting tool (Fig. 5.11 (d)) is an indication for the

above and confirms no self-lubricating material elements on the worn surface at relatively high cutting speed.



**Fig. 5.10.** Built up edge (BUE) formation, tool flank wear ( $V_b$ ) and allowable wear land (wear criterion,  $V_{b_k}$ ) on the cutting edge of uncoated cutting tool at different cutting speeds ( $f = 0.2$  mm/rev,  $a_p = 2$  mm): (a) 150 m/min, (b) 175 m/min, (c) 200 m/min, (d) 225 m/min, (e) 250 m/min, and (f) 300 m/min.




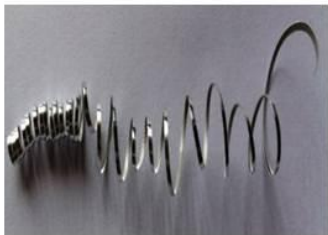
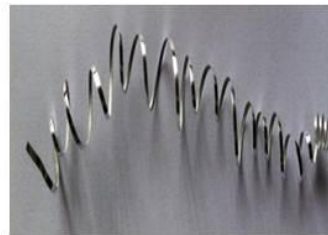



**Fig. 5.11.** (a) BUE formation on the tool cutting edge at 150 m/min speed, (b) flank wear on the tool surface at speed 200 m/min, (c) magnified view corresponding to (b), and (d) EDS chemical composition analysis on the worn surface corresponding to (c) during machining with EMSL coated cutting tools ( $f = 0.2$  mm/rev and  $a_p = 2$  mm).

### 5.3.3. Chip formation

The form of chip produced in a machining process is one of the most important parameters as it influences the surface finish of machined workmaterial and tool life thereby affecting productivity and product quality. Hence, the production of an acceptable form of chip is essential in metal machining. According to ISO 3685 standard, chip shapes during a

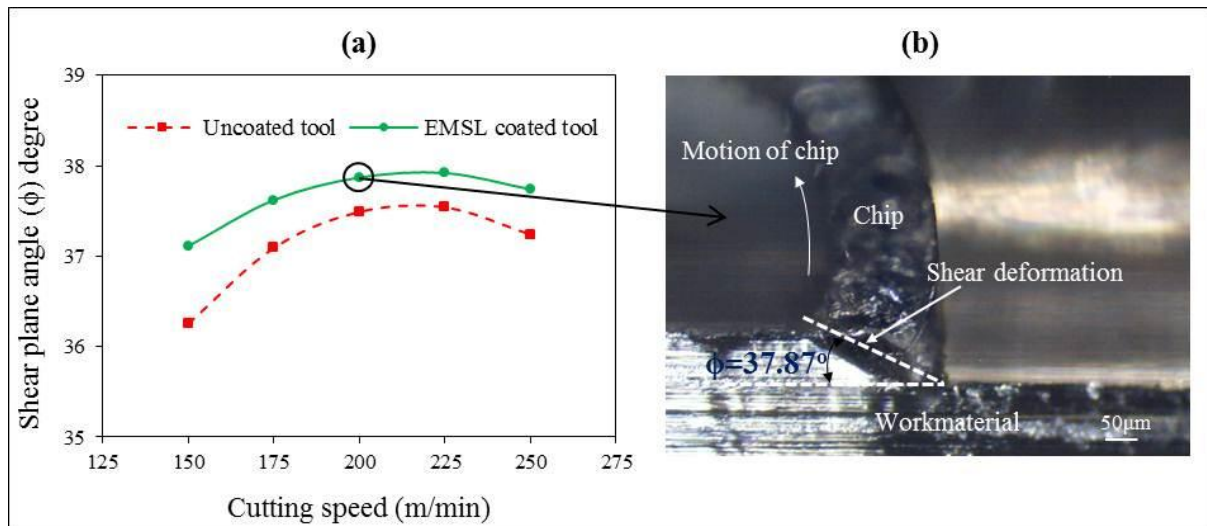


machining process can be classified into several types, which can be either in acceptable form or unacceptable form. Acceptable chip forms (short tubular, washer type, spiral and arc shape) can move easily from the machining zone and do not interfere the machined surface quality. In contrary, unacceptable chips (ribbon, tangled and needle type), can influence the quality of the machined surface as they tend to tangle around the tool and the workpiece and pose safety problems to operators. In the present work, some of the chip shapes obtained during machining of AA7075-T6 workmaterial with uncoated and EMSL coated cutting tools under different cutting conditions is shown in Fig. 5.12.

Cutting Speed (m/min)	Uncoated tool	EMSL coated tool
150	 <p>Snarled</p>	 <p>Washer-type helical (snarled)</p>
200	 <p>Washer-type helical (snarled)</p>	 <p>Washer-type helical (long)</p>
250	 <p>Elemental</p>	 <p>Conical (helical)</p>

**Fig. 5.12.** Comparison of chip shapes during machining of AA7075-T6 with and without coated cutting tools ( $f = 0.2$  mm/rev and  $a_p = 2$  mm).

The chip reduction coefficient, which is calculated as the ratio of chip thickness to the uncut chip thickness, is the prime parameter in knowing the shear angle and determining the cutting process efficiency because it reveals the energy spent during plastic deformation of workmaterial. In the present study, the chip thickness and chip reduction coefficient during machining with uncoated and coated cutting tools were measured and found to be less in the case of machining with EMSL coated cutting tools (detailed results can be seen in chapter 6). This improvement is because of the high shear angle (Fig. 5.13 (a)) due to better lubrication by the presence of MoS<sub>2</sub> solid lubricant coating on the rake face of the cutting tool. The gap between the lines in Fig. 5.13 (a) is an indication for the above improvement. The chip formation showing shear deformation to form chip and its shear angle during machining with EMSL coated cutting tools was presented in Fig. 5.13 (b).

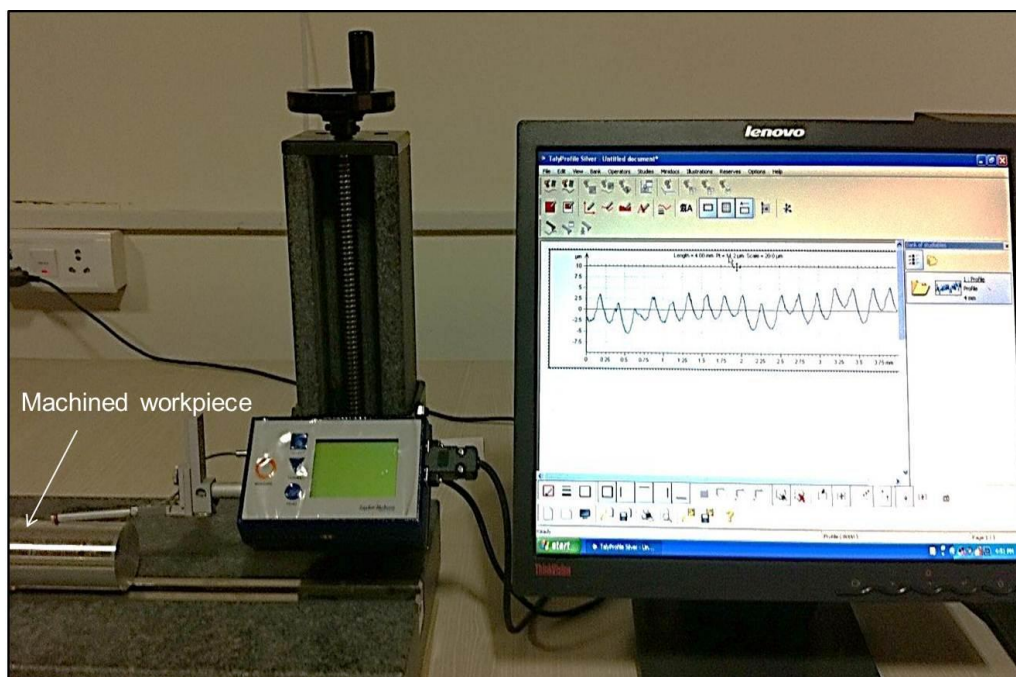


**Fig. 5.13.** (a) Variation of shear angle to form a chip at different cutting speeds, and (b) chip formation showing shear deformation (shear angle,  $\phi = 37.87^\circ$ ) corresponding to cutting speed of 200 m/min during machining with coated cutting tools (cutting conditions:  $f = 0.2$  mm/rev and  $a_p = 2$  mm).



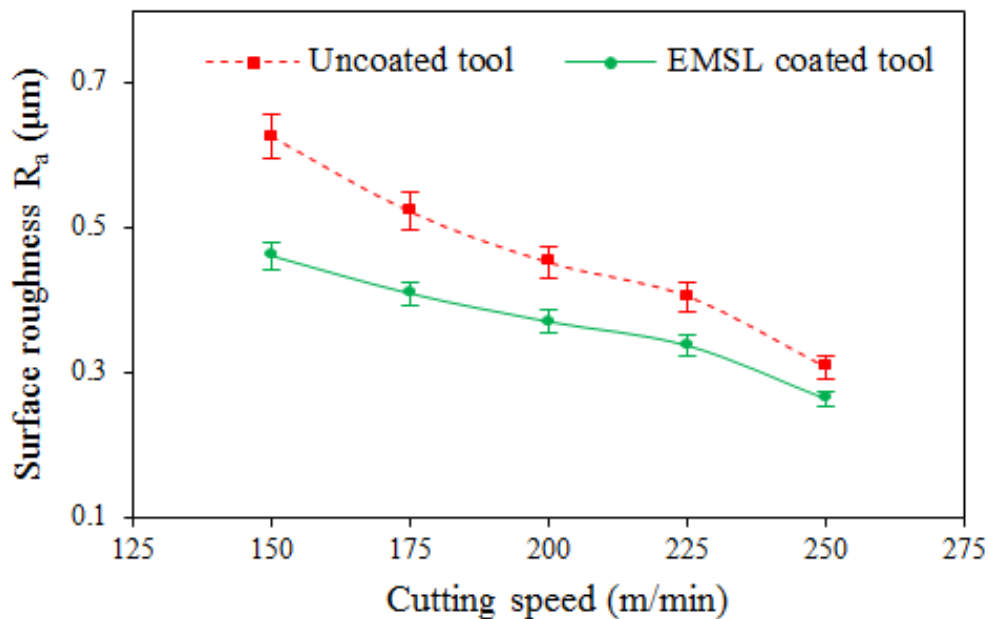
### 5.3.4. Surface roughness

Surface roughness ( $R_a$ ) is an important index not only in predicting the surface quality of machined workmaterial but also in influencing the performance of mechanical parts and production costs. The degradation of surface quality on the machined part often depends on the machining process performance, including selection of cutting conditions, lubricants and the effectiveness of the cutting tool materials. Any improvement in tool-workmaterial interaction by reducing the frictional effects on contact surfaces by proper selection of cutting tool material will affect the surface quality of machined workmaterial and as well as the tool performance to a greater level. In the present research work, an attempt was made to see the effectiveness of EMSL coated cutting tools on the quality of machined surface of workmaterial. A sample surface roughness measurement on workpiece using surface profilometer is shown in Fig. 5.14.



**Fig. 5.14.** A sample measure of surface finish on the machined workmaterial using surface profilometer (Taylor Hobson Surtronic S25).

Fig. 5.15 shows variations in the average surface roughness ( $R_a$ ) as a function of cutting speed during turning of AA7075-T6 workmaterial. It is observed that the measured values of surface roughness during machining with EMSL coated tools are always smaller and surface quality of workmaterial under this machining showed a much better improvement by 20% when compared to that of machining with uncoated cutting tool. This is expected because of the following two phenomena: (i) at higher cutting speeds the BUE on cutting tool surface turn out to be less, chip breakage decreases, and hence the quality of machined workmaterial surface, and (ii) presence of  $\text{MoS}_2$  solid lubricant in EMSL coating on cutting tool can reduce cutting temperatures generated and prevents further tool wear progression. Surface roughness values in this study are found to be in the same trend as it can be seen in the previous work [170], where higher cutting speeds result in relatively easier material removal from the workpiece, resulting in a better surface finish on the machined workmaterial when machining with uncoated cutting tool.



**Fig. 5.15.** Surface roughness as a function of cutting speed during machining with and without coated cutting tools ( $f = 0.2$  mm/rev and  $a_p = 2$  mm).

### 5.3.4.1. Surface roughness under varying cutting conditions

In previous section (i.e. Section 5.3.4), the variation of surface roughness against cutting speed at constant feed and depth of cut condition is discussed. In this section, the plan of experiments is with an objective of relating the influence of the cutting speed, feed rate and depth of cut with surface roughness of machined workmaterial when machining with uncoated and coated cutting tool.

#### 5.3.4.1.1. Plan of experiments

In the present work, in order to see the influence of cutting process parameters on the quality of machined workmaterial surface, Taguchi design approach is employed in experimental plan. Taguchi orthogonal array,  $L_{27}(3^{13})$  is selected for conducting experiments, which is having 27 rows corresponding to the number of experiments and can accommodate up to 13 variables in 13 columns and requires 26 degrees of freedom (DoF). The number of levels used in experiments is 3. The machining process parameters (control factors) considered for the experiments were: (i) cutting speed ( $v_c$ ), (ii) feed ( $f$ ), and (iii) depth of cut ( $a_p$ ). Each process parameters has three levels, denoted with 1, 2, and 3. The number of trial experiments conducted with the 3 levels for each identified factors is illustrated in Table 5.2. Table 5.2 indicates the control factors and their levels used in machining experiments. The experimental results of surface roughness and corresponding S/N (signal to noise) ratios for the results obtained from Taguchi statistical approach are presented in Table 5.3. To ensure the repeatability and minimum error, each experiment was repeated for three times.

**Table 5.2.** Assignment of levels to the control factors (machining parameters).

Control factors	Levels		
	1	2	3
Cutting speed, $v_c$ (m/min)	100	175	250
Feed, $f$ (mm/rev)	0.15	0.25	0.35
Depth of cut, $a_p$ (mm)	0.5	1.5	2.5

**Table 5.3.** Measured surface roughness ( $R_a$ ) on the machined workmaterial at varying cutting conditions.

Exp. No.	Cutting conditions			Surface roughness ( $\mu\text{m}$ )		S/N ratio	
	Cutting speed (m/min)	Feed (mm/rev)	Depth of cut (mm)	uncoated tool	coated tool	uncoated tool	coated tool
1	1	1	1	0.56	0.46	5.0362	6.6300
2	1	1	2	0.61	0.51	4.2934	5.7960
3	1	1	3	0.67	0.56	3.4785	5.0130
4	1	2	1	1.11	0.94	-0.9065	0.5360
5	1	2	2	1.30	1.09	-2.2789	-0.7566
6	1	2	3	1.33	1.10	-2.4770	-0.8430
7	1	3	1	1.90	1.56	-5.5751	-3.8672
8	1	3	2	2.02	1.65	-6.1070	-4.3586
9	1	3	3	2.10	1.71	-6.4444	-4.6853
10	2	1	1	0.42	0.34	7.5350	9.2067
11	2	1	2	0.49	0.40	6.1961	7.9188
12	2	1	3	0.56	0.45	5.0362	6.7454
13	2	2	1	0.79	0.64	2.0475	3.8331
14	2	2	2	0.89	0.72	1.0122	2.8339
15	2	2	3	1.02	0.83	-0.1720	1.6085
16	2	3	1	1.49	1.20	-3.4637	-1.6030
17	2	3	2	1.64	1.32	-4.2969	-2.4507
18	2	3	3	1.75	1.41	-4.8608	-3.0155
19	3	1	1	0.29	0.23	10.7520	12.4430
20	3	1	2	0.39	0.31	8.1787	10.1370
21	3	1	3	0.48	0.38	6.3752	8.3103
22	3	2	1	0.64	0.49	3.8764	6.0338
23	3	2	2	0.80	0.62	1.9382	4.1284
24	3	2	3	0.87	0.68	1.2096	3.2565
25	3	3	1	1.24	0.97	-1.8684	0.2628
26	3	3	2	1.36	1.06	-2.6708	-0.5482
27	3	3	3	1.52	1.20	-3.6369	-1.5911

#### **5.3.4.1.2. Results and discussion**

The influence of cutting parameters such as cutting speed, feed and depth of cut on the measured surface roughness of machined workmaterial is discussed with the help of following statistical approach: (i) Analysis of Variance (ANOVA), and (ii) correlations between the parameters by multiple linear regressions.

##### *5.3.4.1.2.1. ANOVA results*

ANOVA can be useful for interpreting the input data and results in a controlled way after series of experiments. The obtained results in the current work were analyzed using Minitab-16, statistical analysis software which is widely used in many engineering applications. Table 5.4 shows the results of ANOVA with the surface roughness ( $R_a$ ) of machined workmaterial during machining with uncoated and coated cutting tool. The last column of the ANOVA table indicates the percentage of contribution ( $P$ ) of the each parameter on the total variation indicating then, the degree of influence on the result, surface roughness.

From the ANOVA of results (Table 5.4), it indicates that the feed rate is the most significant parameter among the factors considered. The percent contribution of each factor on the measured surface roughness is as follows: feed rate factor (84.31% with uncoated tool, 81.74% with coated tool), cutting speed factor (11.37% with uncoated tool, 14.04% with coated tool) and depth of cut factor (3.31% with uncoated tool, 3.23% with coated tool). This is true because it is well accepted that for a specified nose radius of cutting tool, the quality of surface finish is primarily a function of the feed rate [172].

From the measured surface roughness values and corresponding S/N ratios presented in Table 5.3, it is understood that the optimal cutting parameters for surface roughness of machined workmaterial with and without coated cutting tool were the cutting speed at level 3 (250 m/min), feed at level 1 (0.15 mm/rev) and the depth of cut at level 1 (0.5 mm). This is

true because in general among all the available quality characteristics in the analysis of the S/N ratio, a greater S/N ratio corresponds to the better quality characteristics. The optimum values cutting parameters are presented Table 5.5.

**Table 5.4.** ANOVA results for average surface roughness ( $R_a$ ).

Factors	Degree of freedom	Test F		$F_{table}$	Percentage of contribution P (%)	
		uncoated tool	coated tool		uncoated tool	coated tool
Feed	2	2557.9	4108.33	4.46	84.31	81.74
Cutting speed	2	345.1	705.66	4.46	11.37	14.04
Depth of cut	2	100.5	162.66	4.46	3.31	3.23
Cutting speed x depth of cut	4	5.0	8.66	3.84	0.32	0.34
Feed x depth of cut	4	4.3	6.33	3.84	0.28	0.25
Cutting speed x feed	4	3.7	7.16	-	0.24	0.28
Error	8	-	-	-	0.13	0.09
Total	26	-	-	-	100.00	100.00

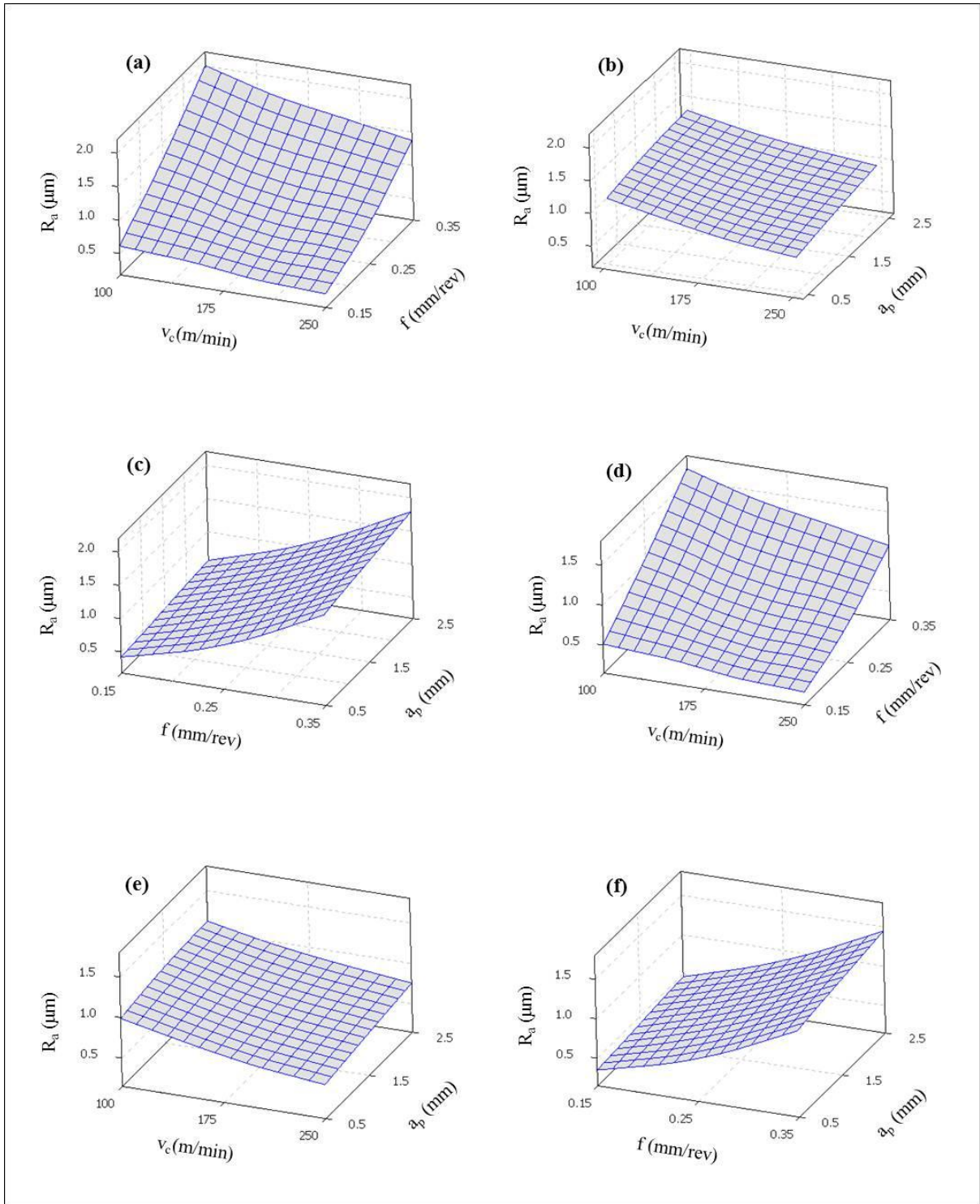
**Table 5.5.** The optimum values of cutting parameters.

Cutting speed (m/min)	Feed (mm/rev)	Depth of cut (mm)
250	0.15	0.5

- *Effect of cutting parameters on surface roughness*

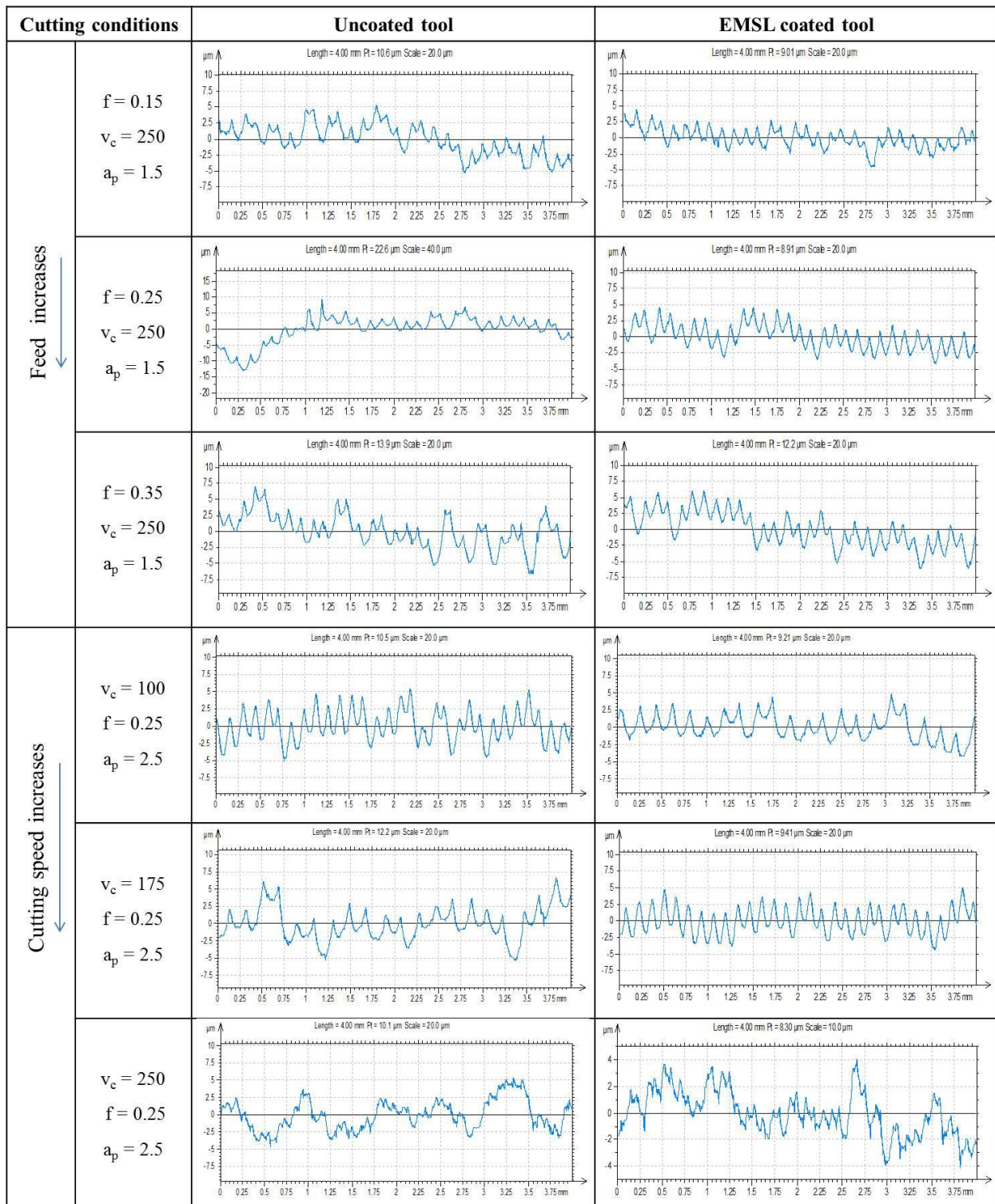
Variations of workmaterial surface finish with respect to different cutting parameters such as cutting speed, feed and depth of cut when machining with and without coated cutting tools are shown in Fig. 5.16. From this figure, it can be observed that for given cutting speed, the quality of surface finish on the machined workmaterial in both the machining environments (machining with uncoated cutting tool and machining with EMSL coated cutting tool) sharply increases with increase in feed value. On the other hand, surface roughness has a tendency to reduce with an increase in cutting speed at constant feed rate. However, the measured values of surface roughness on the machined workmaterial when machining with EMSL coated cutting tool are always smaller than those with uncoated cutting tool. Results show that it was much better in quality of surface finish (about 20-25%) of machined work material under similar operating conditions when machining with EMSL coated cutting tool. The lower values of surface roughness produced by the EMSL coated cutting tool could be due to the MoS<sub>2</sub> solid lubricant presence on cutting tool and its strong inherent lubricating properties. It can be concluded here that lower surface roughness values or high quality of surface finish on the machined workmaterial in both the machining at higher cutting speeds are due to lower cutting forces and less heat dissipated to the workmaterial during machining process.

The measured surface roughness ( $R_a$ ) on the machined workmaterial surface during machining with and without coated cutting tool at different cutting conditions is presented in Fig. 5.17. The corresponding observations of surface quality (microscopic surface) of machined workmaterial are illustrated in Fig. 5.18. The observations from Fig. 5.17 and Fig. 5.18 signifies a well understanding of cutting parameters and its influence on the measured surface roughness with a comparative judgment.



**Fig. 5.16.** Surface plots for effects of cutting conditions (cutting speed, feed and depth of cut) on average surface roughness of machined workmaterial: **(a)-(c)** during machining with uncoated cutting tool, and **(d)-(f)** during machining with EMSL coated cutting tool.





$v_c$  is in m/min,  $f$  is in mm/rev and  $a_p$  is in mm

**Fig. 5.17.** Comparison of measured surface roughness on the machined work material at different cutting conditions: (a) during machining with uncoated tool, and (b) during machining with coated tool.

Cutting conditions		Uncoated tool	EMSL coated tool
Feed increases ↓ (Surface quality decreases)	$f = 0.15$ $v_c = 250$ $a_p = 1.5$		
	$f = 0.25$ $v_c = 250$ $a_p = 1.5$		
	$f = 0.35$ $v_c = 250$ $a_p = 1.5$		
Cutting speed increases ↓ (Surface quality increases)	$v_c = 100$ $f = 0.25$ $a_p = 2.5$		
	$v_c = 175$ $f = 0.25$ $a_p = 2.5$		
	$v_c = 250$ $f = 0.25$ $a_p = 2.5$		

$v_c$  is in m/min,  $f$  is in mm/rev and  $a_p$  is in mm

**Fig. 5.18.** Optical micrographs showing the quality of machined workmaterial at varying cutting conditions when machining with and without coated cutting tools.

#### 5.3.4.1.2.2. Correlations and confirmations

In the present study, in order to understand the influence of cutting parameters on the surface roughness and verify the accuracy of developed regressive model, correlation and confirmation tests were performed. The correlation between the cutting parameters (cutting speed, feed and depth of cut) and measured surface roughness of machined workmaterial when machining with and without coated tool is determined from the developed multiple linear regression models as shown in Eq.5.3 and Eq.5.4.

Table 5.6 presents the error between the measured and predicted (from model) results of surface roughness for some randomly selected cutting conditions. From the analysis of results, it is noticed that the calculated error for surface roughness is very less in both the machining, i.e. machining with uncoated tool and machining with EMSL coated cutting tool. Therefore, Eq.5.3 and Eq.5.4 correlate the relationship of surface roughness with the cutting parameters with realistic degree of approximation. Further, the effectiveness of the model has been checked by calculating the coefficients of determination ( $R^2$ ). The obtained  $R^2$  values for the models are presented in the Eq.5.3 and Eq.5.4. It is observed that the coefficients of determination values of developed models have very good correlations between the experimental and predicted values of surface roughness and hence the models are very effective.

$$R_a \text{ (with coated tool)} = 0.30716 - 0.00298 v_c + 2.27285 f + 0.03269 a_p + 0.00001 v_c^2 + 8.42494 f^2 - 0.01012 a_p^2 - 0.01205 v_c f + 0.00017 v_c a_p + 0.20254 f a_p \quad (R^2 = 94.3\%) \quad (5.3)$$

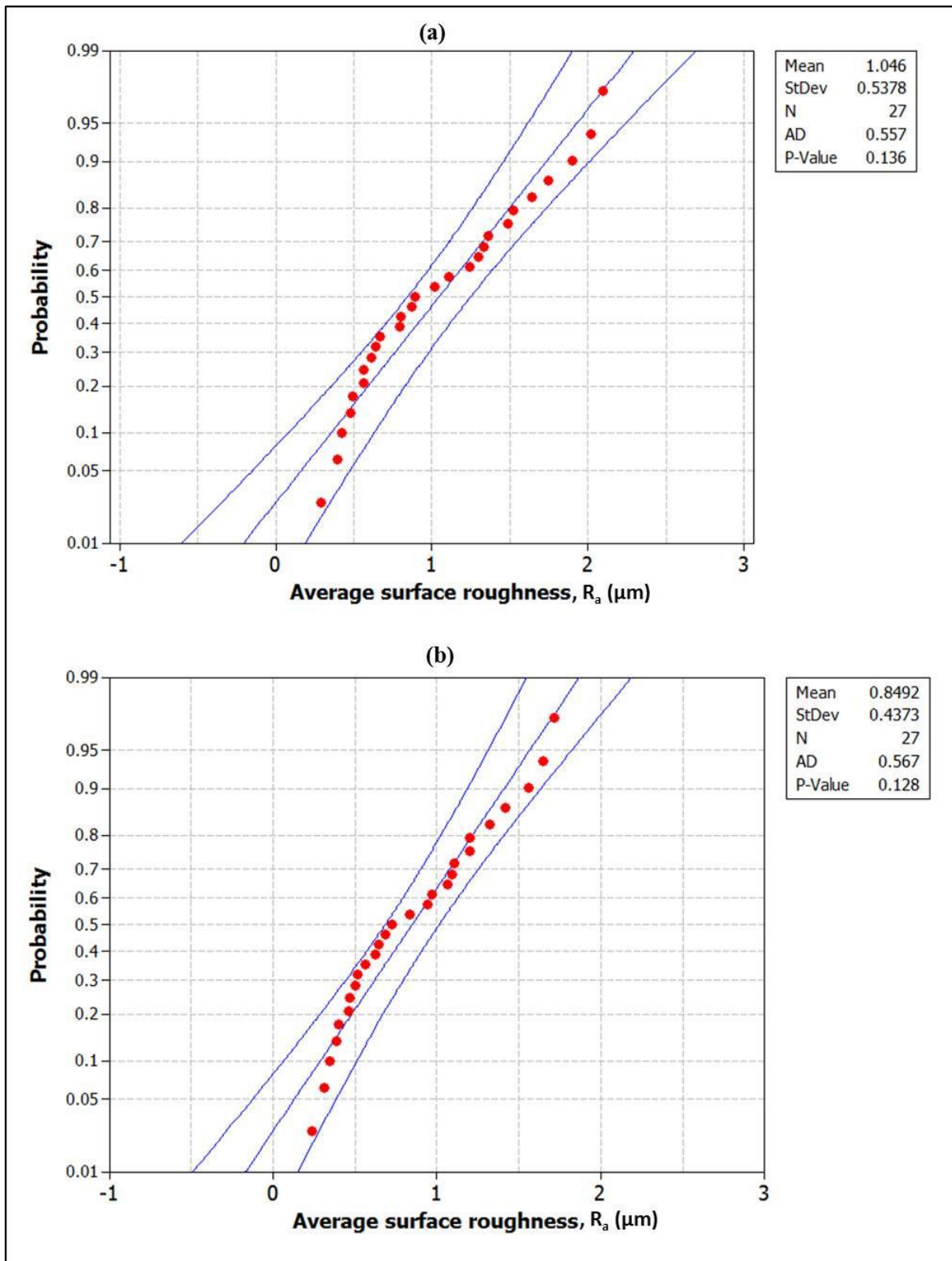
$$R_a \text{ (with uncoated tool)} = 0.3795 - 0.0036 v_c + 2.3306 f + 0.0511 a_p + 0.0001 v_c^2 + 11.0556 f^2 - 0.0144 a_p^2 - 0.0136 v_c f + 0.0002 v_c a_p + 0.25 f a_p \quad (R^2 = 95.7\%) \quad (5.4)$$

**Table 5.6.** Percentage of error (%) between measured and model predicted surface roughness.

Test No.	Randomly selected cutting parameter values			Error (%) between experimental and predicted value	
	Cutting speed (m/min)	Feed (mm/rev)	Depth of cut (mm)	Coated tool	Uncoated tool
1	150	0.2	1	5.09	5.37
2	225	0.3	2	6.73	6.16
3	250	0.3	2	6.24	6.38

In addition to the above, the adequacy of the developed models was tested using the ANOVA statistical technique and the calculated value of the F-test of the model does not exceed the standard tabulated value of F-table for a desired confidence level of 95%. The 95% prediction interval is the range in which we can expect any individual value to fall into 95% of the time. From the ANOVA results, it is evident that both the models are adequate at 95% confidence level. Further, the Anderson–Darling test and normal probability plots of the residuals versus the predicted surface roughness results are plotted in Fig. 5.19. The data presented in Fig. 5.19 closely follows the straight line. The null hypothesis is that the data distribution law is normal and the alternative hypothesis is that it is non-normal. Using the ‘*p*’ value which is greater than ‘ $\alpha$ ’ of 0.05 (level of significance), the null hypothesis cannot be rejected (i.e., the data follow a normal distribution). It implies that the models proposed for predictions of surface finish quality of machined workmaterial during machining with and without coated cutting tools are adequate.





**Fig. 5.19.** Normal probability plots for average surface roughness ( $R_a$ ) measured on the machined workmaterial: **(a)** during machining with uncoated cutting tool, and **(b)** during machining with coated cutting tool.

## 5.4. Summary

To endorse the performance of novel EMSL coated cutting tools, machining experiments were conducted when turning an aerospace workmaterial, aluminum alloy AA7075-T6, on commercial high-precision lathe machine. The performance of EMSL coated cutting tools during cutting tests has been demonstrated successfully. Results from machining tests reveal that the EMSL coated cutting tools can endow superior process performance compared to that of conventional cutting tools (uncoated cutting tools) and can make a potential coating to cutting tools with additional benefits of being able to accomplish sustainable machining.

EMSL coated cutting tools demonstrate the benefits in curtailing the tool-chip contact frictional effects and contribute to the favorable control of heat generation at tool-workmaterial contacts. This is due to the fact that the presence of lamellar structured orientation of MoS<sub>2</sub> solid lubricant, which shears easily along the chip-tool rake face sliding direction and leading to such favorable benefits. Machining with EMSL coated cutting tools results in lower specific cutting energy due to thermal softening at tool-work interface leading to reasonable lower cutting forces than those in machining with uncoated cutting tools under same cutting conditions. As a result of lesser cutting forces and cutting temperatures, average tool flank wear in EMSL coated cutting tools is very less (about 25%) as compared to that of uncoated cutting tool. Shear deformation to form chips under all experimental condition was judged and observed favorable tool-chip interaction in machining with EMSL coated cutting tools. In both the machining conditions, high cutting speeds result in a better quality of surface finish on the machined workmaterial. However, surface quality of machined workmaterial when machining with EMSL coated cutting tool showed a much better improvement by 20-25% when compared to that of machining with uncoated cutting tool. In addition, optimum machining parameters and their influence on the measured surface roughness results were presented with the help of Taguchi design approach and ANOVA.

The optimal cutting parameters for surface roughness of machined workmaterial were the cutting speed at level 3 (250 m/min), feed at level 1 (0.15 mm/rev) and the depth of cut at level 1 (0.5 mm). Correlations between the cutting parameters and measured surface roughness are determined using multiple linear regression equation. Further, to see the adequacy of the results, the Anderson-Darling test and normal probability plots of the residuals versus the predicted response for the surface roughness are plotted.

In summary, experimental investigations reveal that the machining with EMSL coated cutting tools results in improved machinability parameters without affecting the quality of machined surface produced. The results expected to be possible avenues to cater the present industrial requirements and open a new way to implement these coatings prepared by electrostatic deposition process and can endow a new alternative coating to make the machining from pollution free environment (sustainable machining).

# **CHAPTER 6**

## **FINITE ELEMENT (FE) MODELLING AND SIMULATION OF MACHINING PROCESS**

---

Previous chapter presents the experimental tests to understand the physical cutting process variables such as cutting temperature, cutting force, tool life, etc. during machining with and without coated cutting tools under different cutting conditions. The use of the finite element (FE) tool here is to give a better understanding of the cutting process presented in chapter 5 and to see the accuracy of machining results and have a relative comparison of numerical predictions with experimental findings. The current chapter is organized as follows: Section 6.1 presents the brief introduction about the importance of FE modelling. Section 6.2 presents the FE modelling approach to machining process. Section 6.3 deals with the FE machining simulations with the help of FE modelling code, DEFORM<sup>TM</sup>. Section 6.4 involves the experimental tests in two machining environments in accordance with the experimental condition presented in chapter 5 and followed by results and discussions in Section 6.5. Finally, Section 6.6 presents the summary of this chapter.

### **6.1. Introduction**

The impetus in prognostic process engineering of machining process using FE tool is due to its science-based approach in comprehending the physical cutting process variables. FE modelling provides an insight for further understanding of the machining process, through the predictive capability of machinability parameters such as cutting force, cutting temperature and chip formation, etc. Further, application of FE tool in metal cutting simulations has a great importance in predicting some results that are experimentally very difficult to be evaluated. Success and reliability of FE machining model are heavily dependent upon how



accurately selecting the material constitutive relation, friction parameters between the cutting tool and workmaterial contact and simulation settings during FE modeling of machining process. The application of FE codes and their computational improvements that make this tool one of the most promising approach in simulating the cutting processes include turning, milling, drilling and grinding. In the present chapter, FE modeling of machining process when simulating AA7075-T6 cutting process is presented in accordance with the material and experimental conditions adopted in chapter 5. In FE modelling of machining, workpiece plastic flow is accounted by formulated constitutive equation. Friction modelling is based on combination of shear friction and Coulomb friction defined as function of normal stress at tool-chip contact over the sticking and sliding region. FE modelling of machining process is presented with the help of commercial FE modelling code, DEFORM<sup>TM</sup>.

## **6.2. FE modelling of the machining process**

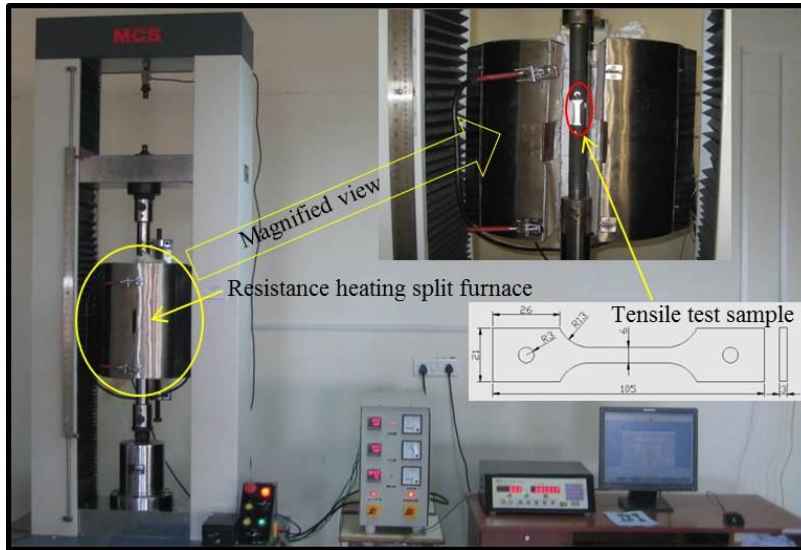
Regardless of the machining process being modelled, accuracy of FE modelling of machining process is greatly dependent upon the following attributes: (i) the workmaterial constitutive relation - used as input to the FE simulations to denote elastic, plastic and thermo-mechanical behavior of workmaterial, (ii) friction parameters between the cutting tool and workmaterial interfaces should be modelled fairly enough to account the forces, stresses and temperatures developments, (iii) FE model should not require chip separation criteria - continuous remeshing and quality of the mesh is maintained throughout the chip formation, and (iv) simulation settings (mesh structure, mesh density, element size or number of elements, time-step size, error tolerances, remeshing criterion, assumptions, solver techniques, etc.). More detailed information on these attributes is explained in subsequent sections.

### 6.2.1. Selection of material constitutive model

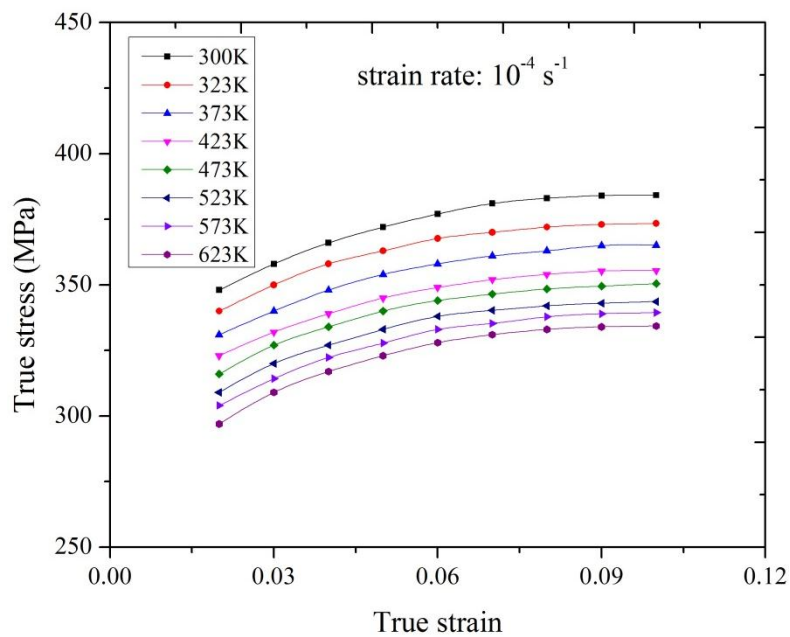
In any FE machining model, an essential input is the accurate definition of workmaterial properties. It is observed from the literature review (chapter 2) that the selection of constitutive model to describe the flow behavior accurately is a difficult situation, and there is no general method to help the selection of constitutive model for metal or alloys. However, irrespective of the manufacturing application such as machining, forming, forging, rolling, extrusion, etc., the basic criterion in selection of constitutive model depends upon the following factors: (i) applicability range or working domain, (ii) accuracy needed, (iii) computational time required, and (iv) the amount of data required to evaluate material constants.

In the present research work, to ensure the accuracy of the numerical simulations and choose the best material constitutive relation for FE modelling of machining process, four constitutive models, such as Johnson-Cook (JC) model, Zerilli-Armstrong (ZA) model, Arrhenius (Arr) model and Norton-Hoff (NH) model are studied. The accuracy of material constitutive relation is greatly depend upon the flow stress data and corresponding strain rate condition. Hence, in this work, the predicative capability of each model at different strain rate conditions is evaluated by conducting a trial FE analysis at particular cutting condition (see forthcoming Section 6.3). For this purpose, the flow stress data of the AA7075-T6 workmaterial is considered based on the following: (i) by conducting a series of tensile tests on a computer controlled universal testing machine (UTM) as shown in Fig. 6.1 – to relate workmaterial deformations at low strain rate, and (ii) flow stress data from previous study - to relate high strain rate condition. Fig. 6.2 shows the typical true stress-true strain curves obtained from tensile tests at low strain rate conditions. Fig. 6.3 shows the existing flow stress data [144] for the workmaterial at high strain rate and deformation temperatures. The workmaterial constants at specified reference strain rate and reference temperature for JC,

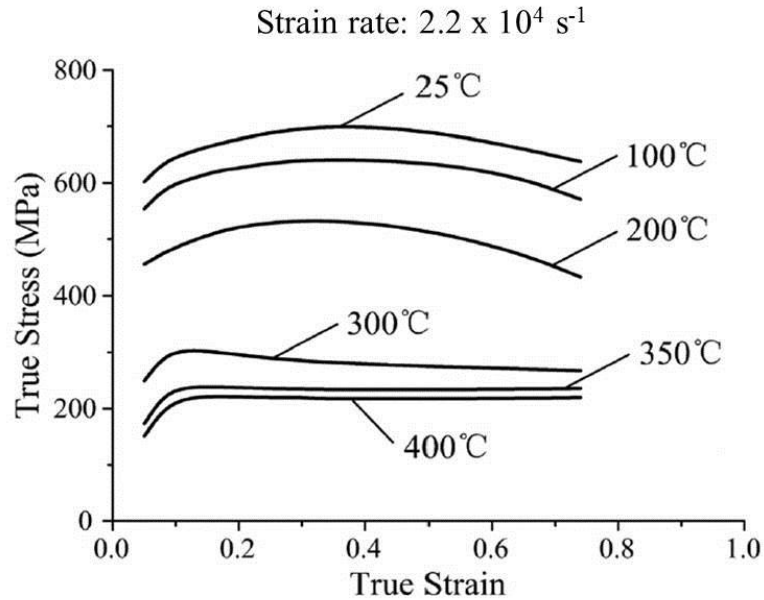
ZA, Arr and NH models are determined as per the standard material evaluation procedure mentioned in SFTC DEFORM<sup>TM</sup> finite element software [173].



**Fig. 6.1.** Computer controlled UTM with high temperature contact type extensometer and three-zone resistance heating split furnace with a tensile test sample.



**Fig. 6.2.** Flow stress of AA7075-T6 workmaterial under various deformation temperatures at low strain rate ( $10^{-4} \text{ s}^{-1}$ ).



**Fig. 6.3.** Flow stress of AA7075-T6 workmaterial under various deformation temperatures at high strain rate ( $2.2 \times 10^4 \text{ s}^{-1}$ ) [144].

#### 6.2.1.1. Johnson-Cook (JC) model

In order to account the flow stress of workmaterial, the Johnson-Cook (JC) constitutive material model was used in the present work when simulating AA7075-T6 machining process. The original JC material constitutive model as shown in Eq.6.1 [145] provides a good description of metal material behavior undertaking high strains, strain rates and temperature dependent visco-plasticity. Due to its simplicity and less number of material constants, JC model is one of the most extensively employed in a wide variety of manufacturing processes and engineering materials and a benchmark for comparison of different models.

$$\sigma = f(\varepsilon) g(\dot{\varepsilon}) h(T) \quad (6.1)$$

where

$$f(\varepsilon) = (A + B \varepsilon^n) \quad (6.2)$$

$$g(\dot{\varepsilon}) = (1 + C \ln \frac{\dot{\varepsilon}}{\dot{\varepsilon}_o}) \quad (6.3)$$

$$h(T) = (1 - (\frac{T-T_r}{T_m-T_r})^m) \quad (6.4)$$

The combined form of JC model (considering equations 6.2 to 6.4) can be mathematically expressed with the following equation (Eq.6.5).

$$\sigma = (A + B \varepsilon^n) \left[ 1 + C \ln \frac{\dot{\varepsilon}}{\dot{\varepsilon}_o} \right] \left[ 1 - (\frac{T-T_r}{T_m-T_r})^m \right] \quad (6.5)$$

The JC model (Eq.6.5) describes the flow stress of the material with the product of strain, strain rate and temperature and fails to take into account the damage to a material element during a machining process. Furthermore, chip-separation criterion is always necessary in FE modelling approach of machining process with the Lagrangian or Arbitrary Lagrangian- Eulerian (ALE) analysis. This chip-separation criterion triggers the material fracture resulting in separation of chip from workmaterial. Hence, in the present work, a JC model (Eq.6.6) [173] with damage initiation criterion is used. Material constants obtained at low and high strain rate condition (reference temperature 300 K) are listed in Table 6.1.

$$\sigma = (A + B \bar{\varepsilon}^n) \left[ 1 + C \ln \left( \frac{\dot{\varepsilon}}{\dot{\varepsilon}_o} \right) \right] \left( \frac{\dot{\varepsilon}}{\dot{\varepsilon}_o} \right)^\alpha \left( D - E \left( \frac{T-T_r}{T_m-T_r} \right)^m \right) \quad (6.6)$$

where,

$$D = D_o \exp[ k (T - T_r)^\beta ] \quad (6.7)$$

where, ‘ $\sigma$ ’ is the flow stress (MPa), ‘ $A$ ’ is the yield stress (MPa), ‘ $B$ ’ is the coefficient of strain hardening (MPa), ‘ $n$ ’ is the strain hardening exponent, ‘ $m$ ’ is the thermal softening exponent, ‘ $\bar{\varepsilon}$ ’ is the effective strain, ‘ $C$ ’ is the coefficient dependent on the strain rate, ‘ $\dot{\varepsilon}$ ’ is

the strain rate ( $s^{-1}$ ), ' $\dot{\epsilon}_0$ ' is the reference strain rate ( $s^{-1}$ ), ' $D_0$ ', ' $\alpha$ ', ' $\beta$ ' and ' $k$ ' are material constants, ' $E$ ' material dependent constant, ' $T$ ' is the current absolute temperature (Kelvin), ' $T_r$ ' is the reference temperature (Kelvin), and ' $T_m$ ' is the melting temperature; for AA7075-T6, the melting temperature is about 900 K.

**Table 6.1.** Material constants for JC model.

Parameter / reference strain rate	A	B	C	n	m	$D_0$	E	$\alpha$	$\beta$	k
$10^{-4} s^{-1}$	317.37	166.95	-0.0073	0.5091	1.5724	1.1	1	0.3482	0.8360	1.3312
$2.2 \times 10^4 s^{-1}$	378.62	141.16	0.002	0.485	0.791	1.1	1	0.9319	1.3893	0.8355

### 6.2.1.2. Zerilli-Armstrong (ZA) model

In the present study to account the flow stress behavior of AA7075-T6 workmaterial during machining process, physically based constitutive model proposed by Zerilli and Armstrong [147] is used. Zerilli and Armstrong used theory of dislocation mechanics to formulate a flow stress model (Eq.6.8) that accounts for strain, strain rate and temperature in a coupled manner, which can be incorporated in dynamics related numerical codes. They worked on different materials to analyze their temperature and high strain rate response and noticed a significant difference between these materials.

$$\sigma = C_0 + C_1 \exp(-C_3 T + C_4 T \ln \frac{\dot{\epsilon}}{\dot{\epsilon}_0}) + C_5 \bar{\epsilon}^n \quad (6.8)$$

where, ' $\sigma$ ' is the flow stress (MPa) and ' $C_0$ ', ' $C_1$ ', ' $C_3$ ', ' $C_4$ ' and ' $C_5$ ' are material dependent constants, ' $\dot{\epsilon}$ ' is the strain rate ( $s^{-1}$ ), ' $\dot{\epsilon}_0$ ' is the reference strain rate ( $s^{-1}$ ), ' $\bar{\epsilon}$ ' is the effective

strain and 'T' is the absolute temperature (Kelvin). In this study, material constants obtained at low and high strain rates (reference temperature 300 K) for the ZA model are listed in Table 6.2.

**Table 6.2.** Material constants for ZA model.

Parameter / reference strain rate	C <sub>0</sub>	C <sub>1</sub>	C <sub>3</sub>	C <sub>4</sub>	C <sub>5</sub>	n
10 <sup>-4</sup> s <sup>-1</sup>	207.34	459.1056	-0.001831	-0.00211	329.409	0.00174
2.2 x 10 <sup>4</sup> s <sup>-1</sup>	326.45	121.37	0.000817	5909.47	583.424	0.315

### 6.2.1.3. Arrhenius (Arr) model

In the present work, to formulate constitutive relation for the material AA7075-T6, the Arrhenius type equation [174] which is extensively used by several researchers to describe the flow behavior of workmaterial under high temperatures, strains and strain rates as shown in Eq.6.9 was employed. In addition, the temperature and strain rate effects on the material deformation behavior can also be formulated by Zener-Hollomon parameter (Z), in an exponential form as shown in Eq.6.10.

$$\dot{\varepsilon} = A F(\sigma) \exp\left(\frac{-Q}{RT}\right) \quad (6.9)$$

$$Z = \dot{\varepsilon} \exp\left(\frac{Q}{RT}\right) \quad (6.10)$$

where,

$$F(\sigma) = \sigma^n \text{ for } \alpha\sigma < 0.8 \quad (6.11)$$

$$= \exp(\beta\sigma) \text{ for } \alpha\sigma > 1.2 \quad (6.12)$$

$$= [\sinh (\alpha \sigma)]^n \text{ for all } \sigma \quad (6.13)$$

where, ' $Q$ ' is the activation energy (kJ/mol), ' $\sigma$ ' is the flow stress (MPa), ' $R$ ' is the universal gas constant ( $8.314 \text{ J mol}^{-1} \text{ K}^{-1}$ ), ' $T$ ' is the current absolute temperature (Kelvin), ' $Z$ ' is the temperature compensation strain rate factor during hot deformation, ' $A$ ', ' $\alpha$ ', ' $n$ ' are the material constants determined from flow stress data (where,  $\alpha = \beta/n$ ) and ' $\dot{\epsilon}$ ' is the strain rate ( $\text{s}^{-1}$ ). For all the stress levels, Eq.6.9 can be written in the form shown in Eq.6.14. Further, the constitutive form that relates flow behavior and Zener-Holloman parameter (combining Eq.6.9 and Eq.6.14) can be mathematically expressed with Eq.6.15. In this work, material constants obtained at low and high strain rates (reference temperature 300 K) for the Arr model are listed in Table 6.3.

$$\dot{\epsilon} = A [\sinh \alpha \sigma]^n \exp \left( \frac{-Q}{RT} \right) \quad (6.14)$$

$$\sigma = \frac{1}{\alpha} \ln \left\{ \left( \frac{Z}{A} \right)^{1/n} + \left[ \left( \frac{Z}{A} \right)^{2/n} + 1 \right] \right\} \quad (6.15)$$

**Table 6.3.** Material constants for Arr model.

Parameter / reference strain rate	A	$\alpha$	n	Q
$10^{-4} \text{ s}^{-1}$	1.305	0.875	1.36	576109
$2.2 \times 10^4 \text{ s}^{-1}$	3744	0.538	1.4	645626

#### 6.2.1.4. Norton-Hoff (NH) model

A thermo-viscoplastic model [175] with a power law function of strain, strain rate and temperature introduced by the Norton-Hoff constitutive model is chosen to predict the



observed dependence of the flow stress of AA7075-T6 material under a domain of strain rates and deformed temperatures. The equivalent flow stress of the material at high deformations introduced by Norton-Hoff can be mathematically expressed with the Eq.6.16.

$$\sigma = K (\dot{\epsilon}_o + \bar{\epsilon})^n \dot{\epsilon}^m \exp \left[ \frac{\beta}{T} \right] \quad (6.16)$$

where, ' $\sigma$ ' is the true stress (MPa), ' $K$ ' is the material constant, ' $\dot{\epsilon}_o$ ' is the reference strain rate ( $s^{-1}$ ), ' $\bar{\epsilon}$ ' is the equivalent plastic strain, ' $\dot{\epsilon}$ ' is the strain rate ( $s^{-1}$ ), ' $n$ ' is the strain hardening exponent, ' $m$ ' is the strain rate hardening exponent, ' $\beta$ ' is the temperature (Kelvin) and ' $T$ ' is the absolute temperature (Kelvin). In this study, material constants obtained at low and high strain rates (reference temperature 300 K) for NH model are listed in Table 6.4.

**Table 6.4.** Material constants for NH model.

Parameter / reference strain rate	K	m	n
$10^{-4} s^{-1}$	270.31	0.000871	0.219
$2.2 \times 10^4 s^{-1}$	133.65	0.00198	0.201

### 6.2.2. Tool-chip interfacial friction modelling

As commonly seen from machining experimental observations [176], there are two distinct regions forms along the tool-chip contact area, i.e., sticking and sliding regions (see Fig. 2.7, chapter 2). In the sticking region along the tool-chip interface the equivalent shear stress limit is imposed, whereas along the sliding region, a constant coefficient of friction is assumed. The frictional stress in the sticking and sliding region are therefore expressed by Eq.6.17 and Eq.6.18 respectively.

$$\tau_{fr} = \bar{\tau}_{max} \quad \text{when} \quad \tau_{fr} \geq \bar{\tau}_{max} \quad (6.17)$$

$$\tau_{fr} = \mu \sigma_n \quad \text{when} \quad \tau_{fr} < \bar{\tau}_{max} \quad (6.18)$$

where, ' $\bar{\tau}_{max}$ ' is the equivalent shear stress (MPa), ' $\tau_{fr}$ ' is the frictional shear stress (MPa), ' $\sigma_n$ ' is the normal stress over the tool rake face (MPa) and ' $\mu$ ' is the mean friction coefficient. This normal stress is very small in sliding region and frictional stress follows simple Coulomb's law with ' $\mu$ ' as mean friction coefficient. In the present research work, as an approximation for numerical simulations, mean coefficient of friction between tool and chip in orthogonal cutting is calculated from the measured cutting force and feed force as given by Eq.6.19. The detailed information about measured cutting forces at different cutting conditions is presented in chapter 5.

$$\mu = \tan \beta = \frac{F_f + F_c \tan \gamma}{F_c - F_f \tan \gamma} \quad (6.19)$$

where, ' $\beta$ ' is the friction angle, ' $\gamma$ ' is the rake angle, ' $F_c$ ' is the cutting force (N) and ' $F_f$ ' is the feed force (N).

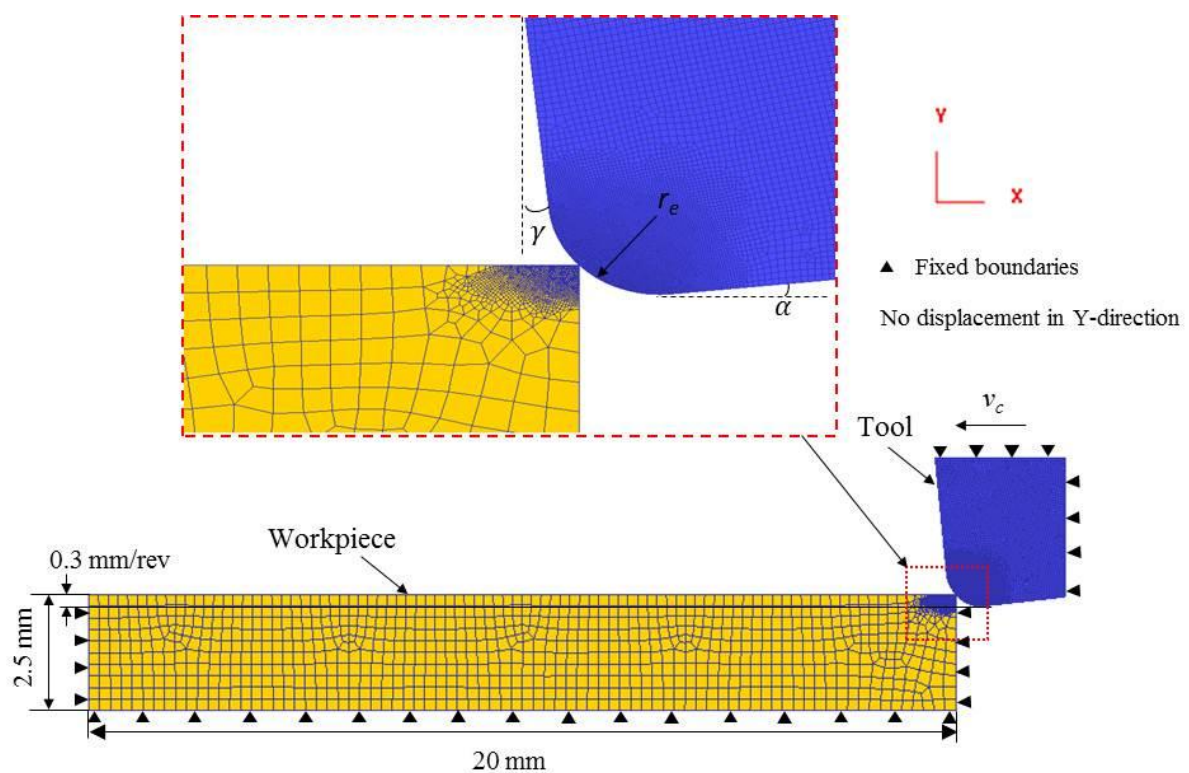
Further, to account the equivalent shear stress limit ( $\bar{\tau}_{max}$ ) in FE cutting simulations, equivalent shear stress,  $\bar{\tau}_{max}$  is calculated based on the following relation (Eq.6.20).

$$\bar{\tau}_{max} = \frac{A}{\sqrt{3}} \quad (6.20)$$

where,  $A$  is the initial yield stress (MPa) of the workmaterial.

### 6.3. FE machining simulations

A two-dimensional FE machining model using commercially available FE modelling code, SFTC DEFORM<sup>TM</sup> is set-up to evaluate the cutting forces, cutting temperatures, chip thickness and shear angle during AA7075-T6 turning with and without coated cutting tools. An example of FE analysis geometry configuration of the cutting process is presented in Fig. 6.4.



**Fig. 6.4.** The two-dimensional FE cutting model used in machining simulations.

Numerical code uses an updated Lagrangian approach for chip separation from workpiece and to achieve continuous remeshing. The workpiece shape is represented by a simplified model with about 6 to 8 mm cut length. The workpiece is modelled as plastic material and was initially meshed with 4000 iso-parametric quadrilateral elements while the carbide cutting tool, modeled as rigid, was meshed into 8000 elements. To ensure the

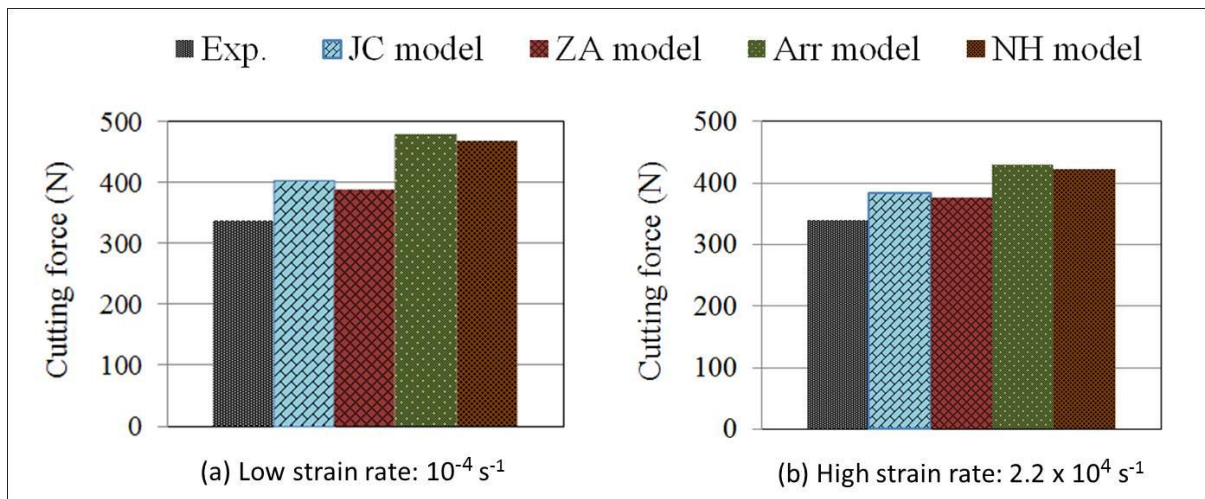
simulation accuracy, the number of elements on workmaterial is chosen by performing convergence analysis on the results of cutting temperature and cutting force. After convergence analysis, to achieve steady-state mechanical conditions, the FE simulation was performed by updated Lagrangian implicit formulation and automatic remeshing technique. In the convergence analysis, JC, ZA, Arr and NH material models were employed at different strain rate conditions in order to choose the best material model for FE machining simulations. Mechanical and thermal boundary conditions of materials used in numerical simulations are defined (Table 6.5) accordingly [73,177-179] in order to allow heat transfer between workpiece and cutting tool.

**Table 6.5.** Mechanical and thermo-physical properties of materials used in FE simulations.

Material	Young's modulus (GPa)	Thermal expansion ( $\mu\text{m.m}/^\circ\text{C}$ )	Thermal conductivity ( $\text{W/m}/^\circ\text{C}$ )	Heat capacity ( $\text{J/kg}/^\circ\text{C}$ )	Poission's ratio	Density ( $\text{kg/m}^3$ )
AA7075-T6	70	25	180.1	910	0.3	2700
MoS <sub>2</sub>	238	6.9	0.44	272	0.13	4800
WC	534	25	50	400	0.22	11900

The ability of formulated constitutive models in relating thermo-mechanical behavior in FE machining simulations was demonstrated by taking cutting forces as performance index. As far as friction modelling is considered, contact conditions between tool and workpiece are defined as per the procedure explained in section 6.2.2. As an example, at particular cutting condition (cutting speed 250 m/min and feed 0.3 mm/rev), the predictive capabilities of formulated constitutive models with different strain rate conditions (low and high) when simulating AA7075-T6 machining process with uncoated cutting tool are presented in Fig. 6.5. The relative error between experimental and FE simulated results of cutting forces with

different material constitutive models under two different strain rate conditions are presented in Table. 6.6.



**Fig. 6.5.** Comparison of experimental and FE simulated cutting forces at low and high strain rate conditions with different constitutive models (cutting conditions: 250 m/min and 0.3 mm/rev).

**Table 6.6.** Percentage of error (%) between experimental and FE simulated cutting forces with different constitutive models for different strain rates.

Strain rate/ constitutive model	Error percentage between experimental and simulated cutting forces with different constitutive models			
	JC model	ZA model	Arr model	NH model
$10^{-4} \text{ s}^{-1}$	19.52	14.79	42.30	39.05
$2.2 \times 10^4 \text{ s}^{-1}$	13.31	10.65	26.92	24.55

## 6.4. Machining experiments

To realize the experimental investigation, a set of machining tests were carried out on high-precision lathe machine as per the experimental conditions presented in Table 6.7. The detailed experimental procedure and method employed in machining tests was explained in chapter 5.

**Table 6.7.** Conditions adopted in FE simulations and machining experiments.

<i>Workmaterial:</i> AA7075-T6 aluminum alloy
<i>Workmaterial size:</i> Initial diameter = 65 mm and length = 550 mm
<i>Cutting conditions:</i> Cutting speed ( $v_c$ ) = 50, 100, 150, 200, 250 m/min; feed ( $f$ ) = 0.2, 0.3, 0.4 mm/rev; machining time for each test = 10 min
<i>Machining test environments:</i> (i) machining with EMSL coated cutting tools, and (ii) machining with uncoated cutting tools
<i>Cutting tool and tool geometry:</i> Carbide tool insert (P-30 grade, grain size 1.4 $\mu\text{m}$ ) rake angle ( $\gamma$ ) = $-6^\circ$ , clearance angle ( $\alpha$ ) = $6^\circ$ and nose radius ( $r_e$ ) = 0.8 mm
<i>Cutting force measurement:</i> Strain gauge dynamometer
<i>Cutting temperatures measurement:</i> Thermal infrared (IR) imaging camera (FLIR E60) with 320 x 240 pixels having thermal sensitivity less than $0.05^\circ\text{C}$ at $30^\circ\text{C}$
<i>Chip thickness measurement:</i> Tool maker's microscope (Olympus STM6)

All the turning experiments were carried out on a cylindrical workmaterial with initial values of length and diameter equal to 550 mm and 65 mm, respectively. Two different machining test environments were chosen are as follows: (i) machining with EMSL coated tools (see chapter 5), and (ii) machining with uncoated tools. Each machining test was conducted for 10 min for all the cutting conditions. Each experiment was repeated three times at every cutting condition, and the average of three measurements was used to represent the

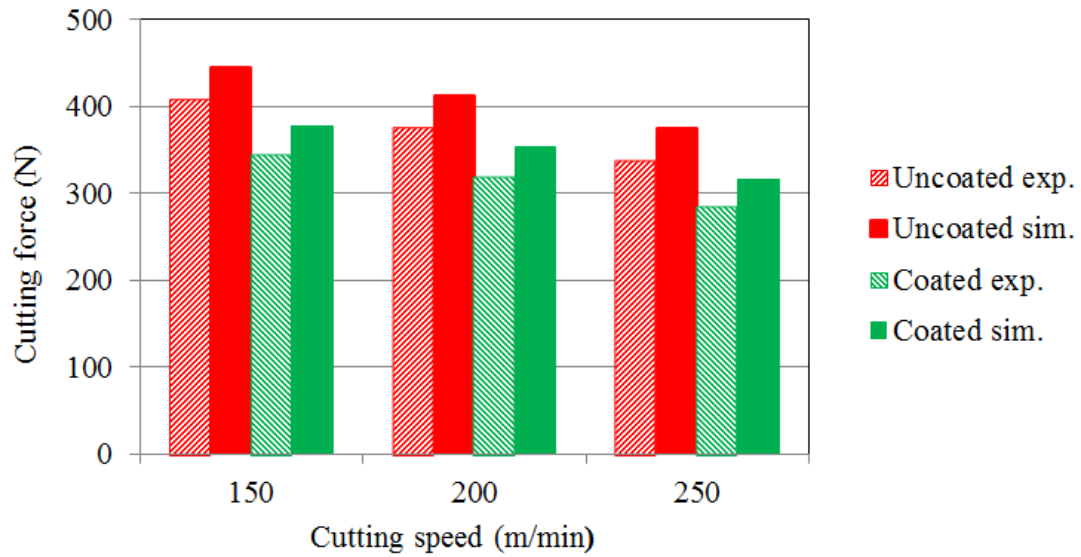
performance parameters such as cutting forces, cutting temperatures, chip thickness and shear angle.

## **6.5. Results and discussion**

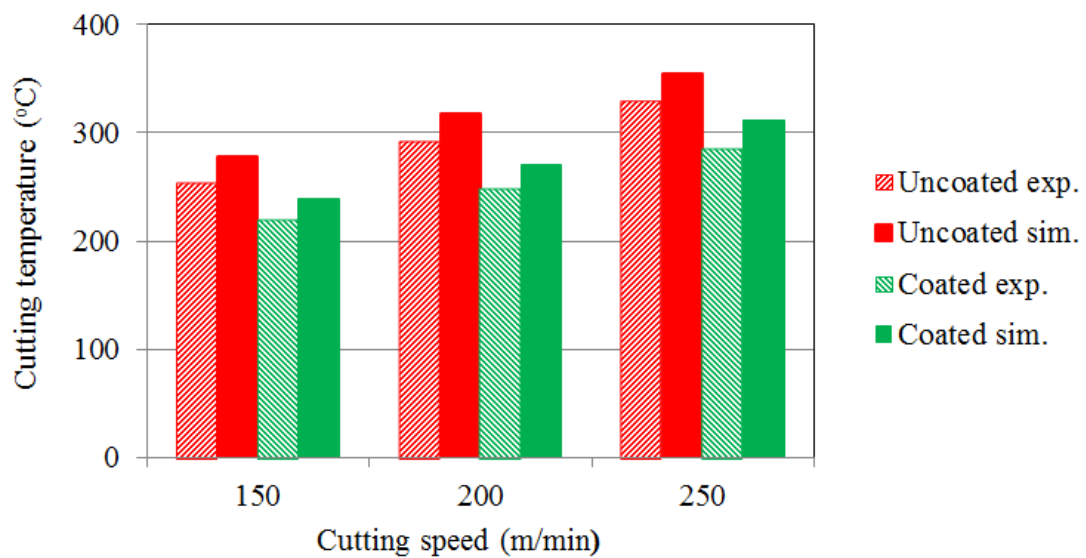
FE modelling of machining process by taking into account the frictional effects based on combination of shear friction and Coulomb friction and material flow behavior based on the formulated model was demonstrated on different cutting conditions. The predicted results such as cutting forces, cutting temperatures, chip thickness and shear angle when simulating the AA7075-T6 machining process with and without coated cutting tools at different cutting conditions were compared with the experimental results.

From the comparison of predictive capability of different models (Table 6.6), it was observed that ZA model show a very high degree of accuracy (low error) in predicting cutting forces when compared to other models (JC, Arr and NH), which indicates that the ZA model can give an accurate and precise estimate of the flow behavior for the AA7075-T6 material under high strain rate condition and can be used to predictive process engineering to analyze the machining process. Hence, in the present study to have a relative comparison of performance of EMSL coated cutting tools with uncoated cutting tools, FE modelling of machining process has been carried out by taking into account of flow behavior of AA7075-T6 material at high strain rate condition as defined by ZA model and numerical predictions of cutting process variables were compared with the experimental results.

Fig. 6.6 and Fig. 6.7 show the experimental and numerical predictions of the cutting force and cutting temperature respectively when cutting AA7075-T6 aluminum alloy with and without coated cutting tools under different cutting speeds.



**Fig. 6.6.** Comparison of experimental and FE simulated cutting force during AA7075-T6 machining with and without coated tools at different cutting speeds ( $f = 0.3$  mm/rev).

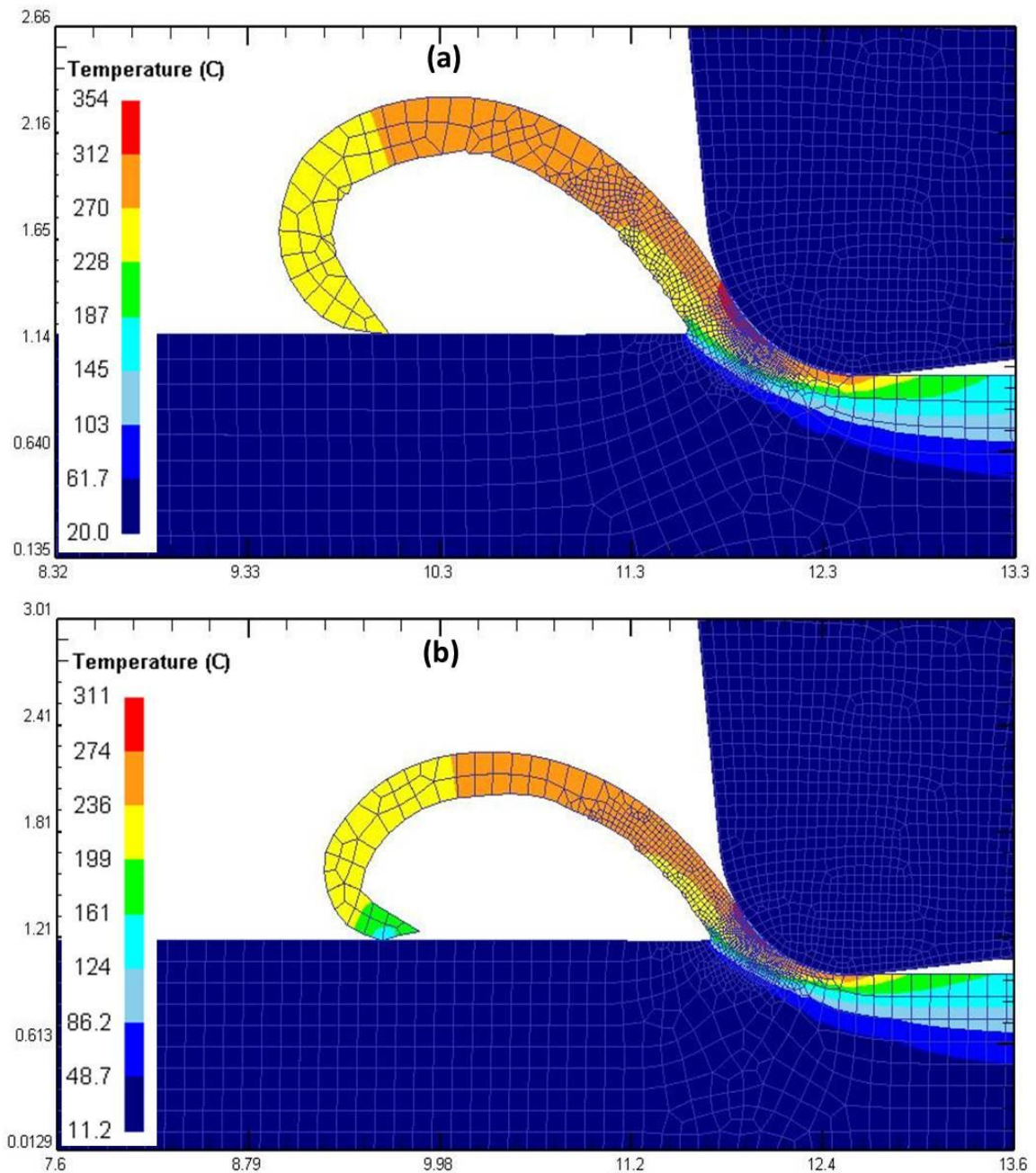


**Fig. 6.7.** Comparison of experimental and FE simulated cutting temperature during AA7075-T6 machining with and without coated tools at different cutting speeds ( $f = 0.3$  mm/rev).

As an example, a steady-state thermal condition outlining the temperature distribution at tool-chip contact when simulating AA7075-T6 machining process using uncoated and coated



cutting tool is presented in Fig. 6.8. From the results, it can be noticed that the maximum cutting temperature is higher for  $V_c = 250$  m/min (Fig. 6.7). This confirms that as the cutting speed progresses it produces workmaterial thermal softening, hence reduction in cutting force was observed, which validates the results presented in chapter 5.



**Fig. 6.8.** FE predictions of cutting temperatures when simulating AA7075-T6 machining process: (a) with uncoated tool, and (b) EMSL coated tool at 250 m/min and 0.3 mm/rev.

The relative error between experimental and numerical predictions of cutting forces and cutting temperatures at different cutting speeds ( $f = 0.3$  mm/rev) is calculated using the expression as shown in Eq.6.21 and results are presented in Table 6.8.

$$\text{Percentage of error} = \frac{[X_{fem} - X_{exp}]}{X_{exp}} \times 100 \quad (6.21)$$

where, ' $X_{exp}$ ' is the experimental value, and ' $X_{fem}$ ' is the FE simulated value.

**Table 6.8.** Percentage of error (%) between experimental and FE simulated results of cutting forces and cutting temperatures when machining AA7075-T6 material with and without coated cutting tool.

Cutting tool	Cutting speed (m/min)					
	150		200		250	
	$\Delta_1$	$\Delta_2$	$\Delta_1$	$\Delta_2$	$\Delta_1$	$\Delta_2$
Uncoated	8.82	9.01	9.54	8.53	10.65	7.51
Coated	9.25	8.63	10.31	8.83	10.52	8.74

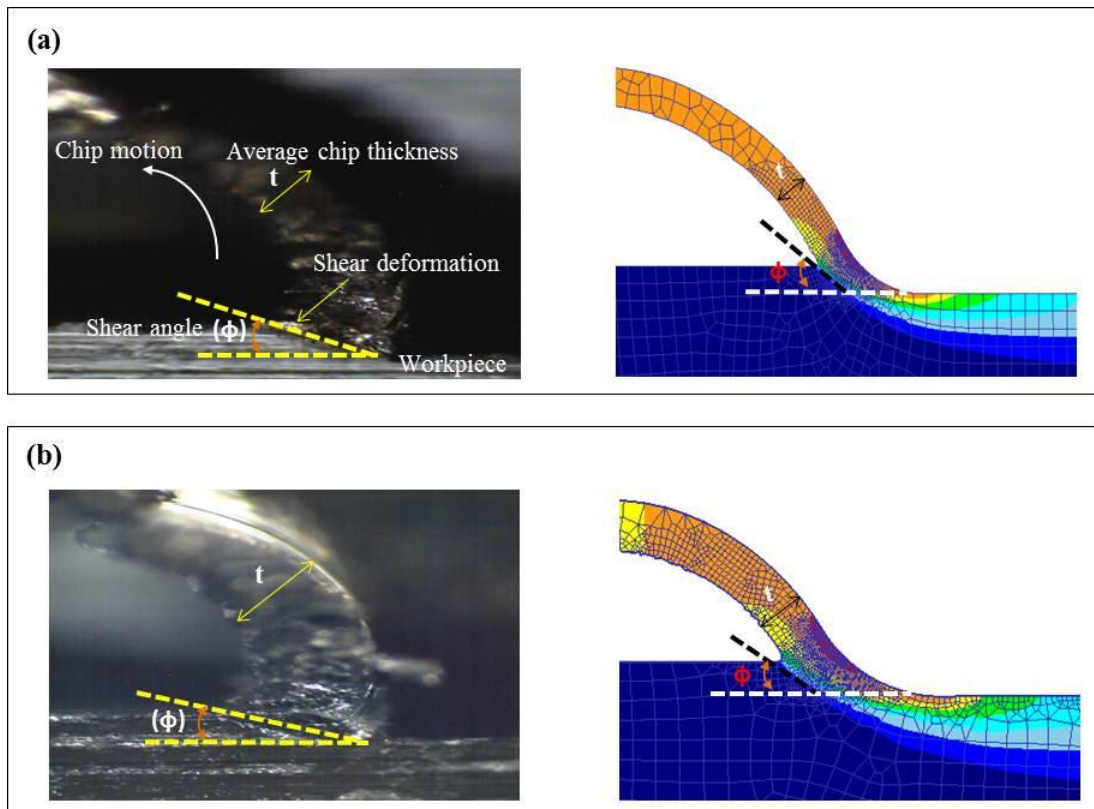
$\Delta_1$  = Error (%) between measured and predicted cutting forces

$\Delta_2$  = Error (%) between measured and predicted cutting temperatures

It can be observed from the Table 6.8 that the agreement between experimental and predicted results of cutting forces and cutting temperatures when cutting AA7075-T6 with and without coated cutting tool is reasonably well as the relative error is very low at all cutting speed conditions. The relative error in all the cutting conditions about 10% was observed. Further, in all the cutting conditions, the simulated results of cutting forces and cutting temperatures are little high when compared to the experimental results due to discretization of the tool-chip contact and the frequent remeshing of the deformed region

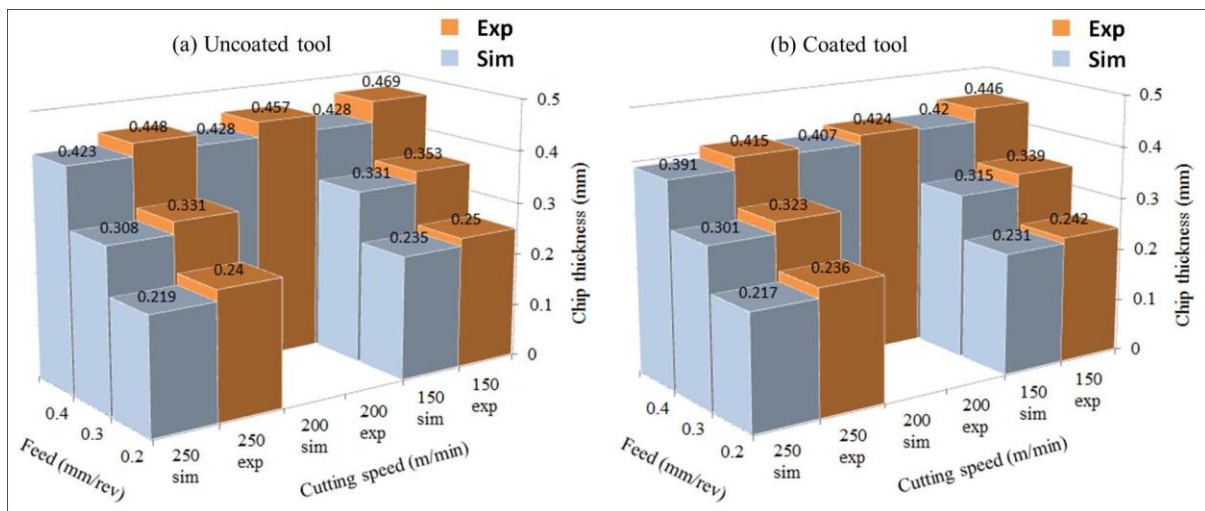
representing chip geometry. It can be concluded here that the proposed FE machining model allows to predict accurately the cutting forces and cutting temperatures and is helpful in better understanding of the physical cutting process variables and to relate the same with practical conditions of machining process before resorting to costly and time consuming experimental trials.

Chip thickness is another important parameter that can be readily monitored and measured. The chip thickness is as a function of the shear angle, feed and rake angle. In the current research work, chip morphology was characterized by the chip thickness to compare the experimental chip thickness with the FE simulation results. It is noticed that continuous chip morphology exists in both the simulated and experimental results during machining with both coated and uncoated cutting tool (Fig. 6.9).



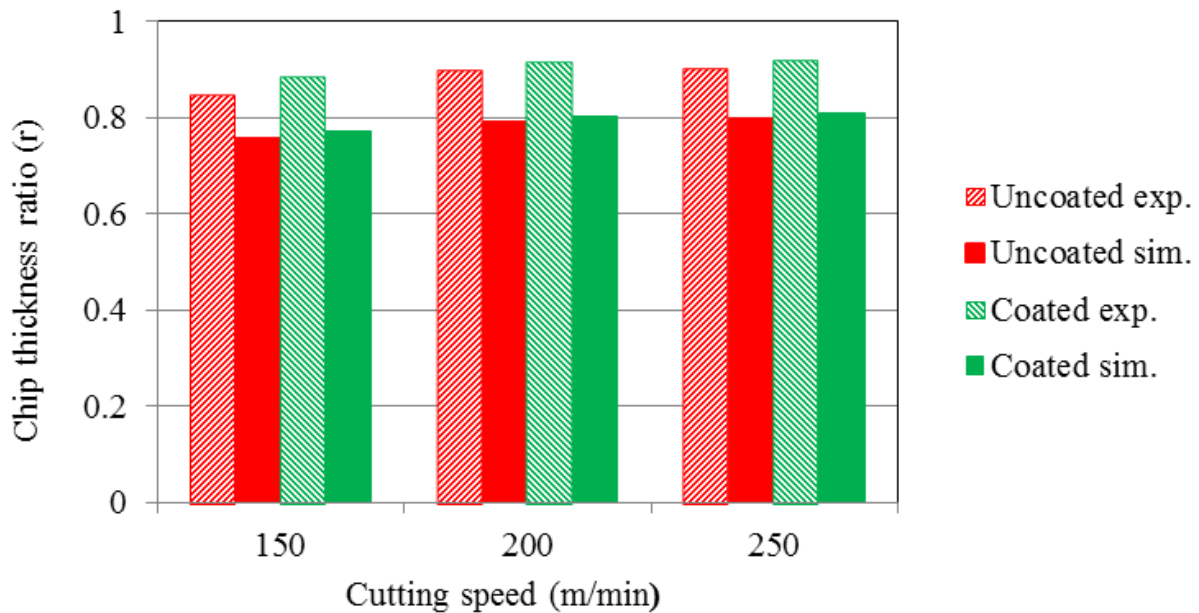
**Fig. 6.9.** Experimental and FE simulated chip formation: (a) with coated cutting tool, and (b) with uncoated cutting tool (cutting conditions: 200 m/min and 0.3 mm/rev).

Fig. 6.10 presents the FE simulated and measured chip thicknesses when machining AA7075-T6 workmaterial with and without coated cutting tools at different cutting speed and feed conditions. It can be seen that the chip thicknesses are in best agreement at all feed rates irrespective of cutting speeds. The machining simulations reveal that chip thickness is a function of feed and cutting speed. The chip thickness increase with increasing feed rate, but cutting speed does not have a major influence. This can be seen from Fig. 6.10 as the cutting speed increases there is no much considerable change in the predicted values of chip thickness.



**Fig. 6.10.** Experimental and FE simulated chip thicknesses during AA7075-T6 machining with and without coated cutting tool at different cutting speeds and feeds.

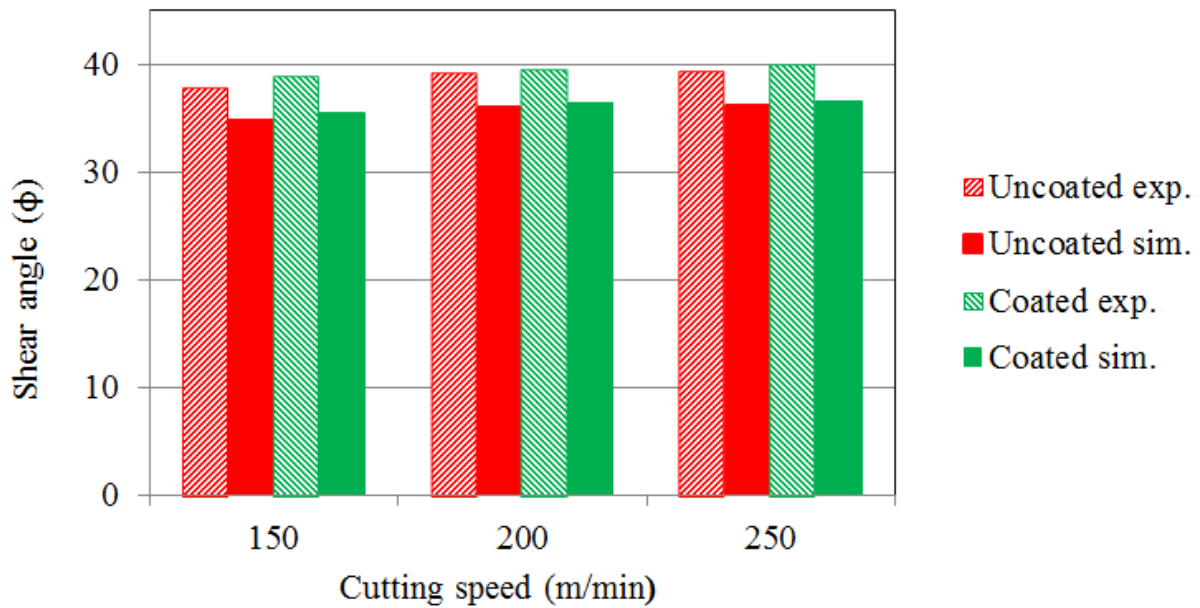
The chip thickness ratio (reciprocal of chip reduction coefficient), which is calculated as the ratio of uncut chip thickness to deformed chip thickness, is the prime parameter in knowing the shear angle and determining the cutting process efficiency. In the current work, the calculated chip thickness ratio when simulating the AA7075-T6 cutting process using uncoated and coated cutting tool is presented in Fig. 6.11.



**Fig. 6.11.** Comparison of experimental and FE simulated results of chip thickness ratio during AA7075-T6 machining process with and without coated cutting tools at different cutting speeds ( $f = 0.3$  mm/rev).

The shear angle is an important parameter that factors into cutting forces as well as the cutting temperatures of the machining process. The shear angle measured between the direction of cutting speed and the plane of separation (shear plane) of workmaterial layer in the form of chip from the workmaterial (see Fig. 6.9). In all the cutting conditions at different cutting speeds and feed rates, it is observed that for both the machining, i.e. machining with coated cutting tool and machining with uncoated cutting tool, the shear angle measurements are in good agreements with FE simulated results. As an example at specified cutting condition, the comparison of experimental and FE simulated results of shear angle in both the machining conditions is presented in Fig. 6.12. Further, from Fig. 6.12 it is noticed that the shear angle is significantly depending on the cutting speed. The increase of shear angle with cutting speed is in accordance with the principle of minimum rate of work. The increasing

shear angle reduces the primary shear area and thus reduces the induced specific cutting energy at tool-chip contact (please see the results of chapter 5).



**Fig. 6.12.** Comparison of experimental and FE simulated results of shear angle during AA7075-T6 machining process with and without coated cutting tools at different cutting speeds ( $f = 0.3$  mm/rev).

The relative error between experimental and numerical predictions of chip thickness ratio and shear angle results is presented in Table 6.9. Results indicate that the FE simulated values are very well correlated with the experimental results as the percentage error in all the cutting conditions below 13% was observed. From the results presented in chapter 5, it was observed that as the cutting speed progresses results in lower specific cutting energy due to thermal softening in the material, which in turn reduces the cutting forces. This same phenomenon is also observed during FE machining process. Further, the FE simulated results of shear angle with coated tool machining is more than that of uncoated one and this trend is very well correlated with experimental observation. From Fig. 6.12, in both the cases i.e.



numerical simulations and experiment results, it is noticed that as the cutting speed increases, the shear angle increases due to improvement in cutting ratio (chip thickness ratio). So, it implies that FE model can work effectively as a prognostic tool when simulating AA7075-T6 machining process and comprehending machining process variables.

**Table 6.9.** Percentage of error (%) between experimental and FE simulated results of chip thickness ratio and shear angle when machining AA7075-T6 material with and without coated cutting tool.

Cutting tool	Cutting speed (m/min)					
	150		200		250	
	$\Delta_1$	$\Delta_2$	$\Delta_1$	$\Delta_2$	$\Delta_1$	$\Delta_2$
Uncoated	11.07	7.80	11.90	8.16	11.73	8.06
Coated	12.55	8.79	12.43	7.81	12.05	8.31

$\Delta_1$  = Error (%) between measured and predicted chip thickness ratio

$\Delta_2$  = Error (%) between measured and predicted shear angle

## 6.6. Summary

FEM approach of machining process concurrently with machining experiments under varying cutting conditions was presented to have a relative comparison of performance of coated cutting tools with uncoated cutting tools. FE modelling of machining process by taking into account the frictional effects based on combination of shear friction and Coulomb friction and material flow behavior based on formulated Zerilli-Armstrong (ZA) model was demonstrated with the help of numerical code, DEFORM<sup>TM</sup>. Numerical predictions in terms of cutting force, cutting temperature, chip thickness and shear angle were compared with the experimental one when machining AA7075-T6 workmaterial with and without coated cutting tools. The FE simulated values are very well correlated with the experimental results in both

the cases, i.e. during machining with coated tool and machining with uncoated tool. The percentage error observed between the experimental and FE simulated results of cutting force and cutting temperature is about 10% in all the conditions when machining with and without coated cutting tool. Further, in all the cutting conditions and in both the machining environment, it is observed that the average chip thickness and shear angle values from machining tests reasonably agrees with the FE simulation results. Therefore, the FEM will be used effectively for predicting the physical cutting process variables such as cutting forces, cutting temperatures, chip thickness and shear angle during machining process.



# CHAPTER 7

## CONCLUSIONS AND FUTURE WORK

---

### 7.1. Summary

Demands on products and production processes are the driving factors behind developments in today's cutting technologies. Innovations such as the application of advanced workmaterial concepts, together with the needs for sustainable machining processes, increased flexibility and improved cost-effectiveness trigger the application of high performance processes, imposing higher stresses on development of new cutting tools. In this direction, coating technology is one means of achieving a crucial enhancement in tool performance. However, there is such a huge variety of available coating materials, coating structures and coating processes that careful selection of a suitable coating system is essential in producing coated tools. In the present research work, applying electrostatic charging principle in coating deposition know-how may contribute to the development of first-ever bonded solid lubricant coatings for machining operations.

### 7.2. Specific contribution

The thesis has contributed to the comprehensive understanding of EMSL coatings on tool substrates as an appreciated approach in enhancing tribological as well as machining process performance. It is expected that the outcomes of current research will not only help to improve the productivity and product quality in machining industry but also contribute to the promotion of manufacturing sustainability. The research also offers a scientific step (through novel coatings) in extending cutting performances in machining such as cutting force, cutting temperature, chip formation and the quality of finish on the machined surface and assist in optimization of cutting process parameters. Further, the research on EMSL coatings can

contribute towards improving the competitiveness of manufacturing industry, universities and research centers and enabling to dissemination of knowledge transfer to researchers working in the relevant fields.

### **7.3. Conclusions**

Based on the review of literature on lubrication/cooling approaches in machining processes for the effect of controlling cutting temperatures, cutting forces and frictional influences, the current research work presents a new methodology in developing solid lubricant coated cutting tools for machining processes. The tribological performance of EMSL coatings is assessed in dry sliding conditions over a wide range of sliding speeds and applied loads. In addition to this, the effectiveness of coated cutting tools in terms of cutting forces, cutting temperatures, tool wear, chip formation, shear angle and surface roughness of machined workmaterial is studied at different cutting conditions. Finally, FE modelling was incorporated to cutting process in order to predict the performance of coated cutting tools in terms of cutting forces, cutting temperatures, chip thickness and shear angle when metal machining and analyze the FE simulated results with experimental performance. For this purpose, formulated Zerilli-Armstrong (ZA) model is used as constitutive relation to denote elastic-plastic behavior of workmaterial when simulating the machining process. Tool-chip interfacial friction modelling is based on the combined frictional effects along the sticking and sliding region on the tool-chip contact area. It was observed during the course of this investigation that the method of applying novel solid lubricant coatings on cutting tools and their influence in tribological and as well as in machining processes have a significant bearing on the performance measures. FE simulated results of cutting process variables are very well correlated with the experimental findings.

The following are the major conclusions which can be drawn from the research work.

1. The developed EMSL coating deposition experimental setup appears to be very helpful in depositing micron-sized solid lubricant particles on cutting tools. The tested performance of EMSL coated tools is quite agreeable in dry sliding and machining conditions. Experimental findings could herald widespread advantages of EMSL coatings over a range of experimental domain and opens a new way to implement the EMSL coatings prepared by an inexpensive process and can endow an alternative coating for tribological and as well as machining operations.
2. From scratch testing on the coated surface, it is observed that the highest critical load of bonded MoS<sub>2</sub> coating prepared by EMSL coating process is about 69 N, indicating that electrostatically deposited MoS<sub>2</sub> coating has quite reasonable coating strength and compared favorably with a reported (previous study) critical load of about 80 N measured by scratch testing for conventional MoS<sub>2</sub> and MoS<sub>2</sub>/metal based coatings prepared by sputtering deposition process.
3. The tribological performance of novel coatings, EMSL coatings, has been demonstrated successfully in dry sliding conditions. EMSL coatings have a high tendency in adhering to the tool substrate and demonstrate the benefits in curtailing the contact frictional effects, enhancing wear resistance and contribute to the favorable control of heat generation at the sliding contact. The performance of EMSL coatings was most obvious at all sliding conditions (on average about 50% friction reduction). The positive results with EMSL coating specimen are owing to the inherent low shear strength of lamellar structured MoS<sub>2</sub> solid lubricant, which can transfer to the sliding track on the disc surface during sliding and contribute to the lower frictional forces.

4. In both the tribological pairs under investigation (see chapter 4), the wear volume of the specimen is linear and satisfying the classical Archard's wear law and directly dependent on the mechanical energy dissipated in the sliding contact. Further, the specific wear rate of EMSL coatings is very low (42% less) when compared to that of uncoated one. Wear rate values of the solid lubricant coated specimen in this study are in reasonable agreement with the results presented in previous studies. Thus, the EMSL bonded MoS<sub>2</sub> coating has a strong potential to enhance the process performance and are able to use quite satisfactorily in tribological applications.
5. In all the tribological conditions tested, the depth of the wear scars present on the disc material when sliding against uncoated specimen is deeper than that of a disc material sliding against EMSL coated specimen. The high material removal from the disc material surface against uncoated specimen is attributed to mechanical plowing action which resulted in high friction between the opposing surfaces and considerable plastic deformation of asperities caused during sliding motion.
6. The machining performance of EMSL coated cutting tools was judged in comparison with the uncoated cutting tools during turning process. Under the same cutting conditions, machining with EMSL coated cutting tools results in lower tool-chip contact frictional effects and cutting temperature and minimum specific cutting energy due to thermal softening at tool-work interface leading to reasonable lower cutting forces (15-18% less) than those in machining with uncoated cutting tools. As a result of lesser cutting forces and temperatures, tool flank wear in EMSL coated cutting tools is very low on average by 25% less as compared to that of the uncoated cutting tool.
7. The formation of BUE on coated cutting tool edge is found to have a significant effect on the quality of machined surfaces. It is true because as the cutting speed increases,

the adhering tendency is low and the BUE becomes sparse and chip fracture decreases, and hence, surface quality improves (20-25% higher). Shear deformation to form chips under all experiments was judged and observed favorable tool– chip interaction in machining with EMSL-coated tools. This is true because lower cutting temperatures due to the existence of MoS<sub>2</sub> solid lubricant on the tool surface can lead to higher shear deformation (high shear angle).

8. FEM approach of cutting process concurrently with machining experiments under varying cutting conditions was presented to have the relative comparison of performance of coated cutting tools with uncoated cutting tools. The outcome of numerical simulation results indicate that the average relative error between experimental and FE simulated results of cutting forces, cutting temperatures, chip thickness and shear angle when machining with and without coated tools is very well correlated with experimental results. Thus, FEM can be used effectively in prognostic process engineering to comprehend the physical cutting process variables during machining process.
9. The experimental and predicted results in machining, i.e. machining with uncoated cutting tool and machining with coated cutting tool show that as the cutting speed increases, the chip thickness marginally decreases. Although, the experimental and predicted results showed a very good agreement in the trend for chip thickness, the experimental results were found to be little higher than the predicted results. The reason for this could be due to side spreading of the workmaterial occurred at the depths of cut used. Further, in both the machining, it can be seen that the chip thicknesses are in best agreement at all feed rates irrespective of cutting speeds. The chip thicknesses increase with increasing feed rate, but cutting speed does not have a significant effect on the chip thickness results.

## 7.4. Future work

It would be interesting to continue the present investigation using various solid lubricant material combination (for example MoS<sub>2</sub>/Ti, MoS<sub>2</sub>/Zr, MoS<sub>2</sub>/Tic, etc.) effects incorporating to the current approach in order to standardize the performance of EMSL coated tools to further level, especially with different tool–workmaterial groups.

Some possible ways to continue the research could be:

1. Tribological performance testing in different environments (vacuum and high temperatures) and other combinations of tribological contacts (contact surfaces subjected to rolling and rolling sliding). This part of study is not included in the current research because of unavailability of testing facilities and time limitations.
2. In order to spread the application of EMSL coatings in industry practices, study on rotational fretting wear behavior of coatings need to be conducted. Since the use of friction reduction coatings is one of the most effective way to palliate fretting failure. The dissipated energy approach and Archard's wear factor will be used to evaluate and predict the durability of coatings.
3. Predicting cutting tool wear while machining hardened materials, like stainless steel, titanium alloy, inconel, etc. (difficult to cut materials, which are used for aerospace, steam turbine, bearing industry, nuclear and automotive applications). To achieve this, it will involve the prior estimation for the chip geometry and the tool-chip contact length and require number of iterative procedures including changing boundary conditions and mesh design until convergence is achieved.

## APPENDICES

---

### Appendix A

#### Particle surface charge to mass ratio calculation:

Particle surface charge as per Pauthrnie's equation is expressed with Eq.A.1.

$$q = A \varepsilon_o \left[ 1 + 2 \left( \frac{\varepsilon_r - 1}{\varepsilon_r + 2} \right) \right] E \quad (\text{A.1})$$

For particles having  $\varepsilon_r \rightarrow \infty$  (MoS<sub>2</sub> metallic particles), the Eq.A.1 becomes as follows:

$$q_{max} = 12 \pi r^2 \varepsilon_o E \quad (\text{A.2})$$

Mean charge to mass ratio ( $q_{max}/m$ ) of the particle can be estimated using the Eq.A.3.

$$\frac{q_{max}}{m} = \frac{12 \pi r^2 \varepsilon_o E}{\left(\frac{4}{3}\right) \pi r^3 \rho} \quad (\text{A.3})$$

where,

A = Surface area of the particle =  $4 \pi r^2$

where, r = radius of the particle (mean particle size (2r) of solid lubricant is 0.7  $\mu\text{m}$ )

$\varepsilon_o$  = permittivity of the space =  $8.85 \times 10^{-12}$  Coulomb/Volt

$\varepsilon_r$  = ratio of the permittivities of particles to that of space(Coulomb/Volt)

E = strength of the electric field (assumed as  $3 \times 10^5$  Newton/Coulomb)

m = mass of the particle (g)

$\rho$  = density of the particle (4.8 g/cc)

$$\begin{aligned} \frac{q_{max}}{m} &= \frac{12 \pi r^2 \epsilon_0 E}{\left(\frac{4}{3}\right) \pi r^3 \rho} = \frac{9 \epsilon_0 E}{\rho r} \\ &= \frac{9 (8.85 \times 10^{-12})(3 \times 10^5)}{(4.8 \times 10^3)(0.35 \times 10^{-6})} \\ &= 142.2 \times 10^{-4} \text{ Coulomb/kg} \end{aligned}$$

### **Transfer efficiency calculation:**

Transfer efficiency of the developed coating deposition system is estimated by weighing balance method using the following relation (Eq.A.4)

$$\text{Transfer efficiency} = \frac{\text{Amount of powder adhered to the tool substrate}}{\text{Total powder sprayed}} \quad (\text{A.4})$$

Amount of powder (weight) adhered to one tool substrate = density of the particles X volume covered on the tool substrate

*Conditions:*

(Substrate dimensions = 20 X 20 X 10 mm (used in coating experiments for transfer efficiency calculation purpose))

Coating thickness measured = 10  $\mu\text{m}$  (approx.)

Volume covered on each substrate:

$$\begin{aligned} &= [(20 \times 20)10^{-6}][10 \times 10^{-6}][2] + [(20 \times 10)10^{-6}][10 \times 10^{-6}][4] \\ &\hspace{15em} (\text{since substrate is having 6 surfaces}) \\ &= 16 \times 10^{-9} \text{ m}^3 \end{aligned}$$

Therefore, the amount of powder adhered to one tool substrate is equal to

= density of particle X volume covered on each substrate:



$$= [4.8 \times 10^3][16 \times 10^{-9}]$$

$$= 76.8 \times 10^{-6} \text{ kg}$$

$$= 0.0768 \text{ g}$$

Total amount of powder adhered to all tool substrates (4 parts coated) = 0.3072 g

Total weight of material sprayed to achieve desired coating thickness = 0.501 g

Therefore, the transfer efficiency = 61.3%.

*Note:* The calculated powder particle mean charge to mass ratio is about  $142.2 \times 10^{-4}$  Coulomb/kg, which is many times more than the usually required particle charge to mass ratio ( $5 \times 10^{-4}$  Coulomb/kg) in any deposition using electrostatic charging principle. Therefore, the developed EMSL coating process transfer efficiency appears to be quite agreeable as it offer the high particle adhering tendency (high wraparound of particles to the tool substrate).

## Appendix B

Specimen wear volume and wear rate in were calculated according to the following equations B.1 and B.2 respectively.

$$WV = \frac{\pi}{24} (D_2 - D_1) (D_1^2 + D_2^2 + D_1 D_2) \quad (\text{B.1})$$

$$WR = \frac{WV}{F_n L} \quad (\text{B.2})$$

where, 'WV' (mm<sup>3</sup>) is the pin wear volume, 'WR' (mm<sup>3</sup>/(N.m)) is the pin wear rate, 'D<sub>1</sub>' and 'D<sub>2</sub>' (mm) respectively the mean value of an initial diameter and of the final diameter of the pin contact surface, 'F<sub>n</sub>' (N) is the normal load, and 'L' (m) is the sliding distance.

The energy dissipated ( $\Delta E$ ) in the sliding contact is calculated as per the following equation B.3.

$$\Delta E = \bar{F} V \Delta t \quad (\text{B.3})$$

where, 'F' (N) is the frictional force, 'V' (m/min) is the constant sliding speed and ' $\bar{F}$ ' (N) is the average value of frictional force calculated from the acquired friction force data.

Specimen wear rate, wear volume and energy dissipated in two tribopairs were calculated for corresponding normal load and sliding speed conditions and results presented in Table B.1.

**Table B.1** Wear volume, wear rate and dissipated energy obtained from dry sliding tests.

Tribopair	Applied load (N)	Exp. No.	Sliding speed (m/min)	c.o.f	$\Delta t$ (min)	$D_1$ (mm)	$D_2$ (mm)	$D_1^2$	$D_2^2$	$D_1 * D_2$	$D_2 - D_1$	$\frac{\pi}{24}$	$F_n * L$ (N.m)	WV ( $\text{mm}^3$ )	WR ( $\times 10^{-6}$ ) ( $\text{mm}^3/\text{N.m}$ )	$\Delta E$ (J)
1	40	1	50	0.49	10	4	4.00186	16	16.01488	16.00744	0.00186	0.13095	20000	0.01169665	0.584833	9800
		2	100	0.42	10	4	4.00225	16	16.01800	16.009	0.00225	0.13095	40000	0.01415055	0.353764	16800
		3	150	0.36	10	4	4.00337	16	16.02697	16.01348	0.00337	0.13095	60000	0.02120032	0.353339	21600
		4	200	0.33	10	4	4.00428	16	16.03425	16.01712	0.00428	0.13095	80000	0.02693116	0.336640	26400
		5	250	0.31	10	4	4.00426	16	16.03409	16.01704	0.00426	0.13095	100000	0.02680518	0.268052	31000
	60	1	50	0.46	10	4	4.00213	16	16.01711	16.00855	0.00213	0.13095	30000	0.01345208	0.448403	13800
		2	100	0.4	10	4	4.00225	16	16.01806	16.00903	0.00225	0.13095	60000	0.01420089	0.236682	24000
		3	150	0.35	10	4	4.00241	16	16.01935	16.00967	0.00241	0.13095	90000	0.01521406	0.169045	31500
		4	200	0.31	10	4	4.00253	16	16.02031	16.01015	0.00253	0.13095	120000	0.01596927	0.133077	37200
		5	250	0.29	10	4	4.00293	16	16.02349	16.01174	0.00293	0.13095	150000	0.01846807	0.123120	43500
	80	1	50	0.44	10	4	4.00251	16	16.02014	16.01006	0.00251	0.13095	40000	0.01583081	0.395770	17600
		2	100	0.39	10	4	4.00286	16	16.02292	16.01145	0.00286	0.13095	80000	0.01801485	0.225186	31200
		3	150	0.33	10	4	4.00310	16	16.02488	16.01243	0.00310	0.13095	120000	0.01955712	0.162976	39600
		4	200	0.31	10	4	4.00331	16	16.02654	16.01326	0.00331	0.13095	160000	0.02086662	0.130416	49600
		5	250	0.28	10	4	4.00341	16	16.02734	16.01366	0.00341	0.13095	200000	0.02148995	0.107450	56000
2	40	1	50	0.34	10	4	4.00134	16	16.01072	16.00536	0.00134	0.13095	20000	0.00842552	0.421276	6800
		2	100	0.31	10	4	4.00153	16	16.01224	16.00612	0.00153	0.13095	40000	0.00962064	0.240516	12400
		3	150	0.29	10	4	4.00209	16	16.01672	16.00836	0.00209	0.13095	60000	0.01314376	0.219063	17400
		4	200	0.27	10	4	4.00349	16	16.02793	16.01396	0.00349	0.13095	80000	0.02195588	0.274449	21600
		5	250	0.25	10	4	4.00379	16	16.03033	16.01516	0.00379	0.13095	100000	0.02384500	0.238450	25000
	60	1	50	0.32	10	4	4.00162	16	16.01300	16.0065	0.00162	0.13095	30000	0.01021825	0.340608	9600
		2	100	0.31	10	4	4.00173	16	16.01387	16.00693	0.00173	0.13095	60000	0.01090395	0.181733	18600
		3	150	0.28	10	4	4.00179	16	16.01438	16.00719	0.00179	0.13095	90000	0.01130659	0.125629	25200
		4	200	0.25	10	4	4.00193	16	16.01548	16.00774	0.00193	0.13095	120000	0.01216852	0.101404	30000
		5	250	0.24	10	4	4.00206	16	16.01650	16.00825	0.00206	0.13095	150000	0.01297388	0.864925	36000
	80	1	50	0.3	10	4	4.00213	16	16.01704	16.00852	0.00213	0.13095	40000	0.01339545	0.334886	12000
		2	100	0.29	10	4	4.00289	16	16.02313	16.01156	0.00289	0.13095	80000	0.01818480	0.227310	23200
		3	150	0.27	10	4	4.00310	16	16.02485	16.01242	0.00310	0.13095	120000	0.01953194	0.162766	32400
		4	200	0.25	10	4	4.00328	16	16.02628	16.01313	0.00328	0.13095	160000	0.02065886	0.129118	40000
		5	250	0.23	10	4	4.00335	16	16.02687	16.01343	0.00335	0.13095	200000	0.02112476	0.105624	46000

## REFERENCES

---

- [1] V.S. Sharma, Manu Dogra, N.M. Suri, Cooling techniques for improved productivity in turning, *International Journal of Machine Tools & Manufacture*, 49 (2009), 435-453.
- [2] J.P. Davim, P.S. Sreejith, R. Gomes, C. Peixoto, Experimental studies on drilling of aluminium (AA1050) under dry, minimum quantity of lubricant, and flood-lubricated conditions, *Proceedings of the Institution of Mechanical Engineers, Part B: Journal of Engineering Manufacture*, 220 (10) (2006), 1605-1611.
- [3] E.O. Bennett, Water based cutting fluids and human health, *Tribology International*, 16 (3) (1983), 133-136.
- [4] P.C. Raynor, S.W. Kim, M. Bhattacharya, Mist generation from metalworking fluids formulated using vegetable oils, *The Annals of Occupational Hygiene*, 49 (4) (2005), 283-293.
- [5] A. Birova, A. Pavlovicova, J. Cvenros, Lubricating oils based on chemically modified vegetable oils, *Journal of Synthetic Lubrication*, 18 (4) (2002), 291-299.
- [6] Deng Jianxin, Cao Tongkun, Yang Xuefeng, Liu Jianhua, Self lubrication of sintered ceramic tools with CaF<sub>2</sub> additions in dry cutting, *International Journal of Machine Tool & Manufacture*, 46 (9) (2006), 957-963.
- [7] Deng Jianxin, Cao Tongkun, Liu Lili, Self-lubricating behaviors of Al<sub>2</sub>O<sub>3</sub>/TiB<sub>2</sub> ceramic tools in dry high-speed machining of hardened steel, *Journal of the European Ceramic Society*, 25 (7) (2005), 1073-1079.
- [8] Deng Jianxin, Cao Tongkun, Ding Zeliang, Liu Jianhua, Sun Junlong, Zhao Jinlong, Tribological behaviors of Al<sub>2</sub>O<sub>3</sub>/TiC ceramic composites with the additions of CaF<sub>2</sub> solid lubricants, *Journal of the European Ceramic Society*, 26 (8) (2006), 1317-1323.

- [9] B.C. Schramm, H. Scheerer, H. Hoche, E. Broszeit, E. Abele, C. Berger, Tribological properties and dry machining characteristics of PVD-coated carbide inserts, *Surface & Coatings Technology*, 188-189 (2004), 623-629.
- [10] T. Aizawa, A. Mitsuo, S. Yamamoto, T. Sumitomo, S. Muraishi, Self-lubrication mechanism via the in situ formed lubricious oxide tribofilm, *Wear*, 259 (2005), 708-718.
- [11] V. Fox, A. Jones, N.M. Renevier, D.G. Teer, Hard lubricating coatings for cutting and forming tools and mechanical components, *Surface & Coatings Technology*, 125 (2000), 347-353.
- [12] You-Rong Liu, Jia-Jun Liu, Zhi Du, The cutting performance and wear mechanism of ceramic cutting tools with MoS<sub>2</sub> coating deposited by magnetron sputtering, *Wear*, 231 (1999), 285-292.
- [13] C. Donnet, A. Erdemir, Solid lubricant coatings: recent developments and future trends, *Tribology Letters*, 17 (3) (2004), 389-397.
- [14] R. F. Bunshah, *Handbook of deposition technologies for films and coatings: Science, Technology and Applications*, Second edition, Noyes publications, Park Ridge, New Jersey, USA, 1994.
- [15] A. Jaworek, Electrospray droplet sources for thin film deposition, *Journal of Materials Science*, 42 (2007), 266-297.
- [16] Wenping Jiang, Ajay P. Malshe, R. Calvin Goforth, Cubic Boron Nitride (cBN) based nano-composite coatings on cutting inserts with chip breakers for hard turning applications, *Surface & Coatings Technology*, 200 (2005), 1849-1854.
- [17] Narala Suresh Kumar Reddy, Mohammed Nouari, Minyang Yang, Development of electrostatic solid lubrication system for improvement in machining process

- performance, *International Journal of Machine Tools & Manufacture*, 50 (9) (2010), 789-797.
- [18] N.S.K. Reddy, M. Yang, Development of an electrostatic lubrication system for drilling of SCM 440 steel, *Proceedings of the Institution of Mechanical Engineers, Part B: Journal of Engineering Manufacture*, 224 (2) (2010), 217-224.
- [19] E.M. Trent, P.K. Wright, *Metal Cutting*, Fourth edition, Butterworth–Heinemann, Boston, 2000.
- [20] B. Bhushan, *Modern Tribology Handbook*, CRC Press, New York, 2000.
- [21] P.J. Arrazola, T. Ozel, Investigations on the effects of friction modelling in finite element simulation of machining, *International Journal of Mechanical Sciences*, 52 (2010), 31-42.
- [22] P.J. Arrazola , A. Kortabarria, A. Madariaga, J.A. Esnaola, E. Fernandez, C. Cappellini, D. Ulutan, T. Ozel, On the machining induced residual stresses in IN718 nickel-based alloy: Experiments and predictions with finite element simulation, *Simulation Modelling Practice and Theory*, 41 (2014), 87-103.
- [23] C. Bruni, A. Forcellese, F. Gabrielli, M. Simoncini, Effect of the lubrication-cooling technique, insert technology and machine bed material on the workpart surface finish and tool wear in finish turning of AISI 420B, *International Journal of Machine Tools & Manufacture*, 46 (2006), 1547-1554.
- [24] Annette Norin, Georg Erkens, Product life cycle, Sulzer technical review (<http://www.sulzer.com>), 2013.
- [25] A.T. Simpson, M. Stear, J.A. Groves, M. Piney, S.D. Bradley, S. Stagg, B. Crook, Occupational Exposure to Metalworking Fluid Mist and Sump Fluid Contaminants, *The Annals of Occupational Hygiene*, 47 (1) (2003), 17-30.

- [26] HSE, Health Surveillance of Occupational Skin Diseases, MS 24, HSE Books, London, 1991.
- [27] U.S. Dixit, D.K. Sarma, J. Paulo Davim, Environmentally friendly machining, Springer, New York, 2012.
- [28] P.S. Sreejith, B.K.A. Ngoi, Dry machining: Machining of the future, Journal of Materials Processing Technology, 101 (2000), 287-291.
- [29] Anselmo Eduardo Diniz, Ricardo Micaroni, Cutting conditions for finish turning process aiming: the use of dry Cutting, International Journal of Machine Tools & Manufacture, 42 (2002), 899-904.
- [30] F. Klocke, G. Eisennblatter, Dry cutting, CIRP Annals - Manufacturing Technology, 46 (2) (1997), 519-526.
- [31] A.P.S. Gaur, Sanjay Agarwal, Improvement in Surface Quality With Molybdenum Disulphide as Solid Lubricant in Turning AISI 4340 Steel, ASME 2010 International Mechanical Engineering Congress and Exposition, doi:10.1115/IMECE2010-37367.
- [32] Deep Mukhopadhyay, Sankha Banerjee, N. Suresh Kumar Reddy, Investigation to Study the Applicability of Solid Lubricant in Turning AISI 1040 steel, Journal of Manufacturing Science and Engineering, 129 (2007), 520-526.
- [33] Dilbag Singh, P. Venkateswara Rao, Improvement in Surface Quality with Solid Lubrication in Hard Turning, Proceedings of the World Congress on Engineering, Vol III, London, U.K., 2008.
- [34] Erdemir, Solid Lubricants and Self-Lubricating Films, CRC Press, USA, 2001.
- [35] D. Nageswara Rao, P. Vamsi Krishna, The influence of solid lubricant particle size on machining parameters in turning, International Journal of Machine Tools & Manufacture, 48 (2008), 107-111.

- [36] P. Vamsi Krishna, D. Nageswara Rao, Performance evaluation of solid lubricants in terms of machining parameters in turning, *International Journal of Machine Tools & Manufacture*, 48 (2008), 1131-1137.
- [37] P. Vamsi Krishna, R.R. Srikant, D. Nageswara Rao, Experimental investigation on the performance of nanoboric acid suspensions in SAE-40 and coconut oil during turning of AISI 1040 steel, *International Journal of Machine Tools & Manufacture*, 50 (10) (2010), 911-916.
- [38] P. Vamsi Krishna, D.N. Rao, and R. R. Srikant, Predictive modelling of surface roughness and tool wear in solid lubricant assisted turning of AISI 1040 steel, *Proceedings of the Institution of Mechanical Engineers, Part J: Journal of Engineering Tribology*, 223 (6) (2009), 929-934.
- [39] Singh Dilbag, P. V. Rao, Performance improvement of hard turning with solid lubricants, *The International Journal of Advanced Manufacturing Technology*, 38 (2008), 529-535.
- [40] N. Suresh Kumar Reddy, P. Venkateswara Rao, Experimental investigation to study the effect of solid lubricants on cutting forces and surface quality in end milling, *International Journal of Machine Tools & Manufacture*, 46 (2006), 189-198.
- [41] P. Vamsi Krishna, R.R. Srikant, D. Nageswara Rao, Solid lubricants in machining, *Proceedings of the Institution of Mechanical Engineers, Part J: Journal of Engineering Tribology*, 225 (4) (2011), 213-227.
- [42] S. Shaji, V. Radhakrishnan, An investigation on surface grinding using graphite as lubricant, *International Journal of Machine Tools & Manufacture*, 42 (2002), 733-740.



- [43] S. Shaji, V. Radhakrishnan, Investigations on the application of solid lubricants in grinding, *Proceedings of the Institution of Mechanical Engineers, Part B: Journal of Engineering Manufacture*, 216 (10) (2002), 1325-1343.
- [44] Mukesh Kumar Dubey, Jayashree Bijwe, S.S.V. Ramakumar, PTFE based nano-lubricants, *Wear*, 306 (2013), 80-88.
- [45] M. Lovell, C.F. Higgs, P. Deshmukha, A. Mobley, Increasing formability in sheet metal stamping operations using environmentally friendly lubricants, *Journal of Materials Processing Technology*, 177 (2006), 87-90.
- [46] Erdemir, R. Erck, and J. Robles, Relationship of hertzian contact pressure to friction behavior of self-lubricating boric-acid films, *Surface & Coating Technology*, 49 (1991), 435-438.
- [47] Erdemir, Tribological properties of boric-acid and boric-acid-forming surfaces: Part 1, Crystal-chemistry and mechanism of self-lubrication of boric-acid, *Lubrication Engineering*, 47 (1991), 168-173.
- [48] M.R. Lovell, M.A. Kabir, P.L. Menezes, C.F. Higgs III, Influence of boric acid additive size on green lubricant performance, *Philosophical Transactions of the Royal Society A*, 368 (2010), 4851-4868.
- [49] Pushkarraj Deshmukh, Michael Lovell, W. Gregory Sawyer, Anton Mobley, On the friction and wear performance of boric acid lubricant combinations in extended duration operations, *Wear*, 260 (2006), 1295-1304.
- [50] P. Vamsi Krishna, R.R. Srikant and D.N. Rao, Experimental investigation to study the performance of solid lubricants in turning of AISI1040 steel, *Proceedings of the Institution of Mechanical Engineers, Part J: Journal of Engineering Tribology*, 224 (12) (2010), 1273-1281.

- [51] L.B. Abhang, M. Hameedullah, Control of chip-tool interface temperature for improved productivity through a new lubricating technique, *International Journal of Applied Engineering Research*, 5 (14) (2010), 2373-2382.
- [52] K.P. Rao, C.L. Xie, A comparative study on the performance of boric acid with several conventional lubricants in metal forming processes, *Tribology International*, 39 (2006), 663-668.
- [53] K.P. Rao, Y.V.R.K. Prasad, C.L. Xie, Further evaluation of boric acid vis-a-vis other lubricants for cold forming applications, *Tribology International*, 44 (2011), 1118-1126.
- [54] K.P. Rao, J.J. Wei, Performance of a new dry lubricant in the forming of aluminum alloy sheets, *Wear*, 249 (2001), 86-93.
- [55] William Henry Bragg, *An Introduction to Crystal Analysis*, G. Bell and Sons, London, 1928.
- [56] S. Shaji, V. Radhakrishnan, Analysis of process parameters in surface grinding with graphite as lubricant based on the Taguchi method, *Journal of Materials Processing Technology*, 141 (2003), 51-59.
- [57] Matthew Alberts, Kyriaki Kalaitzidou, Shreyes Melkote, An investigation of graphite nanoplatelets as lubricant in grinding, *International Journal of Machine Tools & Manufacture*, 49 (2009), 966-970.
- [58] D.G. Teer, New solid lubricant coatings, *Wear*, 251 (2001), 1068-1074.
- [59] A.R. Lansdown, *Molybdenum Disulphide Lubrication*, Tribology Series 35, Elsevier, 1999.
- [60] Savan, E. Pfluger, P. Voumard, A. Schroer, M. Simmonds, Modern solid lubrication: Recent developments and applications of MoS<sub>2</sub>, *Lubrication Science*, 12 (2) (2000), 185-203.

- [61] T. Hisakado, T. Tsukizoe, H. Yoshikawa, Lubrication Mechanism of Solid Lubricants in Oils, *Journal of Tribology*, 105 (2) (1983), 245-252.
- [62] P. Voumard, A. Savan, E. Pflüger, Advances in solid lubrication with MoS<sub>2</sub> multilayered coatings, *Lubrication Science*, 13 (2) (2001), 135-145.
- [63] Paul D. Fleischauer, Effects of Crystallite Orientation on Environmental Stability and Lubrication Properties of Sputtered MoS<sub>2</sub> Thin Films, *ASLE Transactions*, 27 (1) (1984), 82-88.
- [64] Hooshang Heshmat, Piotr Hryniewicz, James F. Walton II, John P. Willis, S. Jahanmir, Christopher DellaCorte, Low-Friction Wear-resistant Coatings for High-temperature Foil Bearings, *Tribology International*, 38 (2005), 1059-1075.
- [65] Christopher DellaCorte, Antonio R. Zaldana, Kevin C. Radil, A Systems Approach to the Solid Lubrication of Foil Air Bearings for Oil-Free Turbomachinery, *Journal of Tribology*, 126 (2004), 200-207.
- [66] Song Wenlong, Deng Jianxin, Zhang Hui, Yan Pei, Study on Cutting Forces and Experiment of MoS<sub>2</sub>/Zr-Coated Cemented Carbide Tool, *The International Journal of Advanced Manufacturing Technology*, 49 (2010), 903-909.
- [67] Shtertser, C. Muders, S. Veselov, S. Zlobin, V. Uliantisky, X.Jiang, V.Bataev, Computer controlled detonation spraying of WC/Co coatings containing MoS<sub>2</sub> solid lubricant, *Surface & Coatings Technology*, 206 (2012), 4763-4770.
- [68] Wenping Jiang, Abhijeet S. More, W.D. Brown, Ajay P. Malshe, A cBN-TiN composite coating for carbide inserts: Coating characterization and its applications for finish hard turning, *Surface & Coatings Technology*, 201 (2006), 2443-2449.
- [69] Hao Du, Chao Sun, Weigang Hua, Tiegang Wang, Jun Gong, Xin Jiang, SooWohn Lee, Structure, mechanical and sliding wear properties of WC-Co/MoS<sub>2</sub> - Ni

- coatings by detonation gun spray, *Materials Science and Engineering A*, 445-446 (2007), 122-134.
- [70] Joel Voyer, Basil R. Marple, Tribological performance of thermally sprayed cermet coatings containing solid lubricants, *Surface & Coatings Technology*, 127 (2000), 155-166.
- [71] BailinZha, Xiaojing Yuan, Li Jiang, ZhihongZha, Study on HVOF Sprayed Nickel Coated MoS<sub>2</sub> Coatings, *Advanced Material Research*, 490-495 (2012), 3574-3577.
- [72] Z. Xiaodong, W. Lauwerens, P. Cosemans, M. Van Stappen, J.P. Celis, L.M Stals, H. Jiawen, Different tribological behavior of MoS<sub>2</sub> coatings under fretting and pin-on-disk conditions, *Surface & Coatings Technology*, 163 (2003), 422-428.
- [73] I.L. Singer, S. Fayeulle and P.D Ehni, Wear behavior of triode-sputtered MoS<sub>2</sub> coatings in dry sliding contact with steel and ceramics, *Wear*, 195 (1996), 7-20.
- [74] K. Seock-Sam, A. Chan-Wook and K. Tae-Hyung, Tribological Characteristics of Magnetron Sputtered MoS<sub>2</sub> films in Various Atmospheric Conditions, *KSME International Journal*, 16 (9) (2002), 1065-1071.
- [75] R.C Martins, S.M Paulo, and J.O Seabra, MoS<sub>2</sub>/Ti low-friction coating for gears, *Tribology International*, 39 (12) (2006), 1686-1697.
- [76] N.M. Renevier, J. Hampshire, V.C. Fox, J. Witts, T. Allen, D.G. Teer, Advantages of using self-lubricating, hard, wear-resistant MoS<sub>2</sub> - based coatings, *Surface & Coatings Technology*, 142-144 (2001), 67-77.
- [77] Deng Jianxin, Song Wenlong, Zhang Hui, Zhao Jinlong, Performance of PVD MoS<sub>2</sub>/Zr-coated carbide in cutting processes, *International Journal of Machine Tools & Manufacture* 48 (2008), 1546-1552.
- [78] Dabing Luo, Selection of coatings for tribological applications, Ph.D. thesis, Laboratory of Tribology and System Dynamics (LTDS), France, 2009.

- [79] W. Gisser, H.A. Jehn, *Advanced Techniques for Surface Engineering*, Kluwer Academic Publishers, London, 1992.
- [80] Jan Pana Rabatho, William Tongamp, Atsushi Shibayama, Yasushi Takasaki, Sachihito Nitta, Tetsuo Imai, Investigation of a Flotation Process with De-Sliming and Attrition to Upgrade and Recover Cu and Mo from a Cu-Mo Flotation Tailing, *Materials Transactions, The Mining and Materials Processing Institute of Japan*, 52 (4) (2011), 746-752.
- [81] E.A. Ponomarev, M. Neumann-Spallart, G. Hodes, C. Levy-Clement, Electrochemical deposition of MoS<sub>2</sub> thin films by reduction of tetrathiomolybdate, *Thin Solid Films*, 280 (1996), 86-89.
- [82] M.E. Campbell, John B. Loser, Eldon Sneegas, *Solid Lubricants, Technology Survey by NASA*, Midwest Research Institute, Missouri, USA, 1966.
- [83] O.N. Cora, A. Agcayaz K. Namiki, H. Sofuoglu, M. Koc, Die wear in stamping of advanced high strength steels - investigations on the effects of substrate material and hard-coatings. *Tribology International*, 52 (2012), 50-60.
- [84] L.A. Dobrzanski, L. Wosinska, K. Golombek, J. Mikula, Structure of multicomponent and gradient PVD coatings deposited on sintered tool materials. *Journal of Achievements in Materials and Manufacturing*, 20 (2007), 99-102.
- [85] L.A. Dobrzanski, K. Golombek, Structure and properties of the cutting tools made from cemented carbides and cermets with the TiN+ mono-, gradient- or multi (Ti, Al, Si)N +TiN nanocrystalline coatings, *Journal of Materials Processing Technology*, 164-165 (2005), 805-815.
- [86] L.A. Dobrzanski, L.W. Zukowska, J. Mikula, K. Golombek, D. Pakula, M. Pancielejko, Structure and mechanical properties of gradient PVD coatings, *Journal of Materials Processing Technology*, 20I (2008 ), 310-314.

- [87] A.I. Fernandez-Abia, J. Barreiro, J. Fernandez-Larrinoa, L.N. Lopez de Lacalle, A. Fernandez-Valdivielso, O.M. Pereira, Behaviour of PVD coatings in the turning of austenitic stainless steels, *Procedia Engineering*, 63 (2013), 133-141.
- [88] D.M. Mattox, *Handbook of Physical Vapor Deposition (PVD) Processing*, Noyes publications, USA, 1998.
- [89] E.J. Coad, C.S.J. Pickles, G.H. Jilbert, J.E. Field, Aerospace erosion of diamond and diamond coatings, *Diamond and Related Materials*, 5 (1996), 640-643.
- [90] K.W. Lee, S.J. Harris, Boron carbide films grown from microwave plasma chemical vapour deposition, *Diamond and Related Materials*, 7 (1998), 1539-1543.
- [91] E. Uhlmann, J. Koenig, CVD diamond coatings on geometrically complex cutting tools, *CIRP Annals - Manufacturing Technology*, 58 (2009), 65-68.
- [92] Yoshiko Sato, Junki Kawamura, Takashi Nagase, S.A. Pahlovy, Iwao Miyamoto, Sharpening of CVD diamond coated tools by 0.5–10 keV Ar<sup>+</sup> ion beam, *Diamond and Related Materials*, 20 (7) (2011), 954-959.
- [93] J. Blink, J. Farmer, J. Choi, C. Saw, Applications in the nuclear industry for thermal spray amorphous metal and ceramic coatings, *Metallurgical and Materials Transactions A*, 40 (2009), 1344-1354.
- [94] Y. Gao, X. Xu, Z. Yan, G. Xin, High hardness alumina coatings prepared by low power plasma spraying, *Surface & Coatings Technology*, 154 (2002), 189-193.
- [95] S. Stewart, R. Ahmed, T. Ituskaichi, Rolling contact fatigue of post-treated WCNiCrBSi thermal spray coatings, *Surface & Coatings Technology*, 190 (2005), 171-189.
- [96] J.Y. Bai, Y.X. Cheng, J.B. Cheng, X.B. Liang, B.S. Xu, An automatic high velocity arc spraying system, *Key Engineering Materials*, 373–374 (2008), 89-92.

- [97] S. Stewart, R. Ahmed, Contact fatigue failure modes in hot isostatically pressed WC-12%Co coatings, *Surface & Coatings Technology*, 172 (2003), 204-216.
- [98] R. Ahmed, M. Hadfield, Rolling contact fatigue performance of detonation gun coated elements, *Tribology International*, 30 (1997), 129-137.
- [99] Piao Zhong-yu, Xu Bin-shi, Wang Hai-dou, Wen Dong-hui, Characterization of Fe-based alloy coating deposited by supersonic plasma spraying, *Fusion Engineering and Design*, 88 (2013), 2933-2938.
- [100] Lowenheim, F. A., *Electroplating*, McGraw-Hill, New York, 1978.
- [101] SIRI board of consultant and engineers, *Modern Technology of electroplating: Anodizing and other surface treatments*, Small Industry Research Institute, India, 2004.
- [102] Abhishek Kumar, V.P. Agrawal, Attribute based specification, comparison and selection of electroplating system using MADM approach, *Expert Systems with Applications*, 36 (2009), 10815-10827.
- [103] Yinping Ye, Jianmin Chen, Huidi Zhou, An investigation of friction and wear performances of bonded molybdenum disulfide solid film lubricants in fretting conditions, *Wear*, 266 (2009), 859-864.
- [104] J. Xu, M.H. Zhu, Z.R. Zhou, Ph. Kapsa, L. Vincent, An investigation on fretting wear life of bonded MoS<sub>2</sub> solid lubricant coatings in complex conditions, *Wear*, 255 (2003), 253-258.
- [105] J. Luo, M.H. Zhu, Y.D. Wang, J.F. Zheng, J.L. Mo, Study on rotational fretting wear of bonded MoS<sub>2</sub> solid lubricant coating prepared on medium carbon steel, *Tribology International*, 44 (2011), 1565-1570.
- [106] F.J. Clauss, *Solid Lubricants and Self-lubricating Solids*, Academic Press, New York and London, 1972.

- [107] R. Greenberg, G. Halperin, I. Etsion, and R. Tenne, The effect of WS<sub>2</sub> nanoparticles on friction reduction in various lubrication regimes, *Tribology Letters*, 17 (2) (2004), 179-186.
- [108] Bret C. Windom, W.G. Sawyer, David W. Hahn, A Raman Spectroscopic Study of MoS<sub>2</sub> and MoO<sub>3</sub>: Applications to Tribological Systems, *Tribology Letters*, 42 (2011), 301-310.
- [109] B.C. Stupp, Molybdenum disulfide and related solid lubricants, *Lubrication Engineering*, 14 (1958), 159-163.
- [110] J. Xu, Z.R. Zhou, C.H. Zhang, M.H. Zhu, J.B. Luo, An investigation of fretting wear behaviors of bonded solid lubricant coatings, *Journal of Materials Processing Technology*, 182 (2007), 146-151.
- [111] D.B. Luo, V. Fridrici, Ph. Kapsa, Evaluating and predicting durability of bonded solid lubricant coatings under fretting conditions, *Tribology International*, 44 (2011), 1577-1582.
- [112] M.R. Vaziri, M. Salimi, M. Mashayekhi, Evaluation of chip formation simulation models for material separation in the presence of damage models, *Simulation Modelling Practice and Theory*, 19 (2011), 718-733.
- [113] R. Teti, I.S. Jawahir, K. Jemielniak, T. Segreto, S. Chen, J. Kossakowska, Chip Form Monitoring through Advanced Processing of Cutting Force Sensor Signals, *Annals of CIRP*, 55 (1) (2006), 75-78.
- [114] W. Grzesik, C.A. Van Luttervelt, Analytical Models Based on Composite Layer for Computation of Tool-Chip Interface Temperatures in Machining Steels with Multilayer Coated Cutting Tools, *Annals of CIRP*, 54 (1) (2005), 91-94.



- [115] M.H. Attia, L. Kops, A New Approach to Cutting Temperature Prediction Considering the Thermal Constriction Phenomenon in Multi-layer Coated Tools, *Annals of CIRP*, 53 (1) (2004), 47-50.
- [116] T. Ozel, Taylan Altan, Process simulation using finite element method - prediction of cutting forces, tool stresses and temperatures in high speed flat end milling, *International Journal of Machine Tools & Manufacture*, 40 (2000), 713-738.
- [117] Tugrul Ozel, Erol Zeren, Finite Element Method Simulation of Machining of AISI 1045 Steel with A Round Edge Cutting Tool, *Proceedings of the 8th CIRP International Workshop on Modeling of Machining Operations*, Chemnitz, Germany, 2005.
- [118] T. Ozel, T. Altan, Modeling of high speed machining processes for predicted tool forces stresses and temperatures using FEM simulations, in: *Proceedings of the CIRP International Workshop on Modeling of Machining Operations*, Atlanta, GA, 1998.
- [119] E. Ceretti, C. Lazzaroni, L. Menegardo, T. Altan, Turning simulations using a three-dimensional FEM code, *Journal of Materials Processing Technology*, 98 (2000), 99-103.
- [120] E. Ceretti, E. Taupin, T. Altan, Simulation of metal flow and fracture applications in orthogonal cutting, blanking and cold extrusion, *Annals of CIRP*, 46 (1) (1997), 187-190.
- [121] E. Usui, T. Shirakashi, *Mechanics of Machining - from Descriptive to Predictive Theory*, *On the Art of Cutting Metals - 75 Years Later*, *ASME PED*, 7 (1982), 13-35.

- [122] T. Ozel, The Influence of Friction Models On Finite Element Simulations of Machining, *International Journal of Machine Tools & Manufacturing*, 46 (2006), 518-530.
- [123] T. Ozel, and E. Zeren, Finite Element Modelling the Influence of Edge Roundness on the Stress and Temperature Fields Induced by High Speed Machining, *International Journal of Advanced Manufacturing Technology*, 35 (2007), 255-267.
- [124] Attanasio, E. Ceretti, S. Rizzuti, D. Umbrello, F. Micari, 3D finite element analysis of tool wear in machining, *CIRP Annals-Manufacturing Technology*, 57 (2008), 61-64.
- [125] J.P. Davim, and C. Maranhao, A Study of Plastic Strain and Plastic Strain Rate in Machining of Steel AISI 1045 Using Fem Analysis, *Materials and Design*, 30 (2009), 160-165.
- [126] Guoqin Shi, Xiaomin Deng, Chandrakanth Shet, A finite element study of the effect of friction in orthogonal metal cutting, *Finite Elements in Analysis and Design*, 38 (2002), 863–883.
- [127] Chandrakanth Shet, Xiaomin Deng, Finite element analysis of the orthogonal metal cutting process, *Journal of Materials Processing Technology*, 105 (2000), 95-109.
- [128] P.J. Arrazola, D. Ugarte, J. Montoya, A. Villar, S. Marya, Finite element modelling of chip formation process with Abaqus/explicit<sup>TM</sup> 6.3, VIII International Conference on Computational Plasticity COMPLAS VIII , Barcelona, 2005.
- [129] Maranhao, J. Paulo Davim, Finite element modelling of machining of AISI 316 steel: Numerical simulation and experimental validation, *Simulation Modelling Practice and Theory*, 18 (2010), 139-156.

- [130] P.J. Arrazola, T. Ozel, Investigations on the effects of friction modelling in finite element simulation of machining, *International Journal of Mechanical Sciences*, 52 (2010) 31-42.
- [131] L. Filice, F. Micari, S. Rizzuti, D. Umbrello, A critical analysis on the friction modelling in orthogonal machining, *International Journal of Machine Tools & Manufacture*, 47 (2007), 709-714.
- [132] P.J. Arrazola, T. Ozel, D. Umbrello, M. Davies, I.S. Jawahir, Recent advances in modelling of metal machining processes, *CIRP Annals - Manufacturing Technology*, 62 (2013), 695-718.
- [133] O. Pantale, J.L. Bacaria, O. Dalverny, R. Rakotomalala, S. Caperaa, 2D and 3D numerical models of metal cutting with damage effects, *Computer Methods in Applied Mechanics and Engineering*, 193 (2004), 4383-4399.
- [134] J.S. Strenkowski, J.T. Carroll, A finite element model of orthogonal metal cutting, *Journal of Manufacturing Science and Engineering*, 107 (4) (1985), 349-354.
- [135] H. Bil, S.E. Kılıc, A.E. Tekkaya, A comparison of orthogonal cutting data from experiments with three different finite element models, *International Journal of Machine Tools & Manufacture*, 44 (2004), 933-944.
- [136] B. Zhang, A. Bagchi, Finite element simulation of chip formation and comparison with machining experiment, *Journal of Manufacturing Science and Engineering*, 116 (8) (1994), 289-297.
- [137] Vahid Kalhori, Modelling and Simulation of Mechanical cutting, Lulea University of Technology, Ph.D. Thesis, Sweden, 2001.
- [138] A.G. Mamalis, M. Horvath, A.S. Branis, D.E. Manolakos, Finite element simulation of chip formation in orthogonal metal cutting, *Journal of Materials Processing Technology*, 110 (2001), 19-27.

- [139] S.P.F.C. Jaspers, J.H. Dautzenberg, Material behaviour in metal cutting: strains, strain rates and temperatures in chip formation, *Journal of Materials Processing Technology*, 121 (2002), 123-135.
- [140] N. Fang, A new Quantitative Sensitivity Analysis of the Flow Stress of 18 Engineering Materials in Machining, *Journal of Engineering Materials and Technology*, 127 (2) (2005), 192-196.
- [141] Y.C. Lin, Xiao-Min Chen, Ge Liu, A modified Johnson–Cook model for tensile behaviors of typical high-strength alloy steel, *Materials Science and Engineering A*, 527 (2010), 6980-6986.
- [142] T. Ozel, Taylan Altan, Determination of workpiece flow stress and friction at the chip–tool contact for high-speed cutting, *International Journal of Machine Tools & Manufacture*, 40 (2000), 133-152.
- [143] T. Ozel, Erol Zeren, Determination of work material flow stress and friction for FEA of machining using orthogonal cutting tests, *Journal of Materials Processing Technology*, 153-154 (2004), 1019-1023.
- [144] Shuhui Li, Bo Hou, Material Behavior Modeling in Machining Simulation of 7075-T651 Aluminum Alloy, *Journal of Engineering Materials and Technology*, 136 (2014), 11001-14.
- [145] G.R. Johnson, W.H. Cook, *Proceedings of Seventh International Symposium on Ballistics*, The Hague, Netherlands, 1983, 541-547.
- [146] P.L.B. Oxley, *The Mechanics of Machining: An Analytical Approach to Assessing Machinability*, Ellis Horwood Limited, Chichester, UK, 1989.
- [147] F.J. Zerilli, R.W. Armstrong, Dislocation-mechanics-based constitutive relations for material dynamics calculations, *Journal of Applied Physics*, 61 (1987), 1816-1825.

- [148] K. Maekawa, T. Shirakashi, E. Usui, Flow Stress of Low Carbon Steel at High Temperature and Strain-Rate (Part 2) - Flow Stress Under Variable Temperature and Variable Strain-Rate, *Bulletin of the Japan Society of Precision Engineering*, 17 (1983), 167–172.
- [149] N.N. Zorev, Interrelationship between Shear Processes Occurring along the Tool Face and Shear Plane in Metal Cutting, *International Research in Production Engineering*, ASME, 1963.
- [150] Angelos P. Markopoulos, *Finite Element Method in Machining Processes*, Springer Briefs in Manufacturing and Surface Engineering, New York, 2013.
- [151] E.G. Ng, T. El-Wardany, M. Dumitrescu, M.A. Elbestawi, *Proceedings of the 5<sup>th</sup> CIRP International Workshop on Modeling of Machining Operations*, West Lafayette, IN, USA, 2002.
- [152] E. Usui, T. Shirakashi, *Mechanics of machining from descriptive to predictive theory*, ASME Publications, PED Sciences, 39 (1997), 369-389.
- [153] E. Usui, K. Maekawa, T. Shirakashi, Simulation Analysis of Built-up Edge Formation in Machining of Low Carbon Steels, *Bulletin of the Japan Society of Precision Engineering*, 15 (1981), 237-242.
- [154] T.H. Childs, K. Maekawa, T. Obikawa, Y. Yamane, *Metal Machining: Theory and Applications*, Elsevier, Amsterdam, 2000.
- [155] M.H. Dirikolu, T.H. Childs, K. Maekawa, Finite element simulation of chip flow in metal machining, *International Journal of Mechanical Sciences*, 43 (2001), 2699-2713.
- [156] T. H. C. Childs, K. Maekawa, *Computer Aided Simulation and Experimental Studies of Chip Flow and Tool Wear in the Turning of Low Alloy Steels by Cemented Carbide Tools*, *Wear*, 139 (1990), 235-250.

- [157] P.J. Arrazola, D. Ugarte, X. Dominguez, A new approach for the friction identification during machining through the use of finite element modeling, *International Journal of Machine Tools & Manufacture*, 48 (2) (2008), 173-183.
- [158] G.B. Adrian, The science and technology of electrostatic powder spraying, transport and coating, *Journal of Electrostatics*, 45 (1998), 85-120.
- [159] S. Singh, B.C. O'Neill, A.W. Bright, A parametric Study of Electrostatic Powder Coating, *Journal of Electrostatics*, 4 (4) (1978), 325-334.
- [160] S. Singh, Charging Characteristics of Some Powders used in Electrostatic Coating, *IEEE Transactions on Industry Applications*, IA-17 (1) (1980), 121-124.
- [161] J. Malzbender, J.M.J. Den Toonder, A.R. Balkenende, G. De With, Measuring mechanical properties of coatings: a methodology applied to nano-particle-filled sol-gel coatings on glass, *Materials Science and Engineering R*, 36 (2002), 47-103.
- [162] T. Kagnaya, C. Boher, L. Lambert, M. Lazard, T. Cutard, Wear mechanisms of WC-Co cutting tools from high-speed tribological tests, *Wear*, 267 (2009), 890-897.
- [163] A. Ramalho, J.C. Miranda, The relationship between wear and dissipated energy in sliding systems, *Wear*, 260 (2006), 361-367.
- [164] N.M. Renevier, V.C. Fox, D.G. Teer, and Hampshire, J, Performance of low friction MoS<sub>2</sub>-titanium composite coatings used in forming applications, *Materials & Design*, 21 (4) (2000), 337-343.
- [165] V.S. Sharma, M. Dogra, N.M. Suri, Advances in the turning process for productivity improvement—a review, *Proceedings of Institution of Mechanical Engineers, Part B: Journal of Engineering Manufacture*, 222 (11) (2008), 1417-1442.

- [166] F. Pusavec, D. Kramar, P. Krajnik, J. Kopac, Transitioning to sustainable production—part II: evaluation of sustainable machining technologies, *Journal of Clean Production*, 18 (12) (2010), 1211-1221.
- [167] H. Popke, T. Emmer, J. Steffenhagen, Environmentally clean metal cutting processes—machining on the way to dry cutting, *Proceedings of Institution of Mechanical Engineers, Part B: Journal of Engineering Manufacture*, 213 (3) (1999), 329-332.
- [168] R.R. Srikant, M.M.S. Prasad, M. Amrita, A.V. Sitaramaraju, P.V. Krishna, Nanofluids as a potential solution for minimum quantity lubrication: a review. *Proceedings of Institution of Mechanical Engineers, Part B: Journal of Engineering Manufacture*, 228 (1) (2014), 3-20.
- [169] E. Brinksmeier, A. Walter, R. Janssen, P. Diersen, Aspects of cooling lubrication reduction in machining advanced materials, *Proceedings of Institution of Mechanical Engineers, Part B: Journal of Engineering Manufacture*, 213 (8) (1999), 769-778.
- [170] R.K. Bhushan, S. Kumar and S. Das, Effect of machining parameters on surface roughness and tool wear for 7075 Al alloy SiC composite, *International Journal of Advanced Manufacturing Technology*, 50 (2010), 459-469.
- [171] Valery Marinov, *Manufacturing processes for metal products*, Kendall Hunt Publishing, USA, 2010.
- [172] M.C. Shaw, *Metal Cutting Principles*, Clarendon Oxford, London, 1984.
- [173] Deform 2D V9.0.1. User's Manual, Scientific Forming Technologies Corporation, Columbus, Ohio, 2006.
- [174] C. Zener, H. Hollomon, Effect of strain rate upon plastic flow of steel, *Journal of Applied Physics*, 15 (22) (1944).

- [175] N.J. Hoff, Approximate analysis of structures in presence of moderately large creep deformations, *Quarterly of Applied Mathematics*, 12 (1954), 51-63.
- [176] E. Usui, H. Takeyama, A photoelastic analysis of machining stresses, *ASME Journal of Manufacturing Science and Engineering*, 82 (4) (1960), 303-308.
- [177] Ryan C. McLaren, Thermal conductivity anisotropy in molybdenum disulfide thin films, MS thesis, Graduate College of the University of Illinois, Urbana, Illinois, 2009.
- [178] E.A. Flores-Johnson, Luming Shen, Irene Guiamasia, Giang D. Nguyen, Numerical investigation of the impact behavior of bioinspired nacre-like aluminum composite plates, *Composites Science and Technology*, 96 (2014), 13-22.
- [179] Tarek Mabrouki, Francois Girardin, Muhammad Asad, Jean-Francois Rigal, Numerical and experimental study of dry cutting for an aeronautic aluminum alloy (A2024-T351), *International Journal of Machine Tools & Manufacture*, 48 (2008), 1187-1197.



## LIST OF PUBLICATIONS

---

### International Journals

#### Published

1. Uma Maheshwera Reddy Paturi, Suresh Kumar Reddy Narala, Experimental investigation to study the effect of electrostatic micro-solid lubricant-coated carbide tools on machinability parameters in turning, Proc IMechE Part B: Journal of Engineering Manufacture (SAGE), DOI: 10.1177/0954405414530903.
2. Uma Maheshwera Reddy Paturi, Suresh Kumar Reddy Narala, Rajdeep Pundir, Constitutive flow stress formulation, model validation and FE cutting simulation for AA7075-T6 aluminum alloy, Materials Science & Engineering A (Elsevier), 605 (2014), 176–185.

#### Under review

1. Uma Maheshwera Reddy Paturi, Suresh Kumar Reddy Narala, On a novel solid lubricant coating: A study on the tribological characteristics under dry sliding conditions, Proc IMechE Part J: Journal of Engineering Tribology (SAGE).
2. Uma Maheshwera Reddy Paturi, Suresh Kumar Reddy Narala, Experimental and finite element simulations of aluminum alloy AA7075-T6 machining with and without coated tools, Simulation Modelling Practice and Theory (Elsevier).
3. Uma Maheshwera Reddy Paturi, Suresh Kumar Reddy Narala, Flow stress prediction for AA7075-T6 at elevated temperatures: numerical simulation and experimental validation in machining, Materials and Design (Elsevier).

## **Publications in International conference proceedings**

1. Uma Maheshwera Reddy Paturi, Suresh Kumar Reddy Narala, Investigation on wear behavior of electrostatic micro-solid lubricant coatings under dry sliding conditions, ASME 2012 International Mechanical Engineering Congress and Exposition, Volume 3, DOI:10.1115/IMECE2012-87201.

(<http://proceedings.asmedigitalcollection.asme.org/proceeding.aspx?articleid=1750648>)

2. Uma Maheshwera Reddy Paturi, Suresh Kumar Reddy Narala, Finite element analysis and study of tool wear in machining with coated tools, ASME 2013 International Mechanical Engineering Congress and Exposition, Volume 2B, DOI:10.1115/IMECE2013-64342.

(<http://proceedings.asmedigitalcollection.asme.org/proceeding.aspx?articleid=1857839>)

## BIOGRAPHY OF THE CANDIDATE

Name of the candidate	UmaMaheshwera Reddy Paturi
ID. No.	2011PHXF017H
Experience	Over 8 years of teaching experience
Academic credentials	<ul style="list-style-type: none"> <li>• Ph.D. (pursuing from BITS-Pilani, Hyderabad Campus)</li> <li>• M.Tech in Mechanical Engineering (VTU, Karnataka)</li> <li>• B.Tech in Mechanical Engineering (SKD, Anantapur)</li> <li>• Intermediate in M.P.C (RK Junior College, Hyderabad)</li> <li>• SSC, AP Residential School (Lingampally, Medak Dt.)</li> </ul>
Career achievements	<ul style="list-style-type: none"> <li>• Gold Medal received from VTU (Visveswararajah Technological University) for securing University I Rank in M.Tech</li> <li>• Professor Gopalan (Ex-Professor, IITB) Cash Prize received for the year 2005</li> <li>• JSS Maha Vidya Peta Cash Prize received for the year 2005</li> <li>• JSS Maha Vidya Peta Award of Honor received for the year 2005</li> </ul>
Professional memberships	<ul style="list-style-type: none"> <li>• Life Member of Indian Society for Technical Education</li> <li>• Life Member of Institution of Engineers India</li> <li>• Student Member of ASME</li> </ul>
Personal details	Residential address: Flat-205, Balaji Residency, R.R. Nagar Old Bowenpally, Hyderabad – 500011 Contact Number: +919848484637 Email address: maheshpaturi@gmail.com

## BIOGRAPHY OF THE SUPERVISOR

Name of the Supervisor	Dr. SURESH KUMAR REDDY NARALA
Designation and address	Associate Professor, Department of Mechanical Engineering, BITS, Pilani, Hyderabad Campus
Experience (years)	13
Number of publications	Journals - 14
	International Conferences - 10
Number of citations	312
Sponsored projects	1. Performance evaluation of various coated drills based on wear and hole quality in dry drilling (Sponsor: Oerlikon Balzers)  (Jan 2008 to Nov 2008)
	2. BITS-SG Project on “Development of novel coated tools for green machining”, Rs.11.8 Lakhs.  (2011-2013)
	3. CSIR project- “Development of ES nano-solid lubricant coated tools for sustainable machining”, Rs.18.52 Lakhs.  (2012-15)
	4. DST project – “Novel minimal application method for performance improvement in turning”, Rs.32.50 Lakhs.  (2013-16)
No. of Ph.D. students under supervision	3